ABSTRACT

HYDE, GARY KEVIN. Functional Textiles via Self-assembled Nanolayers and Atomic Layer Deposition. (Under the direction of Gregory N. Parsons and Behnam Pourdeyhimi).

The ability to create novel inorganic-organic-metal ordered structures with molecular level precision opens the possibility of developing multifunctional textiles for a myriad of applications including active filtration, bio-separation of proteins, catalytic mantles, and electronic fabrics as well as novel barrier and anti-counterfeiting materials. Due to the high curvature and heterogeneous nature of textile fibers, existing surface modification technologies are not capable of providing complete coverage of a fiber/fabric surface. The use of self-assembly techniques and self-limiting reactant adsorption processes offer the possibility of achieving fully conformal, uniform functionalization of textile fibers of any continuous shape. Atomic layer deposition and electrostatic self-assembly have been used in the semiconductor industry to produce uniform self-organized molecular assemblies over large areas of uniform and clean surfaces such as silicon wafers. However, the use of these techniques in textiles has been largely unexplored.

The goal of this research was to determine the feasibility of using layer-by-layer and atomic layer deposition as methods of textile modification. This research has also investigated the optimum processing conditions that allow the selective and controlled deposition of organic, inorganic, and metallic substances on textile substrates via self-assembled nanolayers and atomic layer deposition techniques.

FUNCTIONAL TEXTILES VIA SELF-ASSEMBLED NANOLAYERS AND ATOMIC LAYER DEPOSITION

by

GARY KEVIN HYDE

A dissertation submitted to the Graduate Faculty of

North Carolina State University

in partial fulfillment of the

requirements for the Degree of

Doctor of Philosophy

Fiber and Polymer Science

Raleigh, NC

June 2007

APPROVED BY:

Dr. William Oxenham	Dr. Pamela Banks-Lee
Dr. Gregory Parsons (Co- Chair of Advisory Committee)	Dr. Behnam Pourdeyhimi (Co- Chair of Advisory Committee)

DEDICATION

To Mom and Dad

BIOGRAPHY

Gary Kevin Hyde was born on June 24, 1981 to Gary and Karen Hyde of Ellijay, GA. Kevin has one sister, Amanda. He graduated from Gilmer High School in Ellijay, GA in May 1999. Kevin graduated with a Bachelor of Science degree in Textile Engineering Technology in May 2003 from Southern Polytechnic State University in Marietta, GA. After graduation, Kevin began attending North Carolina State University to pursue a Master's of Science degree in Textile Chemistry as an Institute of Textile Technology Fellow. Upon obtaining his Master's in May 2005, Kevin began working towards his Doctorate of Philosophy in Fiber and Polymer Science.

ACKNOWLEDGEMENTS

I owe a tremendous debt to my advisor over the past year and a half, Dr. Gregory Parsons. For some reason still unknown to me, Dr. Parsons adopted me into his group and gave me an incredible opportunity to continue my research and add even more to my education. He has shown tremendous confidence in me, especially when one considers that I have a very different background from any of his other graduate students. I am looking forward to working with him in the future and hope that our work together continues to be successful.

I would like to thank all the members, past and present, of Dr. Parsons' research group including Dr. Kie Jin Park, Dr. Jason Kelly, Dr. Daisuke Hojo, Jeong-Seok Na, Qing Peng, Joe Spagnola, Michael Stewart, Ryan Van Gundy, Zach Nicholson, and Kelly Roth. I have learned something from each of them and they helped make the transition to a new research group very easy. Each of them have helped me in finishing my work. They are good friends in addition to good co-workers.

In particular, I want to thank Dr. Kie Jin Park who helped get me started in Dr. Parsons' research group. Kie Jin's guidance and input was invaluable and I could not have done this research without him. He was very patient with me and a great teacher.

This dissertation would have never been finished without the help and hard work Michael Stewart. Michael is one of the smartest and hardest working students I know and I really can not thank him enough for the past year and a half. In addition to his help at school,

Michael has become a good friend and I will really miss him when he leaves for graduate school.

A special thanks also goes to Joe Spagnola for all of his help since I joined Dr. Parsons' group. Joe has helped with reactor construction, experiments, analysis, and general advice. I have learned a great deal about work in the lab from Joe and his help has allowed me to get all of this work done in time. Joe has also become a good friend outside of school and I would like to thank him for that as well.

Finally, I would like to express my deepest gratitude to my parents, my sister, and my grandma. They stood by me and my decisions and were always around whenever I needed to talk. I could not have gotten through graduate school without their help and support.

TABLE OF CONTENTS

LIST OF FIGURES

LIST OF TABLES

CHAPTER 1: INTRODUCTION

1.1 Purpose of Research

Surface modification is an important element of textile manufacturing. The final properties of a textile material are critical in determining how they perform for their given end use. Electrostatic self-assembly and atomic layer deposition are two methods for depositing nano-scale thin films of various materials. Both methods have been successfully used in the semiconductor industry and are currently popular fields of scientific research. However, little research has been done involving the use of textiles as substrates for either of these processes. This research work has investigated the appropriate conditions that allow textile products to be used as substrates for the controlled deposition of thin films using atomic layer deposition and electrostatic self-assembly. The use of new deposition processes could allow many new materials such as polyelectrolytes, metal oxides, and metal nitrides to be used as coatings for textile materials. This research was also aimed at better understanding the combination of organic and inorganic materials at the nano-scale.

1.2 Challenges

Neither atomic layer deposition or electrostatic self-assembly have been extensively implemented for textile substrates. Fibrous structures present a variety of problems in regards to their morphology, chemical stability, and thermal stability. Organic materials are often much more difficult to work with, in that they require different processing conditions as well as different analytical methods. Deposition onto high-surface area, complex materials

using these deposition techniques is a relatively new area of research, requiring the development of new processes and methods.

1.3 Overview of Dissertation

This dissertation describes two novel methods for the surface modification of textile materials: electrostatic self-assembly and atomic layer deposition. Chapter 2 provides a literature review including an overview of textile finishing, recent advances in textile coating technology, descriptions of each of the deposition processes and also the analysis techniques used during the course of this research. In Chapters 3-5, polyelectrolyte layers are deposited onto fibers and fabrics using layer-by-layer assembly. A variety of analytical techniques such as X-ray photoelectron spectroscopy, transmission electron microscopy, and electrostatic force microscopy are utilized. Both natural and synthetic fibers are investigated as substrates for the layer-by-layer deposition of polyelectrolytes. Chapters 6-9 present results of the use of atomic layer deposition as a method for the modification of textile substrates. Again, both synthetic and natural fibers are utilized, along with several different inorganic coatings.

In Chapter 3, results of the layer-by-layer deposition of polyelectrolytes onto cotton fibers are presented. Particular emphasis is placed on the importance of initial surface preparation, in this case a cationization procedure for cotton. A comparison is made between different preparation recipes and their effect on subsequent polyelectrolyte deposition.

In Chapter 4, an examination of cotton fibers supporting polyelectrolyte nanolayers is made using electrostatic force microscopy. Electrostatic force microscopy is a relatively new

method for the characterization of textile materials and provides new insight into the nature of nano-scale coatings.

In Chapter 5, the deposition of polyelectrolyte nanolayers onto polyester fibers is discussed. This work demonstrates the utility of layer-by-layer assembly by coating synthetic fibers in a knit fabric form. The effect of plasma treatment on polyelectrolyte deposition is also studied.

Chapter 6 discusses the low temperature deposition of aluminum oxide onto cotton fabrics using atomic layer deposition. Imaging of the fibers demonstrates the ability of atomic layer deposition to conformally coat individual fibers within the fabric. This study shows that atomic layer deposition is a viable method for the nano-scale modification of textile materials.

Chapter 7 presents the modification of electrospun fibers using atomic layer deposition. The electrospun fibers are then removed to produce aluminum oxide microtubes. Atomic layer deposition is shown to be a powerful method for the uniform coating of complex, high surface area substrates and for the production of microtubes with controllable characteristics.

In Chapter 8, a study on the deposition of titanium nitride on cotton by atomic layer deposition is presented. Particular attention is given to the ability of atomic layer deposition to pass throughout a fabric sample and coat all exposed fiber surfaces. Changes in the surface energy of the fabrics are also investigated.

In Chapter 9, the atomic layer deposition of titanium dioxide onto cellulose fibers is explored. Characteristics of the films are studied by X-ray photoelectron spectroscopy.

Chapter 10 proposes some general conclusions of this research. In addition, future studies and possible projects are also discussed.

Chapter 11 is comprised of an appendix which presents initial experiments involving the combination of layer-by-layer assembly and atomic layer deposition. The layers are analyzed using x-ray photoelectron spectroscopy and atomic force microscopy.

CHAPTER 2: LITERATURE REVIEW

2.1 Textile Finishing

Finishing is the final step in the textile manufacturing process. During finishing, the final properties of a textile material are determined. Many finishing methods are wet processes. However, any operation that is used to change the appearance or properties of a fiber, fabric, or nonwoven before it is packaged can be considered a finishing procedure. A finish may use chemicals to change the properties of the textile, or it can use mechanical devices to cause changes to the surface of the material. Therefore, textile finishing is often divided into two different categories: chemical and mechanical.[1] In chemical finishing, water is normally used as the medium for applying chemicals that alter the textile substrate in some way. An example of a chemical finish would be the application of a low surface energy film such as polyvinyl chloride to make a fabric waterproof.[2] Mechanical finishing is defined as any operation that improves fabric appearance or function by physical manipulation by some type of machinery. An example of mechanical finishing is calendaring, where a fabric is passed between two rolls under pressure to increase the luster of a fabric.[1] The distinction between chemical and mechanical finishing can often be unclear

since chemical finishing normally requires the use of some machinery and mechanical finishing may use water or steam during processing. The two methods can most easily be classified by determining what aspects, chemical or mechanical, impart the desired characteristics to the material.[1,2]

Many of the traditional methods of textile finishing use large quantities of water. This water must then be separated from the fabric and also requires further processing to remove any remaining chemicals. There is currently an effort in the textile industry to develop finishing techniques that are capable of recycling some of the chemicals used and limit the use of water at the same time.[2]

The type of fiber being used often determines the finishes and methods used to treat the materials. Therefore, it is often difficult to define textile finishing as a step-by-step process. In general, products consisting of natural fibers require more processing when compared to synthetic fibers. At the same time, the different synthetic fibers can require very diverse finishing procedures.[2]

Types of textile finishes can be divided into functional and aesthetic finishes. Functional finishes are used to alter fiber or fabric performance, maintenance, durability, safety, and environmental resistance. Finishes that are applied specifically to alter properties related to care, comfort, and durability are generally considered functional finishes. Most functional fabric properties are imparted using chemical, wet processing methods.[1,2]

Some common functional finishes can be seen in the list below[2] :

- Antimicrobial
- Antistatic
- Durable press
- Flame resistant/retardant
- Soil release/resistant
- Water proof/repellent
- Wrinkle recovery

Aesthetic finishes are finishes used to modify the appearance or hand of a fiber or fabric. Finishes that alter the texture, luster, or drape of a textile material can be considered aesthetic finishes.[2] Mechanical and chemical processes may be used to impart an aesthetic finish, with a greater emphasis being placed on mechanical processes for this type of finishing.[1]

It is beyond the scope of this work to provide a comprehensive review of textile finishing. Many different chemicals and processes are used in the finishing of textile materials. Instead, this literature review will concentrate on some of the recent advances in the field of inorganic and novel finishes on textile materials.

2.2 Inorganic Finishes on Textiles

Inorganic finishes have been used for many years in the textile industry including silver, copper, and various metal oxides.[3] Inorganic finishes are often applied using solution

based methods such as pad-dry-cure. Applications of textile materials treated with inorganic finishes range from increasing the conductivity of material such as carpet to reduce static electricity build-up to anti-bacterial finishes for medical face masks. Over the past decade, new technologies have given manufacturers the ability to create inorganic coatings that are more functional and durable than previous finishes. Various types of finishes may be used to treat textiles. Modern textile products are used in an assortment of applications such as the apparel industry, household textiles, medical items, industrial uses and technical products.

Multifunctional textiles are materials that possess many different properties such as flame retardancy, water repellency, and antibacterial activity, etc. Textile products possessing numerous added properties are closely tied to current developments in the textile industry. New types of textile products are providing the industry with new products and technologies. These multifunctional textiles can be used for a number of different tasks. At the same time however, the products must still meet consumer demand in regards to comfort, ease of care, and health issues. Modified textile materials can protect against mechanical, thermal, chemical, and biological attacks, and at the same time offer improved durability and performance.[4] The list below details the most important requirements of multifunctional textiles.[5]

- Improved stability for mechanical, chemical, photo-chemical, or thermal destruction
- Improved water, oil, and soil repellency properties
- Different light absorption and emission properties in the UV and IR regions
- Changed electric conductivity
- Controlled release or immobilization of various active species

Inorganic coatings on textiles are capable of meeting the different requirements listed above. Coatings of inorganic materials such as silver, copper, and other metals offer an array of functionalities for textile products. Medical research is one of the major driving forces for integration of electronics with nonwovens, which are fiber-based materials that are neither woven or knit. Other studies are looking at the inclusion of conductive circuits and optical fibers into nonwoven structures.[6] New technologies have allowed researchers to create durable coatings without changing the aesthetic nature of the fabrics. These various technologies will lead to a number of new products and processes in the coming years.

2.2.1 Sol-gel Coatings on Textiles

Mahltig and his colleagues have recently developed a method for the coating of nonwovens with inorganic sol-gels. Sol-gels are nanoparticular materials that can be made up of modified silica and other metal oxides. The sol-gel process is described in detail in other studies.[4] Sols based on modified silica and metal oxides having particle diameters less than 50 nm form transparent oxide layers on textiles. These oxide layers are stable against light, heat, chemical, and microbial attacks. The layers have also been shown to improve mechanical properties such as strength and abrasion resistance. Sol-gel coatings can be prepared at room temperature under normal pressure conditions using traditional textile application techniques such as pad application. Dip coatings and spraying may also be used to apply the coatings.[4]

In 2003, Mahltig and Bottcher investigated the use of modified silica sols as a way of producing textiles with improved water repellency.[7] Fabrics of polyamide and

polyester/cotton were used as substrates for the sol deposition. The research showed that the hydrophobicity of the textiles increased as the concentration of silica sols increased. The sols were modified to contain alkylsilane, polysiloxane, and fluorine. Different methods were used to evaluate the water repellent properties of the coatings. Contact angle measurements were made on the textiles. Spray tests and washing tests were also performed. The results of the experiments showed that modified silica sols could be used as an alternative treatment to change the water repellency of nonwoven textile products and at the same time have adequate wash fastness.[7]

Mahltig et al. have also studied the ability of sol-gel coatings to prevent the leaching of dyes from textile products.[8] The diffusion of dye out of the sol layer on the textile can be greatly reduced by modifying the composition of the sol-gel. The dye fastness of negatively charged dyes can be improved by using mixed metal oxide sol-gels such as alumina or titanium dioxide.[8]

Due to the particular interest in coatings to prevent bio-contamination, different methods have been investigated to create sol–gel coatings with biocidal properties. Mahltig and his co-workers studied several ways by which modified sols could be used as antimicrobial finishes for textile products. For this study, silica layers with embedded silver, silver salts, and biocidal quaternary ammonium salts were investigated. Both the growth of fungi and bacteria were found to be inhibited by coatings with embedded biocides.[9]

2.2.2 Metal Coatings as Deodorizers

Deodorizing textiles can be produced using inorganic finishes. As the demand of the consumers for more comfortable products grows, new, more efficient methods of deodorizing textile materials must be developed. Deodorization methods make use of aromatic, masking, and neutralizing compounds as well as physical deodorization techniques. Unfortunately, many of these methods do not provide a permanent solution for the removal of unpleasant odors. Metal phthalocyanine derivatives have been investigated by Cho and colleagues as a method of deodorizing polypropylene fibers.[10]

Metal phthalocyanines act as oxidation catalysts to continuously convert odor causing compounds to odorless substances by cyclic oxidation and reduction reactions. These reactions do not consume the metal phthalocyanines. A disadvantage of metal phthalocyanine is that it is often in the form of a solution or powder and therefore not easily applied to many materials. However, fibers are excellent candidates in that they are easy to handle and provide a large contact area with the odor causing compounds. Many of the technologies used for producing deodorizing fibers are limited to certain types of fibers and are not very durable. Cho and his colleagues used chemical grafting to attach Fe (III)-4, 49, 40, 4-- tetra carboxamide phthalocyanine (Fe-TCMP) to nonwoven polyproplylene (PP) fabric. The Fe-TCAP was grafted onto the PP nonwoven by immersing the fabric into a solution of the Fe-TCAP.[10]

Deodorizing fabric was produced by chemically grafting Fe-TCAP onto plasma treated PP nonwoven fabric at 20 W for 20 min. The grafting reaction was carried out for 5, 15, and 20 hours at various pHs (6, 7, and 8) and reaction temperatures (4, 20, and 40°C).

The optimum condition for the grafting reaction was determined on the basis of the oxidation yield of 2-mercaptoethanol at 20°C. 2-mercaptoethanol is a known odor causing compound. The oxidation yield increased as the grafting time increased until 10 h. It then decreased again with further increases in grafting time. The optimum pH of the solution and grafting temperature was 7 and 20°C, respectively. Lower oxidation yields were obtained when deodorizing fabrics were washed with water before use, which indicates that some portion of the Fe-TCAP was physically adsorbed. However, the deodorizing fabric grafted for 10 h at 20°C and pH 7 showed reasonably good deodorizing performance even after washing. In conclusion, it was determined that Fe-TCMP, a metal phthalocyanine derivative, has good potential for continuous deodorization of odor generating compounds such as 2-mercaptoethanol by cyclic oxidation/reduction.[10]

2.2.3 Metal Oxides in Textile Technology

Metal oxides are of great interest because of their chemical and electrical properties. Tin oxide can be used as an electrical conductor that is optically transparent in the visible spectrum. Tin oxide can also be used in photovoltaic cells, liquid crystal displays, and light-emitting diodes. Another important metal oxide is titanium dioxide, which is a wide band-gap semiconductor and is known to be a good oxidizing agent for photo-excited molecules and/or functional groups. Titanium dioxide has been used as a photocatalyst, sensor material, and in photovoltaic cells. The size of the interfacial area plays an important role in determining the properties in many of these applications. The interface often is composed of nanometer-scale particles of the metal oxide.[11]

Drew et al. used electrospinning to create nonwoven fiber membranes for use as substrates for deposition of continuous films of titanium dioxide (TiO_2) and tin dioxide (SnO_2). Liquid-phase deposition was used to deposit the films on the nonwoven webs. During liquid-phase deposition, a metal precursor was first hydrolyzed in an aqueous solution and then subsequently forms a metal oxide by the condensation of water. Liquid-phase deposition allowed the webs to be coated without binding the fibers together, thereby leaving the high surface area of the membranes unchanged.[11]

Drew et al. also demonstrated that liquid-phase deposition could be used to create thin films of TiO_2 and SnO_2 on electrospun nonwoven webs of polyacrylonitrile. Scanning electron microscopy (SEM) was used to analyze the structure of the coatings and the chemical composition of the coatings was confirmed using X-ray photoelectron spectroscopy. It is thought that metal oxide coated nonwoven membranes will provide functional surfaces offering improved performance for applications such as catalysis, sensing, and photoelectric materials.[11]

Metal oxides can also be used to alter the electrical properties of fibers and fabrics. Lee et al. created polypyrrole and metal compounds on the surface of nonwoven polyester fabrics. Vacuum evaporation was used to deposit silver-palladium compounds onto the surface of the nonwoven webs. The polypyrrole and silver-palladium work to form conducting networks on the surfaces of the individual fibers.[12]

2.2.4 Textiles as Electromagnetic Interference Shields

There is currently a need for conductive fabrics capable of providing electromagnetic interference shielding. Metals and metal oxides can be used to improve the electromagnetic interference (EMI) shielding efficiency (SE) of modified nonwoven fabrics. EMI causes efficiency problems for a variety of electronic products. It is expected that metal/polymeric fabrics will offer enhanced advantages for commercial and military EMI shielding applications. Conductive fabrics can also be used in cable manufacturing, battery electrode substrates, and in biomedical applications. These types of materials can be produced by electroless plating of polyester and polypropylene nonwoven fabrics. The standard electroless plating procedure deposits a catalytically active material, which normally contains palladium, onto the fiber surface from an aqueous solution. The nonwoven fabric is then metallized by immersion in a chemical solution. The metals most commonly used for electroless metallization are copper and nickel. It is often necessary to carry out a pretreatment step that makes the fiber surface hydrophilic in order to create uniform layers of metal. It has been demonstrated that atmospheric pressure plasma treatment is an efficient way of producing hydrophilic groups on the surfaces of the fibers.[13]

Simor et al. used nitrogen plasma to create a hydrophilic polyester nonwoven fabric to be used for the electroless plating of nickel. The electroless process made use of metallization baths. First, the fabrics were placed in an aqueous bath of Pd/Sn to chemically activate the surface. The samples were then immersed in an acidic solution to remove the tin from the compound. Finally, the nonwoven webs were placed in a nickel plating bath. The plated fabrics were then analyzed with SEM. Microscopy results showed good coverage of

the nickel to the polyester fibers. Further experimentation using tape tests showed that the nickel plating was very strongly attached to the polyester fibers.[13]

Stefecka et al. investigated the use of electroless copper plating as a method of improving the EMI SE of polypropylene nonwoven fabrics. In this study, spunbonded polypropylene fabrics were used. Atmospheric pressure surface barrier discharge was used to activate the polypropylene webs. The fabrics were then treated with nitrogen, followed by electroless copper plating. The electroless copper plating was carried out using a multistep process based on commercial metallization baths. The plating process is described in detail in the paper. Results showed that a uniform copper coating can be produced on individual fibers for nitrogen plasma treated polypropylene.[14]

2.2.5 Silver in Textile Technology

Perhaps one of the most commonly used inorganic coatings for textile products is silver. Silver is a very useful antiseptic material. It works by binding with protein molecules, inhibiting cellular metabolism, and finally terminating the micro-organism. Silver is naturally non-toxic making it innocuous to human skin. Silver is often used in nonwoven materials to reduce the bacterial content of air or water filters, medical clothing, and woven textile fabrics, all of which come into direct contact with human skin.[15]

Silver colloids, which are nano-sized particles of silver, have begun to attract attention as materials capable of treating textile fabrics. Silver colloids have been shown to provide a good antibacterial effect on polymers and textile products. In 2004, Lee and Jeong demonstrated the use of silver colloids as antibacterial treatments for polyester nonwovens.

The nonwoven webs were simply immersed in solutions of colloidal silver of varying strengths for several different time ranges. A basic pad-dry-cure process was used to treat the fabric webs.[16]

Jeong, Hwang, and Yi investigated the use of nano-sized silver colloids as antibacterial agents on polyester-polypropylene nonwovens. These nonwovens are used due to their excellent softness, uniformity, and light weight. Consumer demand for materials of this type is on the rise since products of polyester-polypropylene are very absorbent, breathable, and inexpensive. This nonwoven blend is often used in medical disposables, sanitary products, and diapers. However, these materials can often carry infectious disease agents and can be easily contaminated by bacteria from moisture and dirt. Therefore, current research is looking at different methods for producing durable, efficient antibacterial finishes for polyester-polypropylene nonwovens.[17]

Jeong et al. prepared polyester-polypropylene nonwovens using various types of nano-sized silver colloids and then compared their antibacterial efficacy. A pad-dry-cure process was used to apply the silver colloids from solution to the nonwoven webs. The silver colloids were examined by SEM. The efficacy was determined by counting the number of living microorganisms on the nonwovens at an initial time and 24 hours after their treatment. The bacteria present were observed as a function of time. The experimental results showed that polyester-polypropylene nonwovens that were treated with the nano-sized silver colloids had good antibacterial properties. SEM imaging showed that the silver nanoparticles were well-dispersed on the surfaces of the nonwoven fibers. The authors expect that polyester-

polypropylene nonwovens treated with silver colloids will display good performance in applications such as back sheets or cover stocks.[17]

Yuranova et al. have demonstrated the use of RF plasma and vacuum-UV for the surface activation and subsequent chemical reduction of silver onto polyamide-polystyrene textile fabrics. A series of preliminary experiments were conducted in order to determine the optimal conditions for the RF plasma and vacuum-UV activation of the fabric surface. Chemical deposition of silver clusters was then carried out. Deposition was done by simply immersing the fabric in different solutions of $AgNO_3$. The silver was then reduced using a suitable pH. Fabrics with and without silver were tested for bacterial growth. The experimental results showed that both methods of surface activation proved to be efficient ways of preparing the polyamide-polystyrene fabrics for deposition.[18]

In addition to improved antibacterial properties, silver coatings could be used to improve various other properties of nonwoven products. Jiang et al. described how chemical silver plating can change numerous fabric properties. Chemical plating is an autocatalytic deposition method that is used for precision processes in conventional manufacturing. Jiang et al. reported the chemical silver plating of cotton and polyester fabrics. The chemical plating solution used consisted of silver nitrate, a reducing agent, and complex agents (alkali, buffer, and stabilizer). After the chemical silver plating was performed, several characteristics of the fabrics were analyzed: fabric weight, fabric thickness, fabric bending, color changes, UV measurements, antistatic properties, conductivity properties, and antibacterial properties. Results of the studies showed that the fabrics were heavier but exhibited very small changes in thickness. The cotton silver plated fabric had a stiffer handle

than the original while the polyester silver plated fabric was softer. The silver treated fabrics showed little color change and demonstrated good color fastness. Both the cotton and the polyester fabrics exhibited improved UV radiation resistance. It was also determined that the silver plated fabrics possessed improved conductivity. Chemical silver plating of the fabrics was also found to be an efficient method of improving the antibacterial properties of the fabrics.[19]

2.3 Layer-by-Layer Self-assembly

The layer-by-layer self-assembly (LbL) of nanolayers is a novel solution for tailoring the surface of textile fibers. The LbL process involves depositing nanolayers of biocidal, charged nanoparticles, non-reactive dyes, metal compounds, and polyelectrolytes in a controlled manner. The thickness and sequence of the nanolayers tailor and enhance the selectivity, diffusivity, and permeability of materials while maintaining their physical properties. This technique is particularly appealing as the thickness, homogeneity, and sequence of these nanolayers can be precisely controlled by means of molecular architecture, self-assembly, and electrostatic interactions. In addition, the self-healing capability of the electrostatic self-assembly method makes this technique particularly tolerant to defects in the base substrate.[20-23]

2.3.1 Layer-by-Layer Deposition Process

Layer-by-layer deposition is related to the Langmuir-Blodgett (LB) technique which was one of the first methods used to create molecularly controlled nano-structured films. The LB process is a system in which monolayers are formed on a non-solvent surface. The

monolayers are then transferred to a solid support. The LB technique was used by Kuhn and his colleagues to perform many of the initial studies on synthetic nano-scale heterostructures in the 1960s.[20]

Current LbL deposition methods are based on the fundamental work conducted by Decher's group in the early 1990s.[20,22-24] The self-assembly process begins by exposing a charged surface to a solution of an oppositely charged polyelectrolyte. The amount of adsorbed material is self-limiting by the charge density of the substrate.[21] Surplus polymer solution adhering to the support is removed by simply washing it in a neutral solution.[25] Under the proper conditions, the polyion is adsorbed with more than the stoichiometric number of charges relative to the substrate, reversing the sign of the surface charge. When the substrate is exposed to a second solution containing a polyion of opposite charge, an additional polyion layer is adsorbed, reversing the sign of the surface charge once again. Consecutive cycles with alternating adsorption of polyanions and polycations result in step-wise growth of polymer films.[26] The process developed by Decher and his colleagues has greatly increased in popularity since its introduction. This is a result of the method's simplicity and the fact that polyelectrolytes and a variety of other materials can be used to create the nanolayers.[27]

The phenomenon of strong electrostatic attraction between charged surfaces and oppositely charged molecules in solution is understood to be the dominant factor in the adsorption of polyelectrolytes.[22,26,28,29] In theory, the adsorption of molecules possessing more than one equal charge allows for charge reversal on the surface. This behavior implies that (1) equally charged molecules will be repulsed allowing for adsorption self-regulation

and restriction of the deposition to a single layer, and (2) an oppositely charged molecule can be adsorbed in a second step on top of the first one. Both adsorption steps can be repeated cyclically to form multilayer structures on the surface of a substrate.[20]

2.3.2 Characteristics of Layer-by-Layer Deposition

Despite the fact that electrostatic self-assembly has become widely used in recent years, certain details of the process are still not clearly understood. For example, a quantitative evaluation of the assembly process parameters is not available and it is required in order to make the electrostatic self-assembly a practical industrial method. Electrostatic self-assembly is also influenced by a variety of factors that can be difficult to control. Entropy within the polymer chains, charge transfer interactions, hydrogen bonding, and other factors influence the self-assembly process. No single theory has been developed to completely describe the deposition process. However, a variety of studies have been conducted in the past few years that have helped to clarify many aspects of the electrostatic self-assembly method.[27]

Although this technique is based on the electrostatic attraction between positively and negatively charged species, the interaction between these charged species is specific to the nature of the substrate and that of the polyelectrolytes. Polyelectrolyte adsorption is nearly irreversible, so the built-up films do not represent equilibrium structures. This behavior adds to the versatility of the method, but implies that a close kinetic control of the adsorption process is required in order to control film thickness and growth. Electrostatic self-assembly may depend on factors controlling the entropy of the polymer chains, such as molar mass,

flexibility of the chains, ion exchange capacity, hydrophobic interactions, charge transfer interactions, stacking forces, and hydrogen bonding.[26] However, no single theory is available that can provide a complete description of the self-assembly process and deeper understanding of the specificity of ion-ion and ion-substrate interactions remains a challenge.[30]

Another interesting property of the LbL method is the self-healing capability of electrostatic self-assembled nanolayers which provides an increased tolerance to defects. This self-healing ability sets the electrostatic method apart from other self-organization techniques. The electrostatic method can be used on substrates with non-uniform surfaces and compensates for defects caused during the adsorption process. It also allows the use of materials which might not necessarily provide smooth layers. The self-healing process is simply a result of the adsorption of multiple layers. As layers are added, defects are covered up or filled, filling voids in the underlying films.[21,31]

2.3.3 Polyelectrolyte Deposition

Decher's work determined that the use of polyelectrolytes was advantageous when compared to various other small molecules. While good adhesion of a layer to the base substrate requires a particular number of ionic bonds, the overcompensation of the surface charge by the incoming layer was found to be more dependent on the properties of the polymer than on those of the substrate. An additional benefit is that the polyelectrolytes can bridge over underlying defects. The conformation of a given polymer at the surface is then more dependent on the chosen polyelectrolytes and the adsorption conditions and less

sensitive to changes on the surface of the substrate.[20] Numerous studies have shown experimental evidence of a linear increase of film thickness with the number of deposited layers independent of the nature of the initial substrate.[32-35]

Aqueous solutions of polyelectrolytes are commonly preferred for depositing layer-by-layer assemblies. However, organic solvents have proven to be useful as well. The use of polyelectrolytes can be easily adapted to automated systems and is not restricted by the size or shape of the substrates. Polyelectrolytes allow the creation of multiple electrostatic interactions between the polymers and the substrate, improving adhesion to the substrate as well as cohesion between the layers.[27]

Nanolayer polyelectrolyte films are typically deposited using adsorbate concentrations of several milligrams per milliliter. While these concentrations are greater than those needed to reach a plateau in the adsorption isotherm, the excess ensures sure that the solutions do not become depleted during the fabrication of many samples with multiple layers.[20] Washing steps are often used after the adsorption of each layer. The rinsing step is aimed at avoiding contamination of the next adsorption solution as well as to remove weakly adsorbed polymer layers, hence stabilizing the multilayer structure. The adsorption times depend on factors such as the molar mass, concentrations, and agitation of the polyelectrolyte solutions.[36]

A large number of polyelectrolytes have been used to create a variety of nano-structured thin film coatings.[20,37-40] One of the most studied and well understood systems is the poly(allylamine) and poly(styrene sulfonate) system.[32,35,41-44] A number of more complex, functionalized polyelectrolytes have also been used based on their ability to form

structured coatings and their ability to enable secondary chemical modifications. One of the greatest advantages of the layer-by-layer deposition technique is that almost any polyelectrolyte can be used as long as the appropriate oppositely charged partner polyelectrolyte is chosen.[27]

The properties of polyelectrolyte films can be controlled by changing characteristics of the solution such as the pH level. Poly(styrene sulfonate) (PSS) and poly(allylamine hydrochloride) (PAH) are examples of polyelectrolytes that are often deposited at pH values less than 7.0. Recent studies have looked at multilayers composed of weak polyelectrolytes. The charge density of these polyelectrolytes can be controlled by adjusting the pH values of the solutions. Weak polyelectrolytes such as PAH allow for a more precise control over the physical characteristics of the multilayers. Weak polyelectrolytes can be deposited with a high percentage of the chains making loops and tails under pH conditions of incomplete charge. This is in contrast to strong polyelectrolytes which often deposit as molecularly thin layers (about 5 Å). Layer thicknesses greater than 80 Å have been achieved when using weak polyelectrolyte solutions of PAA/PAH.[45] Operational factors such as concentration, adsorption time, ionic strength, temperature, rinsing time, dipping speed, drying time, also affect the thickness of the nanolayers.[21] For a given pair of strongly dissociated polycations and polyanions, the concentration of salt in the deposition solution appears to exert the strongest influence on the thickness of each polymer layer. The thickness of a nanolayer appears to be proportional to the salt concentration.[33]

Natural polyelectrolytes can also be used for layer-by-layer electrostatic self-assembly. Nucleic acids, proteins, and polysaccharides have been used to create multilayer

thin films.[46-48] Studies involving these polyelectrolytes looked at the biological function of films and their ability to simulate biological processes. The main advantage is that the assembly of proteins via layer-by-layer deposition does not require chemical modification and should in theory maintain normal protein behavior.[49,50]

2.3.4 Applications of Layer-by-Layer Films

Polymeric nanolayer films are currently used to modify the surface properties of materials used in electronic products, machinery tools, and medical supplies. These polyelectrolyte based films are capable of self-organization.[20] Self-assembled films can function as barriers with controllable levels of permeability for gases, liquids, covalent molecules, ions, and electrons.[34,51] These properties have been used for the construction of insulators, passivators, sensors, and modified electrodes. Self-assembled nanolayers are also suitable for the construction of devices based on molecular recognition.[24,52,53] Molecules or nanoparticles within a self-assembled layer can be aligned spontaneously, or by changing the temperature, pressure or pH. They can also be aligned by the application of an electric or magnetic field. These characteristics permit the formation of superlattices with the desired architecture and allow the production of a number of photonic, electronic, magnetic, and non-linear optical devices.[52] The layer-by-layer self-assembly of insulators, conductors, and magnetic, ferroelectric and semiconductor films allow the construction of molecularly controlled heterostructures.[54-57]

In addition to the applications and advantages listed above, the self-healing capability of electrostatic self-assembled nanolayers provides an increased tolerance to defects. This

self-healing ability sets the electrostatic method apart from other self-organization techniques. The electrostatic method can be used on substrates with non-uniform surfaces and compensates for defects caused during the adsorption process. It also allows the use of materials which might not necessarily provide smooth layers. The self-healing process is simply a result of the adsorption of multiple layers. As layers are added, defects are covered up or filled.[21,31]

2.3.5 Self-assembled Nanolayers on Textiles

Textile materials have not been used extensively as substrates for the electrostatic self-assembly process due to their high curvature and heterogeneous nature. In order to use LbL deposition on textile materials, it may be necessary to modify the surface of the given substrate to provide an adequate number of surface reaction groups. The cationic nature of cotton can be modified through the use of controlled epoxy-based chemical reactions. It has been previously reported that reacting cotton with 2,3-epoxypropyltrimethylammonium chloride forms cationic charges on the surface of the fibers.[3] This process has been used to modify the surface of cotton fibers for subsequent polyelectrolyte deposition.[44] Plasma treatment is an alternative method for surface preparation of materials.[58,59] Recent research has demonstrated that self-assembled nanolayers of polyelectrolytes can be deposited over cationic cotton fibers. This opens a number of possibilities for a novel fully conformal surface modification technique. The alternating pattern of the N/S cps ratio indicates self-organization and the presence of a layered structure.[44]

2.4 Atomic Layer Deposition

For this research, metal and metal oxide deposition onto fiber and fabric structures using vapor processing will be studied. A specific technique of interest, which has not previously been applied to textile materials, is atomic layer deposition (ALD). The technique of atomic layer deposition can be traced back to the 1970s when Suntola and co-workers developed atomic layer epitaxy, a method for the deposition of amorphous and polycrystalline films.[60-62] Film growth during ALD consists of a repeated binary sequence of self-limiting reactant adsorption and reaction steps. Interest in ALD has rapidly increased in recent years due to the need for highly conformal nano-scale films in the electronics industry and is a possible alternative to other deposition methods such as chemical vapor deposition and plasma vapor deposition.[63]

2.4.1 Atomic Layer Deposition Process

The strategy of atomic layer deposition exploits a set of sequential, self-limiting deposition processes that operate on the principle of alternating saturating surface reactions. During ALD, a specimen is exposed to a precursor vapor that forms a (sub)monolayer of the precursor on the substrate. The precursor molecules react with available surface groups, creating a saturated surface. After excess precursor is removed from the vapor phase by a purge gas (e.g., Ar), the reactant gas is subsequently pulsed onto the substrate, where it reacts with the adsorbed precursor layer to form a layer of the target film-forming material. Since no gas phase reaction occurs, the target film is grown layer-by-layer on the substrate, in which case the thickness of the deposited film can be accurately controlled by the number of

cycles the process is repeated. Because of its unique process characteristics and controllability, ALD can be used to deposit conformal, uniformly thin films with precise thickness and composition control over large scales.[64-67] Atomic layer deposition can create films with thicknesses less than 5 nm, overcoming limitations faced by other deposition techniques.[68]

Atomic layer deposition is chemically versatile and has been used to fabricate layers of metals,[63,69,70] metal oxides,[71] metal nitrides,[63,67] and other materials. An additional benefit of ALD is that the deposition of certain materials such as Al_2O_3,[66,67] TiO2,[72] and TiN[63] can be conducted at relatively low temperatures (<150°C), thereby reducing, if not altogether eliminating, thermal damage to temperature-sensitive substrates such as polymers. Also, selective deposition can be controlled by modifying the surface energy of the deposition rate.[70] ALD has also been used to create nanolaminates of different materials.[73-77]

2.4.2 Characteristics of Atomic Layer Deposition

ALD has several key characteristics. The technique uses gas phase precursors that act as the means for deposition of the films. Self-limiting growth of the films is another unique feature of the ALD process. Deposition by ALD is also characterized by the alternating, sequential exposure of the precursors and the reactants. The ALD process also changes based on the temperature at which the reactions are carried out. This temperature range, which is defined as the "ALD process window", is a key aspect of the growth of films by ALD.[78-80] In an ideal ALD process, a plot of the growth rate versus substrate temperature will show a plateau in which self-limiting ALD behavior occurs.[81] When temperatures are

below this range, the growth rate of the films is generally larger as a result of excess reactant condensation. Insufficient activation energy for chemisorption or reaction can cause decreased growth rate. Dosing of precursors and reactants along with proper purge times are also crucial in obtaining ideal ALD behavior.[82] It is the ability of the ALD process to work at a range of low temperatures that has made it a technique of interest outside of the semiconductor industry.

The self-limitation of the ALD process allows increased conformality of ALD films on various substrates. Due to the fact that surface saturation occurs on all surfaces, conformality can be achieved for very high aspect ratio substrates.[63,83,84] In an ideal ALD process, the thickness of the film would be determined by the self-limiting reaction on the surface. One monolayer would be deposited for each full ALD cycle. However, in reality it is possible that only a fraction of a monolayer may be deposited during each cycle. This behavior can come as a result of steric hindrance of precursor molecules on the substrate, which lead to incomplete saturation.[85] It is therefore possible to control the composition and thickness at the atomic or sub-monolayer level.[63,64]

An important factor in ALD growth is the density of surface adsorption sites since ALD reactions typically occur between gas-phase species and specific reactive sites on the surface of the substrate.[86] Growth initiation depends strongly on the chemical functionalization of the starting surface.[87] Chemically functionalized textiles by plasma treatment, wet chemical treatment, etc., should be suitable substrates for low temperature ALD processes. It is also possible that many textile materials possess sufficient reactive groups on the surface without the need for further modification.

It is the partial reaction of the precursor in each deposition cycle that differentiates ALD from more common chemical vapor deposition (CVD) processes and provides ALD its unique ability for high precision film formation. A common approach to characterize the extent of precursor reaction in ALD processes is measurement of a "saturation curve" which is the film thickness determined as a function of precursor exposure (in Langmuirs) per deposition cycle.

The precursors used in ALD must meet several criteria in order to be effective. Precursors should be sufficiently volatile and thermally stable in order to have efficient transportation into the reactor system. Vapor pressure of precursors is also important. The vapor pressure must be high enough to fill the reaction chamber in order to obtain reasonable cycle times. The precursors must react quickly with both the initial surface groups and the reactant that is used.[63,64]

2.4.3 Low Temperature Atomic Layer Deposition

Many recent studies have focused on low temperature ALD. Low temperature ALD could be considered deposition at temperatures less than 200°C. One commonly researched material is aluminum oxide (Al_2O_3). Aluminum oxide has many desirable traits such as strong adhesion to various surfaces, good dielectric properties, and chemical and thermal stability. All of these properties have led to the use of Al_2O_3 in the semiconductor industry as insulators, protective coatings, and as a high *k* dielectric.[88] Al_2O_3 has been demonstrated on polymer surfaces as well. Groner et al. have shown that Al_2O_3 can be successfully deposited at temperatures as low as 33°C.[66] Of the different processes for creating Al_2O_3

films, the use of trimethylaluminum (TMA) and water is one of the most well understood systems.[89]

Titanium dioxide (TiO_2) thin films are known to have many useful chemical, optical, and electrical properties. These properties have led to the use of TiO_2 films in applications such as anti-reflection optical coatings, high dielectric layers for electronics, coatings for biomaterials, and photosensitive layers. Recent research by Lim and Kim has shown that TiO_2 thin films can be deposited by ALD using tetrakis(dimethylamido) titanium as a precursor and water as a reactant. Deposition was achieved from a range of 120 – 150°C. It was also determined that the reaction was self-limiting. The deposited film had high uniformity and conformality.[90] The characteristics of the process described should be well suited for use with textile substrates. Liu et al. have shown that TiO_2 can be used in nanocomposites by combining TiO_2 nanosized particles and polystyrene molecules. By using the layer-by-layer self-assembly process, ordered structures of polymer/TiO_2 layers were created.[91]

Titanium nitride (TiN) is a material of interest in a variety of devices. Titanium nitride films have low resistivity, high melting points, and good thermal and chemical stability.[92,93] Kim et al. have demonstrated the deposition of TiN films using ALD. The films were deposited using tetrakis(dimethylamido) titanium (TDMAT) as the Ti precursor and NH_3 as the reactant gas. The temperatures ranged from 150 – 250°C during the processing. Films deposited using TDMAT by ALD showed lower carbon content compared to TiN films created by chemical vapor deposition.[94] Several other research groups have also demonstrated that TDMAT and NH_3 are a suitable system for the ALD of TiN.[95-98]

Silver has become an important finishing agent in the textile industry due its natural antimicrobial characteristics, but work to date has focused primarily on impregnation of silver particles into fibers, as discussed in a previous section. Conformal silver coatings developed in this work may have improved antibacterial properties, and may lead to additional applications in fiber systems, including conductivity for electronic and optoelectronic systems. Research conducted by Ritala et al. demonstrated that silver can be deposited by ALD at relatively low temperatures.[99] However, ALD of silver has not been studied in depth due to various difficulties with silver precursors.[100] Chemical vapor deposition, which is a similar vapor phase process for thin film deposition, has also been used to deposit silver films. It may be possible to adapt CVD precursors for ALD of silver.[101-104]

2.4.4 Applications of Atomic Layer Deposition

Atomic layer deposition has been widely adopted for electronic applications over the past ten years, but it has not been widely studied for applications in fiber or textile technologies. It is thought that ALD will provide a viable alternative to other thin film deposition methods in the semiconductor industry such as CVD and PVD. Possible applications of ALD in semiconductor manufacturing are in the production of dynamic random access memory capacitors, interconnect barriers, metal gate electrodes, and high aspect ratio via structures.[71,77]

Atomic layer deposition on polymer surfaces is just beginning to be examined and is a promising area of research. However, new aspects of thin film deposition will need to be

understood in order have a better understanding of ALD on non-traditional substrates. In some cases, the precursors can diffuse into the polymer and react sub-surface, leading to improved barrier and transport processes through the polymer. Better knowledge of the thermodynamics of polymer/precursor mixing, and how the precursor and polymer structure define coating penetration and mixing are key questions.[65,105-107] An improved understanding of mechanisms for ALD on polymer surfaces could enable a wide range of new applications for fiber-based systems, including sensors, actuators, electronic functionality, catalytic capability, etc.

2.5 Equipment and Methods

This work has made use of two particular methods of nano-scale deposition: layer-by-layer deposition and atomic layer deposition. An overview of the equipment used for these deposition techniques is provided below. Numerous analytical tools were employed in an effort to better understand the processes used and to characterize the deposited materials. Each of the analytical methods are discussed in Chapters 3-9. Two types of analysis, X-ray photoelectron spectroscopy (XPS) and transmission electron microscopy (TEM), were used in a majority of the studies presented and are discussed in more detail as part of this literature review.

2.5.1 Deposition Equipment

The manuscripts presented in this dissertation can be divided into two different categories. Chapters 3-5 present work involving the layer-by-layer deposition of polyelectrolytes. One of the advantages of this technique is the lack of complex equipment.

A set of Petri dishes and the necessary chemicals were all that were needed for the LbL deposition of the polyelectrolytes. An established cationization method[108] was used to prepare the cotton fabrics and is described in more detail in Chapter 3. A schematic of the LbL process using PSS and PAH can be seen in Figure 2.1.

Chapter 5 discusses deposition of self-assembled polyelectrolytes on polyester fabrics. In order to prepare the polyester substrates for layer-by-layer deposition, they were treated with helium and oxygen plasma mixtures. A PLASMA-PREEN 1 from Plasmatic Systems, Inc., seen in Figure 2.2, was used to treat the fibers. The operation of the plasma treatment system is discussed in detail in Chapter 5.

Chapters 6-9 present research regarding the modification of textile substrates using atomic layer deposition. A schematic of a typical ALD process can be seen in Figure 2.3. Figure 2.4 shows the ALD system configured for the low temperature deposition of aluminum oxide as discussed in Chapters 6 and 7. A quartz tube is used as the reaction chamber. The temperature within the chamber is regulated using a furnace. The system is pumped to vacuum via a turbo pump backed by a diaphragm pump to a base pressure of approximately $5x10^{-6}$ Torr. During deposition, a hydrocarbon pump is used to pump the system. Samples are loaded into the chamber from one end of the quartz tube which is sealed with an o-ring. The reactor is controlled using a Labview generated program. The exact settings and temperatures used for the experiments discussed in this dissertation are provided in Chapters 6 and 7.

Atomic layer deposition of titanium compounds was carried out in a hot-wall quartz tube reactor shown in Figure 2.5. This system can be evacuated to a base pressure of

approximately $5x10^{-6}$ Torr using a turbo pump backed by a hydrocarbon pump. The system is equipped with a furnace to regulate the reaction temperature. Flow rates are controlled by a needle valve and mass flow controller. A Fomblin pump is used to control the pressure during processing. The timing of the valves and other aspects of the reaction are controlled via a Labview interface. Details regarding the settings and reactants used are provided in Chapters 8 and 9.

2.5.2 X-ray Photoelectron Spectroscopy

X-ray photoelectron spectroscopy is a technique used to analyze the chemical state of a sample's surface. X-ray photoelectron spectroscopy can provide quantitative information regarding the chemical state of a material. All elements can be detected by XPS except for hydrogen and helium. This analytical technique was of particular use for this research because it is a non-destructive technique, allowing samples such as fibers and polymers to be analyzed.[109]

During XPS, a sample is exposed to X-ray photons which results in photoelectron emission from specific energy levels which are characteristic of any elements present in the sample. The kinetic energies of the emitted electrons are measured by an electron spectrometer. This data is used to generate a spectrum with different peaks over a range of kinetic energies. The peaks correspond to specific elements found in the sample surface. Atomic orbitals from atoms of the same element in different chemical environments possess slightly different binding energies. These differences, which are referred to as chemical shifts, are a result of the variations in electrostatic screening experienced by core electrons as

the valence and conduction electrons are drawn towards or away from the specific atom. Differences in oxidation state, molecular environment and co-ordination number all provide different chemical shifts. Photoelectron binding energy shifts are the principal source of chemical information.[110]

All of the XPS measurements discussed were conducted using a Kratos AXIS Ultra spectrometer. This system was equipped with an aluminum source: a spherical mirror analyzer operating in spectrum mode. The pressure in the analysis chamber during measurements was approximately $4x10^{-7}$ Torr. Spectra were collected with the sample stage at 0° while the angle of the electrons was 90° and the angle of incidence of the X-rays was 30°. Specific details regarding scan settings are provided in the following chapters.

2.5.3 Transmission Electron Microscopy

Transmission electron microscopy (TEM) is an imaging technique that places a beam of electrons onto a sample. This causes an enlarged image of the sample to form, which is then magnified and directed to appear on a fluorescent screen. The created image can also be detected by a CCD camera. Electrons have properties of waves and particles. Their wave-like properties cause them to behave like a beam of radiation in certain circumstances. Electron wavelength is defined by the electron energy and can therefore be adjusted by the use of accelerating fields. The wavelength of the electrons can be much smaller than that of light, but can still react with a sample due to their electrical charge. With the use of electrical and magnetic fields, the electrons can be focused onto the sample. This electron beam provides much higher resolution than light microscopes and at the same

time can improve the depth of vision.[111]

One of the most important aspects of TEM is sample preparation. Samples must be prepared so that they are extremely thin, allowing them to be electron transparent. The sample preparation aspects make TEM analysis a somewhat time consuming process. It is also possible that the structure of a sample may be changed during sample preparation.[112]

TEM images were obtained using a Hitachi HF-2000 system. The HF-2000 uses a cold field emission electron source with an accelerating voltage of 200 kV. This type of source creates an electron beam with little energy spread and strong stability, allowing high microscope resolution. The TEM system used was also equipped with an Advanced Microscopy Techniques XR-60B digital camera system for digital imaging. The resolution of the system is .10 nm (lattice) and .23 nm (point to point). The microscope is capable of a maximum magnification value of 1,500,000 X. Three mm diameter samples are used in this device. Detailed procedures for sample preparation and settings used for TEM analysis are presented in the following chapters.

2.6 References

1. Tomasino, C. Chemistry and Technology of Fabric Preparation and Finishing. (North Carolina State University, Raleigh, NC; 1992).

2. Hudson, P.B., Clapp, A.C. & Kness, D. Joseph's Introductory Textile Science, Edn. 6th. (Harcourt Brace Jovanovich College Publishers, New York; 1993).

3. Hauser, P.J. & Schindler, W.D. Chemical finishing of textiles. (Woodhead Publishing Limited, Cambridge, England; 2004).

4. Mahltig, B., Haufe, H. & Bottcher, H. Functionalisation of textiles by inorganic sol-gel coatings. *J. Mater. Chem.* **15**, 4385-4398 (2005).

5. Bajaj, P. Finishing of Textile Materials. *Journal Of Applied Polymer Science* **83**, 631-659 (2002).

6. Black, S., Kapsali, V., Bougourd, J. & Geesin, F. in Textiles for protection. (ed. R.A. Scott) 60-89 (Woodhead Publishing Limited, Cambridge; 2005).

7. Mahltig, B. & Bottcher, H. Modified silica sol coatings for water-repellent textiles. *J. Sol-Gel Sci. Technol.* **27**, 43-52 (2003).

8. Mahltig, B., Bottcher, H., Knittel, D. & Schollmeyer, E. Light fading and wash fastness of dyed nanosol-coated textiles. *Text. Res. J.* **74**, 521-527 (2004).

9. Mahltig, B., Fiedler, D. & Bottcher, H. Antimicrobial sol-gel coatings. *J. Sol-Gel Sci. Technol.* **32**, 219-222 (2004).

10. Cho, D.L., Choi, C.N., Kim, H.J., Kim, A.K. & Go, J.H. Fabrication of deodorizing fabric by grafting of metal phthalocyanine derivative onto nonwoven polypropylene fabric. *Journal Of Applied Polymer Science* **82**, 839-846 (2001).

11. Drew, C. et al. Metal oxide-coated polymer nanofibers. *Nano Lett.* **3**, 143-147 (2003).

12. Lee, C.Y. et al. Conductivity and EMI shielding efficiency of polypyrrole and metal compounds coated on (non) woven fabrics. *Synth. Met.* **119**, 429-430 (2001).

13. Simor, M. et al. Atmospheric-pressure plasma treatment of polyester nonwoven fabrics for electroless plating. *Surf. Coat. Technol.* **172**, 1-6 (2003).

14. Stefecka, M. et al. Electromagnetic shielding efficiency of plasma treated and electroless metal plated polypropylene nonwoven fabrics. *J. Mater. Sci.* **39**, 2215-2217 (2004).

15. Lee, H.J. & Jeong, S.H. Bacteriostasis and skin innoxiousness of nanosize silver colloids on textile fabrics. *Text. Res. J.* **75**, 551-556 (2005).

16. Lee, H.J. & Jeong, S.H. Bacteriostasis of nanosized colloidal silver on polyester nonwovens. *Text. Res. J.* **74**, 442-447 (2004).

17. Jeong, S.H., Hwang, Y.H. & Yi, S.C. Antibacterial properties of padded PP/PE nonwovens incorporating nano-sized silver colloids. *J. Mater. Sci.* **40**, 5413-5418 (2005).

18. Yuranova, T. et al. Antibacterial textiles prepared by RF-plasma and vacuum-UV mediated deposition of silver. *J. Photochem. Photobiol. A-Chem.* **161**, 27-34 (2003).

19. Jiang, S.Q., Newton, E., Yuen, C.W.M. & Kan, C.W. Chemical Silver Plating and Its Application to Textile Fabric Design. *Journal Of Applied Polymer Science* **96**, 919-926 (2005).

20. Decher, G. Fuzzy Nanoassemblies: Toward Layered Polymeric Multicomposites. *Science* **277**, 1232-1237 (1997).

21. Decher, G. in. (eds. G. Decher & J. Schlenoff) 1-46 (Wiley-VCH, 2003).

22. Lvov, Y., Decher, G. & H., M. Assembly, Structural Characterization, and Thermal Behavior of Layer-by-Layer Deposited Ultrathin Films of Poly(vinyl sulfate) and Poly(allylamine). *Langmuir* **9**, 481-486 (1993).

23. Lvov, Y., Haas, H., Decher, G. & Mohwald, H. Assembly of Polyelectrolyte Molecular Films onto Plasma-Treated Glass. *J Phys Chem* **97**, 12835-12841 (1993).

24. Decher, G., Lehr, B., Lowack, K., Lvov, Y. & Schmitt, J. New Nanocomposite Films For Biosensors - Layer-By-Layer Adsorbed Films Of Polyelectrolytes, Proteins Or Dna. *Biosens. Bioelectron.* **9**, 677-684 (1994).

25. Lvov, Y., Ariga, K., Onda, M., Ichinose, I. & Kunitake, T. A Careful Examination of the Adsorption Step in the Alternate Layer-by-Layer Assembly of Linear Polyanion and Polycation. *Coll Surf A* **146**, 337-346 (1999).

26. Hammond, P. Recent Explorations in Electrostatic Multilayer Thin Film Assembly. *Curr Op Coll Inter Sci* **4**, 430-442 (2000).

27. Bertrand, P., Jonas, A., Laschewsky, A. & Legras, R. Ultrathin Polymer Coatings by Complexation of Polyelectrolytes at Interfaces: Suitable Materials, Structure, and Properties. *Macromol Rapid Commun* **21**, 319-348 (2000).

28. Phuvanartnuruks, V. & McCarthy, T. Stepwise Polymer Surface Modification: Chemistry-Layer-by-Layer Deposition. *Macromolecules* **31**, 1906-1914 (1998).

29. Ulman, A. Formation and Structure of Self-Assembled Monolayers. *Chem Rev* **96**, 1533-1554 (1996).

30. Rubner, M.F. pH-controlled fabrication of polyelectrolyte multilayers: assembly and applications. *Multilayer Thin Films*, 133-154 (2003).

31. Kleinfield, E. & Ferguson, G. Healing of Defects in the Stepwise Formation of Polymer/Silicate Multilayer Films. *Chem Mater* **8**, 1575-1578 (1996).

32. Chen, W. & McCarthy, T. Layer-by-Layer Deposition: A Tool for Polymer Surface Modification. *Macromolecules* **30**, 78-86 (1997).

33. Dubas, S. & Schlenoff, J. Factors Controlling the Growth of Polyelectrolyte Multilayers. *Macromolecules* **32**, 8153-8160 (1999).

34. Dubas, S. & Schlenoff, J. Polyelectrolyte Multilayers Containing a Weak Polyacid: Construction and Deconstruction. *Macromolecules* **34**, 3736-3740 (2001).

35. Losche, M., Schmitt, J., Decher, G., Bouwman, W.G. & Kjaer, K. Detailed Structure of Molecularly Thin Polyelectrolyte Multilayer Films on Solid Substrates as Revealed by Neutron Reflectometry. *Macromolecules* **31**, 8893-8906 (1998).

36. Hoogeveen, N.G., Stuart, M.A.C., Fleer, G.J. & Bohmer, M.R. Formation and stability of multilayers of polyelectrolytes. *Langmuir* **12**, 3675-3681 (1996).

37. Onda, M., Lvov, Y., Ariga, K. & Kunitake, T. Sequential actions of glucose oxidase and peroxidase in molecular films assembled by layer-by-layer alternate adsorption. *Biotechnol. Bioeng.* **51**, 163-167 (1996).

38. Onitsuka, O., Fou, A.C., Ferreira, M., Hsieh, B.R. & Rubner, M.F. Enhancement of light emitting diodes based on self-assembled heterostructures of poly(p-phenylene vinylene). *J. Appl. Phys.* **80**, 4067-4071 (1996).

39. Wu, A., Yoo, D., Lee, J.K. & Rubner, M.F. Solid-state light-emitting devices based on the tris-chelated ruthenium(II) complex: 3. High efficiency devices via a layer-by-layer molecular-level blending approach. *J. Am. Chem. Soc.* **121**, 4883-4891 (1999).

40. Wu, A.P., Lee, J. & Rubner, M.F. Light emitting electrochemical devices from sequentially adsorbed multilayers of a polymeric ruthenium (II) complex and various polyanions. *Thin Solid Films* **329**, 663-667 (1998).

41. Arys, X. et al. Ordered polyelectrolyte multilayers. Rules governing layering in organic binary multilayers. *J. Am. Chem. Soc.* **125**, 1859-1865 (2003).

42. Arys, X., Laschewsky, A. & Jonas, A.M. Ordered polyelectrolyte "multilayers". 1. Mechanisms of growth and structure formation: A comparison with classical fuzzy "multilayers". *Macromolecules* **34**, 3318-3330 (2001).

43. Cho, J. & Char, K. Effect of layer integrity of spin self-assembled multilayer films on surface Wettability. *Langmuir* **20**, 4011-4016 (2004).

44. Hyde, K., Hinestroza, J. & Rusa, M. Layer-by-layer deposition of polyelectrolyte nanolayers on natural fibers: cotton. *Nanotechnology* **16**, S422-S428 (2005).

45. Yoo, D., Shiratori, S. & Rubner, M. Controlling Bilayer Composition and Surface Wettability of Sequentially Adsorbed Multilayers of Weak Polyelectrolytes. *Macromolecules* **31**, 4309-4318 (1998).

46. He, J.A., Samuelson, L., Li, L., Kumar, J. & Tripathy, S.K. Photoelectric properties of oriented bacteriorhodopsin/polycation multilayers by electrostatic layer-by-layer assembly. *J. Phys. Chem. B* **102**, 7067-7072 (1998).

47. He, J.A., Samuelson, L., Li, L., Kumar, J. & Tripathy, S.K. Oriented bacteriorhodopsin/polycation multilayers by electrostatic layer-by-layer assembly. *Langmuir* **14**, 1674-1679 (1998).

48. He, J.A., Samuelson, L., Li, L., Kumar, J. & Tripathy, S.K. Bacteriorhodopsin thin film assemblies - Immobilization, properties, and applications. *Adv. Mater.* **11**, 435-+ (1999).

49. Brynda, E., Houska, M., Brandenburg, A., Wikerstal, A. & Skvor, J. The detection of human beta(2)-microglobulin by grating coupler immunosensor with three dimensional antibody networks. *Biosens. Bioelectron.* **14**, 363-368 (1999).

50. Caruso, F., Furlong, D.N., Ariga, K., Ichinose, I. & Kunitake, T. Characterization of polyelectrolyte-protein multilayer films by atomic force microscopy, scanning electron microscopy, and Fourier transform infrared reflection-absorption spectroscopy. *Langmuir* **14**, 4559-4565 (1998).

51. Levasalmi, J. & McCarthy, T.J. Poly(4-methyl-1-pentene)-Supported Polyelectrolyte Multilayer Films: Preparation and Gas Permeability. *Macromolecules* **30**, 1752-1757 (1997).

52. Advincula, R. Supramolecular Strategies Using the Layer-by-Layer Sequential Assembly Technique: Applications for PLED and LC Display Devices and Biosensors. *IEICE Trans Electron* **E83-C**, 1104-1111 (2000).

53. Dermody, D.L., Peez, R.F., Bergbreiter, D.E. & Crooks, R.M. Chemically grafted polymeric filters for chemical sensors: Hyperbranched poly(acrylic acid) films incorporating beta-cyclodextrin receptors and amine-functionalized filter layers. *Langmuir* **15**, 885-890 (1999).

54. Feldheim, D.L., Grabar, K.C., Natan, M.J. & Mallouk, T.E. Electron Transfer in Self-Assembled Inorganic Polyelectrolyte/Metal Nanoparticle Heterostructures. *J. Am. Chem. Soc.*, 7640-7641 (1996).

55. Ferreira, M., Cheung, J.H. & Rubner, M.F. Molecular Self-Assembly Of Conjugated Polyions - A New Process For Fabricating Multilayer Thin-Film Heterostructures. *Thin Solid Films* **244**, 806-809 (1994).

56. Joly, S. et al. Multilayer nanoreactors for metallic and semiconducting particles. *Langmuir* **16**, 1354-1359 (2000).

57. Mendelsohn, J.D. et al. Fabrication of microporous thin films from polyelectrolyte multilayers. *Langmuir* **16**, 5017-5023 (2000).

58. Poletti, G., Orsini, F., Riccardi, C., Raffaele-Addamo, A. & Barni, R. Atomic force microscopy investigation of cold-plasma-treated poly(ethyleneterephthalate) textiles. *Surf Interface Anal* **35**, 410-412 (2003).

59. Riccardi, C. et al. Surface modification of poly(ethylene terephthalate) fibers induced by radio frequency air plasma treatment. *Appl Surf Sci* **211**, 386-397 (2003).

60. Suntola, T. Amorphous Thin-Film Active Elements in Switching Devices. *Thin Solid Films* **34**, 9-16 (1976).

61. Suntola, T. Atomic Layer Epitaxy. *Acta Polytech Sc El*, 242-270 (1989).

62. Suntola, T. & Hyvarinen, J. Atomic Layer Epitaxy. *Annu Rev Mater Sci* **15**, 177-195 (1985).

63. Kim, H. Atomic layer deposition of metal and nitride thin films: Current research efforts and applications for semiconductor device processing. *J Vac Sci Technol B* **21**, 2231-2261 (2003).

64. Gordon, R.G. Review of recent progress in atomic layer deposition (ALD) of materials for micro- and nano-electronics. *Abstracts Of Papers Of The American Chemical Society* **227**, U553-U554 (2004).

65. Ferguson, J.D., Weimer, A.W. & George, S.M. Atomic layer deposition of Al2O3 films on polyethylene particles. *Chemistry Of Materials* **16**, 5602-5609 (2004).

66. Groner, M.D., Fabreguette, F.H., Elam, J.W. & George, S.M. Low-temperature Al_2O_3 atomic layer deposition. *Chemistry of Materials* **16**, 639-645 (2004).

67. Ritala, M. et al. Perfectly conformal TiN and Al_2O_3 films deposited by atomic layer deposition. *Chemical Vapor Deposition* **5**, 7-9 (1999).

68. Sinha, A., Hess, D.W. & Henderson, C.L. Area selective atomic layer, deposition of titanium dioxide: Effect of precursor chemistry. *J Vac Sci Technol B* **24**, 2523-2532 (2006).

69. Park, K.J., Doub, J.M., Gougousi, T. & Parsons, G.N. Microcontact patterning of ruthenium gate electrodes by selective area atomic layer deposition. *Applied Physics Letters* **86** (2005).

70. Park, K.J. & Parsons, G.N. Selective area atomic layer deposition of rhodium and effective work function characterization in capacitor structures. *Applied Physics Letters* **89** (2006).

71. Kim, H. & McIntyre, P.C. Atomic layer deposition of ultrathin metal-oxide films for nano-scale device applications. *Journal Of The Korean Physical Society* **48**, 5-17 (2006).

72. Kemell, M., Pore, V., Ritala, M., Leskela, M. & Linden, M. Atomic layer deposition in nanometer-level replication of cellulosic substances and preparation of photocatalytic TiO2/cellulose composites. *J. Am. Chem. Soc.* **127**, 14178-14179 (2005).

73. Elam, J.W., Sechrist, Z.A. & George, S.M. ZnO/Al2O3 nanolaminates fabricated by atomic layer deposition: growth and surface roughness measurements. *Thin Solid Films* **414**, 43-55 (2002).

74. Kim, Y.S., Kang, J.S., Yun, S.J. & Cho, K.I. Multilayered tantalum-aluminum oxide films grown by atomic layer deposition. *Journal of the Korean Physical Society* **35**, S216-S220 (1999).

75. Kim, Y.S. & Yun, S.J. Nanolaminated Al2O3-TiO2 thin films grown by atomic layer deposition. *J Cryst Growth* **274**, 585-593 (2005).

76. Mitchell, D.R.G. et al. Atomic layer deposition of TiO2 and Al2O3 thin films and nanolaminates. *Smart Mater Struct* **15**, S57-S64 (2006).

77. Ritala, M. & Leskela, M. Atomic layer epitaxy - a valuable tool for nanotechnology? *Nanotechnology* **10**, 19-24 (1999).

78. Kim, J.Y., Kim, Y. & Jeon, H. Characteristics of TiN films deposited by remote plasma-enhanced atomic layer deposition method. *Jpn J Appl Phys 2* **42**, L414-L416 (2003).

79. Kim, J.Y., Seo, S., Kim, D.Y., Jeon, H. & Kim, Y. Remote plasma enhanced atomic layer deposition of TiN thin films using metalorganic precursor. *J Vac Sci Technol A* **22**, 8-12 (2004).

80. Yamada, A. & Konagai, M. Atomic layer deposition of ZnO films and their application to solar cells. *Solid State Phenom* **67-8**, 237-248 (1999).

81. Suntola, T. Surface chemistry of materials deposition at atomic layer level. *Appl Surf Sci* **101**, 391-398 (1996).

82. Ylilammi, M. Mass-Transport in Atomic Layer Deposition Carrier Gas Reactors. *J Electrochem Soc* **142**, 2474-2479 (1995).

83. Aaltonen, T., Alen, P., Ritala, M. & Leskela, M. Ruthenium thin films grown by atomic layer deposition. *Chemical Vapor Deposition* **9**, 45-49 (2003).

84. Kim, H. The application of atomic layer deposition for metallization of 65 nm and beyond. *Surf. Coat. Technol.* **200**, 3104-3111 (2006).

85. Ylilammi, M. Monolayer thickness in atomic layer deposition. *Thin Solid Films* **279**, 124-130 (1996).

86. Gobbert, M.K., Prasad, V. & Cale, T.S. Predictive modeling of atomic layer deposition on the feature scale. *Thin Solid Films* **410**, 129-141 (2002).

87. Aaltonen, T. et al. Atomic layer deposition of noble metals: Exploration of the low limit of the deposition temperature. *J Mater Res* **19**, 3353-3358 (2004).

88. Groner, M.D., Elam, J.W., Fabreguette, F.H. & George, S.M. Electrical characterization of thin Al_2O_3 films grown by atomic layer deposition on silicon and various metal substrates. *Thin Solid Films* **413**, 186-197 (2002).

89. Puurunen, R.L. Surface chemistry of atomic layer deposition: A case study for the trimethylaluminum/water process. *J. Appl. Phys.* **97** (2005).

90. Lim, G.T. & Kim, D.H. Characteristics of TiOx films prepared by chemical vapor deposition using tetrakis-dimethyl-amido-titanium and water. *Thin Solid Films* **498**, 254-258 (2006).

91. Liu, Y.J., Wang, A.B. & Claus, R. Molecular self-assembly of TiO2/polymer nanocomposite films. *J. Phys. Chem. B* **101**, 1385-1388 (1997).

92. Ritala, M., Leskela, M., Rauhala, E. & Jokinen, J. Atomic layer epitaxy growth of TiN thin films from TiI4 and NH3. *J Electrochem Soc* **145**, 2914-2920 (1998).

93. Schulberg, M.T., Allendorf, M.D. & Outka, D.A. Aspects of nitrogen surface chemistry relevant to TIN chemical vapor deposition. *Journal of Vacuum Science & Technology a-Vacuum Surfaces and Films* **14**, 3228-3235 (1996).

94. Kim, J.Y., Choi, G.H., Kim, Y.D., Kim, Y. & Jeon, H. Comparison of TiN films deposited using tetrakisdimethylaminotitanium and tetrakisdiethylaminotitanium by the atomic layer deposition method. *Jpn J Appl Phys 1* **42**, 4245-4248 (2003).

95. Elam, J.W., Schuisky, M., Ferguson, J.D. & George, S.M. Surface chemistry and film growth during TiN atomic layer deposition using TDMAT and NH3. *Thin Solid Films* **436**, 145-156 (2003).

96. Fillot, F. et al. Investigations of titanium nitride as metal gate material, elaborated by metal organic atomic layer deposition using TDMAT and NH3. *Microelectron Eng* **82**, 248-253 (2005).

97. Kim, H.K. et al. Metalorganic atomic layer deposition of TiN thin films using TDMAT and NH3. *Journal of the Korean Physical Society* **41**, 739-744 (2002).

98. Yun, J.H., Choi, E.S., Jang, C.M. & Lee, C.S. Effect of post-treatments on atomic layer deposition of TiN thin films using tetrakis(dimethylamido)titanium and ammonia. *Jpn J Appl Phys 2* **41**, L418-L421 (2002).

99. Ritala, M. in AVS 5th International Conference on Atomic Layer Deposition2005).

100. Aaltonen, T. in Chemistry, Vol. PhD (University of Helsinki, Helsinki, Finland; 2005).

101. Gao, L. et al. Silver metal organic chemical vapor deposition for advanced silver metallization. *Microelectron Eng* **82**, 296-300 (2005).

102. Haase, T. et al. CVD with Tri-(n)butylphosphine silver(I) complexes: Mass spectrometric investigations and depositions. *Chemical Vapor Deposition* **11**, 195-205 (2005).

103. Samoilenkov, S. et al. Low-temperature MOCVD of conducting, micrometer-thick, silver films. *Chemical Vapor Deposition* **8**, 74-78 (2002).

104. Southward, R.E. & Thompson, D.W. Inverse CVD: A novel synthetic approach to metallized polymeric films. *Adv. Mater.* **11**, 1043-1047 (1999).

105. Carcia, P.F., McLean, R.S., Reilly, M.H., Groner, M.D. & George, S.M. Ca test of Al2O3 gas diffusion barriers grown by atomic layer deposition on polymers. *Applied Physics Letters* **89**, - (2006).

106. Groner, M.D., George, S.M., McLean, R.S. & Carcia, P.F. Gas diffusion barriers on polymers using Al2O3 atomic layer deposition. *Applied Physics Letters* **88**, - (2006).

107. Wilson, C.A., Grubbs, R.K. & George, S.M. Nucleation and growth during Al2O3 atomic layer deposition on polymers. *Chemistry of Materials* **17**, 5625-5634 (2005).

108. Hauser, P.J. & Tabba, A.R. Improving the environmental and economic aspects of cotton dyeing using a cationised cotton. *Coloration Technology*, 282-288 (2001).

109. Barr, T.L. Modern ESCA: The Principles and Practice of X-ray Photoelectron Spectroscopy. (CRC Press, Inc., Boca Raton, FL; 1994).

110. Nefedov, V.I. X-ray Photoelectron Spectroscopy of Solid Surfaces. (VSP, Utrecht, The Netherlands; 1988).

111. Horiuchi, S. Fundamentals of High-resolution Transmission Electron Microscopy. (North-Holland, New York; 1994).

112. Dykstra, M.J. & Reuss, L.E. Biological Electron Microscopy: Theory, Techniques, and Troubleshooting, Edn. 2nd. (Kluwer Academic/Plenum Publishers, New York; 2003).

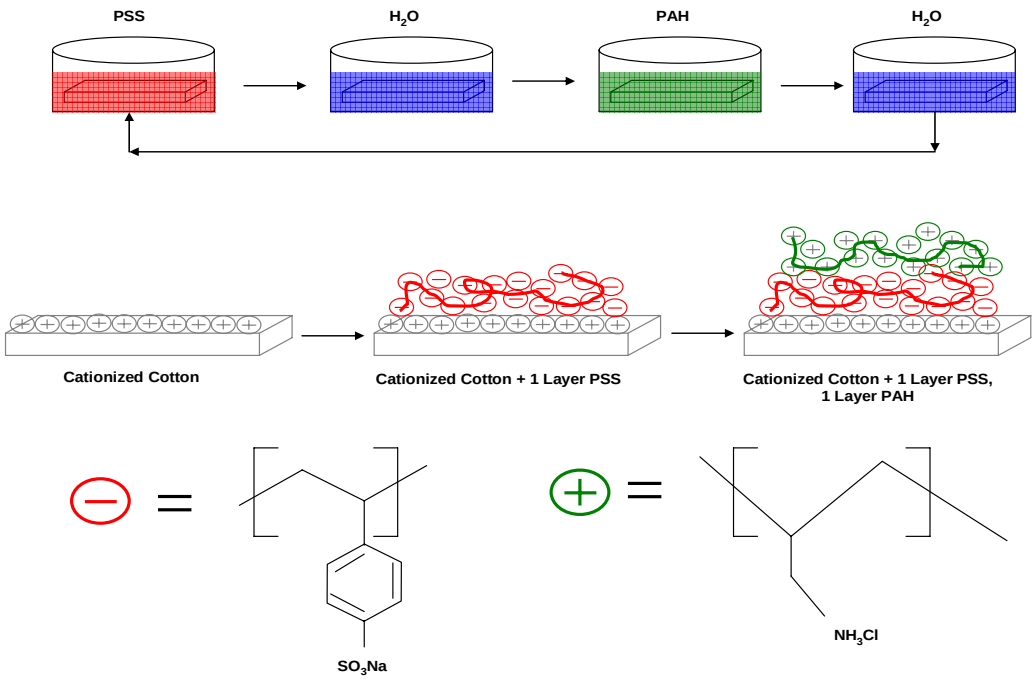

Figure 2.1. Schematic of the layer-by-layer deposition process using the poly(allylamine) and poly(styrene sulfonate) system. First, the cotton undergoes a cationic surface treatment. The polyelectrolytes are then alternately deposited onto the surface of the fabric. Water rinses separate the polyelectrolyte deposition steps to remove loosely adhered molecules.

Figure 2.2. Exterior view of Plasmatic Systems, Inc. PLASMA-PREEN 1 (top) used for modification of polyester fabrics. The bottom picture provides an interior view of the reaction chamber.

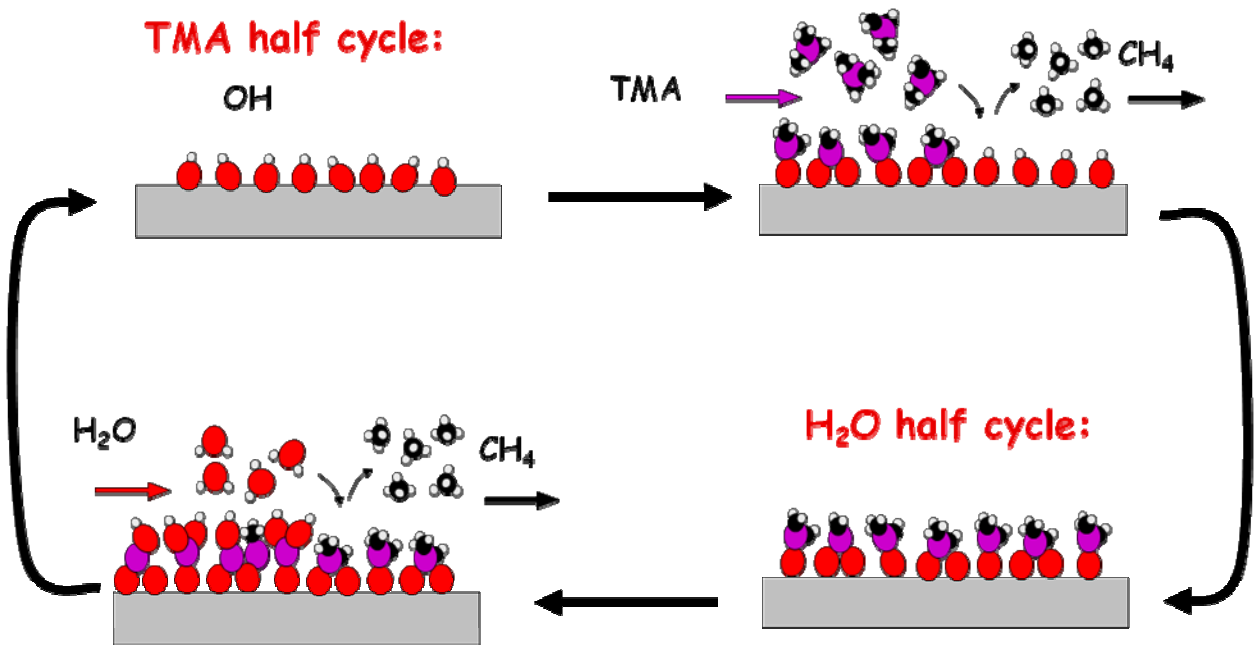

Figure 2.3. Schematic of atomic layer deposition process for aluminum oxide using trimethylaluminum and water as precursor and reactant.

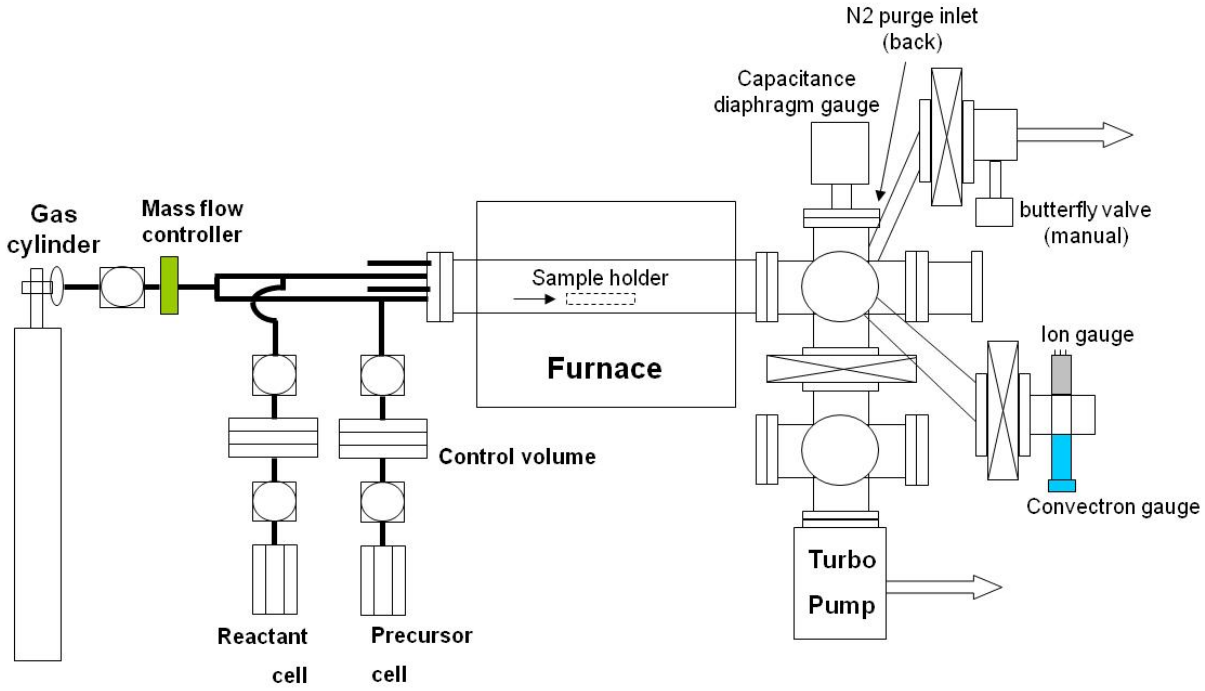

Figure 2.4. Schematic of viscous flow reactor used for deposition of aluminum oxide.

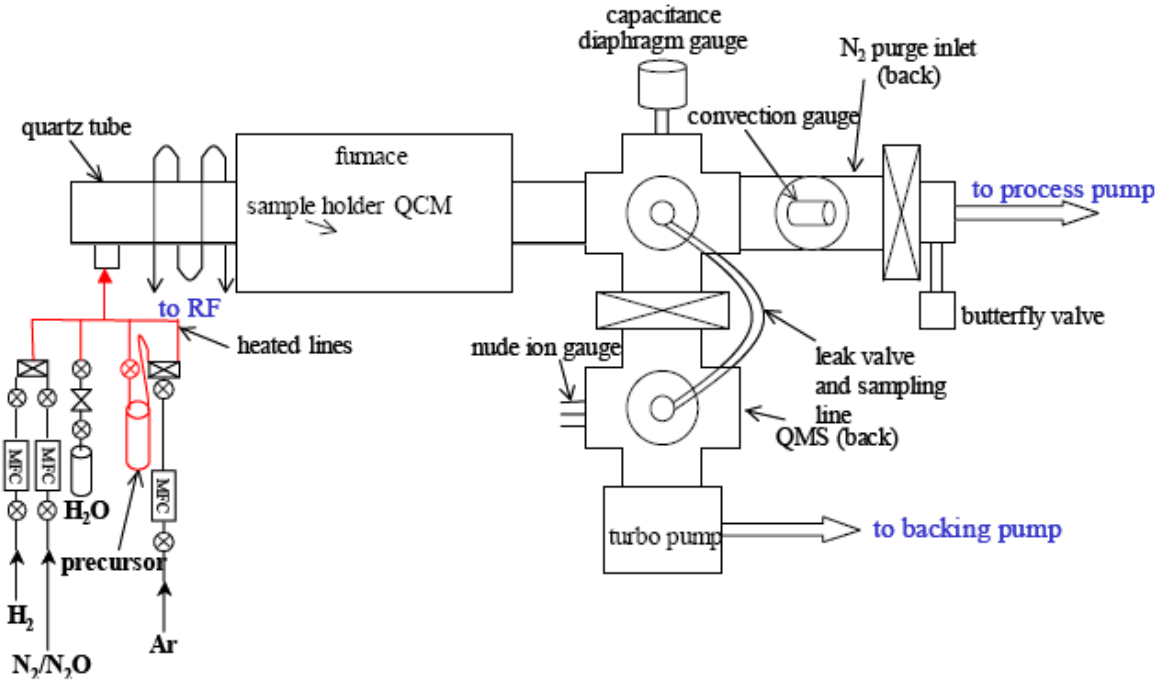

Figure 2.5. Schematic of viscous flow reactor used for deposition of titanium compounds.

Chapter 3 is a reprint of a paper that will appear in Cellulose

Effect of Surface Cationization on the Conformal Deposition of Polyelectrolytes over Cotton Fibers

G. Kevin Hyde[1], Hong Dong[2], and Juan P. Hinestroza[2*]

[1]*Department of Textile Engineering, Chemistry, and Science, North Carolina State University, Raleigh, NC 27695*

[2]*Department of Fiber Science and Apparel Design, Cornell University, Ithaca, NY 14850*

Abstract

The effect of surface cationization on the conformal deposition of alternating nanolayers of poly(sodium styrene sulfonate) (PSS) and poly(allylamine hydrochloride) (PAH) over cotton fibers is reported. Three different levels of cotton cationization were evaluated. Variations in the cationization degree were achieved by manipulating the ratio of 3-chloro-2-hydroxy propyl trimethyl ammonium to NaOH. Experimental results obtained via Carbon-Hydrogen-Nitrogen-Sulfur (CHNS) elemental analysis and X-ray Photoelectron Spectroscopy (XPS) indicated that the deposition process was not significantly influenced by the degree of cotton cationization. The build up of further polyelectrolyte layers was found to be less sensitive to variations in the cationic character of the substrates once a critical number of alternating layers was deposited.

Specific Contribution

For this article, I deposited layers of polyelectrolytes onto cotton fabrics using the LbL deposition method. I began by talking with Dr. Hinestroza to determine the experimental procedure and which cationization mixtures we would analyze. I then treated the cotton fabrics via the cationization procedure discussed in the manuscript. After the fabrics were treated, I cut the cotton fabric into pieces for subsequent deposition of the polyelectrolytes. I then mixed the polyelectrolyte solution and carried out the deposition experiments. After all of the samples were prepared, I analyzed the nanolayer structures using XPS, TEM, and CHNS. I prepared the samples required for the different analysis methods. I was responsible for the data analysis. Once the data had been gathered, I began writing the manuscript. Hong Dong helped with analysis of the CHNS data and the relation of the CHNS results to the other forms of analysis. The paper was submitted to Cellulose by Dr. Hinestroza and after review I revised the manuscript based on the referee's suggestions. Of particular interest for this study was the effect of the initial cationization procedure on the subsequent deposition of the polyelectrolytes. This work demonstrates the importance of initial surface preparation before the LbL process begins. This study showed that after the initial layers are deposited, LbL growth of polyelectrolytes is not substrate dependent.

Chapter 3: Effect of Surface Cationization on the Conformal Deposition of Polyelectrolytes over Cotton Fibers

3.1 Introduction

Layer-by-layer deposition (LbL) is a widely used technique able to create multilayer thin films on the surfaces of a myriad of materials.[1-4] However, the LbL deposition process has not been extensively implemented in textile and natural fibers as they pose unique challenges including the chemical heterogeneity of their surfaces as well as their irregular shapes.

During the LbL deposition process a charged substrate is alternatively immersed in solutions of materials having opposite polarity. The surface charge reversal occurring with each adsorption step leads to the conformation of polyion layers and sometimes layer interpenetration.[5] Numerous factors do determine the composition of the multilayer films and the characteristics of the individual layers. For example, the thickness of a layer appears to be dependent on both the charge density of the underlying surface and the deposition conditions.[6-11] Electrostatic self-assembly processes are also influenced by a variety of factors that can be difficult to control such as polymer entropy, charge transfer interactions, and hydrogen bonding.[12] Therefore, optimization of the LbL deposition process will require judicious selection of proper stabilizers and careful control of the deposition kinetics.[13,14]

Despite the fact that electrostatic self-assembly has become widely used certain details of the process are still not fully understood. Quantitative evaluation of the assembly process will be necessary before making electrostatic self-assembly a practical and scalable

manufacturing method. As of today, no single theory has been developed to completely describe the deposition process. However, a variety of fundamental studies have been conducted helping to clarify many aspects of the electrostatic self-assembly method.[15-19]

Several surface modification techniques, chemical and physical, can be used to alter the surface charge on a substrate. Chemical modification techniques can include surface patterning, photobleaching, plasma treatments or epoxy substitution reactions. For example, recent work by Hauser et al. introduced a chemical process aimed at improving cotton's affinity for anionic dyes by creating cationic charges on the cotton's surface via epoxy substitution. Anionic dyes are of interest to the fiber industry as they improve color fastness in cotton goods while reducing dyeing times, energy consumption, and the use of water.[20] Methods of physical modification comprised of Langmuir-Blodgett films or the use of layers of highly charged polyelectrolytes as primers for the further deposition of multilayers.

It is well documented that the strength of the charge on the surface of the substrate is critical to the LbL process. For example, Fou and Rubner evaluated this effect using microscopic glass slides coated with hydrophilic, hydrophobic, negatively charged, and positively charged surfaces as substrates for LbL. The surface charge of the substrates was found to qualitatively influence the layers' thickness and uniformity.[21] In contrast, the characteristics of the substrate have been found to have a marginal effect on the adsorption of the individual layers as several experimental studies have shown evidence of a linear increase of film thickness with the number of deposited layers independent of the nature of the initial substrate.[6-11, 22-23] Almost all of these studies have been performed on synthetic planar

surfaces with limited interest in curved heterogeneous substrates such as those of natural fibers.

Successful deposition of nanolayers onto natural fibers and textiles via LbL can open an avenue to increase their surface functionality without making major changes to the weight, bulkiness, or comfort of the material. LbL is especially suitable for potential use on natural fibers due to its self-healing capability providing an increased tolerance to defects.[2,12] In a previous publication, we reported a proof-of-concept experiment aimed at establishing the feasibility of depositing polyelectrolyte nanolayers over cotton.[23] In this contribution, we performed a statistically robust design of experiments to assess the effect of cationization on the structure and thickness of the nanolayers.

3.2 Experimental

3.2.1 Materials

Standardized TIC-400 woven cotton fabrics were obtained from Textile Innovators, Inc. (Windsor, NC). Poly (sodium 4-styrene sulfonate) (PSS), Mw 70000, and poly (allylamine hydrochloride) (PAH), Mw 70000, were purchased from Aldrich (St. Louis, MO) and used as received. Aqueous solutions of the polyelectrolytes were made using deionized water at concentrations of 5 mM. Previous reports have shown that this particular polyelectrolyte system is capable of forming self-organized films on a number of different synthetic substrates.[24-28]

3.2.2 Substrate Preparation

Cationic cotton was prepared by using 2,3-epoxypropyltrimethylammonium chloride to insert a cationic group on the cotton's surface.[20] The cationization mechanism is described in Figure 3.1. 2,3-epoxypropyltrimethylammonium chloride (EP3MAC) was prepared in aqueous solution by reacting 3-chloro-2-hydroxy propyl trimethyl ammonium chloride (CHP3MAC) with alkali solutions (50% NaOH in water). EP3MAC reacts with the hydroxyl groups of cellulose creating cationic charges on the surface of the sample. 3-chloro-2-hydroxypropyltrimethylammonium chloride was obtained from The Dow Chemical Company (Freeport, TX) and NaOH crystals were purchased from Sigma Aldrich (St. Louis, MO).

The 3-chloro-2-hydroxypropyltrimethylammonium chloride was pad applied to the cotton specimens at 100% wet pick-up. The samples were dried during 24 hours at ambient conditions (25°C and 70% RH). The specimens were cut into one inch squares and random samples were dyed using anionic dyes to obtain initial qualitative evidence that the process had placed cationic charges on the surface of the fabric. Three different formulations containing different NaOH: CHP3MAC ratios were evaluated as illustrated in Table 3.1.

3.2.3 Polyelectrolyte Layer Deposition

Petri dishes of 2 inches in diameter and one inch depth were used for the deposition of the polyelectrolytes. The dishes were filled up to 90% in order completely immerse the samples. All samples were initially rinsed in water and then placed in PSS solutions dish for five minutes. The specimen was then transferred to a dish containing deionized water. The

sample was allowed to rinse for five minutes and then moved to a dish containing PAH solution. After five minutes, the sample was transferred to a dish containing deionized water to be rinsed again for five minutes. The process was continued until a total of twenty polyelectrolyte layers had been deposited on the cotton substrates. Samples were dried at room temperature for a period of 24 hours.

3.2.4 X-ray Photoelectron Spectroscopy (XPS) Measurements

XPS measurements were conducted using a Kratos AXIS Ultra spectrometer with an Al source and a spherical mirror analyzer working in spectrum mode. The total pressure in the main vacuum chamber during analysis was typically 4 x 10-7 Torr. Spectra were collected with the stage containing the samples at 0°. The take-off angle of the electrons was 90° and the angle of the incident X-rays was 30°. The chemical elements present on the samples were identified from the survey spectra. The survey scans started at 1200 eV and ended at -5 eV taking 1 eV steps with a dwell time of 200 ms. High resolution scans were performed around peaks of interest.

3.2.5 Carbon Hydrogen Nitrogen Sulfur (CHNS) Elemental Analysis

CHNS measurements were performed using a Leco TruSpec CHN analyzer. The TruSpec was equipped with a Sulfur Add-On Module which provided sulfur analysis. Sample size for the CHNS analysis was approximately 100 mg. Tin foil cups were used to hold the samples during measurement. The samples were combusted at 950°C with an afterburner value of 850°C for the CHN measurements. For S analysis, the samples were combusted at 1350°C.

3.2.6 Transmission Electron Microscopy (TEM)

TEM images were obtained using a Hitachi HF-2000 system using a cold field emission electron source with an accelerating voltage of 200 kV. This type of source creates an electron beam that minimizes the energy spread and exhibits strong stability allowing high microscope resolution. The TEM system was equipped with an Advanced Microscopy Techniques XR-60B camera system for digital imaging. Cotton specimens were prepared by pulling individual fibers from the top of the fabric swatches using tweezers. Loctite® super glue gel was used to attach one ends of the fiber to copper 200 mesh grids. A second grid was placed on top of the grids supporting the sample in order to create a grid sandwich.

3.3 Results and Discussion

3.3.1 XPS Measurements

Figure 3.2 illustrates survey spectra for a sample of woven cationic cotton and for a cotton specimen supporting 20 alternating layers of PSS and PAH. As expected, large and well defined peaks for carbon and oxygen can be found in both samples at 281.91 eV and 528.91 eV respectively. Presence of Nitrogen (N 1s) can be noted via a peak at 398.91 eV. A zoom in of the 380 to 420 eV region (left inset in Figure 3.2) illustrates that a small amount of nitrogen is present in the cationic cotton sample. While raw cotton does not contain Nitrogen, the small amount detected is the result of the cationization process as illustrated in Figure 3.1. A larger and more defined peak is noted for the sample coated with the 20 layers corresponding to the presence of PAH nanolayers. The presence of Sulfur in the samples can be noted by tracing the peaks at 164.91 eV and 228.91 eV which correspond

to Sulfur's 2s and 2p electrons. No Sulfur is present in the cationic cotton sample (right inset in Figure 3.2). Further control experiments were performed on raw cotton substrates dipped in PSS and PAH solutions under similar conditions than the cationic specimens. The counts for Sulfur and Nitrogen in the X-ray Photoelectron Spectroscopy survey spectra for these control specimens were found to be below the detection limit of the instrument.

3.3.2 Statistical Analysis

Due to the high surface heterogeneity of the cotton substrates, a statistical analysis was implemented in order to validate the robustness of the cationization process and the ability of the modified substrates to support polyelectrolyte nanolayers. Three different formulations were evaluated using 20 different cotton specimens plus one control. These mole ratios were chosen as they have been previously reported to influence the performance of anionic dyes.[20] Each set of substrates was coated with up to 20 alternating layers of PSS and PAH. XPS survey spectra were obtained for all samples and the N/O and S/O ratios were used to perform a statistical analysis (Anova and F-test). The results of these validation experiments can be observed on Table 3.2 and Figure 3.3.

An ANOVA (Analysis of variance) tests the difference between the means of two or more groups of data. As shown in Table 3.2, ANOVA analysis of the XPS data for each of the three cationization procedures indicates that no significant statistical difference exists regarding their influence on the N/O and S/O ratio measurements. An F-test of the data indicates that the F value for each one of the ratios is smaller than the F-critical for a 95% confidence level.

While the same cotton cationization procedures presented in Table 3.1 have been shown to influence the color and light fastness of some anionic dyes,[20] they do not appear to influence the electrostatic self-assembly deposition of PSS and PAH. This behavior indicates that the deposition process is robust and that LbL can self-adapt to heterogeneous surfaces. However, it is important to note that the large number of anionic/cationic groups present in PSS and PAH contrast with the limited number of charged groups available in dyes allowing a better anchoring of the polyelectrolytes to the charged surface.

As shown in Figure 3.3, each of the cationization procedures appears to provide adequate number of cationic sites for the deposition of the first layer of the anionic PSS polyelectrolyte. As expected, after the critical first layers are deposited the growth of the multilayer structure becomes a function of the polyelectrolyte that is directly underneath and it appears to be no longer influenced by the surface characteristics of the substrate. It has been previously reported that LbL formed multilayer films may have a disordered and intermeshed structure without clear distinction between individual layers preventing a precise determination of their individual thickness.[28-31] A plot of the N/S ratio provides an insight on the degree of interpenetration among the deposited layers. Since the S signal can be associated with the presence of PSS and the N signal corresponds mostly to the presence of PAH, monitoring the evolution of the N/S ratio as a function of the number of deposited layers provide an indication of the level of intercalation or disorder of the resulting structure as shown in Figure 3.4.

Figure 3.4 illustrates that the N/S ratio exhibits large variations during the deposition of the first layers. However, after a critical number of layers from 15 to 16 are deposited, the

N/S ratio levels off exhibiting minor fluctuations. This value indicates that the outermost layers may be not be longer be influenced by the nature of the cotton substrate but by their interactions with the previously deposited polyelectrolyte nanolayer. This behavior is corroborated by comparing the N/S values obtained for the cotton samples with those previously reported in the literature for the same PSS/PAH system. Table 3.3 shows the N/S values for the PSS/PAH pair deposited over several substrates including synthetic polymeric, metals and inorganic materials.

3.3.3 CHNS Analysis

Samples from batch B were selected to perform CHNS elemental analysis. Figure 3.5 shows the evolution of the concentration of Nitrogen and Sulfur on the cotton substrates as a function of the number of deposited layers of PSS and PAH. While the XPS analysis provides an indication of the concentration of certain elements on the surface of the substrates, CHNS measurements are an indication of the concentration of the elements in the whole specimen. As expected, both the concentration of Nitrogen and the concentration of Sulfur exhibited a monotonical increase as a function of the number of deposited layers. The rate of increase in concentration could be estimated from the slope of the trend line. The experimental data in Figure 3.5 indicates that the rate of increase for Sulfur (79 ± 8 ppm per layer) is higher than that for Nitrogen (24 ± 3 ppm per layer). Once these values in ppm per layer are converted to moles/layer they are within agreement with the quantities reported in the XPS measurements. This behavior could be predicted as both the PSS and PAH selected for used in this study were of similar molecular weight.

3.3.4 TEM Imaging

XPS and CHNS analysis do provide indirect evidence of the LbL deposition process and the intercalated nature of the multilayer films over the cotton fibers. TEM was used in order to obtain direct evidence of the presence of the nanolayers. Obtaining useful information via TEM for cotton samples proved to be challenging due to the instability of the cotton fibers inside the TEM vacuum chamber, the thickness of the cotton fibers (10-20 microns) and their high curvature radius.

The specimens from batch A were selected for TEM imaging. The images were obtained without the use of an embedding resin, as described in the experimental section, in order to provide a better insight on the thickness of the multilayered film. Due to the large thickness of the cotton fiber, TEM imaging was only possible on the outermost section of the fibers. Figure 3.6 shows a cross-sectional TEM image of a cotton fiber supporting a 20 layer polyelectrolyte structure. Details of the lumen structure of cotton can be identified as well as a conformal coating. The thickness of the multilayer film is estimated to be between 300 and 400 nm. From this observation and the XPS results it can be estimated that each layer could measure approximately 15-20 nm which is agreement with previously reported data for the PSS/PAH system.[29]

3.4 Conclusions

The use of the LbL method to deposit polyelectrolytes over cotton fibers is reported. The deposition was possible by creating positive charges on the surface of the cotton fibers. Treatment of cotton with 3-chloro-2-hydroxy propyl trimethyl ammonium chloride was

proven to be an effective procedure to create a positively charged substrate able to support multilayer thin films. Three different formulations varying the molar ratio of NaOH to 3-chloro-2-hydroxy propyl trimethyl ammonium chloride CHP3MAC were tested. The three different formulations were found to produce statistically similar results illustrating the robustness of the cationization method. The deposition of the polyelectrolytes was monitored using XPS and CHNS elemental analysis. The values for the N/S ratio on the outermost deposited layers was found to be in quantitative agreement with previously reported data for the PSS/PAH system on several synthetic substrates. These results indicate the feasibility of using the LbL method to modify the surface properties of natural fibers. However, further studies are required to address issues regarding the potential integrity of the nanolayers when exposed to expected conditions of use such as washing and rubbing. Potential applications of this method include the development of active protective clothing and multifunctional textiles.

3.5 Acknowledgements

This research work has been supported through a research grant from The Institute of Textile Technology.

3.6 References

1. Decher, G., Fuzzy Nanoassemblies: Toward Layered Polymeric Multicomposites. *Science* **277**, 1232-1237 (1997).

2. Wagberg, L., Forsberg, S., Johansson, A., and Juntti, P. Engineering of fibre surface properties by application of the polyelectrolyte multilayer concept. Part I. Modification of paper strength. *Journal of Pulp and Paper Science* **22**, 222-228 (2002).

3. Lvov, Y., F. Essler, and G. Decher, Combination of Polycation/Polyanion Self-Assembly and Langmuir-Blodgett Transfer for the Construction of Superlattice Films. *J Phys Chem* **97**, 13773-13777 (1993).

4. Lvov, Y., et al., Assembly of Polyelectrolyte Molecular Films onto Plasma-Treated Glass. *J Phys Chem* **97**, 12835-12841 (1993).

5. Decher, G., Polyelectrolyte Multilayers, an Overview, G. Decher and J. Schlenoff, Editors. 2003, Wiley-VCH. p. 1-46.

6. Chen, W. and T. McCarthy, Layer-by-Layer Deposition: A Tool for Polymer Surface Modification. *Macromolecules* **30**, 78-86 (1997).

7. Cooper, T.M., A.L. Campbell, and R.L. Crane, Formation Of Polypeptide-Dye Multilayers By An Electrostatic Self-Assembly Technique. *Langmuir* **11**, 2713-2718 (1995).

8. Dubas, S. and J. Schlenoff, Factors Controlling the Growth of Polyelectrolyte Multilayers. *Macromolecules* **32**, 8153-8160 (1999).

9. Hoogeveen, N.G., et al., Formation and stability of multilayers of polyelectrolytes. *Langmuir* **12**, 3675-3681 (1996).

10. Losche, M., et al., Detailed Structure of Molecularly Thin Polyelectrolyte Multilayer Films on Solid Substrates as Revealed by Neutron Reflectometry. *Macromolecules* **31**, 8893-8906 (1998).

11. Schmitt, J., et al., Internal Structure of Layer-by-Layer Adsorbed Polyelectrolyte Films: A Neutron and X-ray Reflectivity Study. *Macromolecules* **26**, 7058-7063 (1993).

12. Bertrand, P., et al., Ultrathin Polymer Coatings by Complexation of Polyelectrolytes at Interfaces: Suitable Materials, Structure, and Properties. *Macromol Rapid Commun* **21**, 319-348 (2000).

13. Caruso, F., et al., Ultrathin Multilayer Polyelectrolyte Films on Gold: Construction and Thickness Determination. *Langmuir* **13**, 3422-3426 (1997).

14. Yoo, D., S. Shiratori, and M. Rubner, Controlling Bilayer Composition and Surface Wettability of Sequentially Adsorbed Multilayers of Weak Polyelectrolytes. *Macromolecules* **31**, 4309-4318 (1998).

15. Lvov, Y., et al., A Careful Examination of the Adsorption Step in the Alternate Layer-by-Layer Assembly of Linear Polyanion and Polycation. *Coll Surf A* **146**, 337-346 (1999).

16. Delcorte, A., et al., ToF-SIMS Study of Alternate Polyelectrolyte Thin Films: Chemical Surface Characterization and Molecular Secondary Ions Sampling Depth. *Surface Science* **366**, 149-165 (1996).

17. Fogden, A. and B.W. Ninham, Electrostatics of Curved Fluid Membranes: The Interplay of Direct Interactions and Fluctuations in Charged Lamellar Phases. *Adv Coll Int Sci* **83**, 85-110 (1999).

18. Hammond, P., Recent Explorations in Electrostatic Multilayer Thin Film Assembly. *Curr Op Coll Inter Sci* **4**, 430-442 (2000).

19. Ninham, B.W., K. Kurihara, and O.I. Vinogradova, Hydrophobicity, Specific Ion Adsorption and Reactivity. *Coll Surf A* **123-124**, 7-12 (1997).

20. Hauser, P.J. and A.R. Tabba, Improving the environmental and economic aspects of cotton dyeing using a cationised cotton. *Coloration Technology* **117**, 282-288 (2001).

21. Fou, A.C. and M. Rubner, Molecular-Level Processing of Conjugated Polymers. 2. Layer-by-Layer Manipulation of In-Situ Polymerized p - m e Doped Conducting Polymers. *Macromolecules* **28**, 7115-7120 (1995).

22. Sano, M., Y. Lvov, and T. Kunitake, Formation of Ultrathin Polymer Layers on Solid Substrates by Means of Polymerization-induced Epitaxy and Alternate Adsorption. *Ann Rev Mat Sci* **26**, 153-187 (1996).

23. Hyde, K., J. Hinestroza, and M. Rusa, Layer-by-layer deposition of polyelectrolyte nanolayers on natural fibers: cotton. *Nanotechnology* **16**, S422-S428 (2005).

24. Kleinfield, E. and G. Ferguson, Healing of Defects in the Stepwise Formation of Polymer/Silicate Multilayer Films. *Chem Mater* **8**, 1575-1578 (1996).

25. Lvov, Y., et al., Thin Film Nanofabrication via Layer-by-Layer Adsorption of Tubule Halloysite, Spherical Silica, Proteins, and Polycations. *Coll Surf A* **198-200**, 375-382 (2002).

26. Arys, X., et al., Ordered polyelectrolyte multilayers. Rules governing layering in organic binary multilayers. *Journal Of The American Chemical Society* **125**, 1859-1865 (2003).

27. Arys, X., A. Laschewsky, and A.M. Jonas, Ordered polyelectrolyte "multilayers". 1. Mechanisms of growth and structure formation: A comparison with classical fuzzy "multilayers". *Macromolecules* **34**, 3318-3330 (2001).

28. Cho, J. and K. Char, Effect of layer integrity of spin self-assembled multilayer films on surface Wettability. *Langmuir* **20**, 4011-4016 (2004).

29. Delcorte, A., et al., Adsorption of polyelectrolyte multilayers on polymer surfaces. *Langmuir* **13**, 5125-5136 (1997).

30. Phuvanartnuruks, V. and T. McCarthy, Stepwise Polymer Surface Modification: Chemistry-Layer-by-Layer Deposition. *Macromolecules* **31**, 1906-1914 (1998).

31. Zheng Z.G e t al. Layer-by-layer nanocoating of lignocellulose fibers for enhanced paper properties. *J. Nanoscience and Nanotechnology* **3**, 624-632 (2006).

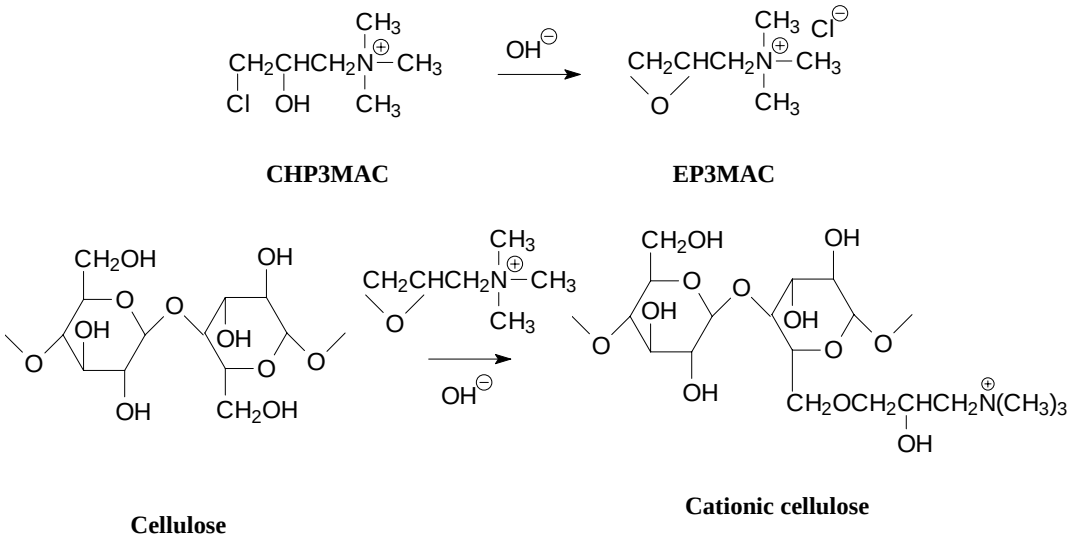

Figure 3.1. Reaction of 3-chloro-2-hydroxypropyltrimethylammonium chloride (CHP3MAC) with alkali to form 2,3-epoxy propyl trimethyl ammonium chloride (EP3MAC) (B) Reaction of (EP3MAC) and the hydroxyl groups in cellulose creating cationic cotton.[20]

Table 3.1. Cationization formulations evaluated.

Formulation	**A**	**B**	**C**
NaOH: 3-chloro-2-hydroxypropyltrimethylammonium chloride	1.2	1.55	1.9
Volume of deionized water [ml]	200	200	200
Mass of 3-chloro-2-hydroxypropyltrimethylammonium chloride [g]	100	100	100
Mass of NaOH [g]	35.2	45.5	55.8

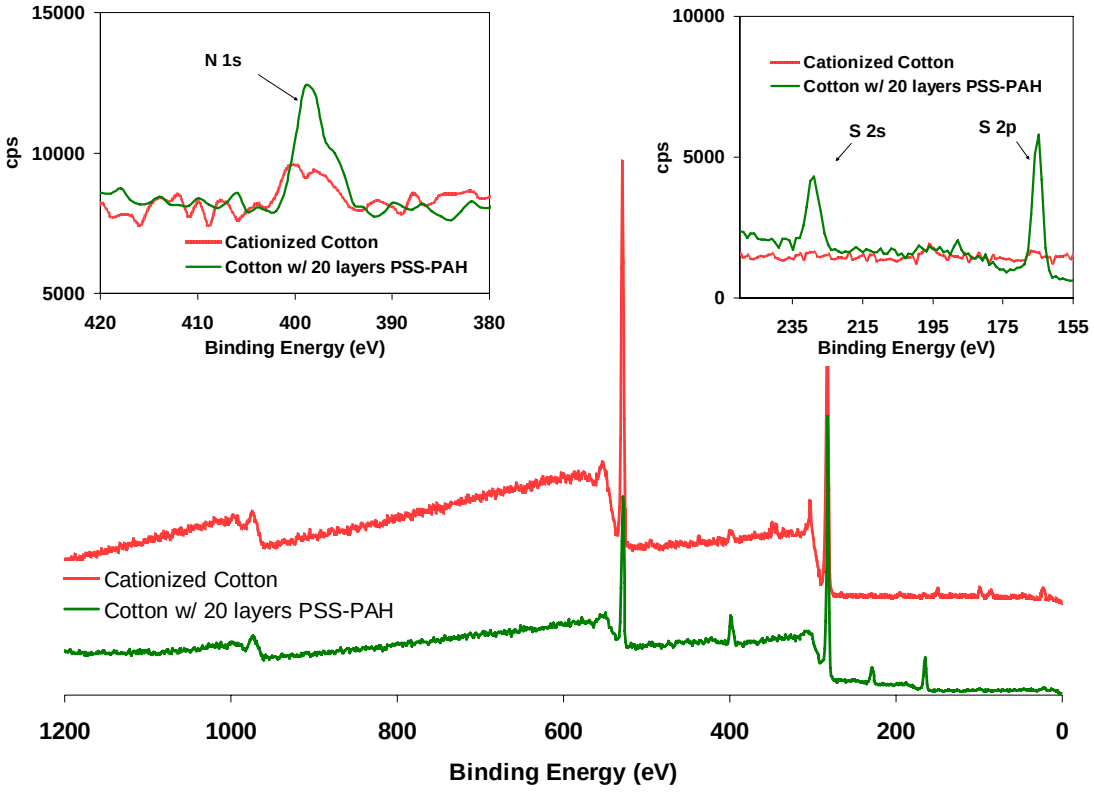

Figure 3.2. XPS spectra for a sample of cationic cotton and one specimen supporting a 20 layer assembly of PSS/PAH. Insets illustrate specific regions were N 1s, S 2s and S 2p counts per second (CPS) were detected.

Table 3.2. Analysis of Variance and F-test for three cotton cationization formulations (mole ratio of NaOH to 3-chloro-2-hydroxy propyl trimethyl ammonium chloride). A= 1.2:1.0 , B=1.55:1.0, C=1.9:1.0

	Formulation	Samples	Sum	Average	Variance	Standard Error
N/O	A	21	2.2531	0.1073	0.0013	0.0077
	B	21	2.4267	0.1156	0.0014	0.0081
	C	21	2.3294	0.1109	0.0019	0.0096
S/O	A	21	2.1608	0.1029	0.0014	0.0081
	B	21	2.2750	0.1083	0.0016	0.0086
	C	21	2.2828	0.1087	0.0030	0.0119

	Source of Variation	Sum of Squares	Degrees of Freedom	F	P-Value	F Critical
N/O	Between Groups	0.0007	2	**0.2380**	0.7890	**3.1504**
	Within Groups	0.0909	60			
	Total	0.0917	62			
S/O	Between Groups	0.0004	2	**0.1124**	0.8939	**3.1504**
	Within Groups	0.1186	60			
	Total	0.1190	62			

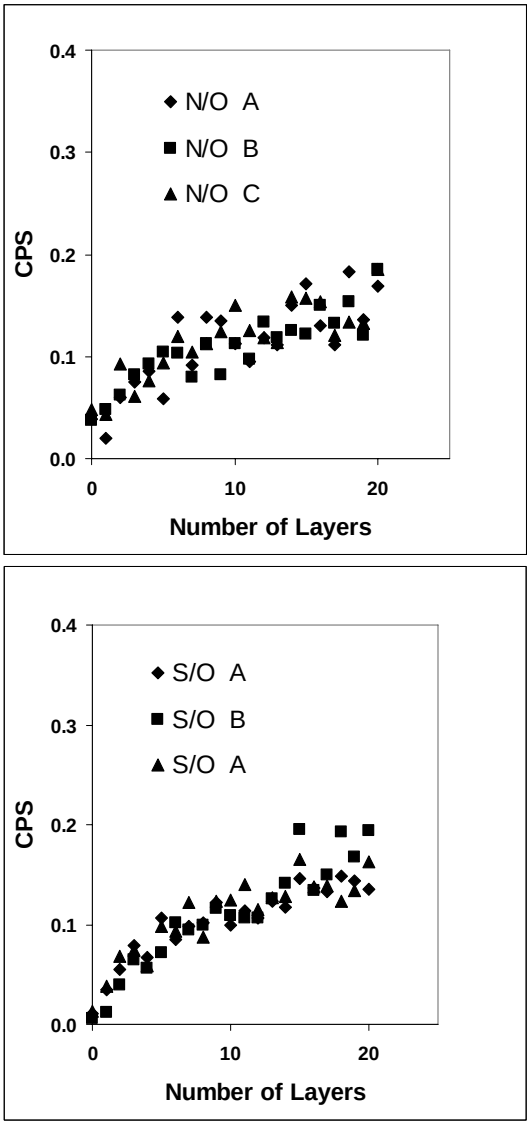

Figure 3.3. N/O and S/O cps (from XPS survey spectra) ratios as a function of the number of deposited nanolayers for three different cationization formulations (Molar ratio of NaOH: 3-chloro -2-hydroxy propyl trimethyl ammonium chloride CHP3MAC). A= 1.2:1.0 , B=1.55:1.0, C=1.9:1.0

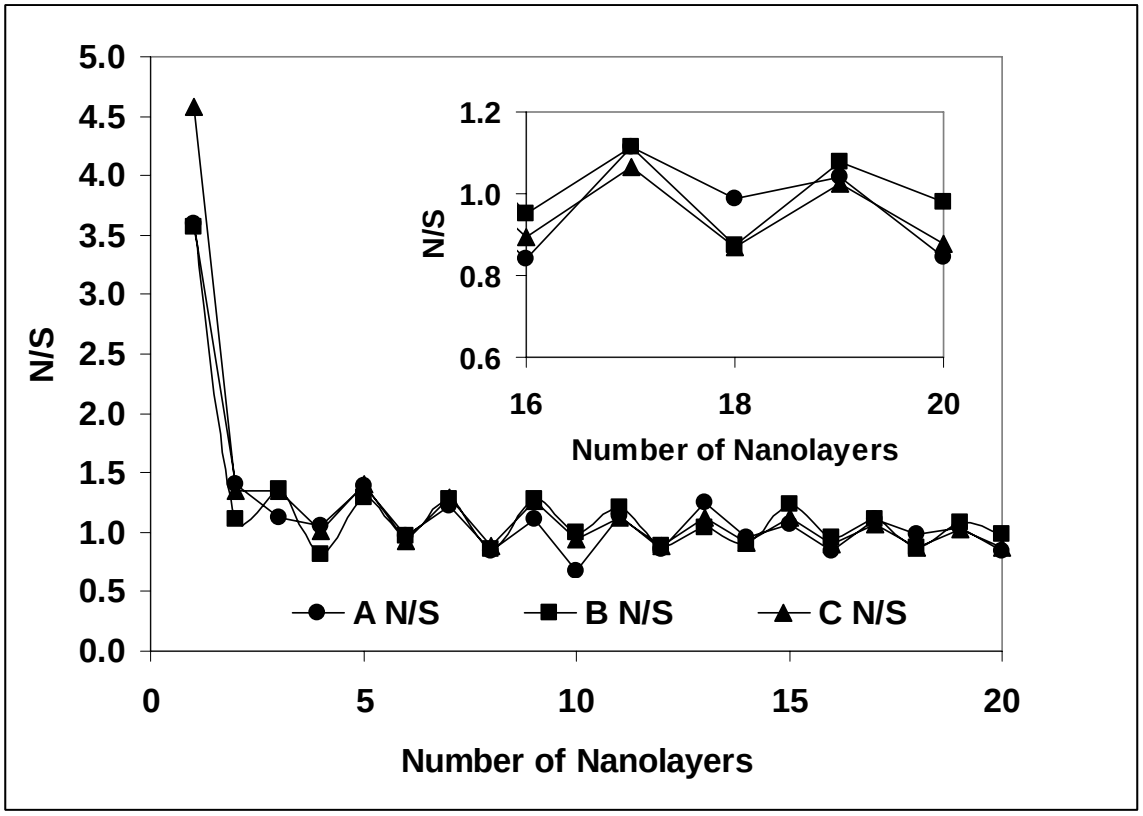

Figure 3.4. Evolution of the N/S ratio (N 1s and S 2p from the XPS spectra) as a function of the number of deposited nanolayers.

Table 3.3. Comparison of N/S ratio for the deposition of PSS/PAH polyelectrolytes on different substrates using the LbL method.[29]

Substrate	N/S ratio
Cotton	1.1
Poly (etherimide)	1.4
Poly (phenylene oxide)	1.2
Poly (ethylene terephthalate)	1.6
Poly (methyl methacrylate)	1.3
Poly (styrene)	1.3
Silicon	1.4
Gold	1.1

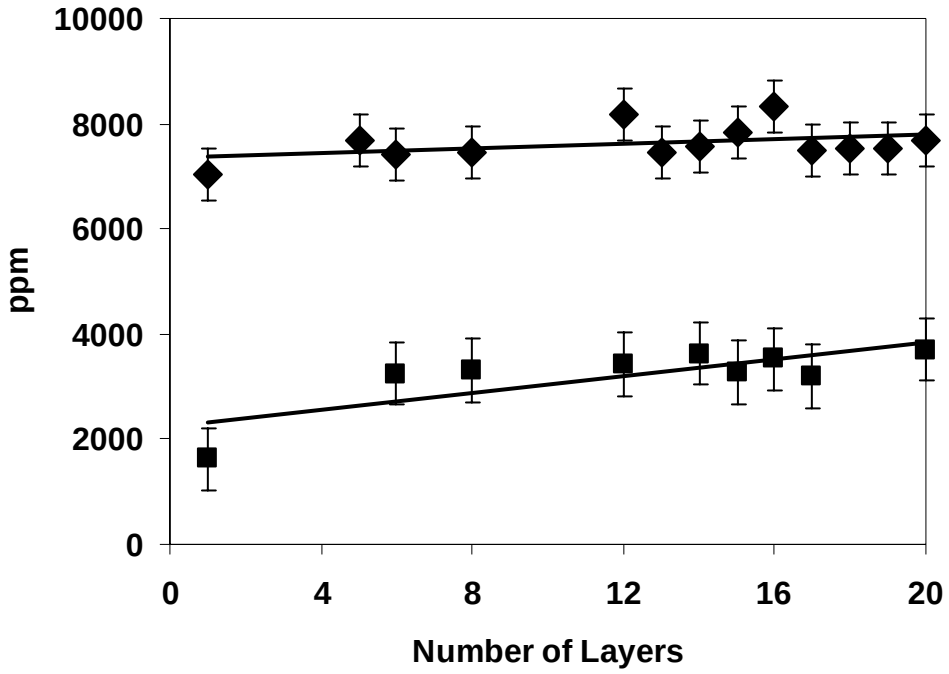

Figure 3.5. Concentration of N (♦) and S (□) as a function of the number of deposited nanolayers obtained from the CHNS analysis.

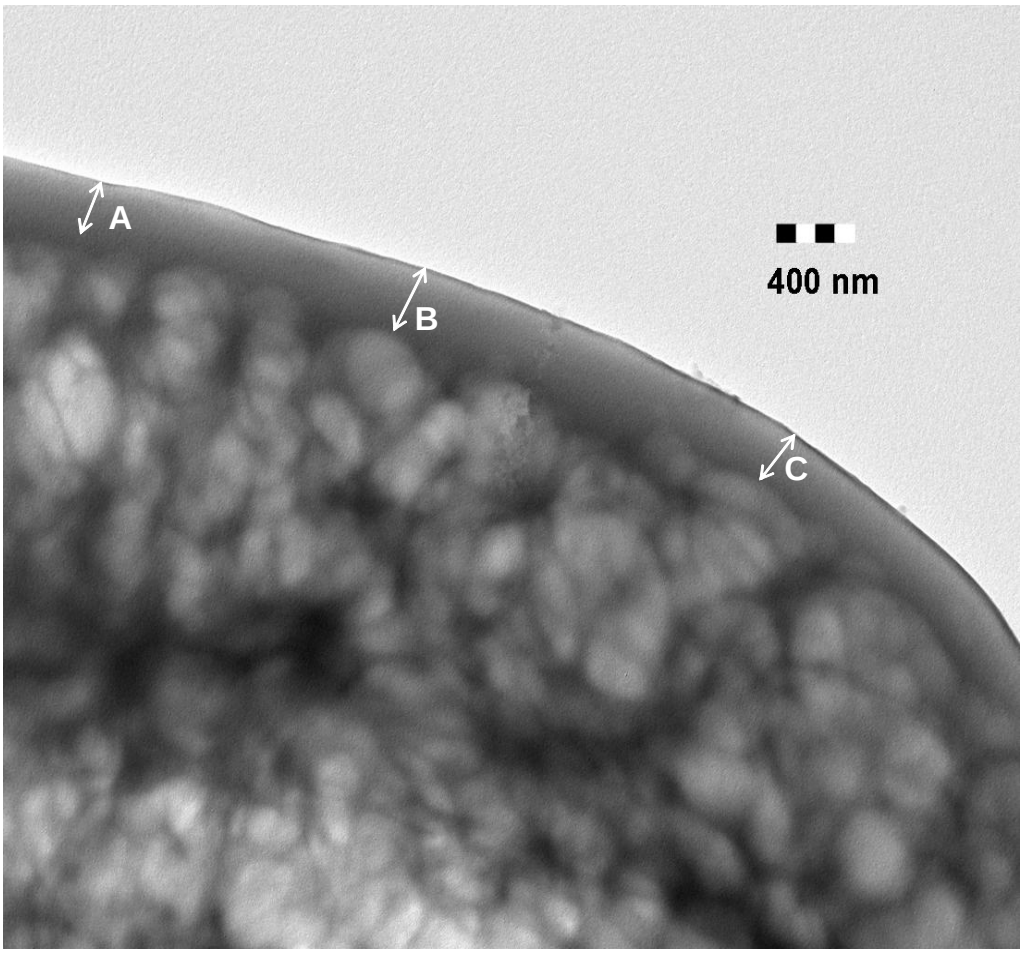

Figure 3.6. TEM Image of a cotton fiber coated with 20 alternating layers of PSS and PAH (batch A). Details of the lumen in the cotton fiber can be identified as well as a conformal coating with varied thickness (A= 365 nm, B= 395 nm and C= 313 nm).

Chapter 4 is a reprint of a paper that will be submitted to Textile Research Journal

Characterization of Nanolayers on Natural Fibers with Electrostatic Force Microscopy

Haoho Huang[1], G. Kevin Hyde[2], and Juan P. Hinestroza[1*]

[1]*Department of Fiber Science and Apparel Design, Cornell University, Ithaca, NY 14850*

[2]*Department of Textile Engineering, Chemistry, and Science, North Carolina State University, Raleigh, NC 27695*

Abstract

Polycations and polyanions were electrostatically deposited over the surface of chemically treated natural fibers to generate layer-by-layer self assembly nano-structures. Such kinds of polyelectrolyte nanolayers can improve a wide variety of the properties of natural fibers. Some surface characterization methods, such as XPS and SEM, have verified the presence of the polyelectrolyte nanolayers, but they could not provide information regarding depth direction. The atomic force microscope (AFM) is ideally suited for characterizing nanolayers in depth direction over the surface of natural fibers. Using electrostatic force microscope, the deposited polyelectrolyte nanolayer in the cross-section of the cotton and wool fibers can be visualized and verified. It was found that a high bias voltage can increase the phase difference in EFM phase images of the fibers deposited with polyelectrolyte multilayers.

Specific Contribution

For this article, I was responsible for preparing the samples where I deposited layers of polyelectrolytes onto cotton and wool fabrics using the LbL deposition method. I began by talking with Dr. Hinestroza to determine the experimental procedure and which cationization mixtures we would analyze. I then treated the fabrics via the cationization procedure discussed in the previous chapter. After the fabrics were treated, I cut the cotton and wool fabric into pieces for subsequent deposition of the polyelectrolytes. I then mixed the polyelectrolyte solution and carried out the deposition experiments. After I finished preparing the samples, they were sent to Dr. Hinestroza's group for EFM analysis. I then helped to write the background of the paper and to analyze the data. I have also helped with the revisions to the current version of the manuscript. This work helped to demonstrate the use of electrostatic force microscopy as a method for analysis of nano-scale modifications.

Chapter 4: Characterization of Nanolayers on Natural Fibers with Electrostatic Force Microscopy

4.1 Introduction

The layer-by-layer (LbL) self assembly technique has been successfully developed since it was first introduced.[1] The technique involves the sequential deposition of oppositely charged polyelectrolytes. A substrate with a charged surface is immersed in a polyelectrolyte solution to adsorb polyelectrolytes on its surface. Then the substrate is rinsed with water to desorb weakly adsorbed polyelectrolytes. The oppositely charged polyelectrolyte is adsorbed on the surface subsequently. The adsorption and washing process is repeated until the desired number of polyelectrolyte layers is reached.

The long range electrostatic interaction between oppositely charged polyelectrolytes plays an important role in the formation of the ordered self-assembly structure. When the polyelectrolyte is adsorbed on a substrate with the opposite charge, the adsorbed polyelectrolyte will overcharge the surface. This charge reversal ensures the consequent adsorption of polyanions and polycations. The short range interactions, such as hydrophobic and van der Waals interactions, may also contribute to the formation of the LbL self assembly.[2] The small molecular weight salts have specific effects on the formation and erosion of multilayers of weak polyelectrolytes.[3]

Recently, LbL assembly has been widely utilized in many fields, such as surface modification and functionalization, capsule preparation, and colloidal stabilization. Layer-by-layer capsules for medical use have been prepared via the LbL technique.[4] In addition, this alternating sequential adsorption approach has been used to deposit not only polymer

molecules to the substrate but also inorganic particles with a size of nanometers up to micrometers. Muller et al.[5] prepared nanocomposite polyelectrolyte/gold fibers via LbL assembly by immersing the poly(allylamine hydrochloride)/poly(styrenesulfonate) coated electrospun fibers into a dispersion of 4-(dimethylamino)pyridine-stabilized gold nanoparticles. Using the LbL approach, Pu et al.[6] prepared polyethylenimine, poly(acrylic acid) and Au nanotubes on the template of sodium sulfate nanowires.

The popularity of the LbL technique is due to its accessibility to generate tailored polymer multilayers with a layer-by-layer delicate self-assembly structure. The thickness of each polymer layer can also be precisely controlled by tuning the polymer concentration, the adsorption time, salt concentration, and the charge densities of the substrate and polymer. The desired number of the layers is easily obtained by increasing the immersion steps. The thickness of the multilayer can range from several nanometers to several micrometers.[1]

Molecular dynamics simulation[7] was carried out to model the formation process of multilayer assembly around charged spherical particles. The simulation shows that the multilayer was only found at a nonequilibrium state. Using a self-consistent field theory, Wang[8] mimicked the deposition and washing of polyanions and polycations in an equilibrium process. This calculation reveals that individual layers electrostatically deposited above the first four layers can be distinguished.

Since the polyelectrolytes possess charges, it was expected to detect the polyelectrolyte multilayer using an electrostatic force microscope (EFM). EFM is based on the two-pass technique. In the first pass, the topography of the sample surface was measured. During the second pass, a voltage is applied between the conductive cantilever and the

sample. Scanning during the second pass is carried out at a constant height *h* above the sample surface in accordance with the profile recorded during the first scan. The phase change due to the tip-sample electrostatic force provides the information of the charge distribution on the surface. Therefore, the electrostatic force microscope can verify the nanolayers as a supplemental method to other techniques, such as FTIR and XPS. Electrostatic force microscopy can provide quantitative information and have a resolution up to nanometers. In addition, electrostatic force microscopy provides vivid visualization and a direct measure of the thickness of the polyelectrolyte multilayer. It was already verified that the polyelectrolytes were well deposited on the surface of the natural fibers using XPS and TEM.[9] XPS measures the element distributions on the surface of fiber and TEM detects the 2D nanolayers in the cross-section of the fiber.

The goal of the present paper is to characterize the polyelectrolyte layers deposited on natural fibers using electrostatic force microscopy (EFM). Wool and cotton fiber were selected since they are the typical examples of natural fibers composed of proteins and cellulose, respectively. The overall thickness of the polyelectrolyte layers should be proportional to the number of the nanolayers deposited. For this reason, the samples deposited with various thicknesses of the nanolayers were scanned. The effect of the bias voltage Ψ applied in EFM scanning on the image quality was also investigated.

4.2 Experimental

4.2.1 Self-assembly Process

The nanolayers on the surfaces of the wool or cotton fibers were generated with the layer-by-layer deposition approach. Woven wool or cotton fabric was first immersed into polyanion solution to adsorb polyanion on its surface and then rinsed with deionized water. After that, the fabric was moved into polycation solution to adsorb polycations. The process was repeated until the desired number of nanolayers was reached. Samples with various numbers of polyelectrolyte layers were prepared for scanning.

4.2.2 Electrostatic Force Microscopy

A single thread made of wool or cotton fibers was taken from the fabrics and embedded in epoxy resin. The embedded sample was then sectioned with an ultra-microtome using a diamond knife to obtain the smooth cross-section of the thread (fibers) for AFM scanning. Trimmed epoxy block with fibers embedded was glued to the metal AFM disk for scanning. NT-MDT NTEGRA Prima AFM was used for electrostatic force microscopy. The EFM cantilever (Micromasch NSC14/Ti-Pt) was coated with Ti-Pt conductive layer. The curvature radius of the cantilever tip is smaller than 40nm. The topography of the cross-section of the fiber was first obtained with tapping mode in the first pass. In the second pass, the EFM phase image was obtained at various bias voltages applied to the cantilever and the sample. Basic image processing, including plane subtracting and line fitting, was performed.

4.3 Results and Discussion

4.3.1 EFM on Cotton Fibers

Cotton fibers are the most extensively used natural fibers. The main component of cotton fibers is cellulose. The cotton fibers were chemically treated to obtain a strong surface charge for the subsequent LbL deposition process. In the LbL deposition process, both polyanion and polycation were adsorbed on the surface. Consequently, both negative and positive charges are present in the multilayer. During the EFM scanning, these charges will induce the phase deviation into the cantilever oscillation due to the electrostatic interactions. As a result, the polyelectrolyte multilayer will be found in the EFM phase images.

Figure 4.1 illustrates the effect of bias voltage on the phase contrast in the EFM images of the cotton fibers with 5 nanolayers. In these images, one can see the polyelectrolyte nanolayers at the interface between the fiber and the epoxy. Compared to the cotton fiber and the epoxy resin, the polyelectrolyte nanolayers are relatively bright in the images and the cotton fiber was partially coated with polyelectrolyte nanolayers. Diffusion restriction of polyelectrolyte into the fabric and the partiality of the surface modification may lead to the partiality of the covering of the polyelectrolyte on the fiber surface.

It was shown in the images that the phase contrast is larger at high voltages than that at low voltages. At zero volts, there is no phase change in the scanning area and the image is almost uniform. At high voltages, the capacitive effect between the cantilever and the sample is larger. However, at low voltages, all interactions, including the electrostatic one, between the sample and the cantilever above the sample are weak. As a result, the phase contrast is small at low voltages.

The EFM phase profiles corresponding to Figure 4.1 for a cross section of the cotton fiber with 5 nanolayers at various bias voltages are shown in Figure 4.2. There is a significant phase change at the boundary of the fiber. It clearly indicates the presence of a charged multilayer on its surface. The phase difference between the polyelectrolyte nanolayers and the cotton fiber is the largest for scanning at the voltage of -9V and +9V. However, for low voltages, even the phase difference between the cotton fiber and the epoxy disappears and the phase profile is almost a straight line.

The effect of the separation between the cantilever and the sample surface on the phase contrast is shown in Figure 4.3. As the separation increases, both the van der Waals and electrostatic interactions between them become weaker. As expected, the contrast in EFM phase images becomes small with increasing separation. At a separation of 1 micrometer, the cotton fiber cannot be distinguished from the epoxy background. The result indicates that the reasonable separation between the sample and the tip in EFM scanning should be below 50 nm for the samples of natural fibers deposited with polyelectrolyte nanolayers.

The EFM phase images for cotton fibers deposited with various numbers of nanolayers are presented in Figure 4.4. As the number of nanolayers increase, the thickness of the multilayer increases. Some studies suggested a relatively small amount of polyelectrolyte is adsorbed during the formation of the first layers. For subsequent adsorptions, the overall thickness of the multilayer becomes proportional to the number of the adsorption layers. However, in the present study, it was shown the first layers were not thinner than the subsequent layers.

4.3.2 EFM on Wool Fibers

The wool fibers were selected as an example because it is a common fiber made of proteins. The wool fiber consists of spindle-shaped cortical cells surrounded by cuticle cells.[10] The successful adsorption of polyelectrolyte on the wool fibers requires a chemical treatment to charge the fiber surface.

Figure 4.5 illustrates the effect of bias voltage on the phase contrast in the EFM images of the wool fibers with 5 nanolayers. Wool fiber is located on the left side. One can see the polyelectrolyte nanolayers on the fiber surface. The polyelectrolyte layers are very bright at both negative and positive voltages because two kinds of polyelectrolyte, i.e. polycations and polyanions, were deposited onto the surface of fibers. For comparison, the topographic image, Figure 4.6, is also given. In the topographic image, the fiber does not have such a bright, sharp and narrow boundary as that shown in EFM phase images. It verifies that the boundary on the fiber surface shown in EFM phase images is due to the electrostatic interaction between the cantilever and the polyelectrolyte nanolayers.

Figure 4.7 shows the dependence of the EFM phase contrast upon the bias voltage for wool fiber deposited with 20 nanolayers. Similar to the sample of wool fibers with 5 nanolayers, the wool fiber with 20 nanolayers was found to also have a very bright boundary outside of the cuticle scale of the wool fiber, except the thickness of the multilayer. The phase contrast is larger for high absolute values of voltage. Moreover, the images at negative voltages are a little clearer than those at positive voltage of the same absolute values. The same rule is applicable to the sample of wool fiber without polyelectrolyte nanolayers deposited shown in Figure 4.8. It was further verified that the negative high voltage (e.g. -

9V) is the most suitable for the characterization of such samples. The multilayer is very clear in the images at large magnification (Figure 4.9, 5.8×5.8μm2).

In the topographic images of the wool fibers embedded in the epoxy presented in Figure 4.10, one can see the clear structure of cortical cells and cuticle cells, which is in agreement with that reported in literature.[10]

Figure 4.11 shows the relation between the number of the nanolayers and the overall thickness of the polyelectrolyte multilayer. The overall thickness of the polyelectrolyte layers increase by increasing the number of nanolayers deposited.

4.4 Conclusions

In the present paper, the polyelectrolyte nanolayers deposited on natural fibers with the layer-by-layer self-assembly technique were characterized with electrostatic force microscopy. The EFM phase images show that the high voltages can increase the phase contrast for both cotton and wool fibers. The thickness of the polyelectrolyte layers increases as the number of the layers deposited increases. It was verified that the negative high voltages are the most suitable for the characterization of the nanolayers deposited on the natural fibers.

4.5 Acknowledgements

This research work has been supported through a research grant from The Institute of Textile Technology and the NCSU Faculty Research and Development Fund.

4.6 References

1. Decher, G., Fuzzy Nanoassemblies: Toward Layered Polymeric Multicomposites. *Science* **277**, 1232-1237 (1997).

2. Kotov, N.A. Layer-by-layer self-assembly: The contribution of hydrophobic interactions. *Nanostruct Mater* **12**, 789-796 (1999).

3. Kovacevic, D., vad der Burgh, S., de Keizer, A. & Stuart, M.A.C. Specific ionic effects on weak polyelectrolyte multilayer formation. *J Phys Chem B* **107**, 7998-8002 (2003).

4. Johnston, A.P.R., Zelikin, A.N., Lee, L. & Caruso, F. Approaches to quantifying and visualizing polyelectrolyte multilayer film formation on particles. *Anal Chem* **78**, 5913-5919 (2006).

5. Muller, K. et al. Polyelectrolyte functionalization of electrospun fibers. *Chem Mater* **18**, 2397-2403 (2006).

6. Pu, Y.C. et al. Water-dissolvable sodium sulfate nanowires as a versatile template for the fabrication of polyelectrolyte and metal-based nanotubes. *J Am Chem Soc* **128**, 11606-11611 (2006).

7. Panchagnula, V., Jeon, J. & Dobrynin, A. V. Molecular dynamics simulations of electrostatic layer-by-layer self-assembly. *Phys Rev Lett* **93**, - (2004).

8. Wang, Q.D., Luo, G.X., Wang, H.P., Hou, C.Y. & Jin, J. Electrostatic interaction between two planar double layers: A further extension to Langmuir's method. *J Disper Sci Tech* **27**, 341-347 (2006).

9. Hyde, K., J. Hinestroza, and M. Rusa, Layer-by-layer deposition of polyelectrolyte nanolayers on natural fibers: cotton. *Nanotechnology* **16**, S422-S428 (2005).

10. Titcombe, L.A., Huson, M.G. & Turner, P.S. Imaging the internal cellular structure of Merino wool fibres using atomic force microscopy. *Micron* **28**, 69-71 (1997).

Figure 4.1. EFM phase images for cotton fiber with 5 nanolayers at various bias voltages. *h*=50nm. a) -9V; b)-6V; c) -3V; d). -1V; e). 0; f). +1V; g) +3V; h). +6V; i).+9V.

(a)

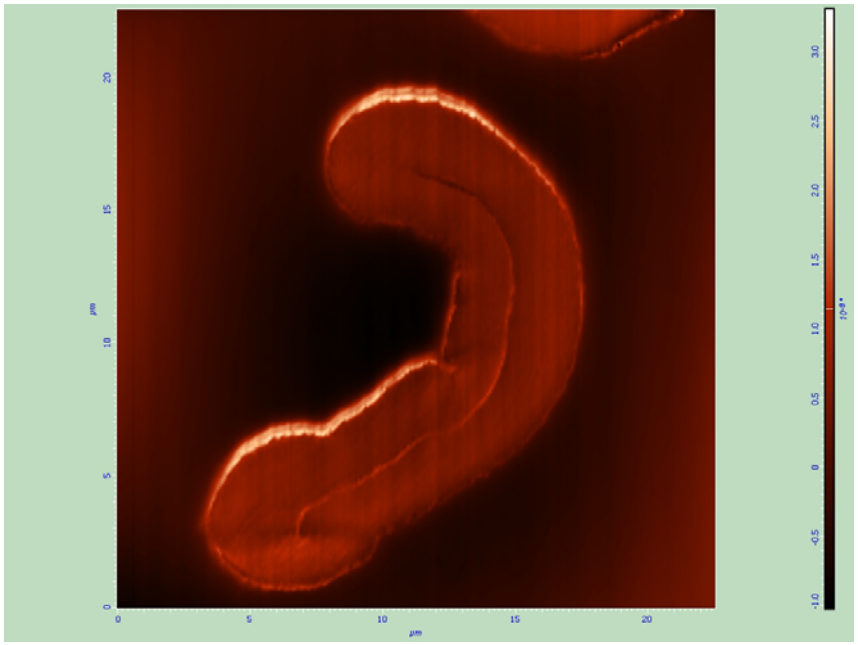
0
5
10
15
20
μm
3.0
2.5
2.0
1.5
1.0
0.5
0
-0.5
-1.0

(b)

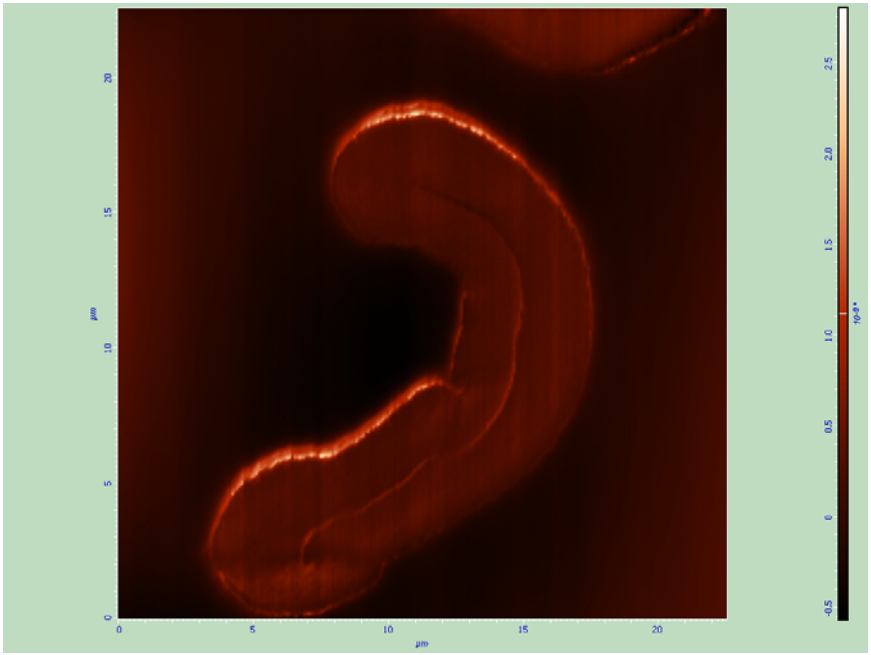
0
5
10
15
20
μm
2.5
2.0
1.5
1.0
0.5
0
-0.5

(c)

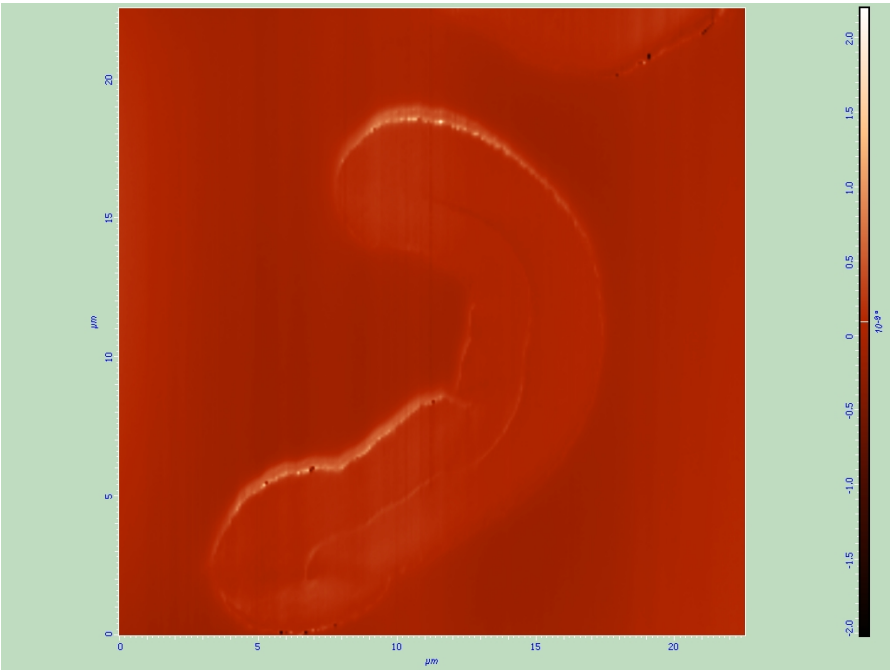

(d)

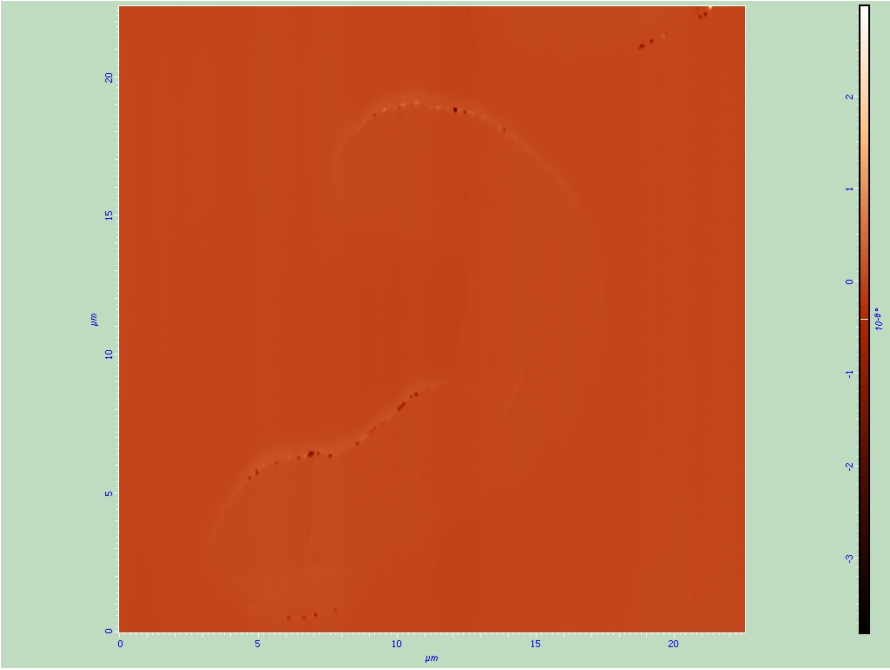

(e)

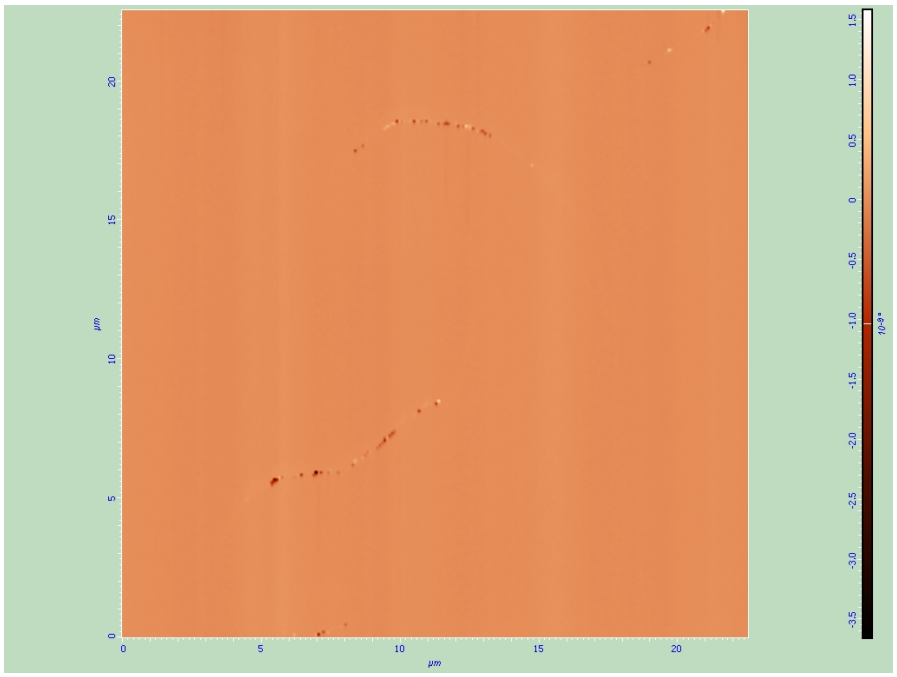
0
5
10
15
20
μm
1.5
1.0
0.5
0
-0.5
-1.0
-1.5
-2.0
-2.5
-3.0
-3.5
10-8 *

(f)

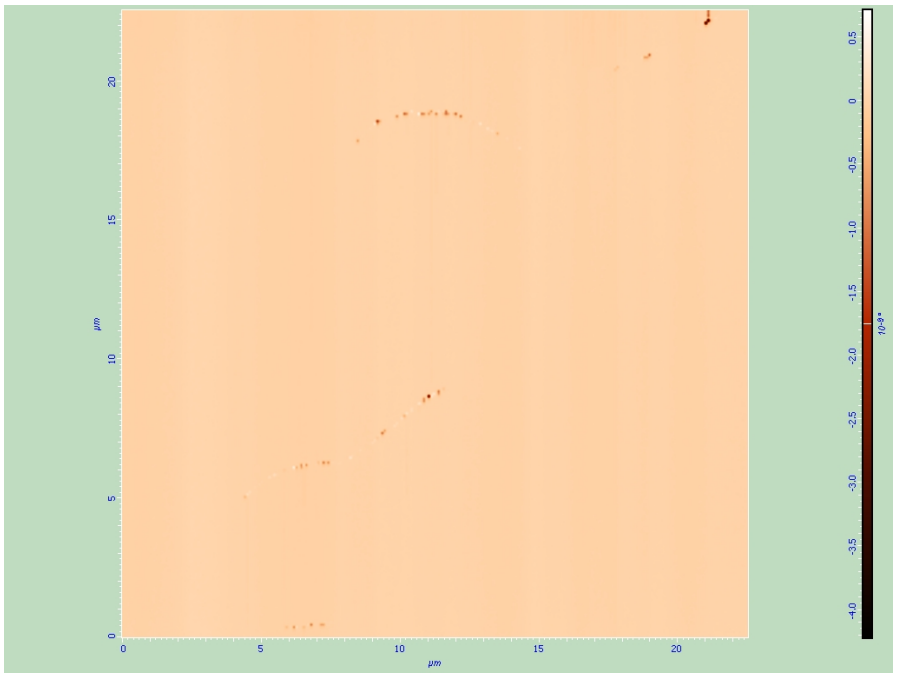
0
5
10
15
20
μm
0.5
0
-0.5
-1.0
-1.5
-2.0
-2.5
-3.0
-3.5
-4.0
10-8 *

(g)

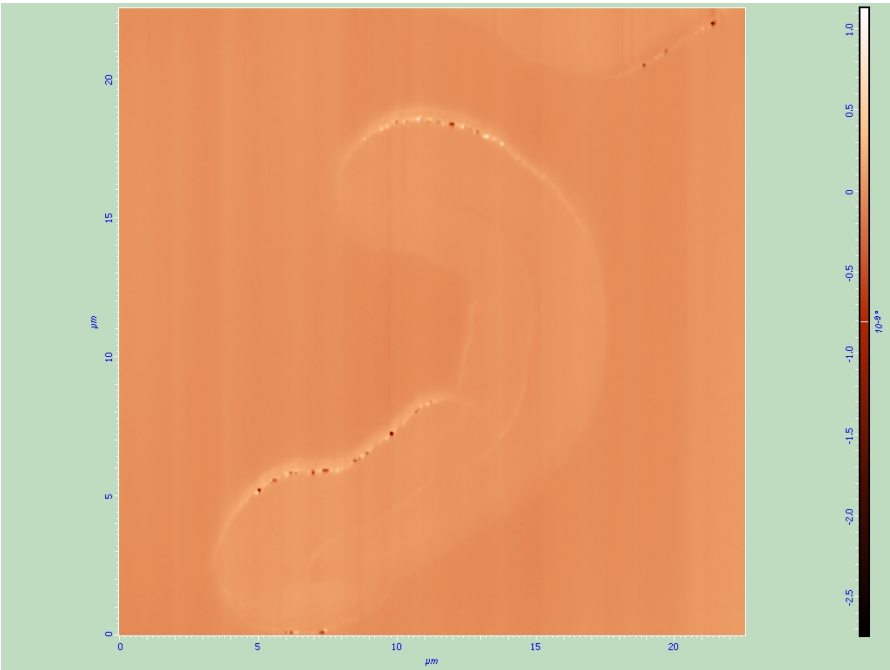

(h)

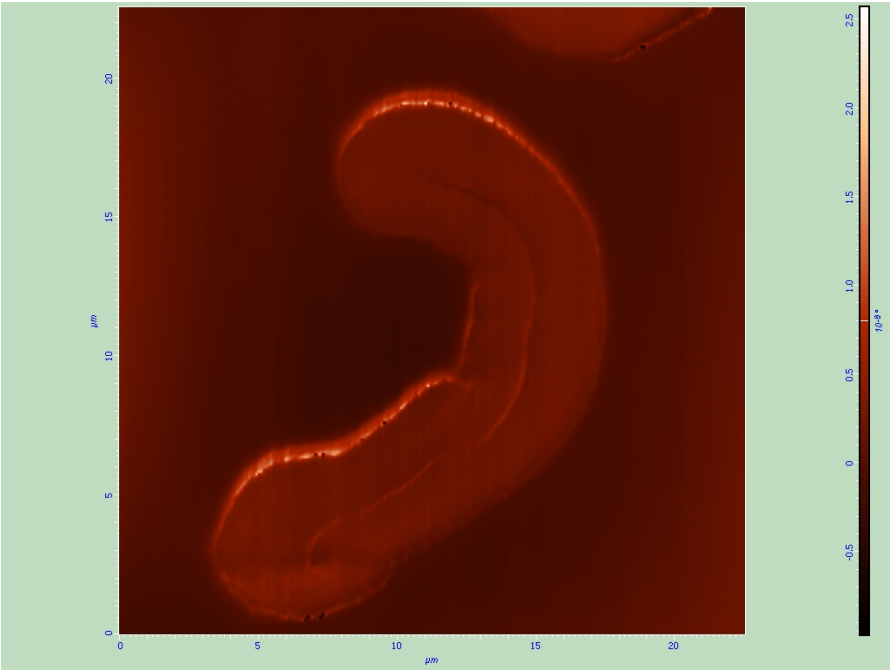

(i)

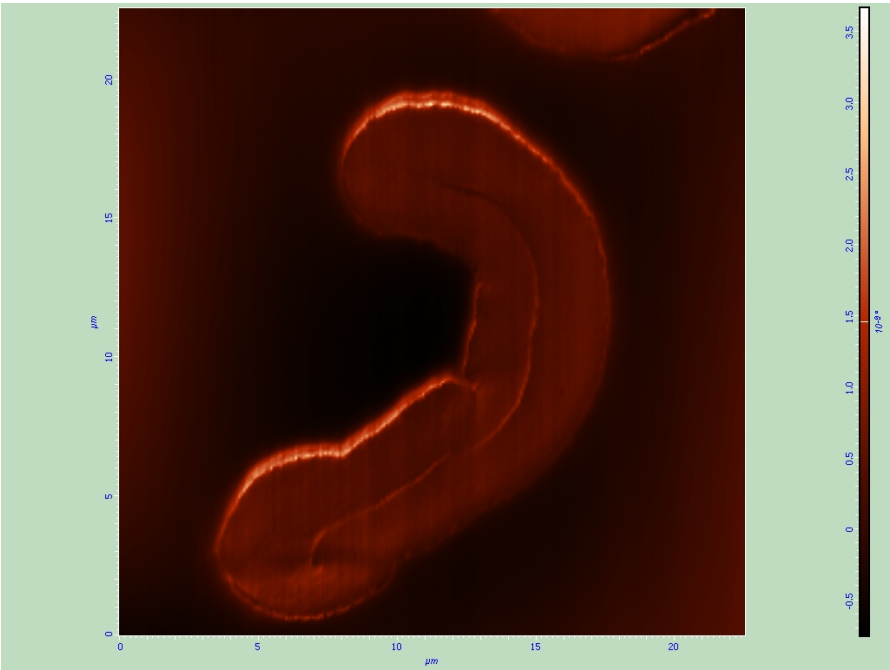

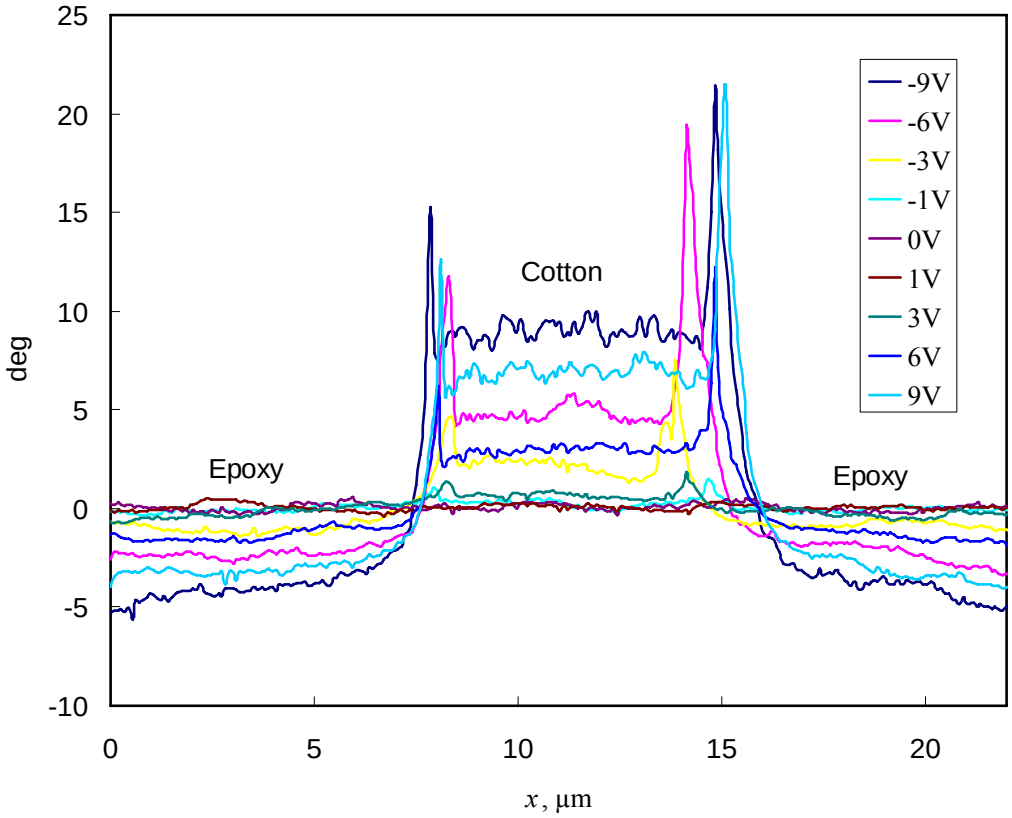

Figure 4.2. EFM Phase profiles for cotton fiber with 5 nanolayers at various bias voltages. *h*=50nm.

Figure 4.3. EFM phase images for cotton fiber with 5 nanolayers at various separation. Ψ=-9V. a). 25nm; b). 50nm; c). 100nm; d). 200nm; e). 500nm; f) 1000nm; g). 1500nm.

(a)

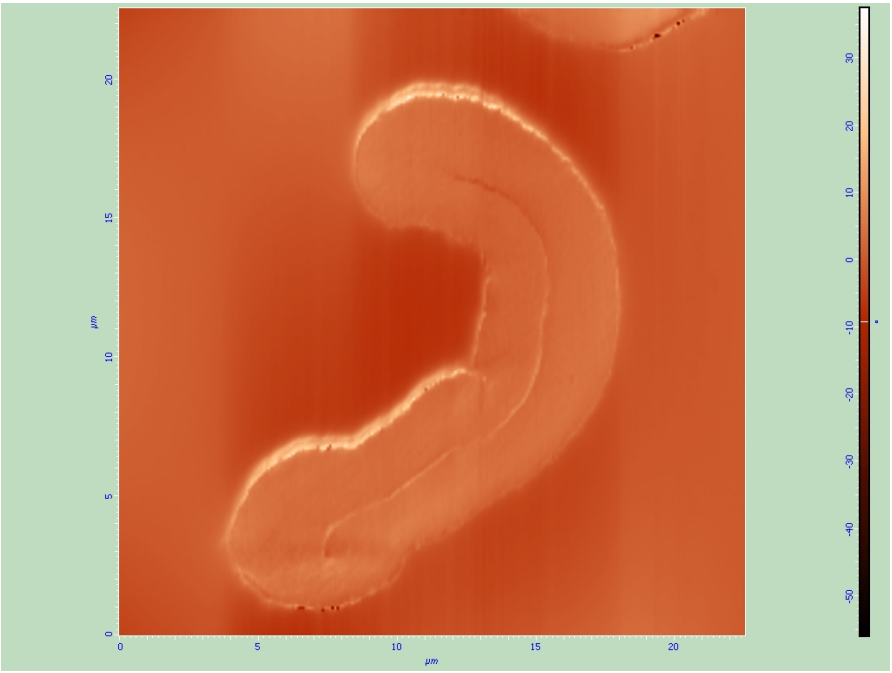
0
5
10
15
20
µm
30
20
10
0
-10
-20
-30
-40
-50
°

(b)

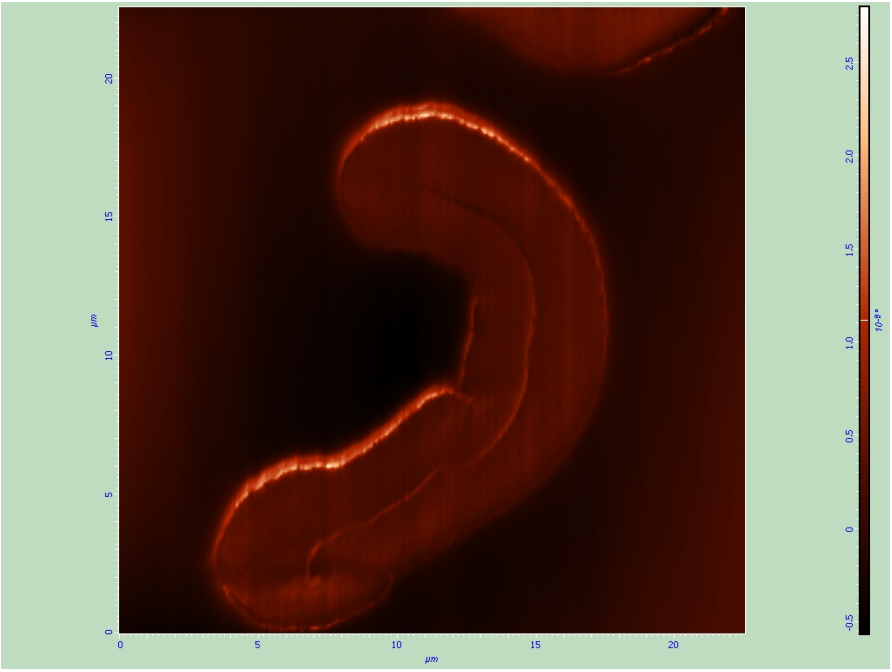
0
5
10
15
20
µm
2.5
2.0
1.5
1.0
0.5
0
-0.5

(c)

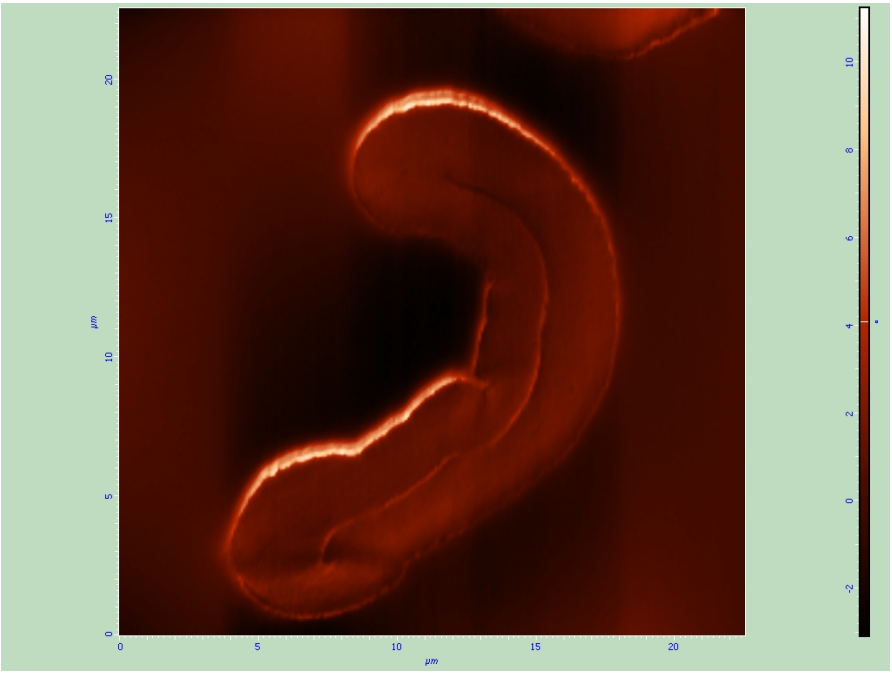

(d)

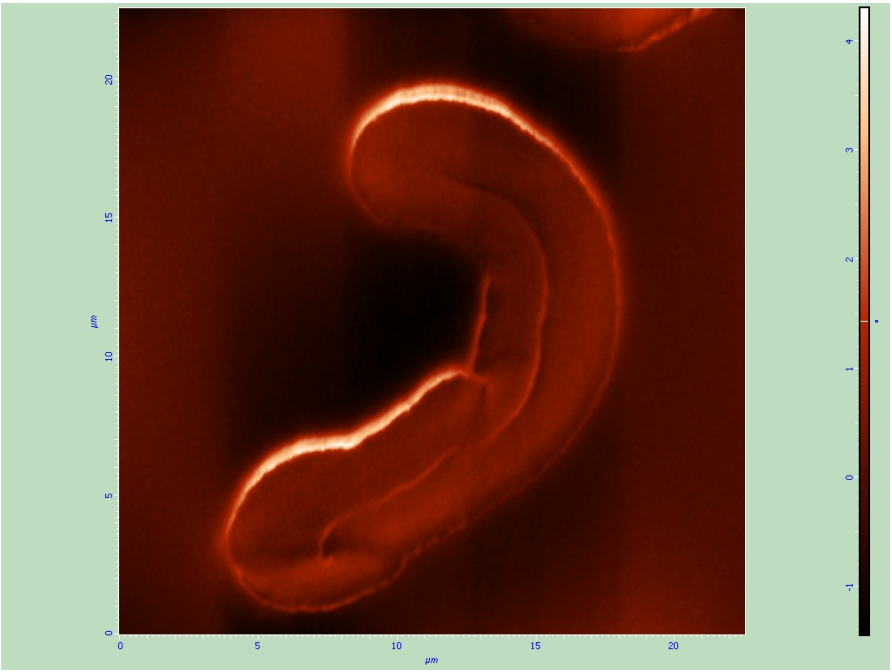

(e)

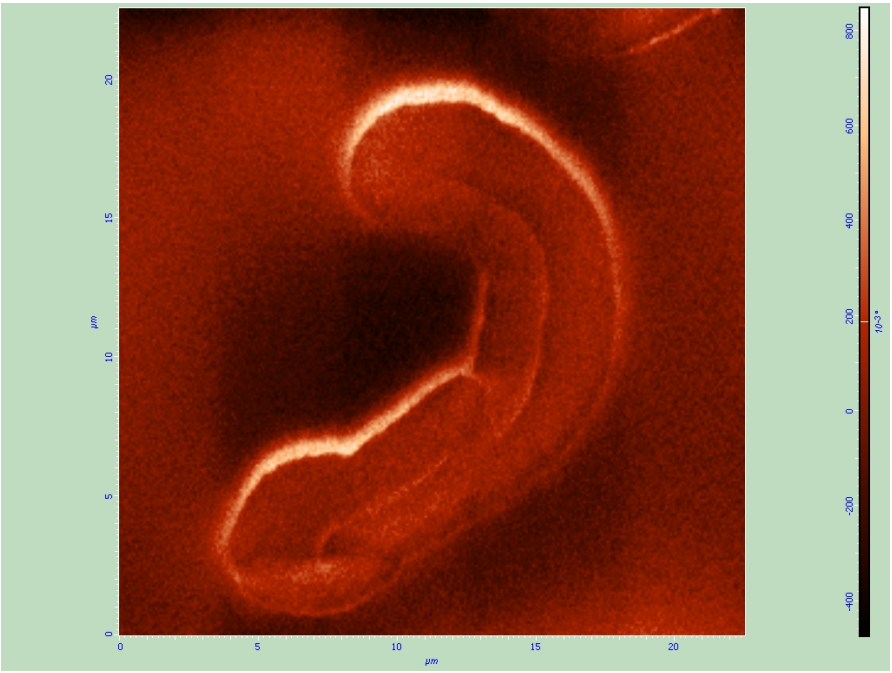
0
5
10
15
20
µm
800
600
400
200
0
-200
-400
10-3 *

(f)

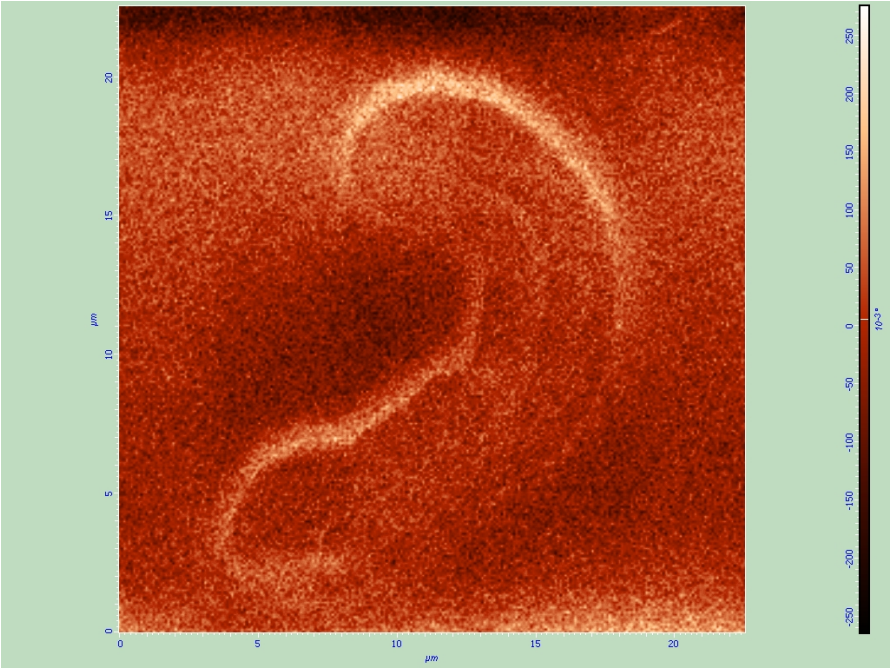
0
5
10
15
20
µm
250
200
150
100
50
0
-50
-100
-150
-200
-250
10-3 *

(g)

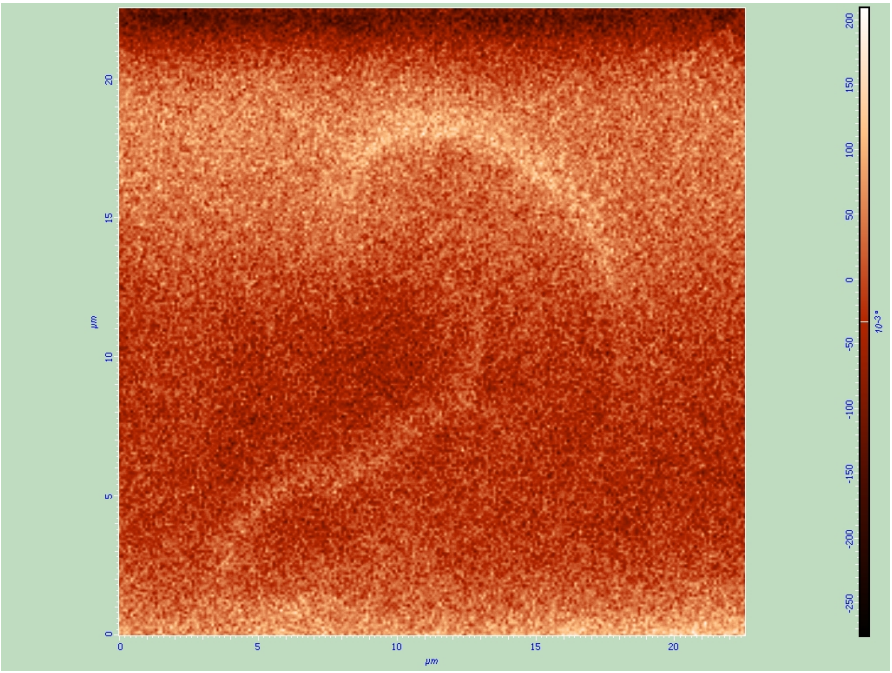

Figure 4.4. EFM phase images for cotton fibers deposited with various numbers of nanolayers. Ψ=-9V, h=50nm. a). 5 layer; b). 15 layers; c). 20 layers.

(a)

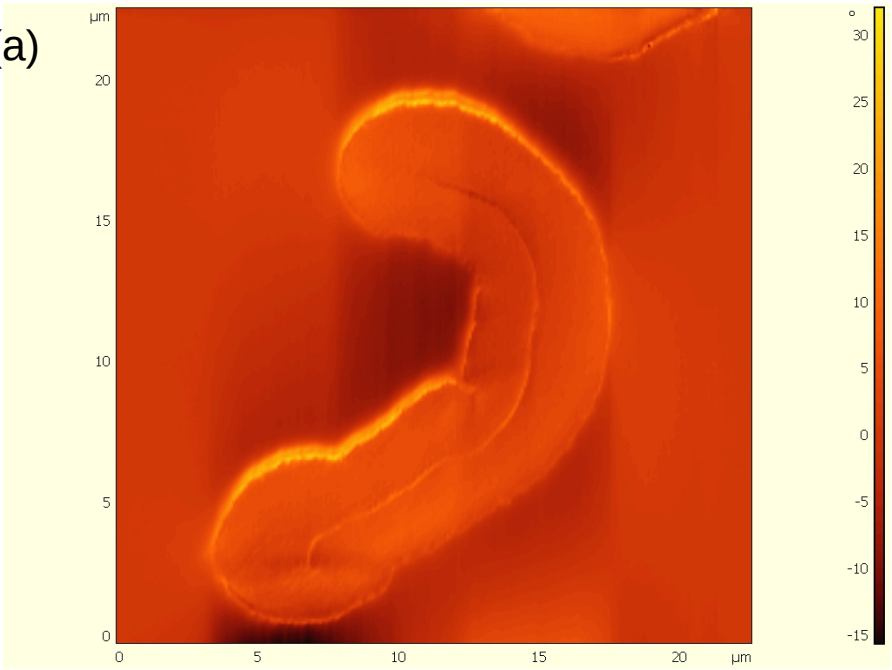
µm
20
15
10
5
0
0
5
10
15
20
µm
°
30
25
20
15
10
5
0
-5
-10
-15

(b)

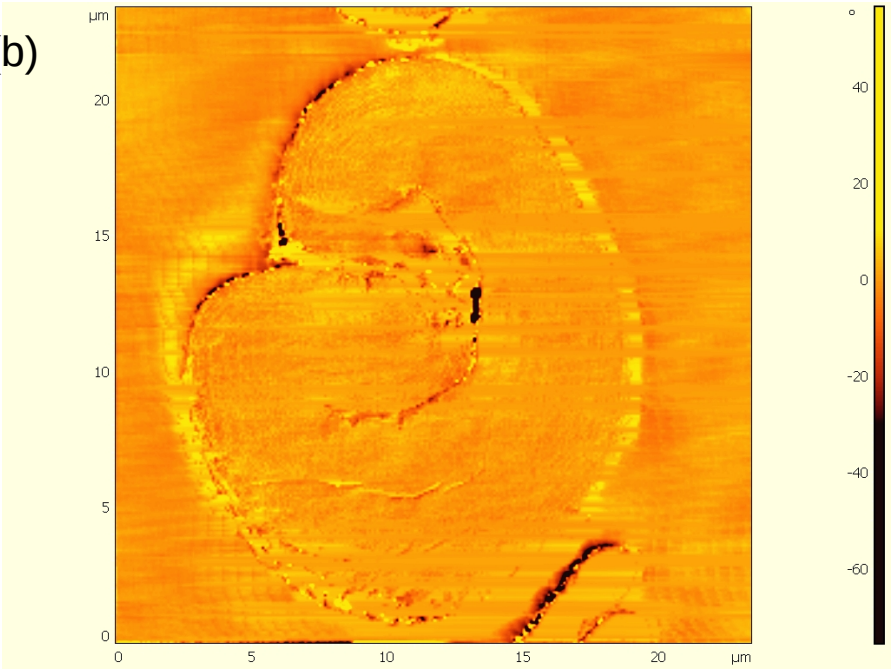
µm
20
15
10
5
0
0
5
10
15
20
µm
°
40
20
0
-20
-40
-60

(c)

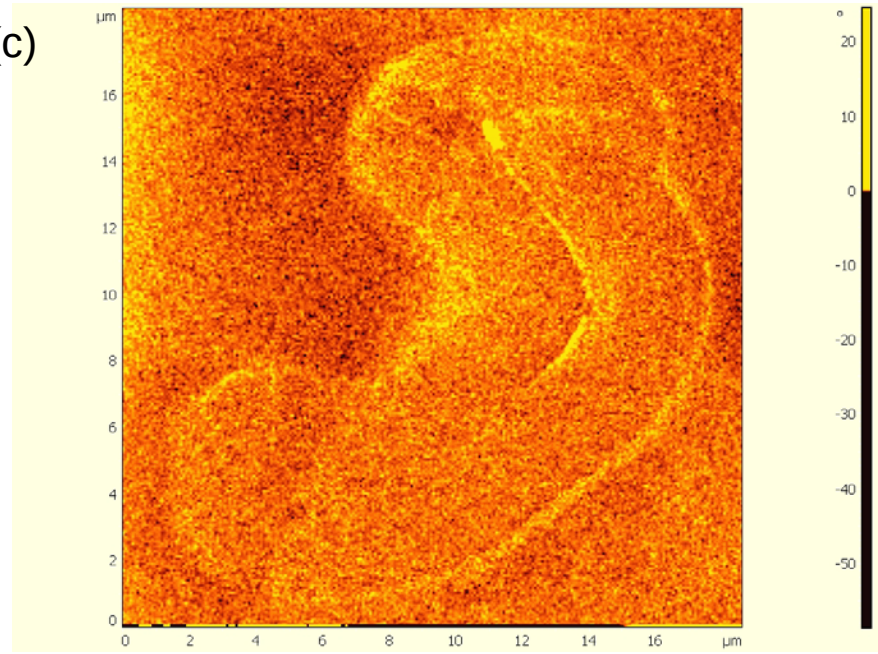

Figure 4.5. EFM phase images for wool fiber with 5 nanolayers at various bias voltages. *h*=50nm. a) -9V; b)-6V; c). -1V; d). +1V; e) +3V; f). +6V; g).+9V.

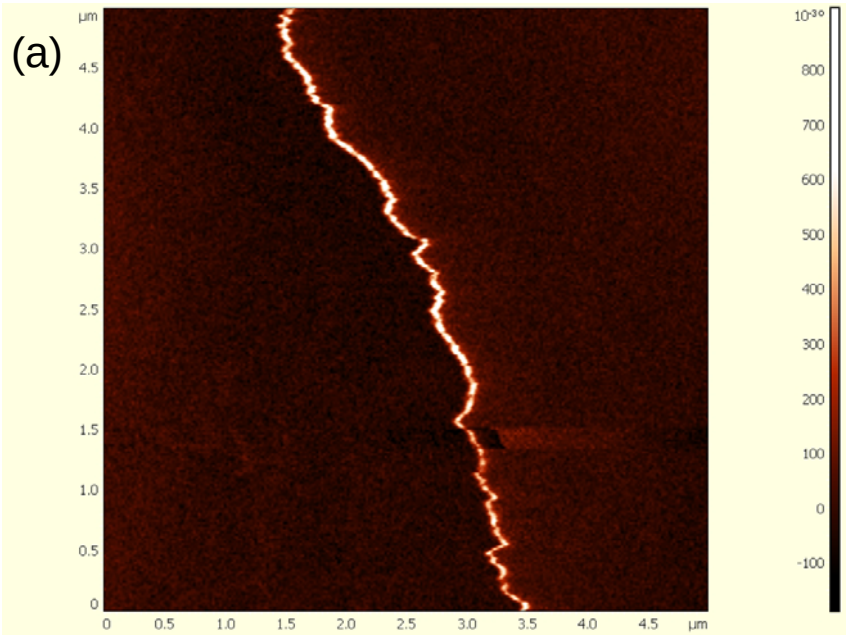
(a)
µm
4.5
4.0
3.5
3.0
2.5
2.0
1.5
1.0
0.5
0
0 0.5 1.0 1.5 2.0 2.5 3.0 3.5 4.0 4.5 µm
10^3°
800
700
600
500
400
300
200
100
0
-100

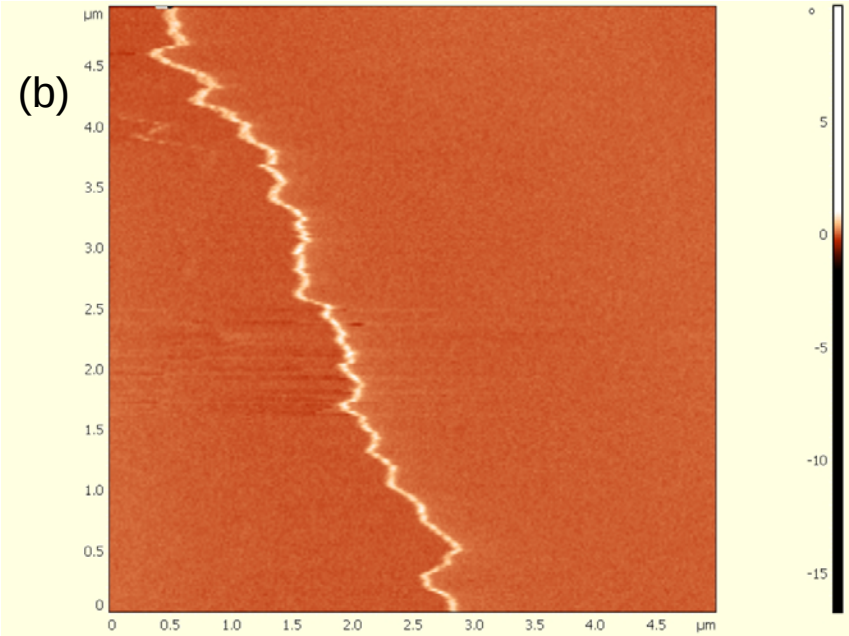
(b)
µm
4.5
4.0
3.5
3.0
2.5
2.0
1.5
1.0
0.5
0
0 0.5 1.0 1.5 2.0 2.5 3.0 3.5 4.0 4.5 µm
°
5
0
-5
-10
-15

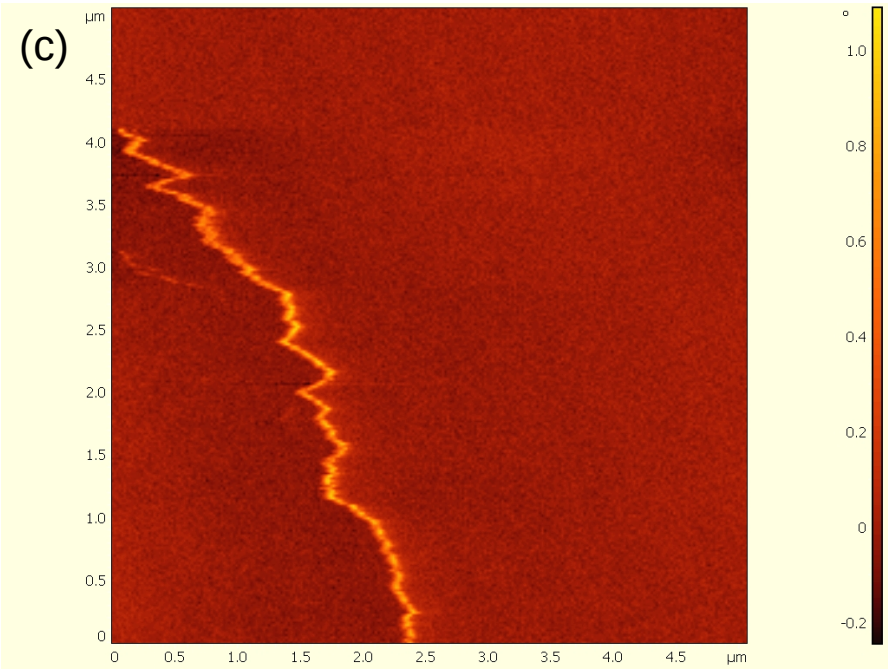
(c)
µm
4.5
4.0
3.5
3.0
2.5
2.0
1.5
1.0
0.5
0
0 0.5 1.0 1.5 2.0 2.5 3.0 3.5 4.0 4.5 µm
°
1.0
0.8
0.6
0.4
0.2
0
-0.2

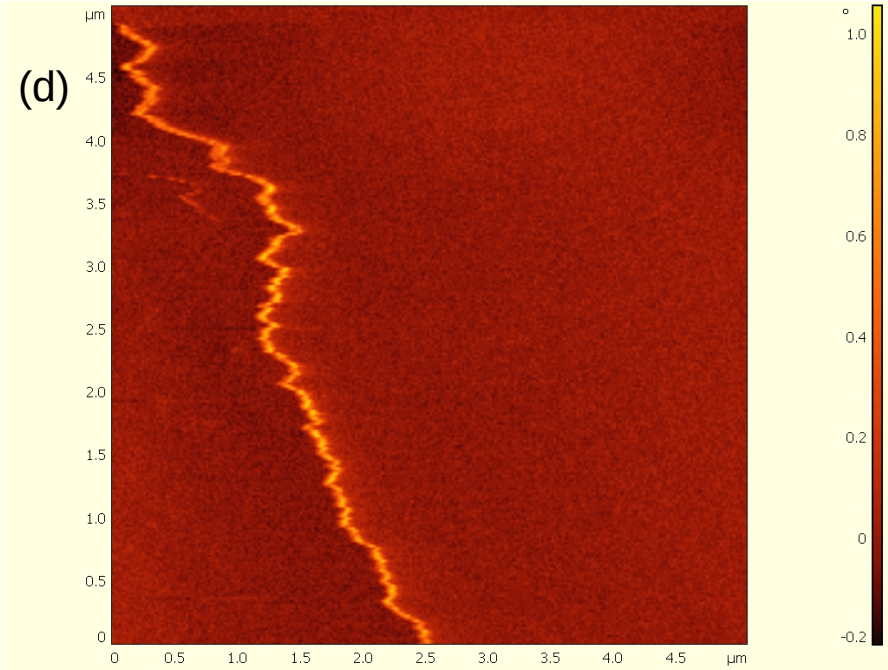
(d)
µm
4.5
4.0
3.5
3.0
2.5
2.0
1.5
1.0
0.5
0
0 0.5 1.0 1.5 2.0 2.5 3.0 3.5 4.0 4.5 µm
°
1.0
0.8
0.6
0.4
0.2
0
-0.2

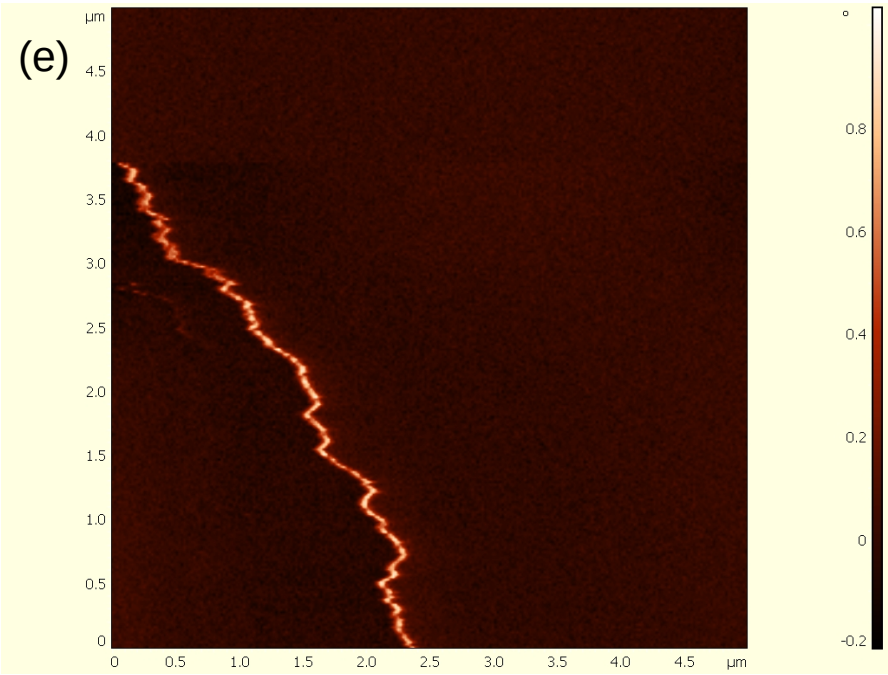
(e)
µm
4.5
4.0
3.5
3.0
2.5
2.0
1.5
1.0
0.5
0
0 0.5 1.0 1.5 2.0 2.5 3.0 3.5 4.0 4.5 µm
°
0.8
0.6
0.4
0.2
0
-0.2

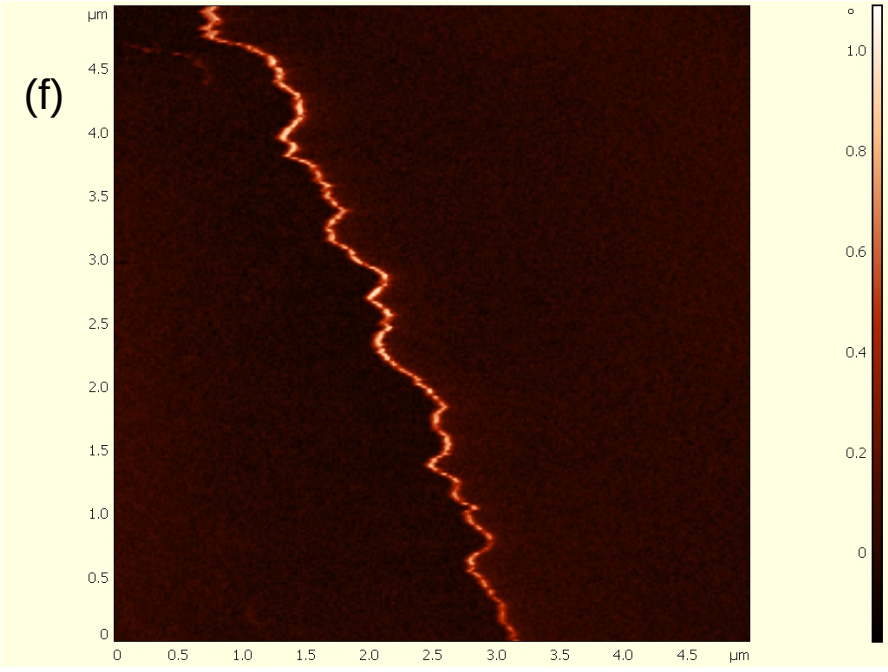
(f)
µm
4.5
4.0
3.5
3.0
2.5
2.0
1.5
1.0
0.5
0
0 0.5 1.0 1.5 2.0 2.5 3.0 3.5 4.0 4.5 µm
°
1.0
0.8
0.6
0.4
0.2
0

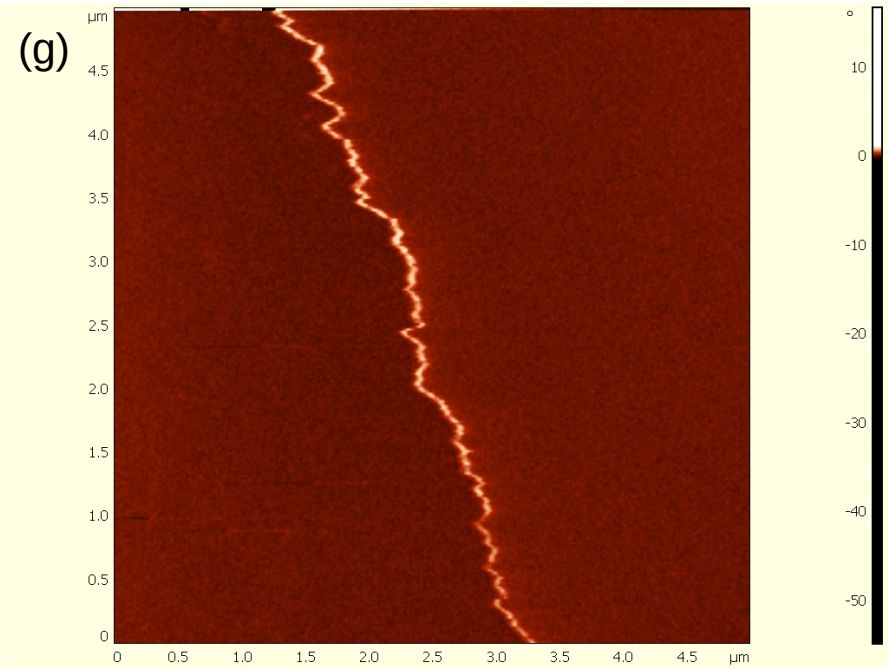
(g)
µm
4.5
4.0
3.5
3.0
2.5
2.0
1.5
1.0
0.5
0
0 0.5 1.0 1.5 2.0 2.5 3.0 3.5 4.0 4.5 µm
°
10
0
-10
-20
-30
-40
-50

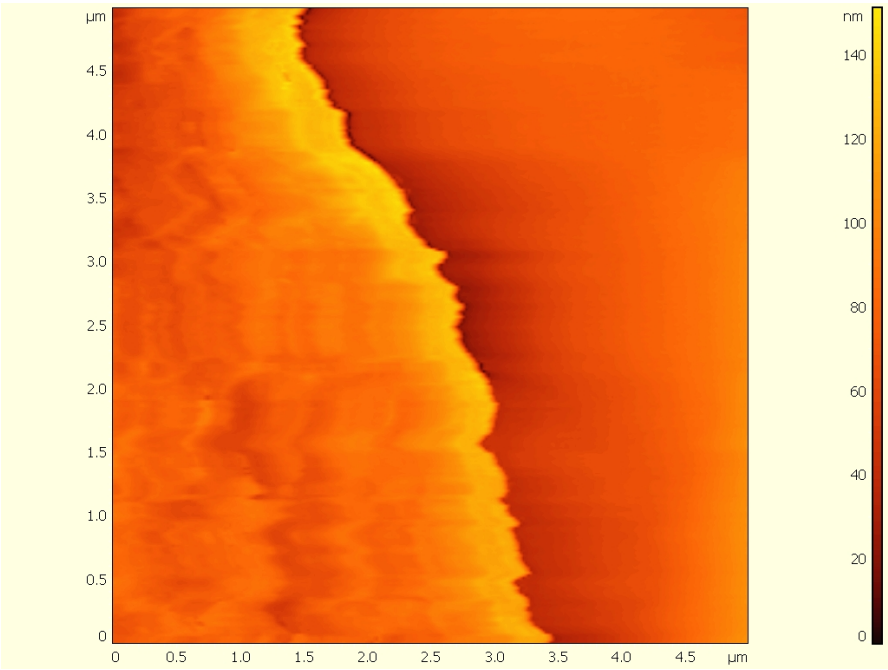

Figure 4.6. Topography of the cross section of wool fiber with 5 nanolayers.

Figure 4.7. EFM phase images for wool fiber with 20 nanolayers at various bias voltages. *h*=50nm. a) -9V; b)-6V; c) -3V; d). -1V; e). +1V; f) +3V; g). +6V; h).+9V.

(a)

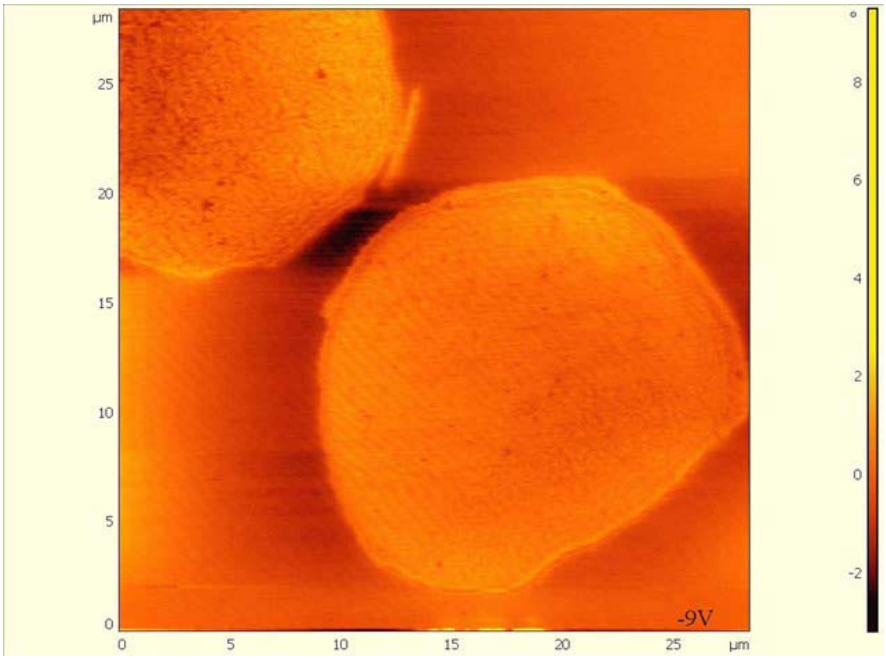
µm
25
20
15
10
5
0
0
5
10
15
20
25
µm
°
8
6
4
2
0
-2
-9V

(b)

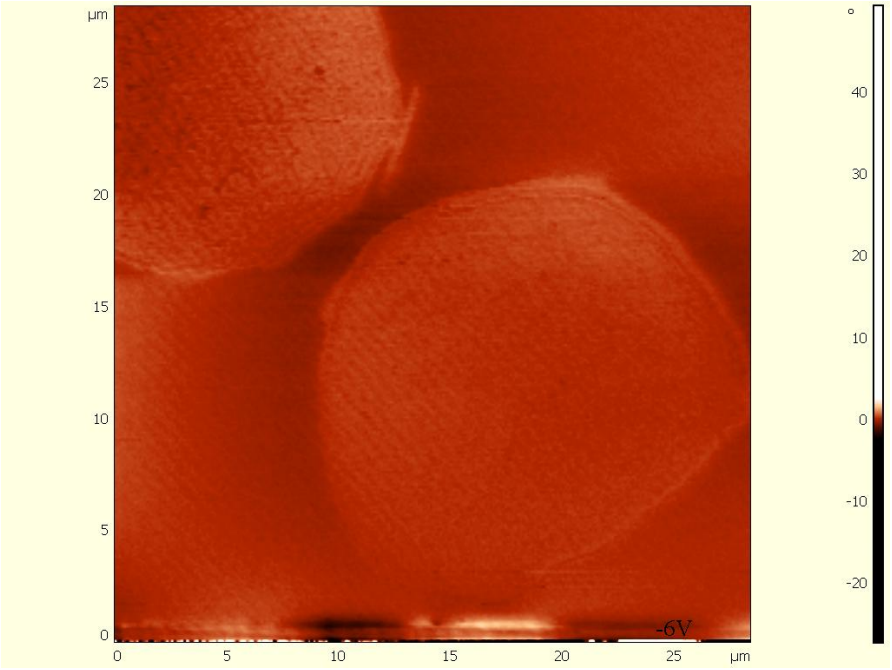
µm
25
20
15
10
5
0
0
5
10
15
20
25
µm
°
40
30
20
10
0
-10
-20
-6V

(c)

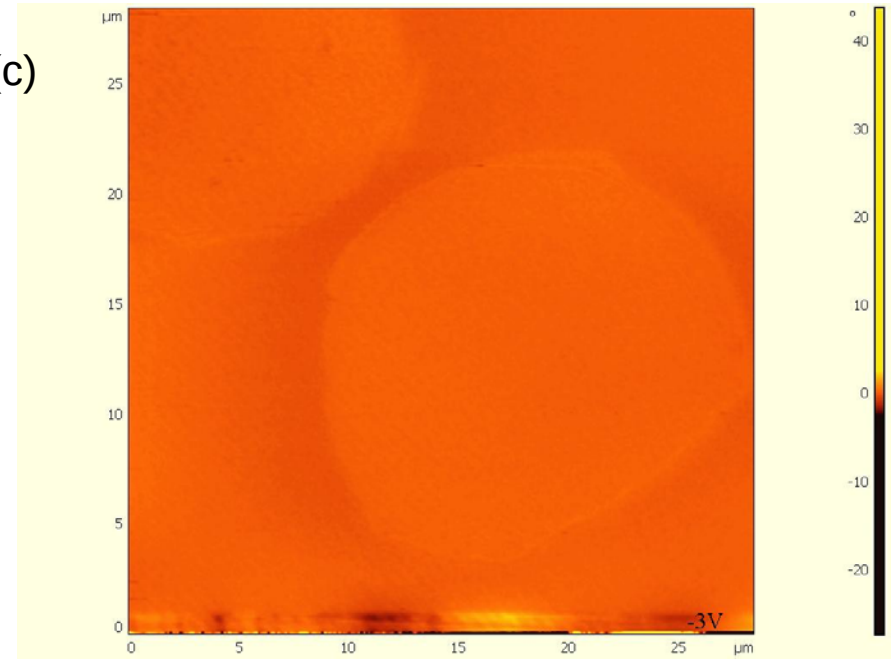
µm
25
20
15
10
5
0
0
5
10
15
20
25
µm
-3V
°
40
30
20
10
0
-10
-20

(d)

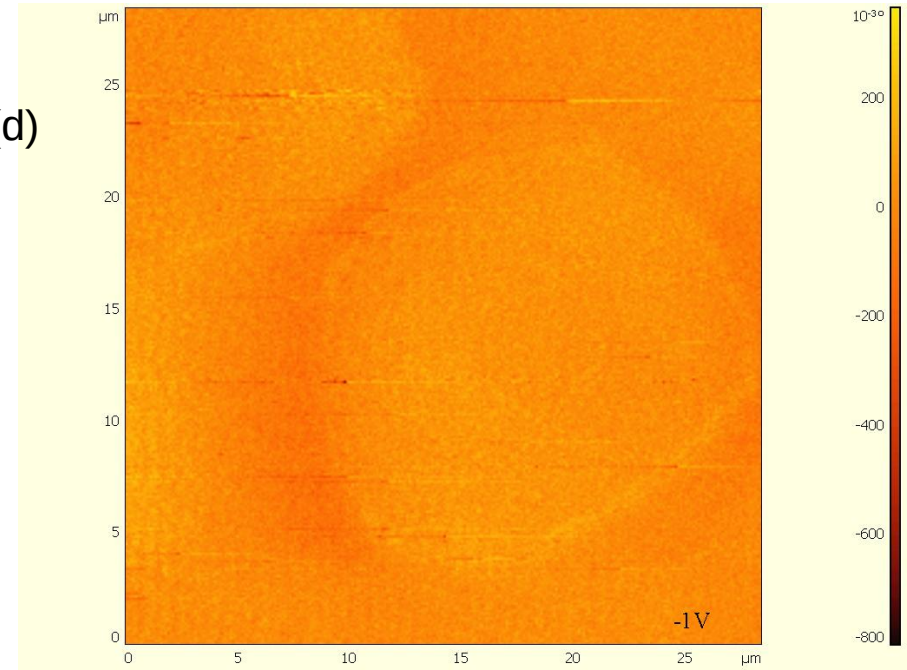
µm
25
20
15
10
5
0
0
5
10
15
20
25
µm
-1V
10⁻³°
200
0
-200
-400
-600
-800

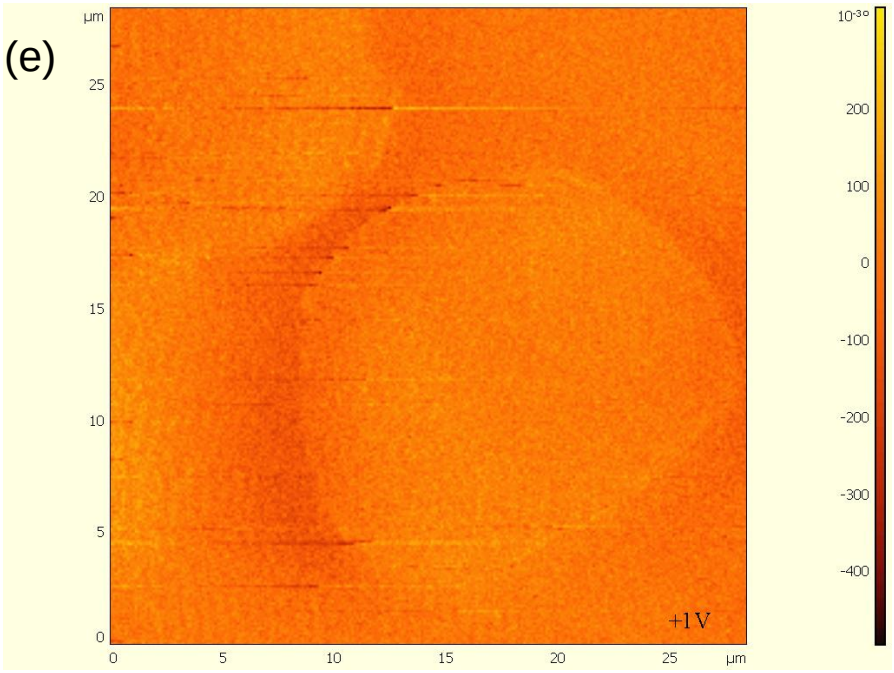
(e)
µm
25
20
15
10
5
0
0
5
10
15
20
25
µm
+1V
10⁻³°
200
100
0
-100
-200
-300
-400

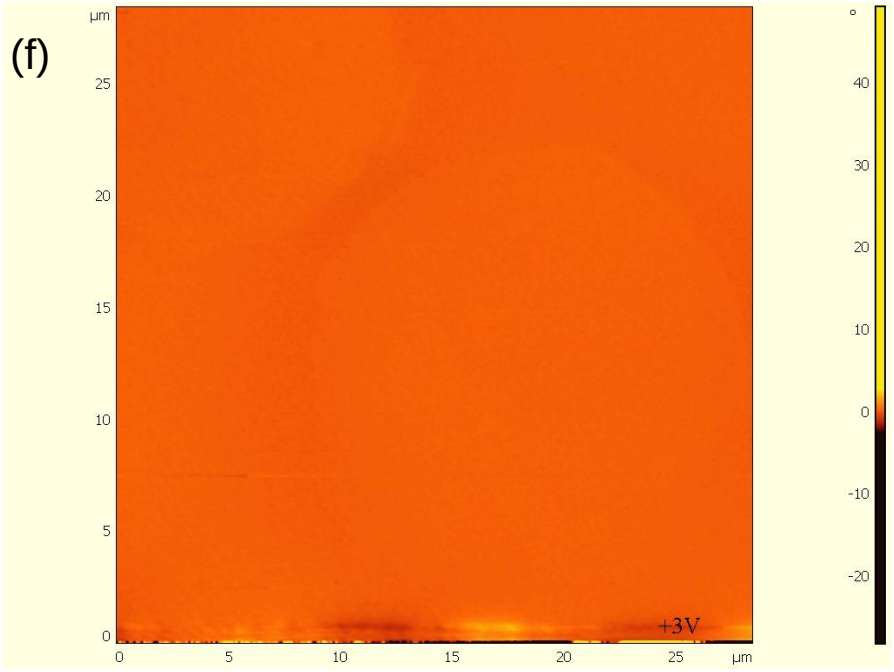
(f)
µm
25
20
15
10
5
0
0
5
10
15
20
25
µm
+3V
°
40
30
20
10
0
-10
-20

(g)

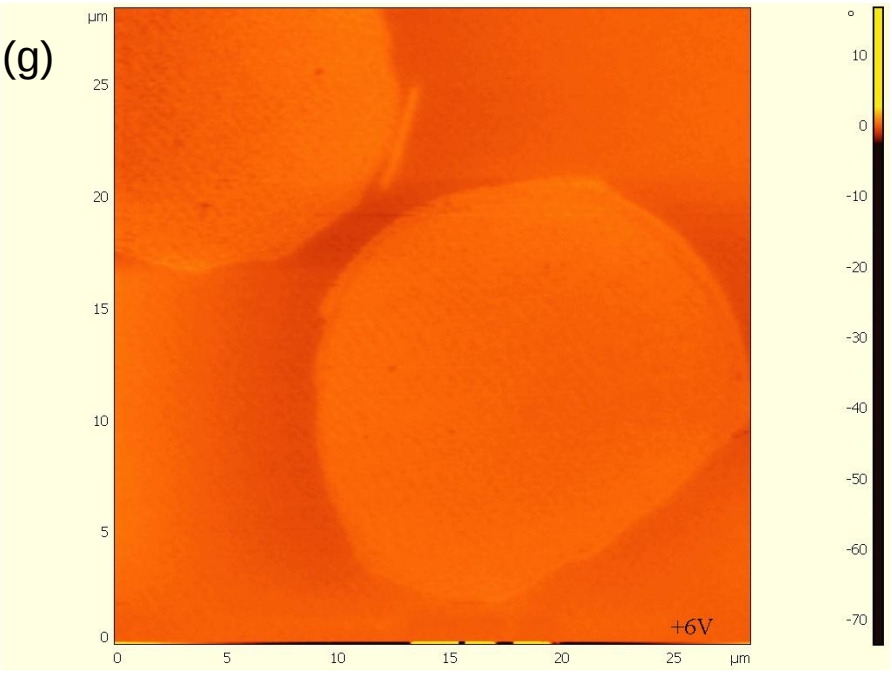
µm
25
20
15
10
5
0
0
5
10
15
20
25
µm
+6V
°
10
0
-10
-20
-30
-40
-50
-60
-70

(h)

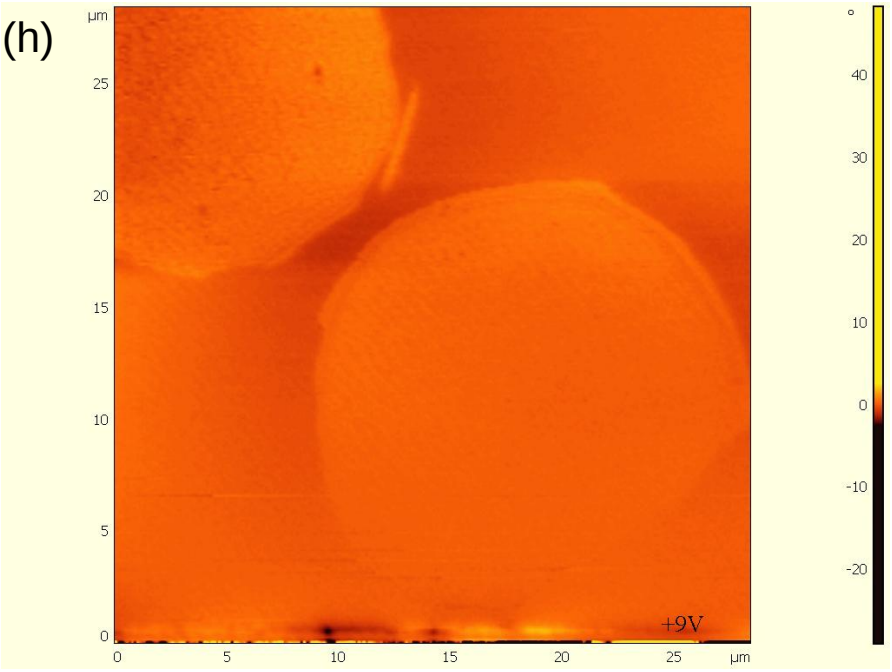
µm
25
20
15
10
5
0
0
5
10
15
20
25
µm
+9V
°
40
30
20
10
0
-10
-20

Figure 4.8. EFM for wool fiber without nanolayers. a) Ψ=-9V; b). Ψ=+9V; c). Ψ=-6V; d). Ψ=+6V; e). Ψ=-3V; f). Ψ=+3V; g). Ψ=-1V; h). Ψ=+1V.

(a)

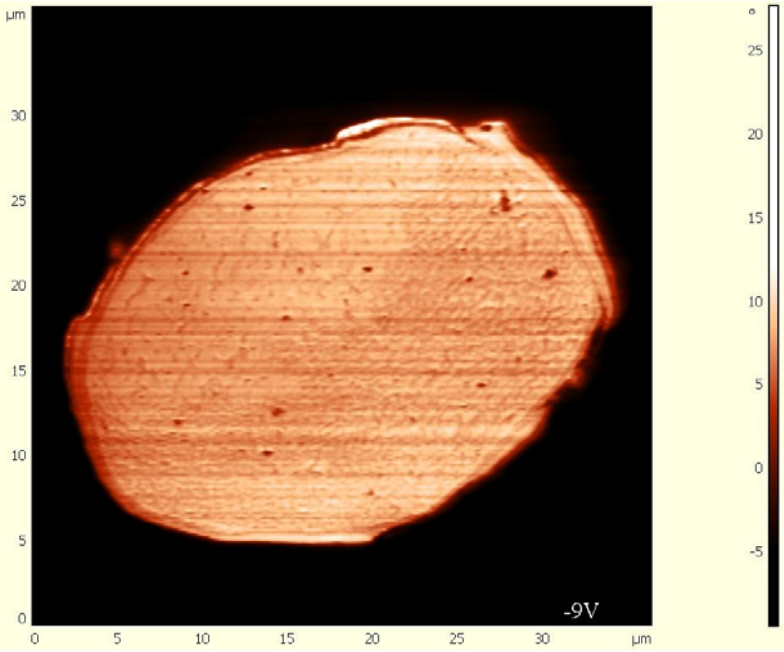
µm
30
25
20
15
10
5
0
-9V
0
5
10
15
20
25
30
µm
°
25
20
15
10
5
0
-5

(b)

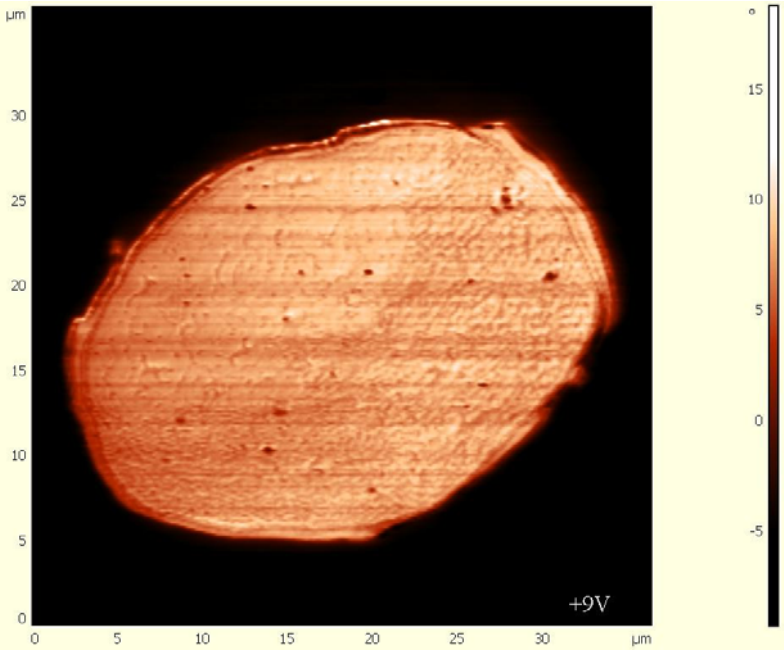
µm
30
25
20
15
10
5
0
+9V
0
5
10
15
20
25
30
µm
°
15
10
5
0
-5

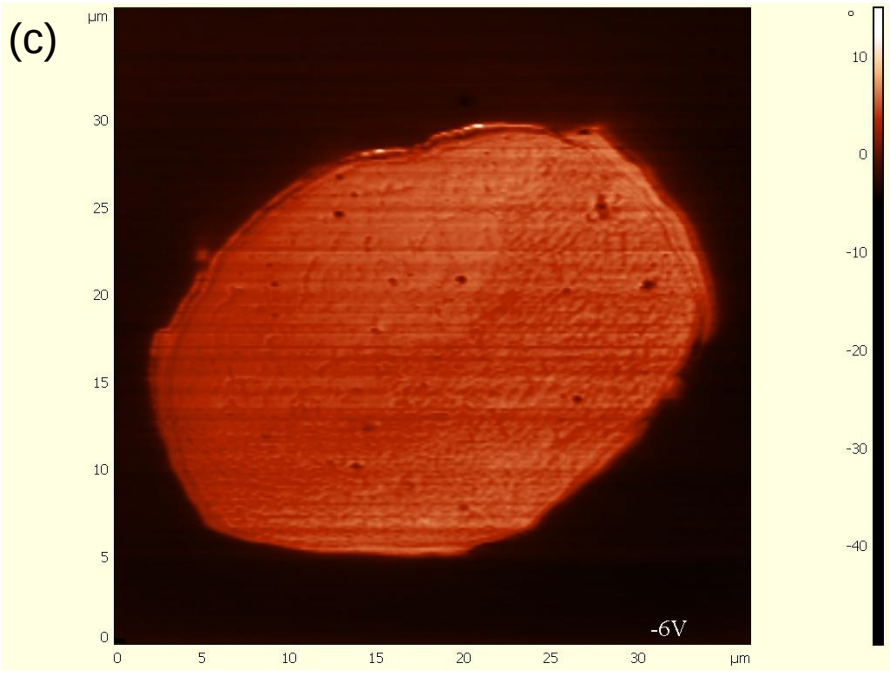
(c)
µm
30
25
20
15
10
5
0
0
5
10
15
20
25
30
µm
-6V
°
10
0
-10
-20
-30
-40

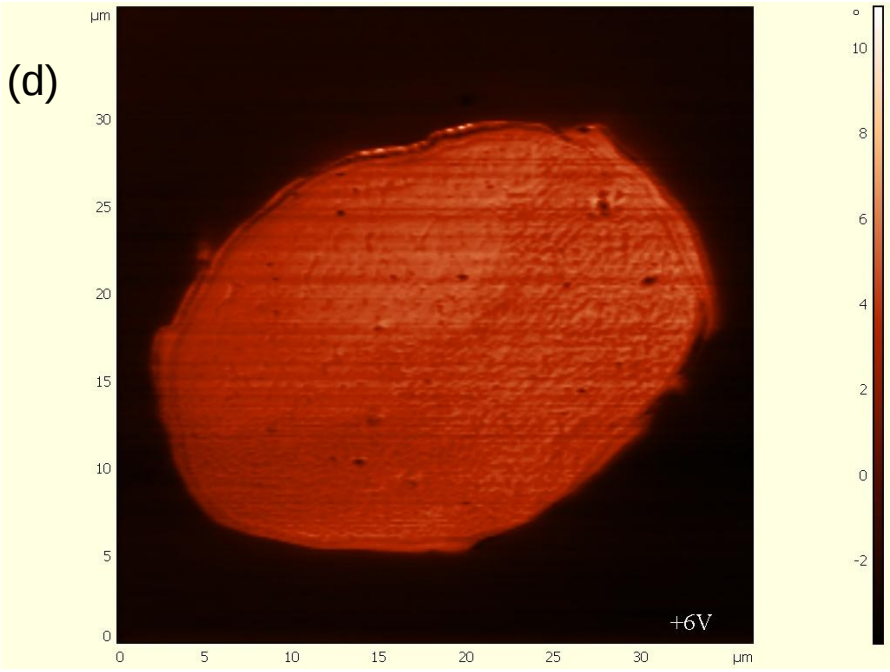
(d)
µm
30
25
20
15
10
5
0
0
5
10
15
20
25
30
µm
+6V
°
10
8
6
4
2
0
-2

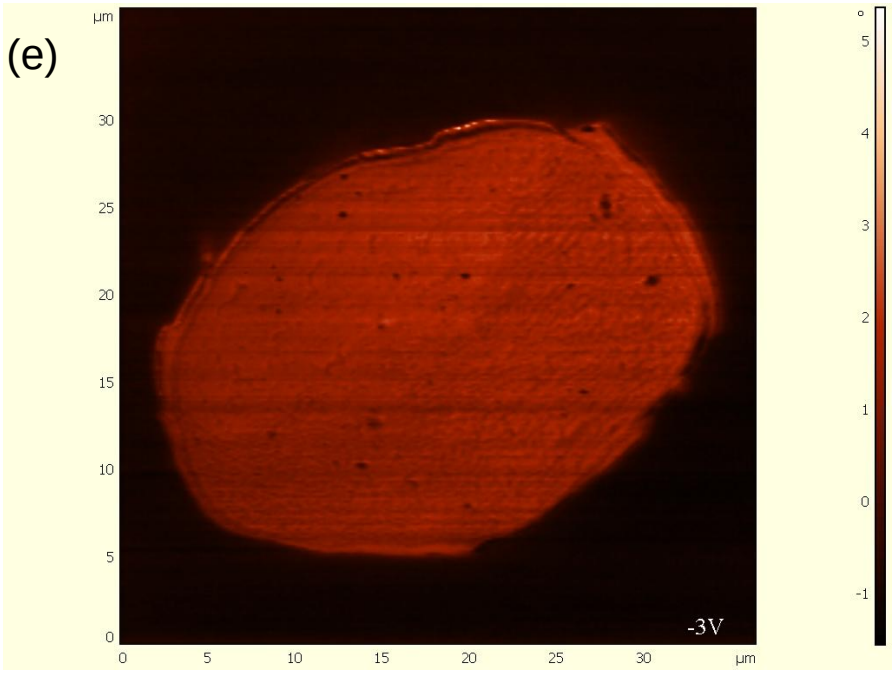
(e)
µm
30
25
20
15
10
5
0
0
5
10
15
20
25
30
µm
-3V
°
5
4
3
2
1
0
-1

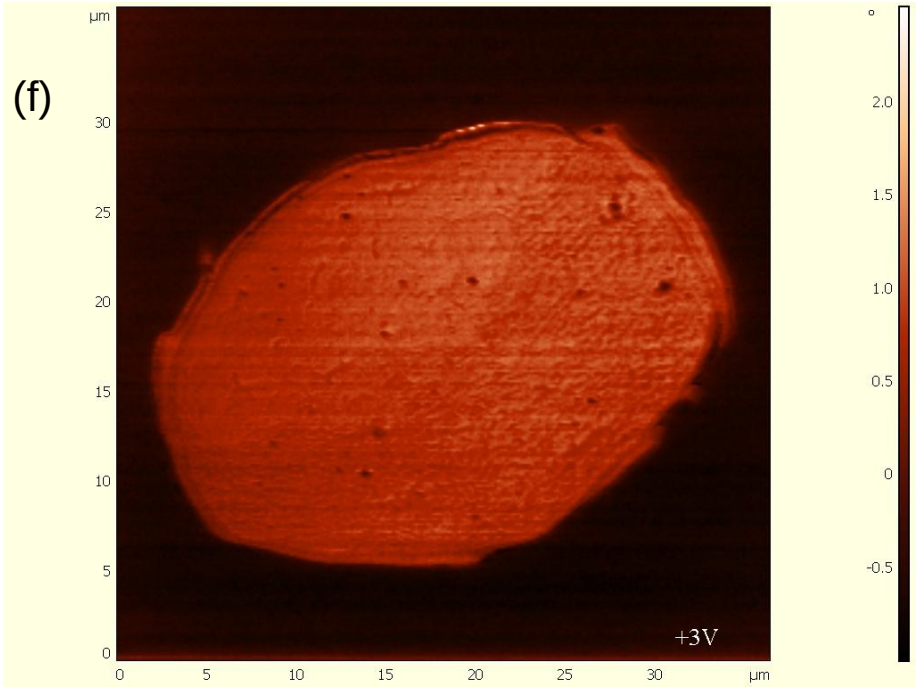
(f)
µm
30
25
20
15
10
5
0
0
5
10
15
20
25
30
µm
+3V
°
2.0
1.5
1.0
0.5
0
-0.5

(g)

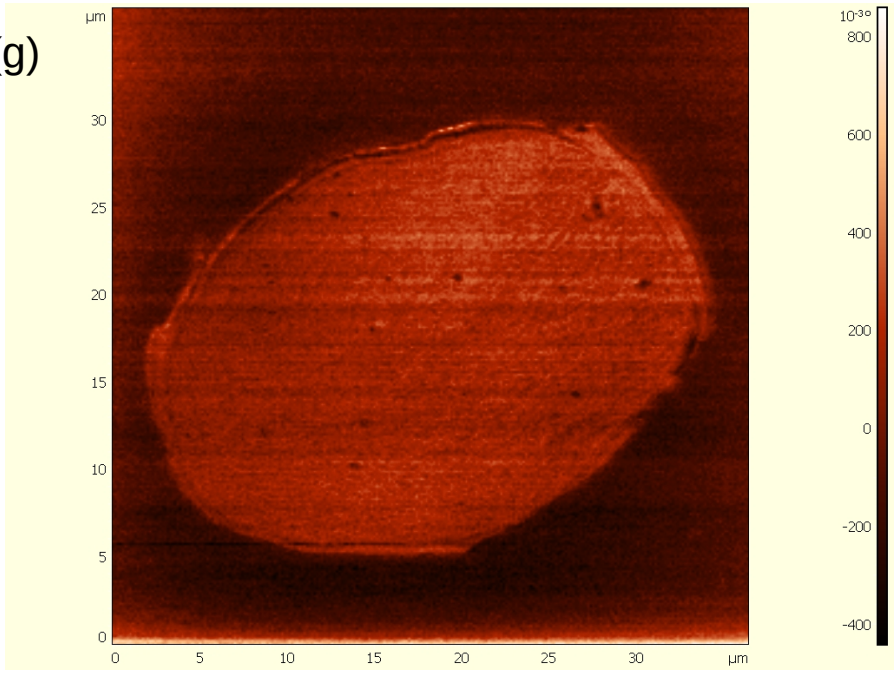
µm
30
25
20
15
10
5
0
0
5
10
15
20
25
30
µm
10-3°
800
600
400
200
0
-200
-400

(h)

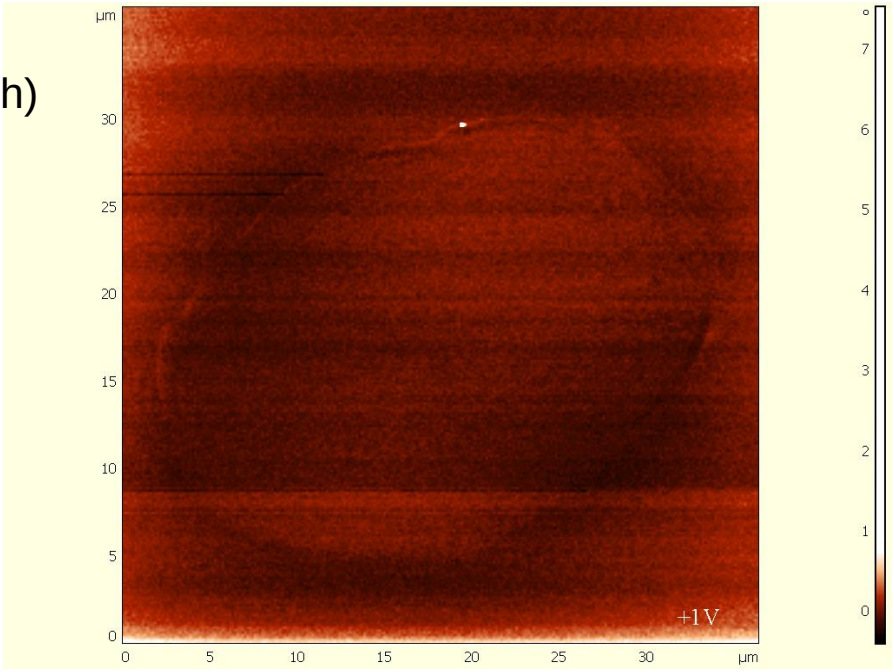
µm
30
25
20
15
10
5
0
0
5
10
15
20
25
30
µm
°
7
6
5
4
3
2
1
0
+1V

Figure 4.9. EFM phase images ($5.8\times5.8\mu m^2$) for wool fibers with 20 nanolayers at various bias voltages Ψ and constant height h=50nm. a). Ψ=-9V; b) Ψ=-3V; c). Ψ=6V; d). Ψ=9V.

(a)

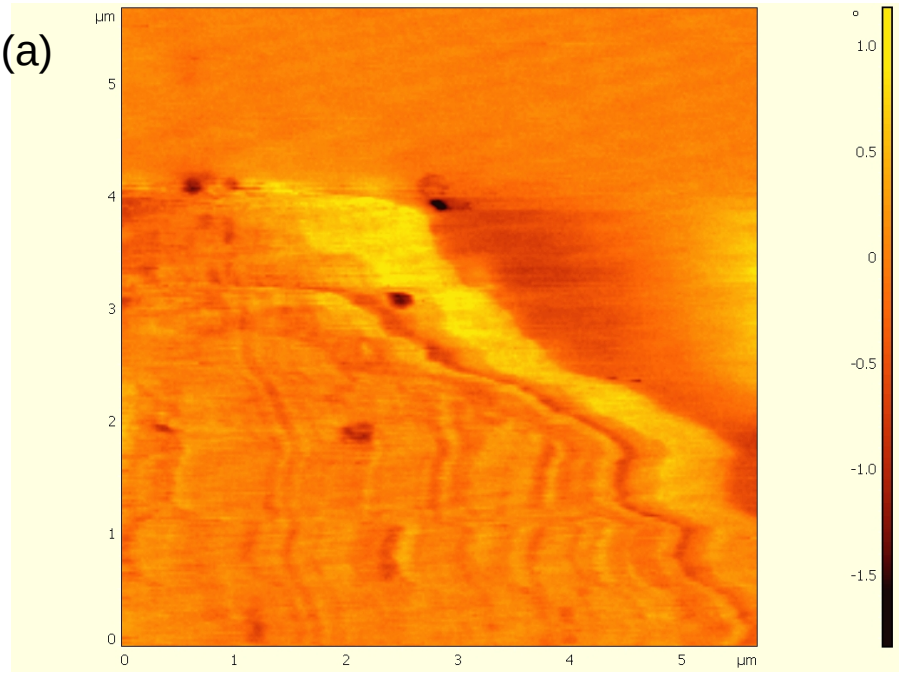
µm
5
4
3
2
1
0
0
1
2
3
4
5
µm
°
1.0
0.5
0
-0.5
-1.0
-1.5

(b)

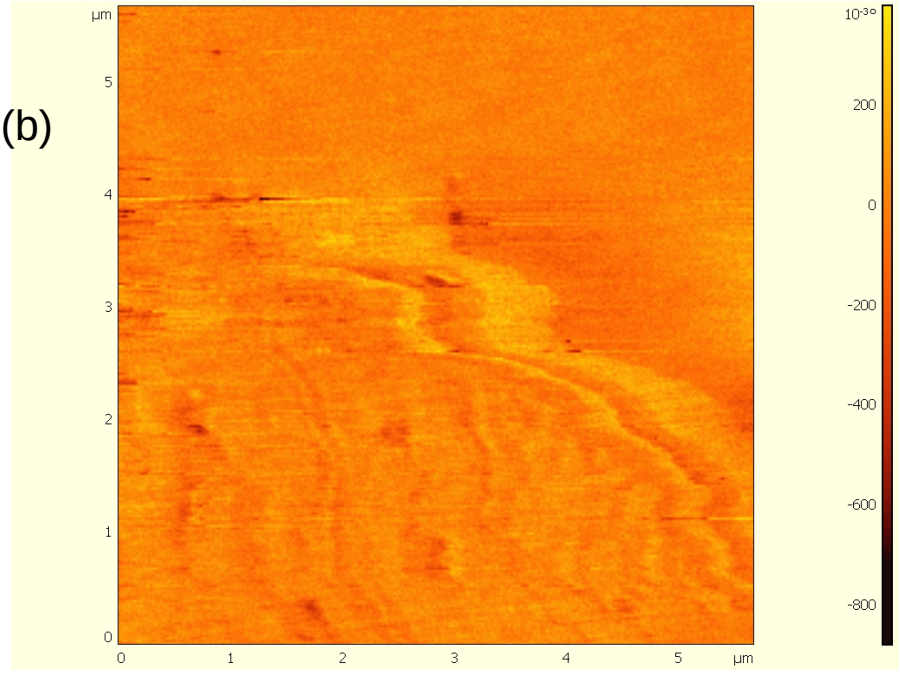
µm
5
4
3
2
1
0
0
1
2
3
4
5
µm
10⁻³°
200
0
-200
-400
-600
-800

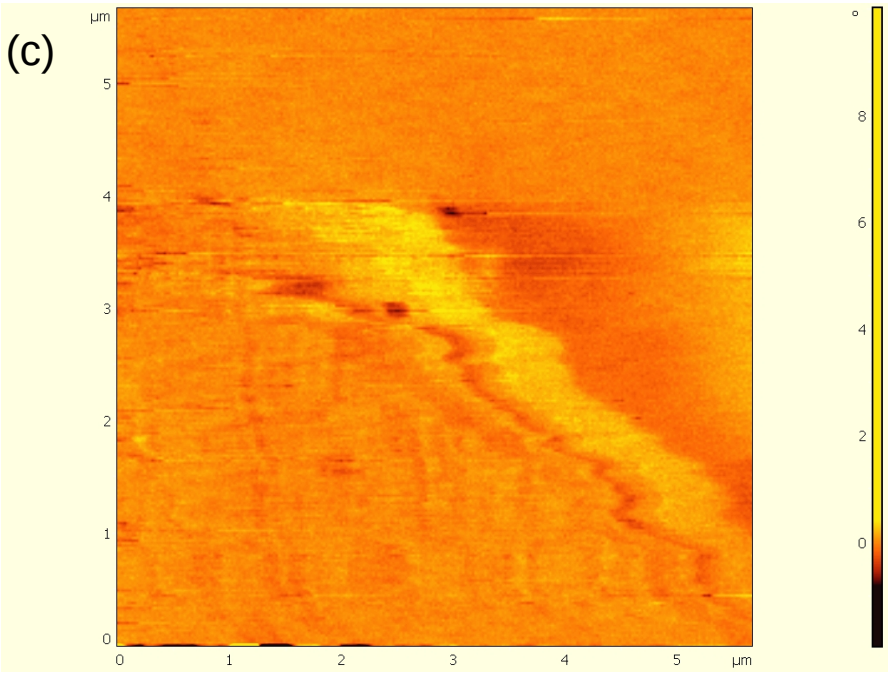
(c)
µm
5
4
3
2
1
0
0
1
2
3
4
5
µm
°
8
6
4
2
0

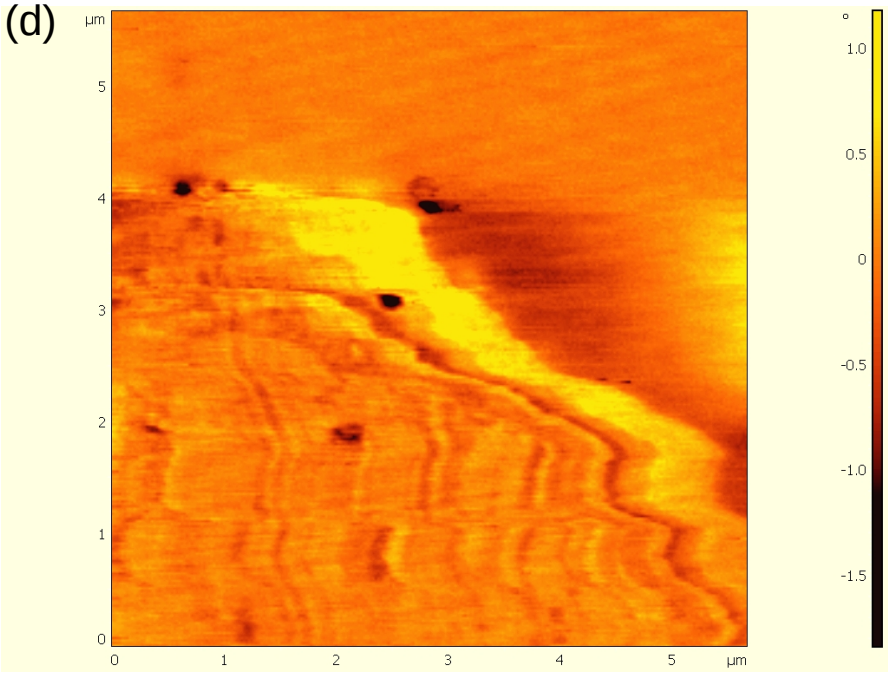
(d)
µm
5
4
3
2
1
0
0
1
2
3
4
5
µm
°
1.0
0.5
0
-0.5
-1.0
-1.5

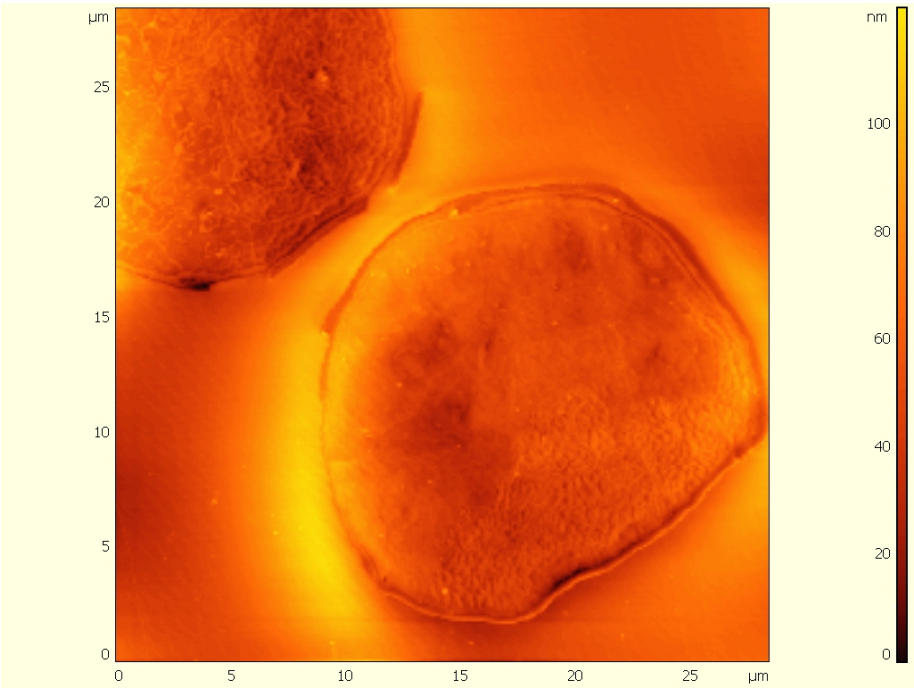

Figure 4.10. Topography of the cross section of wool fiber with 20 nanolayers.

Figure 4.11. EFM phase images for wool fibers deposited with various numbers of nanolayers. Ψ=-9V, h=50nm. a). 0 layer; b). 5 layers; c). 20 layers.

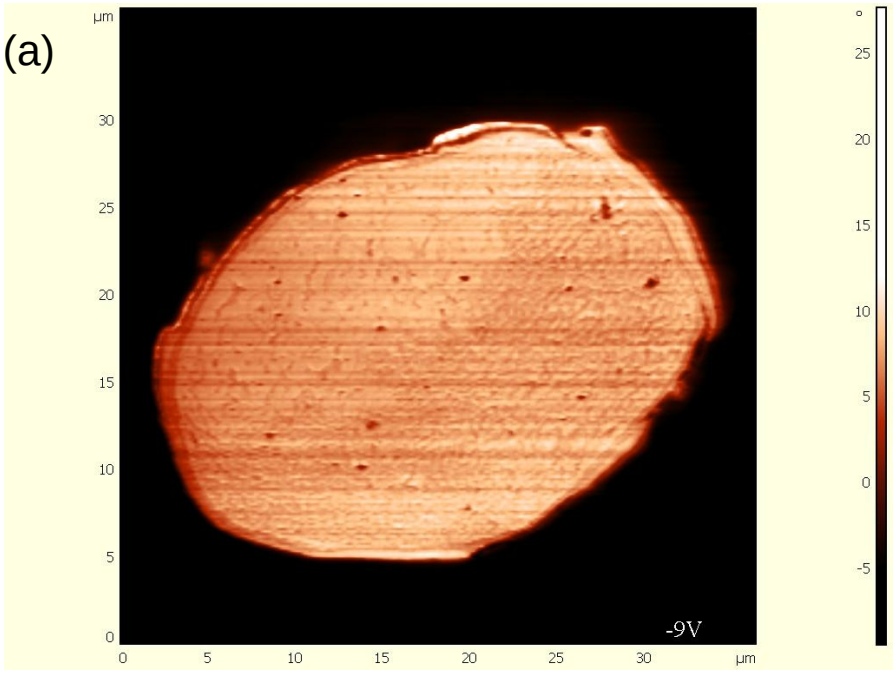
(a)
µm
30
25
20
15
10
5
0
0
5
10
15
20
25
30
µm
-9V
°
25
20
15
10
5
0
-5

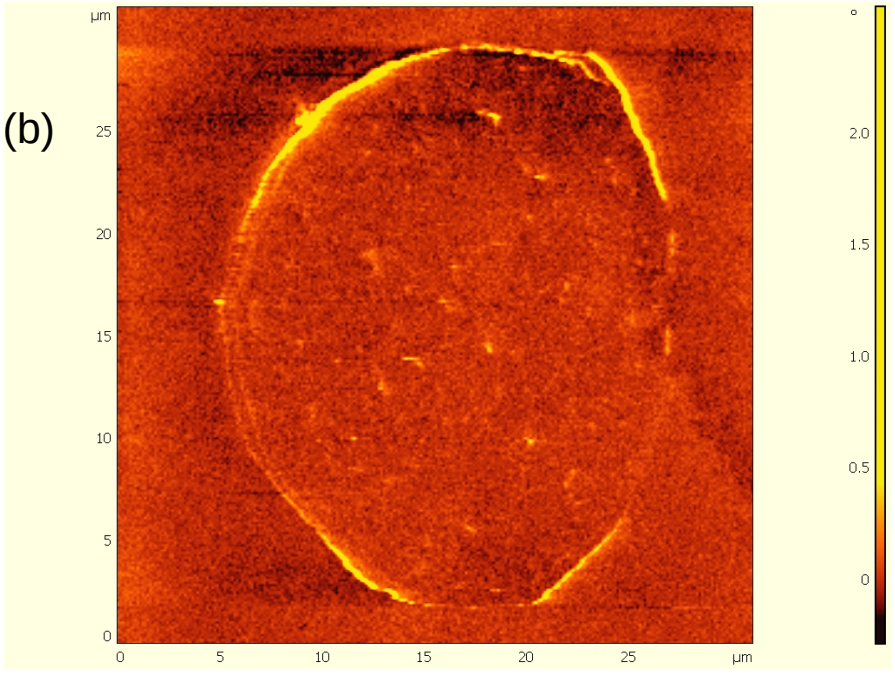
(b)
µm
25
20
15
10
5
0
0
5
10
15
20
25
µm
°
2.0
1.5
1.0
0.5
0

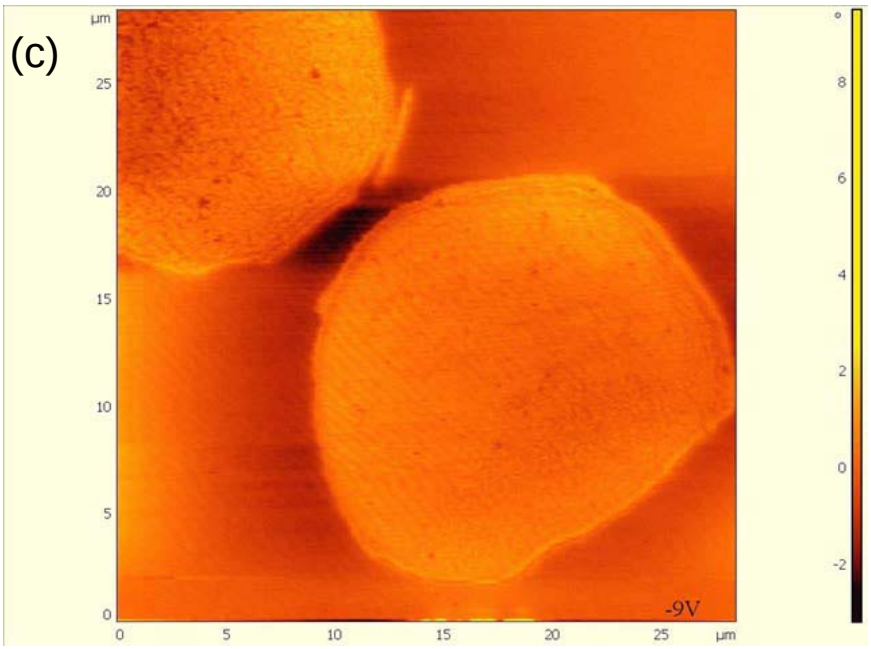
(c)
µm
25
20
15
10
5
0
0
5
10
15
20
25
µm
-9V
°
8
6
4
2
0
-2

Chapter 5 is a reprint of a paper that will be submitted to the Journal of Polymer Engineering and Science

Deposition of Polyelectrolyte Nanolayers on Polyester Fibers Using Electrostatic Self-assembly

G. Kevin Hyde[1] and Juan P. Hinestroza[2*]

[1]*Department of Textile Engineering, Chemistry, and Science, North Carolina State University, Raleigh, NC 27695*

[2]*Department of Fiber Science and Apparel Design, Cornell University, Ithaca, NY 14850*

Abstract

Layer-by-layer deposition of polyelectrolytes onto poly(ethylene terephthalate) (PET) fibers is reported as a method for synthetic fiber surface modification. Poly(sodium styrene sulfonate) (PSS) and poly(allylamine hydrochloride) (PAH) were sequentially adsorbed onto the surface of plasma treated PET fibers. A comparison of four different gas mixtures for plasma treatment was also made. Polyester fibers pose distinctive problems due to their unique cross sections and the physical and chemical heterogeneity of their surface. X-ray photoelectron spectroscopy (XPS) and transmission electron microscopy (TEM) were used to verify the existence of the nanolayers and to confirm their stratification. Analysis of the XPS data showed quantitative agreement to data reported in previous publications involving the deposition of PSS and PAH onto polymer and fiber substrates.

Specific Contribution

For this article, I prepared polyester fabric samples coated with polyelectrolyte nanolayers of PSS and PAH. This study also investigated the use of plasma treatment as a surface modification technique for polyester based textiles. Different plasma treatment specifications were used in order to optimize the subsequent deposition of the polyelectrolyte layers. I began by setting up the plasma treatment system. I was responsible for installing the system and learning how to operate and maintain it. I then discussed the different gas mixtures that would be studied with Dr. Hinestroza. I then made the samples. First, the samples were plasma treated with different mixtures of helium and oxygen. After plasma treatment, the polyester samples were used as substrates for the layer-by-layer deposition of PSS and PAH. After making all of the modified fabric samples, I performed XPS and TEM analysis of the samples in order to characterize the deposited layers. I then analyzed all of the data and created the relevant figures and tables for the manuscript. I wrote the manuscript for this work and gave it to Dr. Hinestroza for further revisions. This work demonstrates the versatility of the LbL technique by coating synthetic fibers in knit fabric form.

Chapter 5: Deposition of Polyelectrolyte Nanolayers on Polyester Fibers using Electrostatic Self-assembly

5.1 Introduction

Multilayer films of polyelectrolytes allow the creation of multicomposite molecular assemblies with great levels of reproducibility and exact molecular architectures. Films created by electrostatic self-assembly (ESA) are able to self-organize. This self-organization allows the production of goods with highly functional surface structures.[1-3]

ESA has been used to alter the surface characteristics of a number of different materials both natural and synthetic. Self-assembled films have been used to produce optical and electronic products as well as medical materials. New research is focusing on the use of ESA as a method of enhancing the performance of textile products.[4-6]

The ESA process, which was first introduced by Decher in the 90s, is a practical method for the creation of nanolayers on charged substrates.[1, 6-9] The ease of use of the procedure has made it a very popular way to modify a number of different substrates. Substrates that have been used include glass, quartz, silica, gold, and silver.[10-12] Polymeric materials have also been used as base substrates for ESA with great success. These polymers include poly(propylene), poly(isobutylene), poly(styrene), poly(methyl methacrylate), poly(ethylene terephthalate), poly(phenylene oxide), and poly(ether imide).[13,14] In addition to the fact that ESA allows a range of substrates to be used, a number of different polyelectrolytes can be used as well. Common polyelectrolytes for ESA include poly(ethyleneimine), poly(allylamine), poly(diallyldimethylammonium chloride), poly(styrene sulfonate), poly(vinyl sulfate) and poly(acrylic acid).[10]

The electrostatic attraction between oppositely charged molecules provides an excellent basis for the creation of nanolayer films. This is due to the fact that it has the least steric demand of all chemical bonds.[1] The ESA process begins with creating a sufficient surface charge on the substrate. Polyanions and polycations are then alternately deposited onto the charged surface. A rinsing step is included between the two adsorption processes in order to remove excess as well as to prevent cross-contamination between the polyelectrolyte solutions. The phenomenon of strong electrostatic attraction between charged surfaces and oppositely charged molecules in solution is understood to be the dominant factor in the adsorption of polyelectrolytes.[2,3,15-17] The ESA process is comprised of these simple steps. The adsorption steps can be repeated cyclically to form multilayer structures on the surface of a substrate.[1]

Textile materials are just beginning to be considered as substrates for the layer-by-layer assembly of polyelectrolytes. The ESA technique offers the possibility to tailor the surface properties of textile fibers by depositing nanolayers of polyelectrolytes, charged nanoparticles, and non-reactive dyes in a controlled manner. ESA will allow control over characteristics such as selectivity, diffusivity, and permeability. This creates the possibility of developing functional textiles for protective clothing and selective filtration applications. The purpose of this experimental work was to determine the feasibility of using the ESA deposition process on polyester fabric substrates and the effect of plasma pre-treatment on the ESA process.

5.2 Experimental

5.2.1 Polyelectrolytes

The polyelectrolytes, poly(sodium 4-styrene sulfonate) (PSS), Mw 70000, and poly(allylamine hydrochloride) (PAH) Mw 70000, were purchased from Aldrich (St. Louis, MO) and were used as received. Aqueous solutions of the polyelectrolytes were made using deionized water at concentrations of 5 mM/L. Previous reports have shown that this polyelectrolyte system is capable of forming self-organized films on a number of different substrates including textile fibers and fabrics.

5.2.2 Substrates

The polyester samples used in this study were knit fabrics. The fabric (scoured, TIC 729, 95-53) was obtained from SDL Textile Innovators Corporation. The samples were cut into approximately 1 inch x 1 inch squares and labeled before being treated.

5.2.3 Substrate Preparation

Helium and oxygen plasma mixtures were used to modify the surface of the polyester samples. Helium and oxygen mixtures have gained interest in plasma treatments due to their ability to produce surface oxidation and at the same time cause a cross linking reaction. Together, these two mechanisms are expected to produce a reactive surface with good stability in regards to ageing.

A Plasmatic Systems, Inc. (North Brunswick, NJ) PLASMA-PREEN 1 was used to plasma treat the polyester samples. The PLASMA-PREEN 1 is a plasma etching system. The system is manufactured from a microprocessor controlled microwave oven and uses the

built in digital controls of the oven. The system was equipped with a quartz-made barrel type process chamber that measured 4.1 inches in diameter and 6.0 inches long.

The PLASMA-PREEN 1 system works by allowing the process gas into the process chamber at reduced pressures (1 to 5 Torr). The plasma discharge is excited by the microwave energy from the microwave oven. The process creates ionized gas species and free radicals within the gas. These active species then react with the sample in the chamber. The PLASMA-PREEN 1 has a power range from 100 up to 750 watts and operates at 2.45 GHz. The polyester fabric was placed into the glass reactor and then treated using different mixtures of helium-oxygen. Batches of 20 1 inch x 1 inch samples were placed in the process chamber and then treated.

Helium and oxygen were provided by Machine & Welding Supply Company (Raleigh, NC). Aalborg mass flow-meter/controllers were used to measure and control the gas flow rate. The pressure within the chamber was measured with a Supco VG64 digital vacuum gauge. The glass reactor was pumped using a Precision Scientific vacuum pump to a typical pressure of 1.0 Torr.

Four different gas mixtures were used for this study: (1) 100% He (2) 20% He / 80% O (3) 50% He / 50% O (4) 80% He / 20% O. The 100% He samples were treated for 1 minute with a power level of 10 and a duty cycle of 10. The samples for the remaining three mixtures were treated for 1 minute with a power level of 10 and a duty cycle of 0. The change in duty cycle was implemented to prevent thermal degradation of the samples. PET film was initially used to test feasibility of the technique and to determine the optimum operation conditions. Untreated PET film is hydrophobic while plasma treated PET film

becomes hydrophilic. The settings on the PLASMA-PREEN 1 were adjusted until the PET film samples exhibited hydrophilic characteristics by measuring the contact angle of water on the film. After the settings were verified, the polyester fabric was treated. Three sets of twenty fabric samples were prepared for each mixture. After treatment, the polyester samples were placed in Ziploc® bags for storage until they were used in the deposition process.

5.2.4 Polyelectrolyte Layer Deposition

Thirty-two glass Petri dishes were used for the deposition. The dishes were laid out in an array of four by eight dishes in order to facilitate the deposition process. The first row of dishes contained the anionic polyelectrolyte solution, PSS; the second and fourth rows contained deionized water for rinsing; and the third row contained the cationic polyelectrolyte solution, PAH. The Petri dishes were filled to a level that would completely immerse the PET fabric samples. Solutions were discarded and replaced when they became cloudy after use. Unused dishes were kept covered in order to prevent evaporation and contamination of the polyelectrolyte solution.

Rinsed samples were placed in the first PSS dish for five minutes. Tweezers were used to transfer the sample to the next dish containing deionized water. The sample was rinsed for five minutes and then moved to the next dish containing PAH. After five minutes, the sample was transferred to the next dish containing deionized water to be rinsed again for five minutes. This process was continued until a total of twenty polyelectrolyte layers had been deposited on the PET substrate. Therefore, the final samples with twenty layers contain

ten layers of PSS and ten layers of PAH that alternate. Samples were dried at room temperature for a period of 24 hours before being placed in Ziploc® bags for storage until they were analyzed.

5.2.5 XPS Measurements

XPS measurements were conducted using a Kratos AXIS Ultra spectrometer with an Al source and a spherical mirror analyzer working in spectrum mode. The total pressure in the main vacuum chamber during analysis was typically 4 x 10-7 Torr. Spectra were collected with the stage containing the samples at 0°. The take-off angle of the electrons was 90° and the angle of the incident X-rays hitting the sample was 30°. The chemical elements present on the samples were identified from survey spectra. Survey scans were of the spectrum type with an Al reference. The survey scans started at 1200 eV and ended at -5 eV taking 1 eV steps with a dwell time of 200 ms. High resolution scans were performed around peaks of interest.

5.2.6 TEM Analysis

TEM images were obtained using a Hitachi HF-2000 system using a cold field emission electron source with an accelerating voltage of 200 kV. This type of source creates an electron beam that minimizes the energy spread and exhibits strong stability allowing high microscope resolution. The TEM system was equipped with an Advanced Microscopy Techniques XR-60B camera system for digital imaging. PET fiber specimens were prepared

by pulling individual fibers from the top of the fabric samples using tweezers. Loctite® super glue gel was used to attach the ends of the fibers to copper 200 mesh grids.

5.3 Results and Discussion

5.3.1 XPS Measurements

X-ray photoelectron spectroscopy was used to examine the surfaces of the knit PET fabric samples. Figure 5.1 illustrates a survey spectrum for an unmodified sample of plasma treated (80% He / 20% O) polyester fabric. Large peaks can be seen at 281.91 eV and 528.91 eV demonstrating the presence of carbon and oxygen respectively. A survey spectrum of a 20-layer PSS/PAH polyelectrolyte film supported on a knit plasma treated polyester fabric can be seen in Figure 5.2. Well-defined peaks can now be seen at 398.91 and 164.91 eV. These peaks represent the presence of N and S and these elements come from the PAH and PSS respectively. A comparison of Figures 5.1 and 5.2 shows that XPS spectra can be used to observe the electrostatic deposition of the polyelectrolytes onto the polyester fabric.

Figure 5.3 shows the C/O counts per second (cps) ratio as a function of the number of deposited nanolayers. As the number of layers increases, the C/O ratio becomes more uniform. The O present on the samples is a result of the chemical structure of the polyester. Increasing the number of polyelectrolyte layers causes a decrease in the amount of O present on the surface of the fabric. Large initial increases in the C/O ratio can be seen. This behavior is similar to that of the PSS/PAH system on natural fiber substrates.[6] The results

for the deposition of PSS and PAH onto polyester fabric are comparable to the results for the same polyelectrolyte system on substrates of polyester film.[13,14]

Figures 5.4 and 5.5 illustrate the N/O and S/O ratios respectively. A large variance is again seen for the initial layers in a similar pattern as that exhibited by the C/O ratio of Figure 5.1. This behavior is similar to that reported when working with other types of textile substrates. The high degree of non-uniformity of the polyester fabric explains this variance in the early polyelectrolyte layers. Eventually, both the N/O and S/O ratios gradually level off as the number of layers deposited increases. This is in agreement with previously published reports.[13,14,16,18]

XPS analysis was also used determine if the nanolayers of polyelectrolytes were deposited over the polyester fabric samples in a self-organized and ordered manner. In order to determine the stratification of the polyelectrolytes, a plot of the N/S ratios was generated from the XPS survey spectra as shown in Figure 5.6. The alternating behavior of the N/S ratio as a function of the number of layers demonstrates the stratification of the deposited layers as previously reported for electrostatic self-assembly of PSS/PAH layers on natural and synthetic substrates. This behavior is in agreement with published data and it is due to the fact that samples with PAH on top have higher N/S ratio than the samples with PSS on top. Once again, large amounts of variance can be seen for the initial layers while higher layers exhibit a more level trend.

The XPS spectra of plasma treated knit polyester samples supporting alternating layers of PSS and PAH are in quantitative agreement to spectra obtained in previous studies involving ESA films of PSS and PAH on both natural and synthetic substrates.[6,13,14]

Due to the high surface heterogeneity of the polyester fabric substrates, a thorough full factorial statistical analysis of the substrate preparation procedure was implemented. The four different ratios of He and O gas mentioned previously were evaluated. The objective of these experiments was to determine the reproducibility of the technique as well as to quantify the effect of the plasma treatment on the electrostatic self-assembly deposition process.

Figure 5.7 illustrates the C/O cps ratio as a function of the number of deposited nanolayers for the four different plasma treatment procedures. The average value of the C/O cps ratio as well as bars indicating the standard error are also presented in Figure 5.7

Based on the experimental results, it was observed that no statistical significant differences existed between the four plasma treatment procedures. Figures 5.8 and 5.9 validate this assessment as they show a similar trend for the evolution of the N/O and S/O ratios as the number of nanolayers deposited increased. The ratios of gas used for plasma treatment do not appear to affect the electrostatic self-assembly deposition of nanolayers. This behavior is in agreement with the nature of electrostatic self-assembly indicating that the deposition process is robust and can self-adapt to heterogeneous surfaces.

5.3.2 TEM Imaging

Figure 5.10 shows a TEM image of a polyester fiber coated with 20 polyelectrolyte layers. The multilayer film can be seen to provide uniform conformal coating to the surface of the fiber and it is estimated to be approximately between 400 nm in thickness. Figure 5.11 shows a higher resolution image of the top layer of the polyelectrolyte film, which is PAH. The outermost layer can again be seen in Figure 5.12. Clear boundaries can be seen between

the top layer of PAH and the layer of PSS underneath. The polyelectrolyte layers are approximately 20 nm thick.

The difficulties involving direct measurement of individual nanolayers films have been documented elsewhere. These problems are compounded when using substrates with high curvature, in this case polyester fibers. The samples used in this study posed their own unique problems due to the instability of the polyester fibers when exposed to the electron beam. The following TEM images allow the outermost layers to be directly measured and provide direct proof of the deposition of the polyelectrolytes and their ability to adhere to the non-uniform surface of polyester fibers.

5.4 Conclusions

The ESA process was used to deposit alternate nanolayers of PSS and PAH on polyester fabric substrates. Plasma treatment of the samples with mixtures of He and O gas was shown to be a successful method of charging polyester fabrics in order for them to support polyelectrolyte thin films. XPS and TEM provided direct and indirect evidence of the effectiveness of the deposition process. In addition, quantitative agreement of the N/S ratio with previously published data using natural and synthetic substrates further confirms the belief that ESA is greatly dependent on the nature of the polyelectrolyte system that is used and not as dependent on the underlying substrate. The results of this experimentation demonstrate that ESA could be used to develop surface functional textile products for a number of different applications.

5.5 Acknowledgements

This research work has been supported through a research grant from The Institute of Textile Technology and the NCSU Faculty Research and Development Fund.

5.6 References

1. Decher, G., Fuzzy Nanoassemblies: Toward Layered Polymeric Multicomposites. *Science* **277**, 1232-1237 (1997).

2. Hammond, P., Recent Explorations in Electrostatic Multilayer Thin Film Assembly. *Curr Op Coll Inter Sci*. **4,** 430-442 (2000).

3. Ulman, A., Formation and Structure of Self-Assembled Monolayers. *Chem Rev* **96**, 1533-1554 (1996).

4. Mendelsohn, J.D., et al., Fabrication of microporous thin films from polyelectrolyte multilayers. *Langmuir* **16**, 5017-5023 (2000).

5. Yoo, D., et al., New electro-active self-assembled multilayer thin films based on alternately adsorbed layers of polyelectrolytes and functional dye molecules. *Synthetic Metals* **85**, 1425-1426 (1997).

6. Hyde, K., J. Hinestroza, and M. Rusa, Layer-by-layer deposition of polyelectrolyte nanolayers on natural fibers: cotton. *Nanotechnology* **16**, S422-S428 (2005).

7. Decher, G., Polyelectrolyte Multilayers, an Overview, G. Decher and J. Schlenoff, Editors. Wiley-VCH, 1-46 (2003).

8. Decher, G., et al., Layer-By-Layer Adsorbed Films Of Polyelectrolytes, Proteins Or Dna. *Abstracts Of Papers Of The American Chemical Society* **205**, 334- (1993).

9. Decher, G., Y. Lvov, and J. Schmitt, Proof of Multilayer Structural Organization in Self-assembled Polycation-Polyanion Molecular Films. *Thin Solid Films* **244**, 772-777 (1994).

10. Bertrand, P., et al., Ultrathin Polymer Coatings by Complexation of Polyelectrolytes at Interfaces: Suitable Materials, Structure, and Properties. *Macromol Rapid Commun* **21**, 319-348 (2000).

11. Caruso, F., et al., Ultrathin Multilayer Polyelectrolyte Films on Gold: Construction and Thickness Determination. *Langmuir* **13**, 3422-3426 (1997).

12. Losche, M., et al., Detailed Structure of Molecularly Thin Polyelectrolyte Multilayer Films on Solid Substrates as Revealed by Neutron Reflectometry. *Macromolecules* **31**, 8893-8906 (1998).

13. Chen, W. and T. McCarthy, Layer-by-Layer Deposition: A Tool for Polymer Surface Modification. *Macromolecules* **30**, 78-86 (1997).

14. Delcorte, A., et al., Adsorption of polyelectrolyte multilayers on polymer surfaces. *Langmuir* **13**, 5125-5136 (1997).

15. Lvov, Y., G. Decher, and M. H., Assembly, Structural Characterization, and Thermal Behavior of Layer-by-Layer Deposited Ultrathin Films of Poly(vinyl sulfate) and Poly(allylamine). *Langmuir* **9**, 481-486 (1993).

16. Phuvanartnuruks, V. and T. McCarthy, Stepwise Polymer Surface Modification: Chemistry-Layer-by-Layer Deposition. *Macromolecules* **31**, 1906-1914 (1998).

17. Tieke, B., et al., Ultrathin Self-assembled Polyelectrolyte Multilayer Membranes. *Eur Phys J E* **5**, 29-39 (2001).

18. Levasalmi, J. and T.J. McCarthy, Poly(4-methyl-1-pentene)-Supported Polyelectrolyte Multilayer Films: Preparation and Gas Permeability. *Macromolecules* **30**, 1752-1757 (1997).

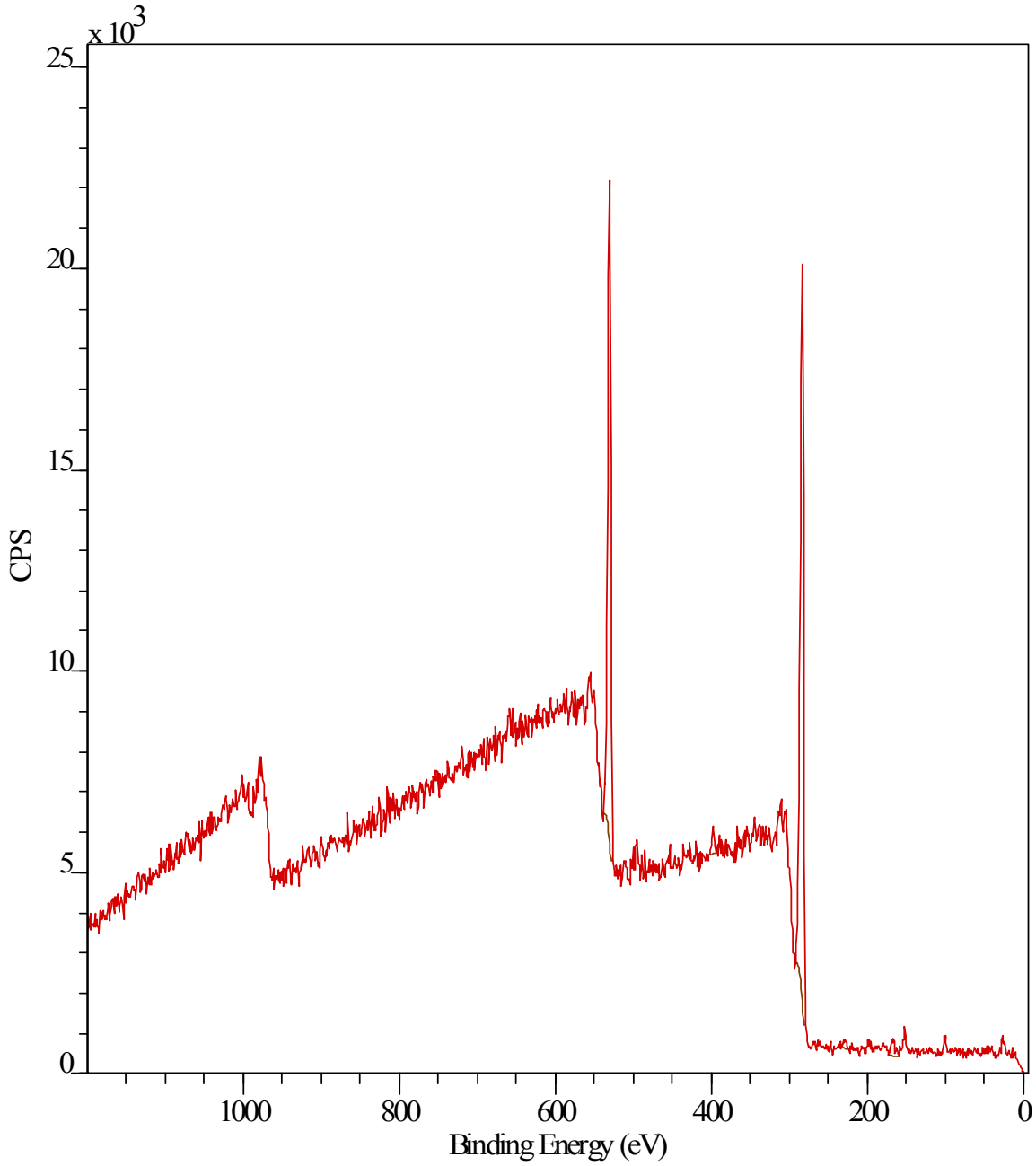

Figure 5.1. XPS spectra for plasma treated (80% He / 20% O) knit polyester fabric.

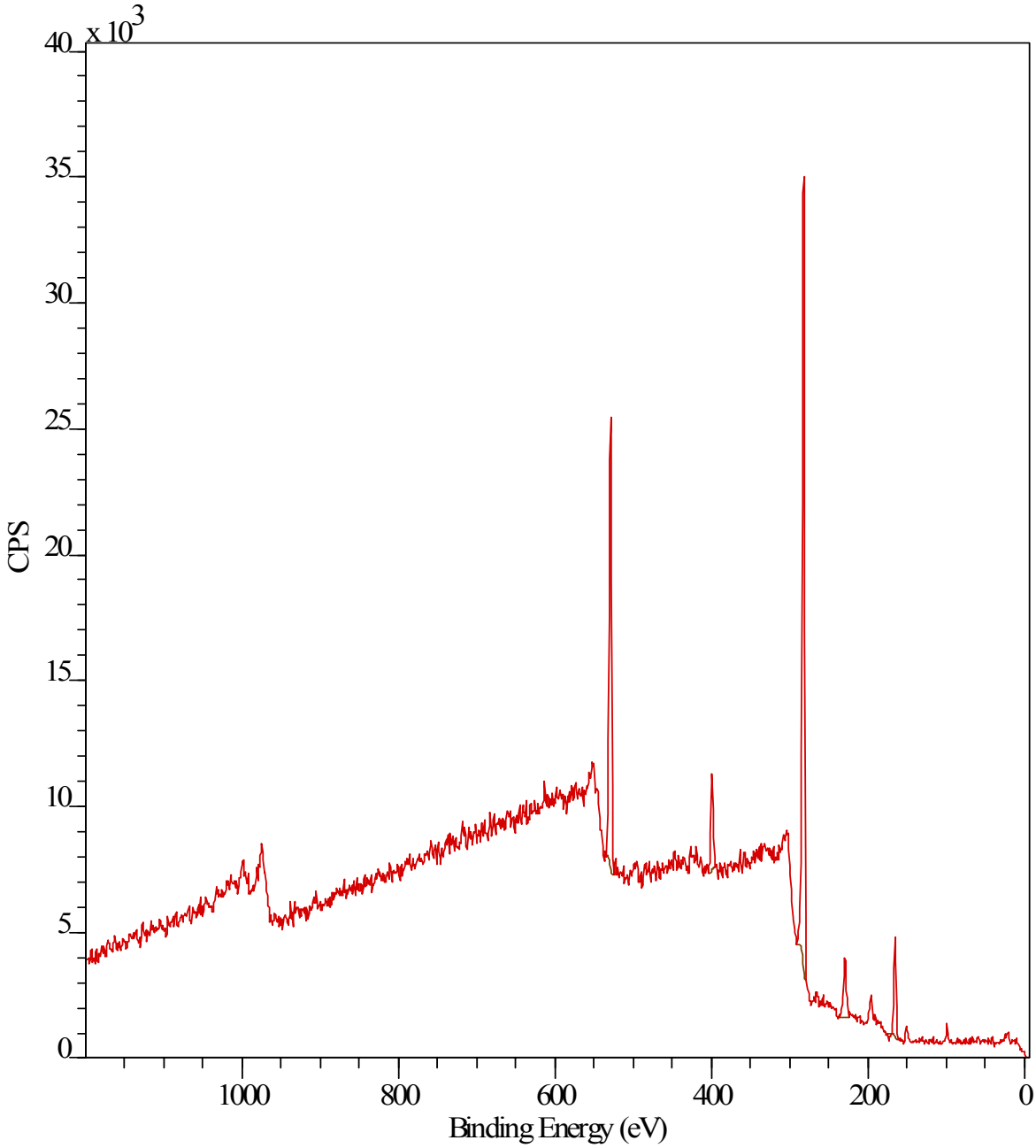

Figure 5.2. XPS spectra for plasma treated (80% He / 20% O) knit polyester fabric supporting 20 self-assembled layers of PSS/ PAH.

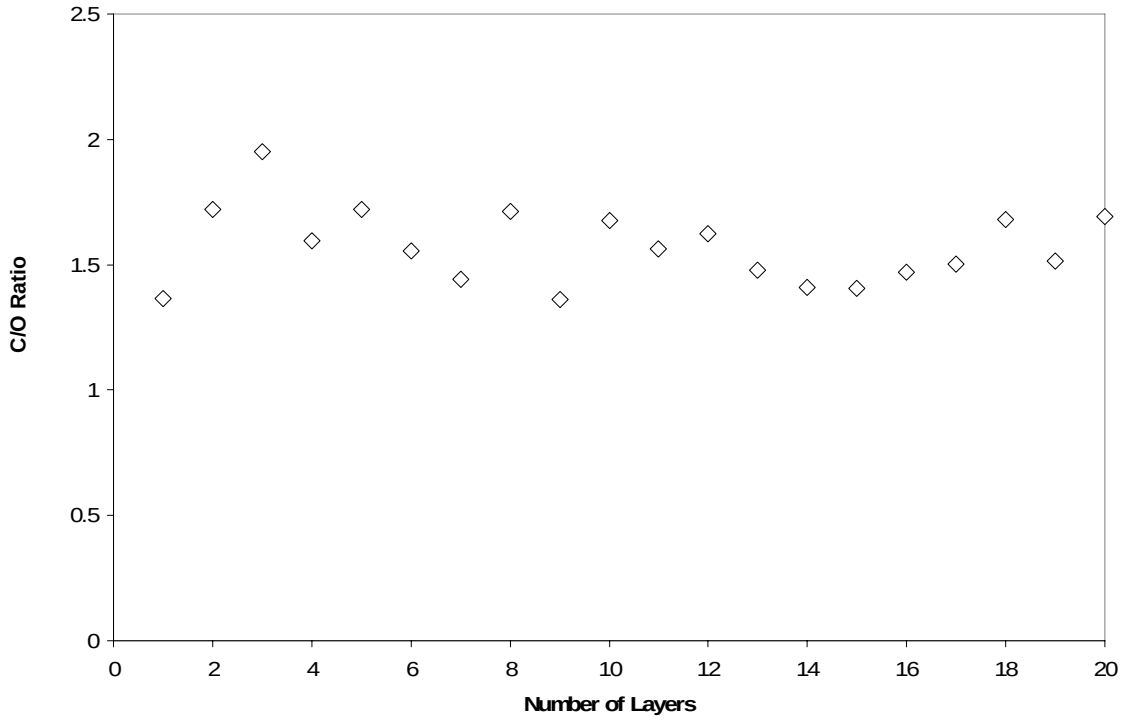

Figure 5.3. C/O ratio for knit polyester samples coated with PSS/PAH layers.

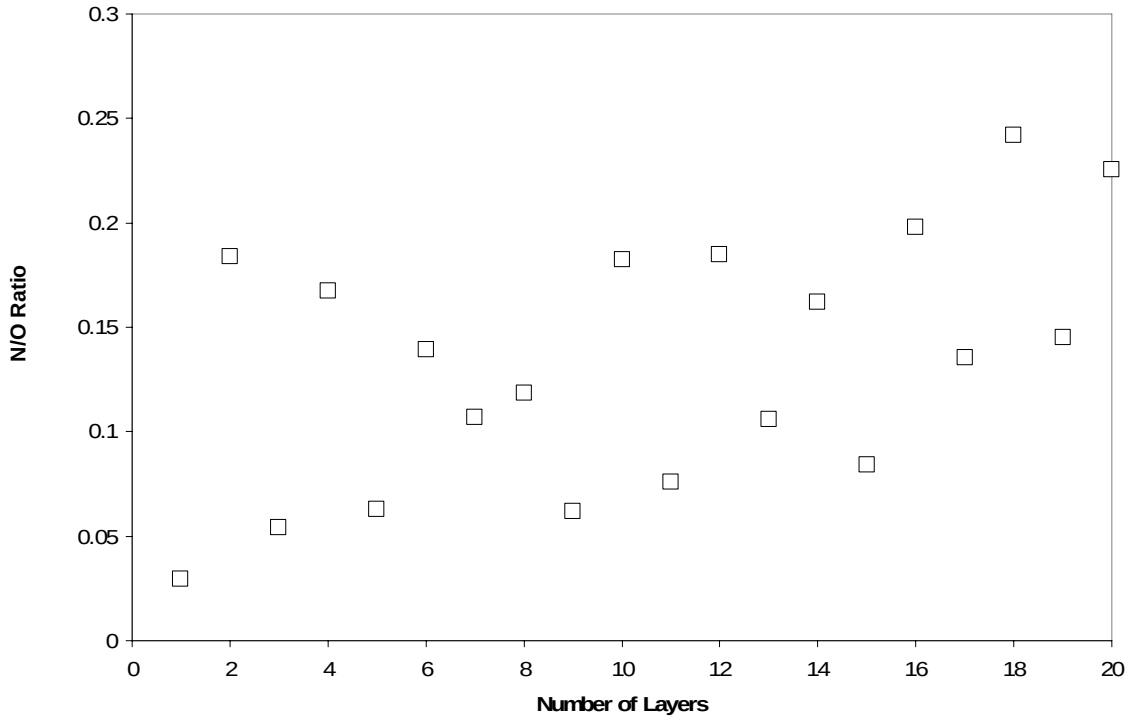

Figure 5.4. N/O ratio for knit polyester samples coated with PSS/PAH layers.

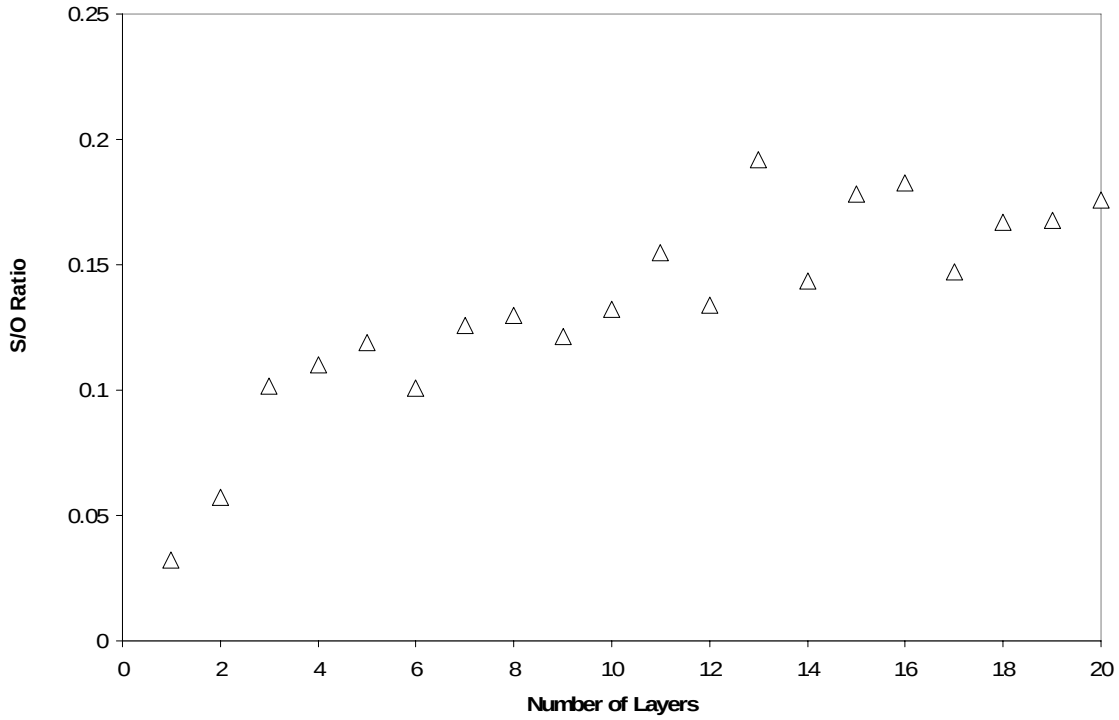

Figure 5.5. S/O ratio for knit polyester samples coated with PSS/PAH layers.

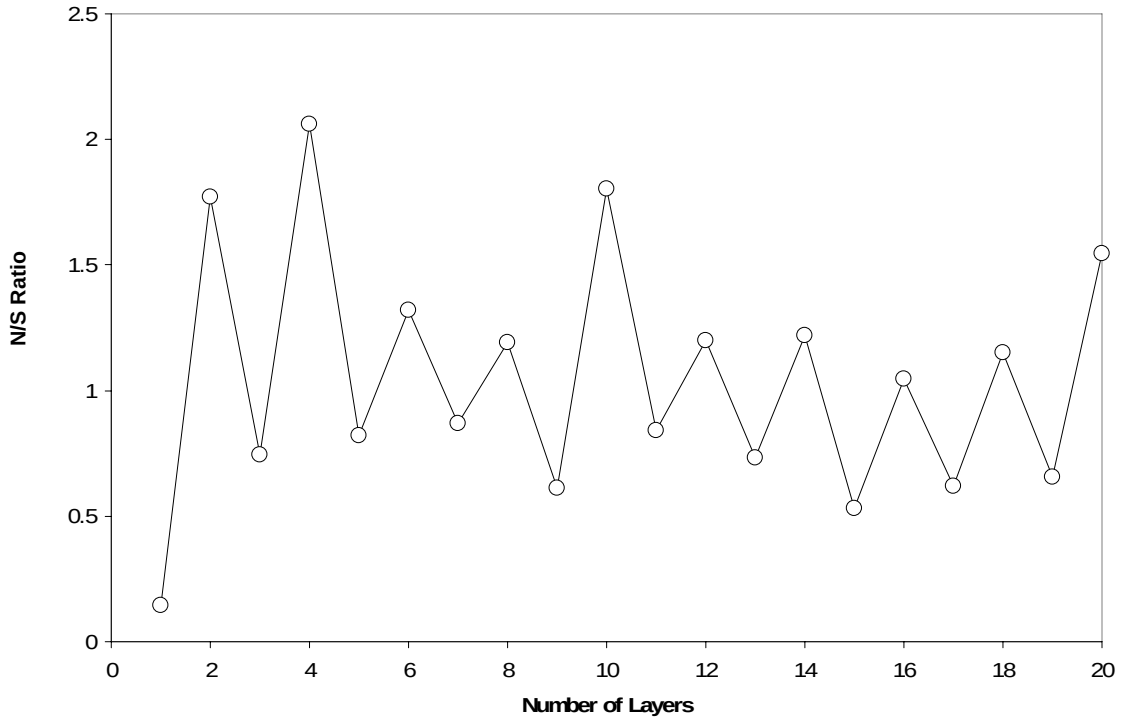

Figure 5.6. N/S ratio for knit polyester samples coated with PSS/PAH layers.

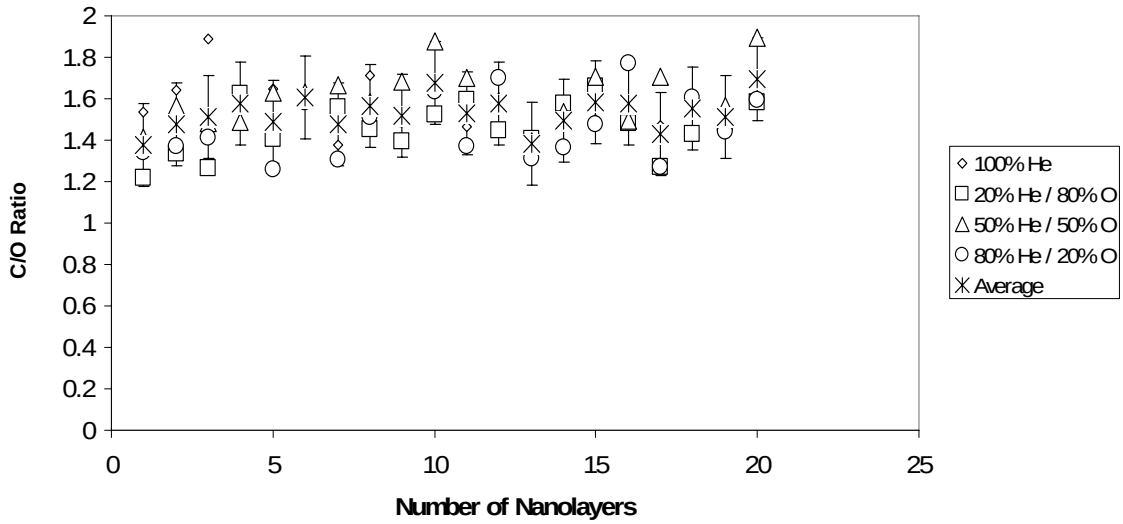

Figure 5.7. C/O cps ratio as a function of the number of deposited nanolayers for four different plasma treatment procedures.

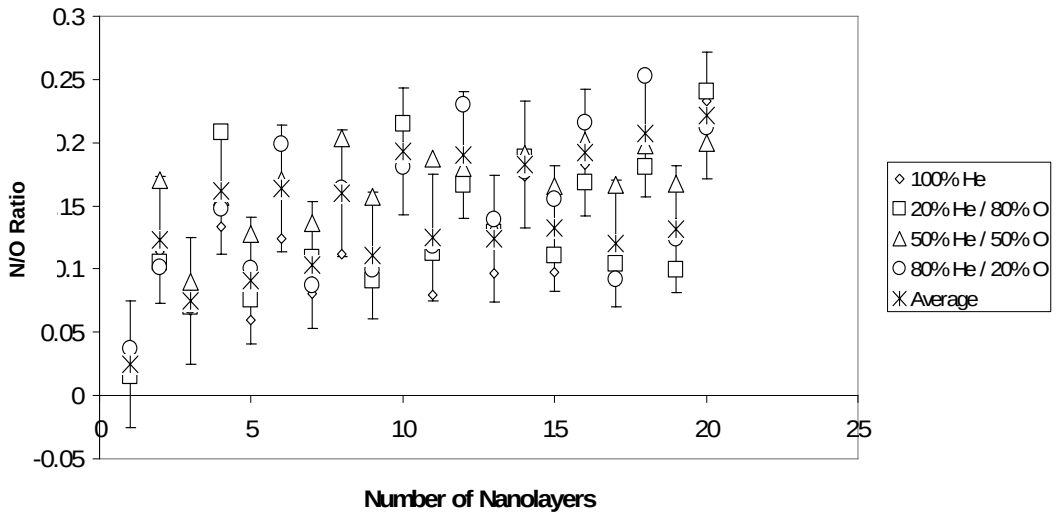

Figure 5.8. N/O cps ratio as a function of the number of deposited nanolayers for four different plasma treatment procedures.

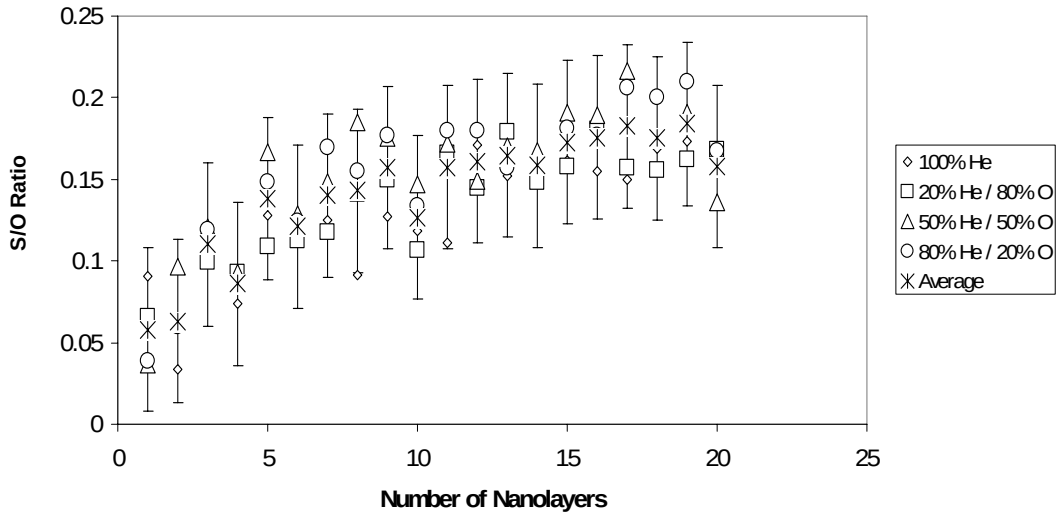

Figure 5.9. S/O cps ratio as a function of the number of deposited nanolayers for four different plasma treatment procedures.

Figure 5.10. Planar TEM image of a polyester fiber coated with a multilayer PSS/PAH film.

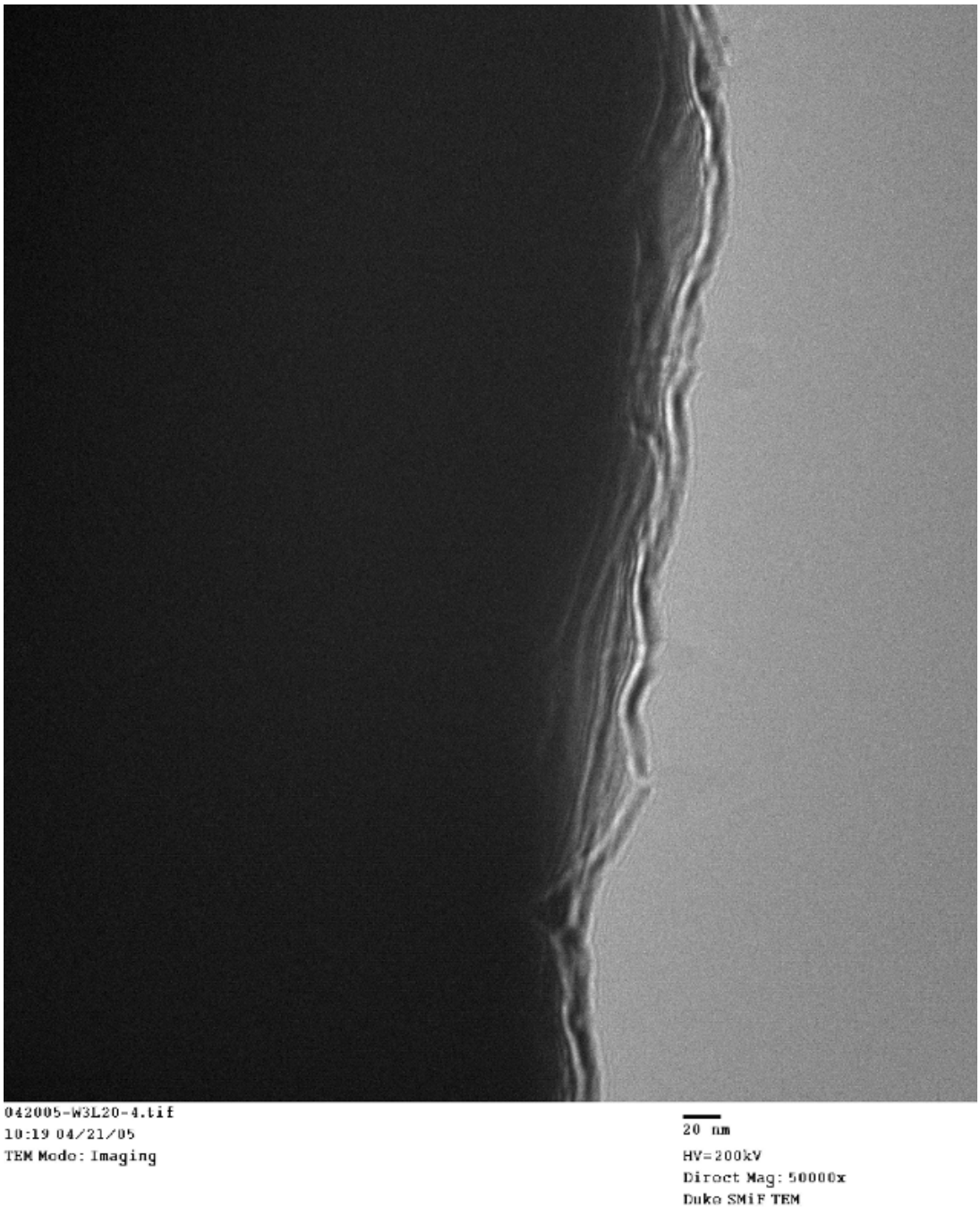

Figure 5.11. High resolution planar TEM image of a polyester fiber coated with 20 layers of PSS/PAH film.

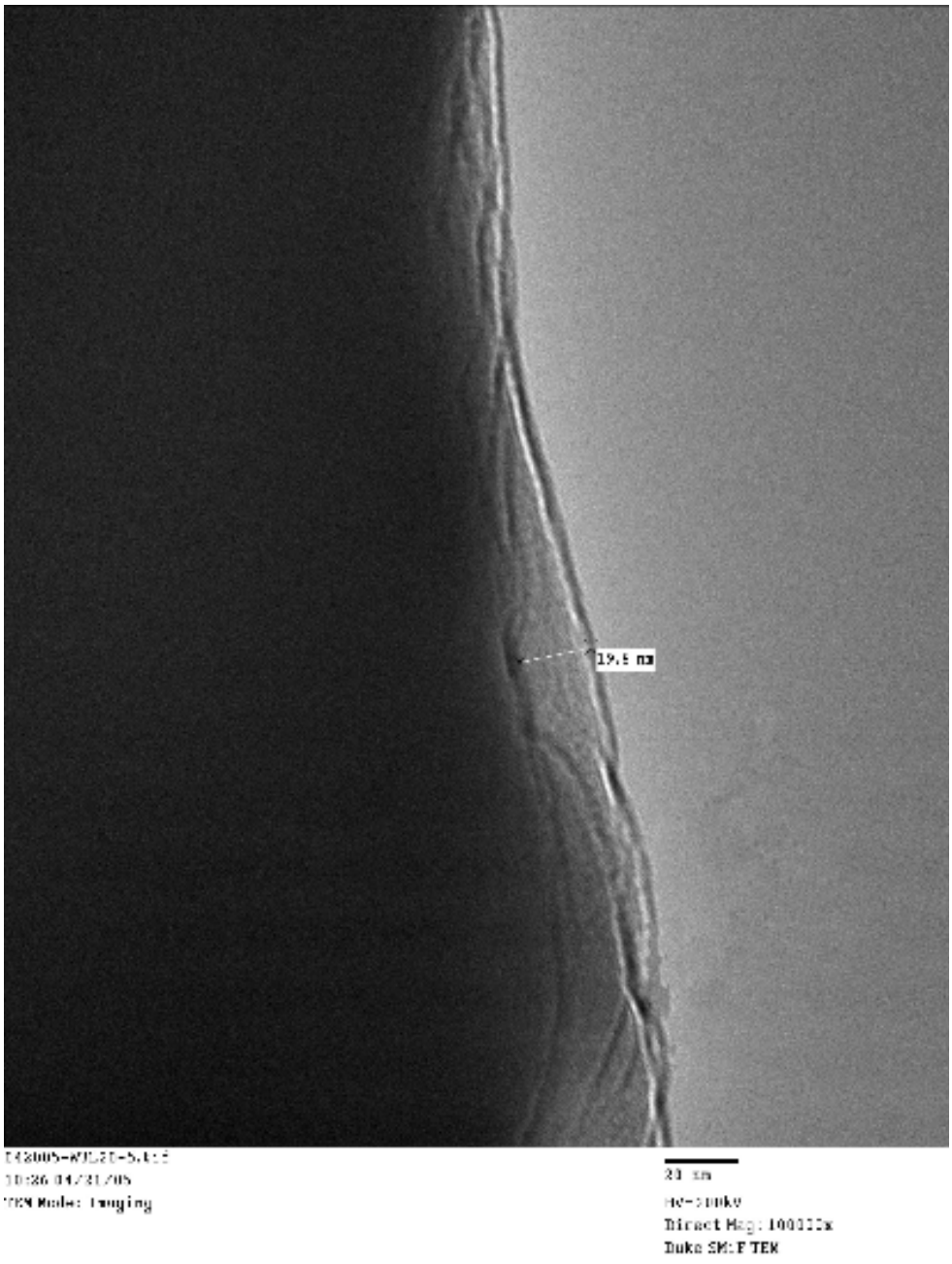

Figure 5.12. High resolution planar TEM image of a polyester fiber coated with 20 layers of PSS/PAH film.

Chapter 6 is a reprint of a paper submitted to Langmuir

Atomic Layer Deposition of Conformal Inorganic Nano-scale Coatings on Three-Dimensional Natural Fiber Systems: Effect of Surface Topology on Film Growth Characteristics

G. Kevin Hyde[1], Kie Jin Park[2], S. Michael Stewart[2], Juan P. Hinestroza[3], and Gregory N. Parsons[2*]

[1]*Department of Textile Engineering, Chemistry, and Science*
[2]*Department of Chemical and Biomolecular Engineering*
North Carolina State University, Raleigh, NC 27695

[3]*Department of Textiles and Apparel*
Cornell University, Ithaca, NY 14853

Abstract

Atomic-scale material deposition is utilized to achieve uniform coverage and modify the surface properties of natural fiber and woven fabric materials, where irregular nano-scale features are imbedded in a macroscale interpenetrating fiber network. The complex surface topology of the woven fabric results in significantly different film growth thickness per ALD cycle as compared to planar surfaces coated using the same process conditions, likely due to reactant adsorption within the fiber starting material, as well as impeded reactant transport out of the fabric system during the purge cycle. Cotton textiles modified with conformal nano-scale Al_2O_3 are found to show extreme hydrophobic effects, distinctly different from planar surfaces that receive the same coatings. The results highlight key concerns for achieving controlled conformal coatings on complex surfaces, and open the possibility for

new textile finishing approaches to create novel fabric-based materials with specialized function and performance.

Specific Contribution

For this manuscript, I worked with Dr. Kie Jin Park and Michael Stewart to plan and construct a reactor designed for the low temperature deposition of aluminum oxide. I helped in ordering parts for the reactor and then with the actual construction of the reactor system. Together with Dr. Park, I helped test the new system to ensure it was operating correctly. I was responsible for writing the operating instructions for the reactor. I also contributed to the general maintenance of the reactor. After the preliminary experiments were completed, I prepared the cotton samples coated with aluminum oxide. I also prepared silicon samples with the cotton samples that the growth characteristics could be compared for the two different substrates. I was trained to use the ellipsometer so that the film thickness could be measured for the silicon samples. I worked with Dr. Park to determine the optimum conditions for deposition onto the cotton substrates. We then developed a series of experiments to carry out. Michael Stewart and I worked together to create all of the samples. After the samples were done, I was responsible for XPS and planar TEM analysis of the samples. I prepared samples for cross-sectional TEM and sent them to Dr. Hinestroza's group. I worked with Dr. Park and Michael to analyze the results. I then wrote the manuscript and have revised the manuscript based on the reviews of referees from the journal Small. I then submitted the manuscript to Langmuir. This work helped determine the feasibility of using ALD as a modification technique for textile materials and also studied the nature of the deposited films over complex substrates.

Chapter 6: Atomic Layer Deposition of Conformal Inorganic Nano-scale Coatings on Three-Dimensional Natural Fiber Systems: Effect of Surface Topology on Film Growth Characteristics

6.1 Introduction

More than 6,000 years ago the Egyptians learned to spin natural cellulosic and proteinaceous fibers, including cotton and wool, into bundled yarns and weave the yarns into fabrics for clothing and other uses.[1] During the 19th Century, wet chemical treatments such as mercerization and bleaching were developed to improve fabric color and luster, strength, and resistance to organic degradation.[2] Currently, there is need for new multifunctional textiles with performance that extends well beyond traditional materials for advanced apparel, medical devices, military and other specialty applications.[3-8] Of particular interest are new materials that can protect against mechanical, chemical, biological and thermal exposure, and effectively repel undesirable foreign substances, while maintaining the benefits of light-weight breathable fabrics. Textile materials that can modify light absorption, reflection, or emission, change electrical conductivity, or control the release or immobilization of active chemical compounds are also of interest. Inorganic coatings on fibers are capable of meeting some of these objectives.[3] Inorganic coating methods including sol-gel[5-7,9] and solution immersion[8,10-12] have recently been studied for surface finishing of textile products, but these and other liquid-based practices require laborious drying and/or curing steps that demand significant energy use and create large amounts of waste. Moreover, the uniformity of conventional coating processes on fiber surfaces are often not ideal, resulting in detrimental variations in material performance which can

severely limit applications.[3,8,13,14] New methods for conformal inorganic coating onto complex textile topologies could improve material performance in new applications, and significantly broaden the scope of this early traditional technology for new functional systems.

Atomic layer deposition (ALD) involves a binary series of vapor-phase self-limiting deposition chemical reactions to form highly uniform coatings of metals and metal oxides with thickness controlled at the atomic-scale.[15,16] For ALD processing, the surface temperature is typically less than that for chemical vapor deposition, and in some cases, ALD can be readily performed at 100°C or less,[17-20] making it an attractive approach for coating thermally sensitive materials. This method can be used to deposit highly conformal coatings with precise thickness and composition over large scales and onto substrates with complex topologies. Moreover, the ALD process is sufficiently flexible that it can used to fabricate layers of metals, metal oxides, metal nitrides and other materials.[19,21,22] Vapor phase processes, including atmospheric pressure plasma exposure, are currently used for textile modification and can be scaled to the rates required for high throughput processing,[23-27] but they often result in non-uniform surface modification. Vapor phase methodologies that can fully penetrate the network could be used, for example, to increase robustness, heat and fire resistance, and improve durability and cleaning, as well as enable electronic conduction, and catalytic and biocidal activity. Recent studies have demonstrated the ability of ALD to coat temperature sensitive substrates of wool fibers,[28,29] cellulose-based papers,[28,30] and polymers.[18,29] In this work, we have used spectroscopic and cross-sectional imaging techniques to examine the nature of the nano-scale conformality on the complex surface

topology of natural fibers. Film growth rate on cotton is also assessed and compared to the rate on planar substrate surfaces obtained with the same process conditions.

Metal oxides are of interest for their chemical and electrical function. For example, tin oxide is visibly transparent and can conduct charge for applications in photovoltaic cells, liquid crystal displays, and light-emitting diodes. Titanium dioxide is a wide band-gap semiconductor that can act as a good oxidizing agent for photo-excited molecules and/or functional groups in photocatalysis and photovoltaic cells, and has unique gas sensing capabilities. Al_2O_3 is also of interest as an insulator for electrical applications and for barrier properties with controllable levels of permeability on polymer substrates.[16,18,31] In certain applications, the working area of these oxide surfaces affect the sensitivity and overall device efficiency. Methods to produce conformal coatings of metals and metal oxides onto complex high surface-area networks of textile-based fibers are not currently available, but could enable unique material integration solutions and provide new functional platforms for high surface area device operation.

Atomic layer deposition can be used to form coatings on planar and irregular non-planar surfaces. When scaling ALD from two to three dimensions, it is necessary to account for the increased surface area which must be coated, and for the increased time for reactant and product species diffusion in and out of the reaction zone. Natural fabric systems, where irregular nano-scale features are imbedded in a macroscale interpenetrating fiber network, offer a unique challenge to hybrid material coating technologies. In this article, atomic layer deposition is demonstrated as an approach for highly conformal and uniform coatings of aluminum oxide onto natural textile fibers and fabrics. Examination of growth on planar and

three-dimensional cotton surfaces gives important insight into fundamental chemical process issues on complex material surfaces.

6.2 Experimental Procedure

Atomic layer deposition was applied to silicon and woven bundles of natural cotton fibers to form conformal coatings of Al_2O_3 with precisely controlled thickness. The cotton fabric had been previously treated with chlorine bleach to remove unwanted contaminants and to whiten the cotton fibers, and it underwent mercerization which includes immersion in caustic soda followed by neutralization with acid. Mercerization is commonly performed to increase luster, strength, dye affinity, resistance to mildew, and to reduce lint. Fiber-based fabric ~1 mm thick was cut into samples approximately 2 cm x 2 cm for deposition experiments. Silicon wafers (n+ type, MEMC Electronic Materials, Inc.) were also cut into 2 cm x 2 cm pieces and cleaned by wet chemical treatment (BakerClean® JTB-100) to produce a hydroxylated silicon oxide surface. An aluminum sample boat was used to hold one of each sample substrates in the reactor during deposition.

For these studies, atomic layer deposition of aluminum oxide was performed in a hot-wall viscous-flow tube reactor described elsewhere.[20] Trimethylaluminum (TMA) (98%, Strem Chemical, Inc.) and deionized water were used as reactants for the deposition of Al_2O_3. TMA is a liquid with a vapor pressure of ~9 Torr at 20ºC. The reactant lines were heated to 60°C in order to prevent condensation of water. Directly before deposition process, the substrates were placed in the reactor and heated in vacuum ($5x10^{-7}$ Torr) to ~100°C and allowed to equilibrate for 60 minutes. To begin deposition, the reactor was flushed with

argon, and ambient temperature vapors of TMA and water were separately introduced into the reactor in pulses of 1 and 2 seconds respectively, with a 20 second Ar purge between each reactant exposure step. The TMA and water were carried into the reactor using Ar flow, and the Ar flow rate was constant at 100 standard cubic centimeters per minute (sccm). The pressure was fixed between 0.5 and 1 Torr using a variable orifice valve downstream from the reactor. The substrate temperature was held constant between 75°C and 200°C. At ~150°C or higher, the cotton substrates were observed to be discolored and physically brittle after deposition, likely due to a combustion reaction between the fiber and oxygen in the water reactant. Therefore, results reported here for deposition on cotton were obtained from runs done at ≤100°C. An operating temperature of 100°C is sufficient for adequate deposition of Al_2O_3 and is low enough to limit damage to the cotton fibers.

Aluminum oxide deposition by thermal ALD using TMA and H_2O is one of the most well understood ALD systems on planar substrate surfaces.[16] The growth mechanism is based on the chemisorption of $Al(CH_3)_3$ on –OH surface groups. This reaction forms adsorbed $(\text{-O-})_n Al(CH_3)_{3-n}$ with CH_4 as a by-product. The H_2O then recreates –OH surface groups by oxidation of the Al while also forming CH_4. For the deposition of Al_2O_3 on cotton with TMA and H_2O, the growth mechanism likely follows this process. Cellulose fibers $(C_6H_{10}O_5)_n$ are the primary constituent in natural cotton, and the cellulose polymer presents a large number of –OH groups on the surface to react with the TMA.

Ellipsometry was used to examine the Al_2O_3 films deposited on the Si substrates. A Rudolph Technologies Inc., Auto EL ellipsometer was used to conduct the measurements

with an incidence angle of 75°. Three measurements were made at random spots on each sample in order to analyze the uniformity of the Al_2O_3 films.

Transmission electron microscopy (TEM) was used for characterizing film conformality and uniformity. TEM also allowed the thickness of the layers on the coated fibers to be determined. TEM images were obtained using a Hitachi HF-2000 system using a cold field emission electron source with an accelerating voltage of 200 kV. This type of source creates an electron beam that minimizes the energy spread and exhibits strong stability allowing high microscope resolution. The TEM system was equipped with an Advanced Microscopy Techniques XR-60B camera system for digital imaging. Planar samples were prepared by randomly pulling individual fibers from the cotton fabrics using tweezers. The fibers were mounted to 200 mesh Cu grids using double sided tape. A second grid was then placed on top to hold the fibers between the grids. Cross-sectional TEM samples were prepared by embedding fabric samples in resin. Spurr low viscosity embedding medium (Ladd Research Industries), which is based on ERL 4221, was used to prepare the samples. Samples were cured for 12 hours at 70°C. The embedded samples were then sectioned by microtome and attached to Cu grids using an adhesive.

X-ray photoelectron spectroscopy (XPS) was performed using a Kratos AXIS Ultra spectrometer with an Al source and a spherical mirror analyzer working in spectrum mode to examine film composition on the cotton fabric substrates. Characterization was performed on the cotton fabric samples ~5 mm x 5 mm in size attached to the XPS sample holder using double sided copper tape. The pressure in the main vacuum chamber during analysis was ~ 4×10^{-7} Torr. The take-off angle of the electrons was 90° relative to the sample stage, and the

angle of the incident X-ray beam hitting the sample was 30°. The chemical elements present on the samples were identified from survey spectra. The survey scans started at 1200 eV and ended at −5 eV taking 1 eV steps with a dwell time of 200 ms. High resolution detail scans were performed for the peaks of interest. Charging effects were corrected using C1s at 285.0 eV as a reference position. In addition to XPS, Auger electron spectroscopy (AES) was considered as an analytical method. However, because of the intensity of the electron beam used for AES, the cotton decomposed during analysis. On the other hand, the X-rays used during XPS did not degrade the cotton sample.

6.3 Results and Discussion

Atomic layer deposition of Al_2O_3 was performed on planar silicon substrates at various temperatures using fixed deposition conditions, and thickness was determined from ellipsometry as a function of the number of deposition cycles. Figure 6.1(a) shows results for deposition at 200°C. The film thickness increased linearly with the number of cycles corresponding to ~1.1 Å per cycle.[18] Similar experiments were performed at other temperatures keeping other process conditions fixed, and the results are shown in Figure 6.1(b). The growth rate increased by a factor of ~2 as temperature decreased from 200ºC to 75ºC consistent with some excess TMA and/or water absorption at lower temperature. At 100°C, the process pressure was also observed to affect the ALD Al_2O_3 growth per cycle, as shown in Figure 6.1(c), where an increase in pressure results in an increase in film growth per cycle, also likely due to an increase in reactant coverage with increased exposure. At 100°C and 0.5 Torr, increasing the TMA or water exposure time per cycle did not change the

growth per cycle on planar substrates, consistent with self-limiting saturation within each half-cycle, typical of an atomic layer deposition process.

Figure 6.2(a) is an image of an untreated cotton fabric sample, and Figure 6.2(b) shows a similar sample after treatment with 500 cycles of ALD Al_2O_3 at 100°C. The images point out that the cotton fabric is comprised of fiber-based woven yarns, and the samples present a wide range of size scales associated with the fibers, fiber bundles and the gaps and cavities within the material. After Al_2O_3 deposition, the sample appeared visually indistinguishable from the initial starting material, with similar feel and flexibility. The surface energy characteristics of the fabric did change markedly upon oxide deposition, as discussed below.

Figure 6.3 shows plan-view and cross-sectional TEM images of untreated cotton fiber and cotton fiber treated with 100 cycles of Al_2O_3 ALD at 100°C and 0.5 Torr. The images on the left are planar, high resolution TEM images taken before (Figure 6.3(a)) and after (Figure 6.3(c)) deposition, and the figures on the right show related cross sectional images. Consider the images in Figures 6.3(a) and 6.3(c). In the high resolution image of an uncoated fiber in Figure 6.3a, the solid cotton fiber is at the bottom of the image and nano-scale fibrils are observed extending from the fiber surface. After exposing the fabric sample to 100 cycles of Al_2O_3 ALD at 100°C, (Figure 6.3(c)) the nano-scale fibrils extending from the surface are no longer visible. Instead the surface of the fiber is covered by an aluminum oxide coating approximately 49 nanometers in thickness. In the lower resolution cross-sectional TEM images in Figures 6.3(b) and 6.3(d), the natural cotton fiber shows its characteristic “bean” shape, corresponding to a hollow fiber that is collapsed upon itself,

resulting in a long inner surface that is exposed to the outside through a "pinched" opening that varies in size along the length of the fiber. After exposing to 100 Al_2O_3 ALD cycles at 100°C, the cross sectional images show a uniform, conformal coating of the surface of the fibers, including uniform coating with the same thickness within the long inner surface. The thickness is ~50 nm, consistent with the high resolution images shown in the left-side panels. The similar thicknesses from the high resolution and cross-sectional TEM images collected from different samples demonstrates reproducibility in the technique.

Another example of conformal ALD coating on cotton is shown in the TEM images in Figure 6.4 where fibers were coated with 500 ALD cycles of Al_2O_3. Figure 6.4(a) shows a cross-sectional image, and of particular interest is the area highlighted by the arrow where the surface of a fiber has created a pinched contact where ALD growth is not obtained. Growth is observed in the sub-micron open region adjacent to the pinched area, indicating that vapor-phase reactants were able to access this area, likely by diffusing laterally along the length of the fiber (i.e. in the direction into or out of the plane of the image). Figure 6.4(b) presents a magnified image of 500 cycles of ALD Al_2O_3 coating on another cotton fiber sample. A conformal film ~175 nm in thickness can be observed in this image as the film follows the irregular surface of the cotton fiber. The lighter area in this image (and in Figure 6.4(a)) represents a zone where the epoxy resin has separated from the coated fiber, likely during curing or microtome cutting. Some cracking and other discontinuities of the Al_2O_3 film are also evident, which are also attributed to fracture during TEM sample preparation.

We note that the images of coated fibers in Figures 6.3 and 6.4 were obtained from individual fibers randomly extracted (after the ALD coating procedure) from cotton yarns

that were woven into fabric samples ~1 mm thick. More than 30 fiber samples randomly extracted from the woven fabric were imaged by TEM, and all showed uniformity similar to that shown in Figure 6.3. While results suggest uniform coverage throughout the fiber bundle, the growth rate per cycle on the cotton is substantially different from that on planar substrates indicating non-ideal growth conditions which could result in non-uniformities in the sample, as discussed below.

The Al_2O_3 film thicknesses on several cotton samples was measured by TEM as a function of the number of ALD cycles (using the same deposition conditions as Figures 6.3 and 6.4), and the results are plotted in Figure 6.5. A growth rate of ~2 Å per cycle was expected at 100°C based on results in Figure 1a from experiments on the planar SiO_2 surface. However, the growth rate on cotton appears to be initially very high (~5 Å per cycle), followed by a decrease to ~3 Å per cycle as growth proceeds. If precursor depletion was an issue, the significant higher surface area of the woven fiber system compared to the planar surface could result in a decreased growth rate on the fibers. However, in the ALD process, water absorbed in the cotton before growth is expected to lead to significant reaction with the TMA in the initial growth cycles, resulting in high growth rates during the early growth cycles. This is consistent with the rate of 5 Å per cycle observed over the first 50-100 cycles in Figure 6.5. The growth rate of 3 Å per cycle during later cycles is likely due to the very different reactant flow in the three-dimensional fiber network, where excess water and TMA remains within the fiber network upon reactant purging. In the woven fiber system, the pathway required for the reactant flow into and out of the woven sample during each ALD cycle is relatively long and considerably tortuous, requiring longer purge times to allow for

complete diffusion of vapor by-products out of the fiber network. Specifically, one may expect that the diffusivity of the highly polar water molecules in the narrow confined regions of the fabric is distinctly reduced as compared to the non-polar trimethylaluminum reactant and methane by-product, resulting in a higher effective surface exposure for the water molecules, and hence a larger growth thickness during each ALD cycle, as observed in Figure 5. This non-ideal growth may also result in a gradient in the precursor concentration through the sample, leading to non-uniformities in the film thickness, for example, as distance into the woven sample increases. Therefore, achieving more ideal growth per cycle would necessitate longer purge times to eliminate non-reacted species from the tightly woven growth zone. One method to address this issue utilized by Ritala et al.[32] is to use a flow-through reactor geometry to increase the reactant transmission through the fiber network. The results in Figures 6.3 and 6.4 suggest that the process conditions utilized in this study result in relatively good uniformity across the sample thickness. A more conclusive analysis of uniformity throughout the relatively thick woven sample will require a more statistical data set and analysis methodology.

X-ray photoelectron spectroscopy was used to examine the chemical composition and bonding of the coating on the woven cotton samples. All XPS scans were collected from whole fabric samples where many individual fibers were analyzed simultaneously. Surface charging effects were adjusted using the C 1s signal at 285.0 eV as a reference. Figure 6.6(a) shows results of an XPS detail scan of Al 2p for untreated cotton and cotton with 50 and 300 cycles of ALD Al_2O_3. No Al peak is observed for the uncoated sample, whereas an Al 2p peak appears at 74.5eV after 50 ALD cycles. The intensity of the peak increases for 300

ALD cycles, demonstrating Al_2O_3 deposition on the cotton fibers. The relative magnitude of the peaks is consistent with a relatively large initial growth per cycle shown in Figure 6.5. Figure 6.6(b) shows the O 1s spectra obtained from untreated cotton samples and samples with 50 and 300 cycles of ALD Al_2O_3. The O 1s signal at 533.0 eV for untreated cotton is consistent with the expected peak position for C-O bonds.[33,34] After Al_2O_3 deposition, the peak position is observed to shift to a lower binding energy consistent with oxygen binding primarily to aluminum. The C 1s spectra are shown in Figure 6.6©. Peaks at 285.0, 286.7, and 288.0 eV are expected for C-C, C-O, and O-C-O bonds found in untreated cotton fibers.[33,35] As the ALD cycle proceeds, it is observed that the intensity of the C-O and O-C-O peaks decrease. The samples with the thickest Al_2O_3 coating show evidence only for C-C bonds, ascribed to the presence of adventitious C. These spectra are consistent with the Al_2O_3 film completely covering the surfaces of the cotton fibers during the ALD process, consistent with the TEM images.

Static water contact angle measurements were also conducted on the coated samples and the results are shown in Figure 6.7. The initial bleached and mercerized cotton fabric was extremely hydrophilic and readily absorbed water. After treatment with Al_2O_3 by ALD, the fabric samples were observed to be significantly more hydrophobic. For example, after a cotton fabric was treated with 100 cycles of Al_2O_3 the initial static water contact angle was approximately 127°. This is in contrast to a contact angle of 0° for an untreated cotton sample, and a contact angle of 62° for the SiO_2 sample treated with 100 cycles of Al_2O_3 under the same growth conditions. When the water droplet remained on the surface for some time, the contact angle was observed to slowly decrease, reaching 104° after 30 minutes and

53° after 60 minutes under ambient air exposure. Numerous reports have shown that the wettability of a surface is controlled by both the surface energy and surface topography of the sample material.[36-39] The observed increase in hydrophobicity of the cotton fabric upon Al_2O_3 deposition likely results from an increase in the rigidity of the individual fibers by the more incompliant inorganic coating. This rigidity can effectively reduce the total contact area between the fiber and the water droplet, thereby enhancing the hydrophobicity of the fabric surface.

The results show that atomic layer deposition uniquely allows reactive growth precursors to penetrate throughout a typical tightly woven fiber network to provide for a highly conformal inorganic coating on the intricate convoluted surfaces often found in natural textile materials. The same process conditions on planar and complex surface structures are shown to result in significantly different film growth thickness per ALD cycle, likely due to reactant adsorption within the starting material, as well as impeded reactant transport out of the fabric system during the purge cycle. Alumina coatings on cotton are shown here to modify the effective surface energy of a woven fiber system to convert a highly hydrophilic surface to predominantly hydrophobic. This ability to conformally modify woven textile materials with near monolayer precision may help enable new multifunctional textiles with properties and performance that deviate radically from current structured fabrics

6.4 Acknowledgements

The authors acknowledge support from the National Science Foundation under grant CTS-0626256.

6.5 References

1. Adanur, S. Handbook of Weaving. (Technomic Publishing Company, Inc., Lancaster; 2001).

2. Adanur, S. Wellington Sears Handbook of Industrial Textiles. (Technomic Publishing Company, Inc., Lancaster; 1995).

3. Bajaj, P. Finishing of Textile Materials. *J. Appl. Polym. Sci.* **83**, 631-659 (2002).

4. Black, S., Kapsali, V., Bougourd, J. & Geesin, F. in Textiles for protection. (ed. R.A. Scott) 60-89 (Woodhead Publishing Limited, Cambridge; 2005).

5. Mahltig, B. & Bottcher, H. Modified silica sol coatings for water-repellent textiles. *J. Sol-Gel Sci. Technol.* **27**, 43-52 (2003).

6. Mahltig, B., Bottcher, H., Knittel, D. & Schollmeyer, E. Light fading and wash fastness of dyed nanosol-coated textiles. *Text. Res. J.* **74**, 521-527 (2004).

7. Mahltig, B., Haufe, H. & Bottcher, H. Functionalisation of textiles by inorganic sol-gel coatings. *J. Mater. Chem.* **15**, 4385-4398 (2005).

8. Stull, J.O. in Textiles for protection. (ed. R.A. Scott) 295-354 (Woodhead Publishing Limited, Cambridge; 2005).

9. Mahltig, B., Fiedler, D. & Bottcher, H. Antimicrobial sol-gel coatings. *J. Sol-Gel Sci. Technol.* **32**, 219-222 (2004).

10. Drew, C. et al. Metal oxide-coated polymer nanofibers. *Nano Lett.* **3**, 143-147 (2003).

11. Jeong, S.H., Hwang, Y.H. & Yi, S.C. Antibacterial properties of padded PP/PE nonwovens incorporating nano-sized silver colloids. *J. Mater. Sci.* **40**, 5413-5418 (2005).

12. Jiang, S.Q., Newton, E., Yuen, C.W.M. & Kan, C.W. Chemical Silver Plating and Its Application to Textile Fabric Design. *J. Appl. Polym. Sci.* **96**, 919-926 (2005).

13. Chen, X. & Chaudhry, I. in Textiles for protection. (ed. R.A. Scott) 529-556 (Woodhead Publishing Limited, Cambridge; 2005).

14. Leonas, K.K. in Textiles for Protection. (ed. R.A. Scott) 441-464 (Woodhead Publishing Limited, Cambridge; 2005).

15. Kim, H. Atomic layer deposition of metal and nitride thin films: Current research efforts and applications for semiconductor device processing. *Journal Of Vacuum Science & Technology B* **21**, 2231-2261 (2003).

16. Puurunen, R.L. Surface chemistry of atomic layer deposition: A case study for the trimethylaluminum/water process. *J. Appl. Phys.* **97** (2005).

17. Du, Y., Du, X. & George, S.M. SiO2 film growth at low temperatures by catalyzed atomic layer deposition in a viscous flow reactor. *Thin Solid Films* **491**, 43-53 (2005).

18. Groner, M.D., Fabreguette, F.H., Elam, J.W. & George, S.M. Low-temperature Al2O3 atomic layer deposition. *Chem. Mat.* **16**, 639-645 (2004).

19. Kim, S.K. et al. Low temperature (< 100 degrees C) deposition of aluminum oxide thin films by ALD with O-3 as oxidant. *J. Electrochem. Soc.* **153**, F69-F76 (2006).

20. Peng, Q. et al. Atomic Layer Deposition on Electrospun Polymer Fibers as a Direct Route to Al2O3 Microtubes with Precise Wall Thickness Control. *Nano Lett.* (2007).

21. Park, K.J., Doub, J.M., Gougousi, T. & Parsons, G.N. Microcontact patterning of ruthenium gate electrodes by selective area atomic layer deposition. *Appl Phys Lett* **86**, - (2005).

22. Ritala, M. et al. Perfectly conformal TiN and Al2O3 films deposited by atomic layer deposition. *Chem Vapor Depos* **5**, 7-9 (1999).

23. Cho, D.L., Choi, C.N., Kim, H.J., Kim, A.K. & Go, J.H. Fabrication of deodorizing fabric by grafting of metal phthalocyanine derivative onto nonwoven polypropylene fabric. *J. Appl. Polym. Sci.* **82**, 839-846 (2001).

24. Rahel, J. et al. Hydrophilization of polypropylene nonwoven fabric using surface barrier discharge. *Surf. Coat. Technol.* **169**, 604-608 (2003).

25. Simor, M. et al. Atmospheric-pressure plasma treatment of polyester nonwoven fabrics for electroless plating. *Surf. Coat. Technol.* **172**, 1-6 (2003).

26. Stefecka, M. et al. Electromagnetic shielding efficiency of plasma treated and electroless metal plated polypropylene nonwoven fabrics. *J. Mater. Sci.* **39**, 2215-2217 (2004).

27. Yuranova, T. et al. Antibacterial textiles prepared by RF-plasma and vacuum-UV mediated deposition of silver. *J. Photochem. Photobiol. A-Chem.* **161**, 27-34 (2003).

28. Niskanen, A., Arstila, K., Leskela, M. & Ritala, M. Radical enhanced atomic layer deposition of titanium dioxide. *Chem Vapor Depos* **13**, 152-157 (2007).

29. Niskanen, A., Arstila, K., Ritala, M. & Leskela, M. Low-temperature deposition of aluminum oxide by radical enhanced atomic layer deposition. *J. Electrochem. Soc.* **152**, F90-F93 (2005).

30. Kemell, M., Pore, V., Ritala, M., Leskela, M. & Linden, M. Atomic layer deposition in nanometer-level replication of cellulosic substances and preparation of photocatalytic TiO2/cellulose composites. *J Am Chem Soc* **127**, 14178-14179 (2005).

31. Groner, M.D., Elam, J.W., Fabreguette, F.H. & George, S.M. Electrical characterization of thin Al2O3 films grown by atomic layer deposition on silicon and various metal substrates. *Thin Solid Films* **413**, 186-197 (2002).

32. Ritala, M. et al. Rapid coating of through-porous substrates by atomic layer deposition. *Chem Vapor Depos* **12**, 655-658 (2006).

33. Beamson, G. & Briggs, D. High Resolution XPS of Organic Polymers. (Wiley, Chichester, England; 1992).

34. Yeqiu, L., Jinlian, H., Yong, Z. & Zhuohong, Y. Surface modification of cotton fabric by grafting polyurethane. *Carbohydrate Polymers*, 276-280 (2005).

35. Mitchell, R., Carr, C.M., Parfitt, M., Vickerman, J.C. & Jones, C. Surface chemical analysis of raw cotton fibres and associated materials. *Cellulose* **12**, 629-639 (2005).

36. Daoud, W.A., Xin, J.H. & Tao, X.M. Superhydrophobic silica nanocomposite coating by a low-temperature process. *J Am Ceram Soc* **87**, 1782-1784 (2004).

37. Feng, L. et al. Super-hydrophobic surfaces: From natural to artificial. *Adv Mater* **14**, 1857-1860 (2002).

38. Gao, L.C. & McCarthy, T.J. "Artificial lotus leaf" prepared using a 1945 patent and a commercial textile. *Langmuir* **22**, 5969-5973 (2006).

39. Gao, L.C. & McCarthy, T.J. A perfectly hydrophobic surface (theta(A)/theta(R)=180 degrees/180 degrees). *J Am Chem Soc* **128**, 9052-9053 (2006).

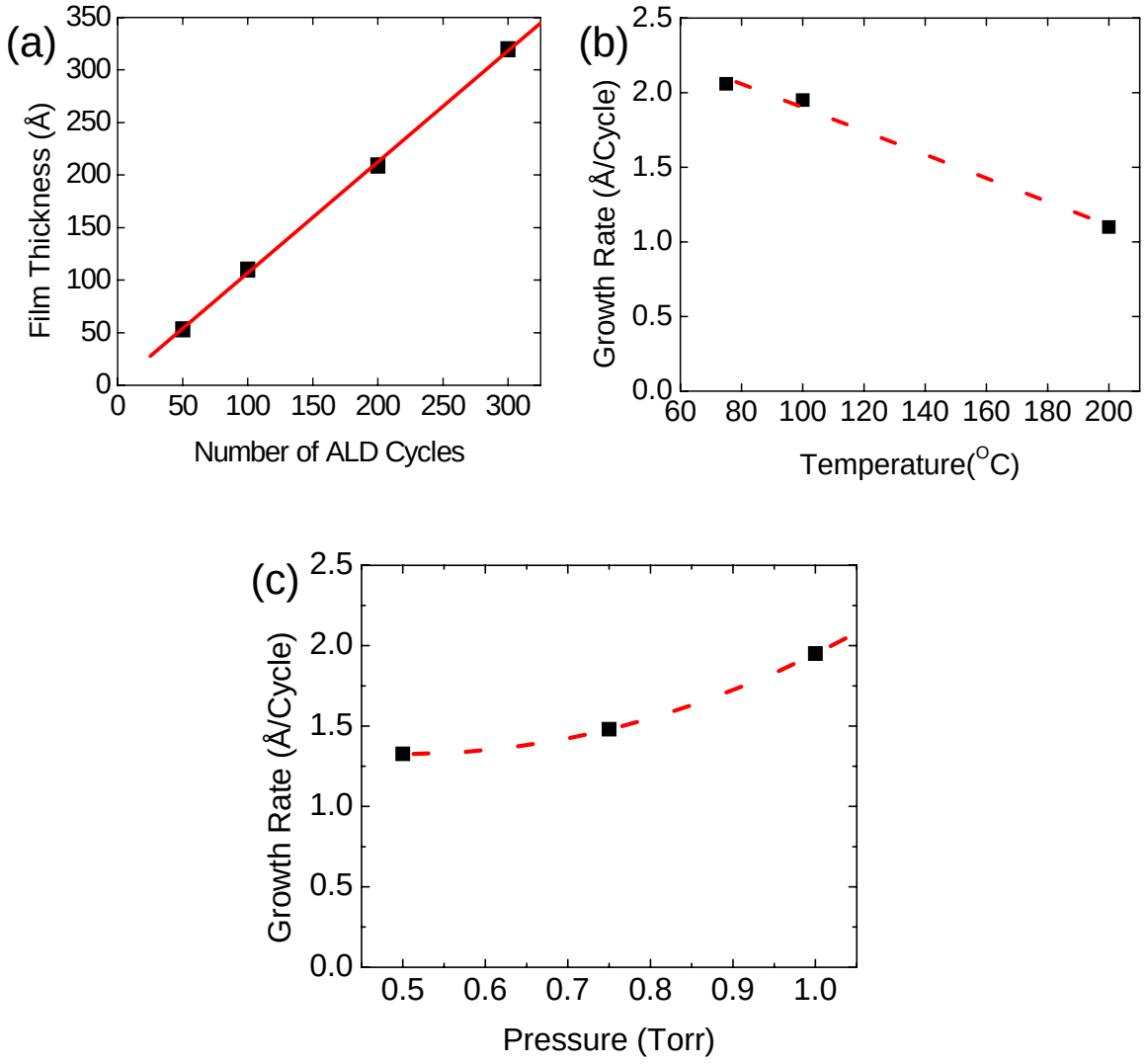

Figure 6.1. Growth rate of Al_2O_3 on silicon. (a) ALD cycle number versus Al_2O_3 film thickness (as measured by ellipsometry) deposited on Si at 200°C with a pressure of 1 Torr, (b) Growth rate versus temperature with process pressure of 1 Torr; the dashed line is a guide to the eye, and (c) Growth rate versus pressure at 100°C; the dashed line is a guide to the eye.

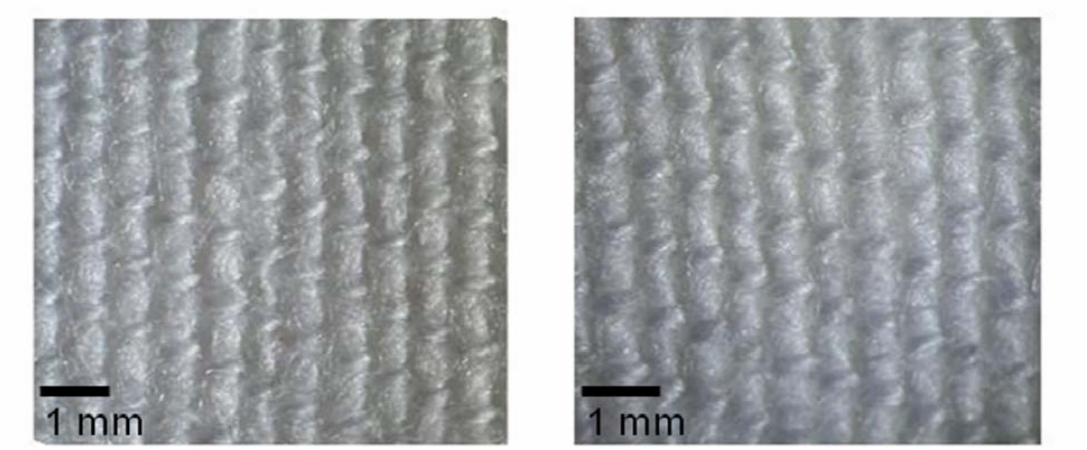

Figure 6.2. Images of cotton fabric. (a) Untreated cotton fabric, (b) Cotton fabric treated with 500 cycles of Al_2O_3.

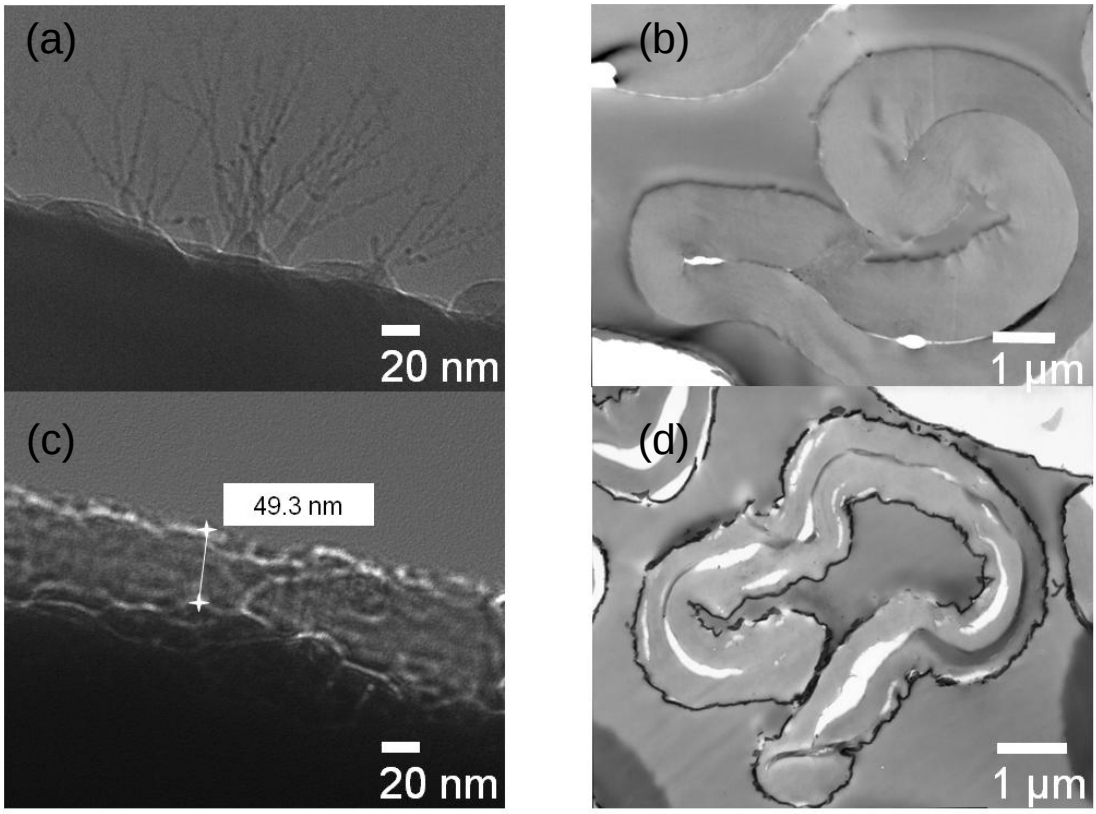

Figure 6.3. Transmission electron microscope (TEM) images of untreated cotton fiber and cotton fiber treated with 100 cycles of Al_2O_3 ALD. (a) Planar image of untreated cotton fiber, (b) Cross-sectional image of untreated cotton fiber, (c) Planar image of cotton fiber coated with 100 cycles Al_2O_3 ALD showing coverage of fibrils on fiber surface, (d) Cross-sectional image of cotton fiber coated with 100 cycles Al_2O_3 ALD demonstrating uniform, conformal coating of fiber surface.

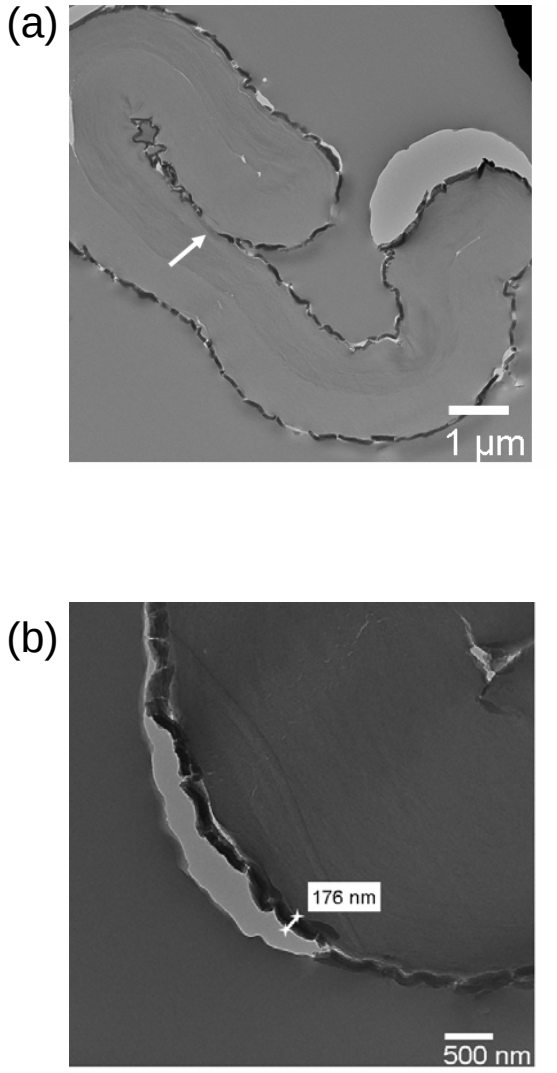

Figure 6.4. Transmission electron microscope (TEM) images of cotton fiber treated with 500 cycles of Al_2O_3 ALD. (a) Cross-sectional image of cotton fiber showing conformal coating of Al_2O_3. The arrow points out a portion of the fiber that is pinched together where no deposition is visible. (b) Cross-sectional image of cotton fiber detailing nature of Al_2O_3 coating. A defect can be seen in the film where the embedding resin has pulled the Al_2O_3 coating from the surface of the fiber.

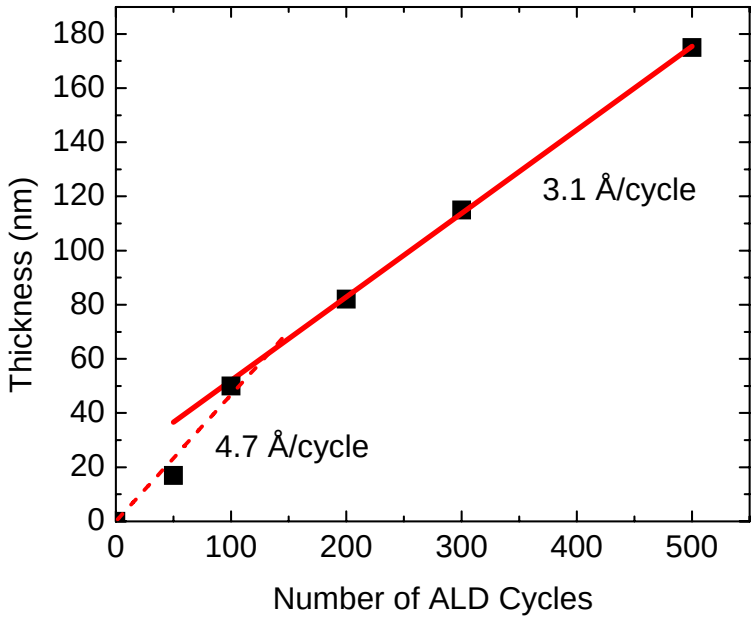

Figure 6.5. ALD growth rate of Al_2O_3 on cotton substrates. ALD cycle number versus Al_2O_3 film thickness for deposition at 100°C. Thickness measurements were made using TEM.

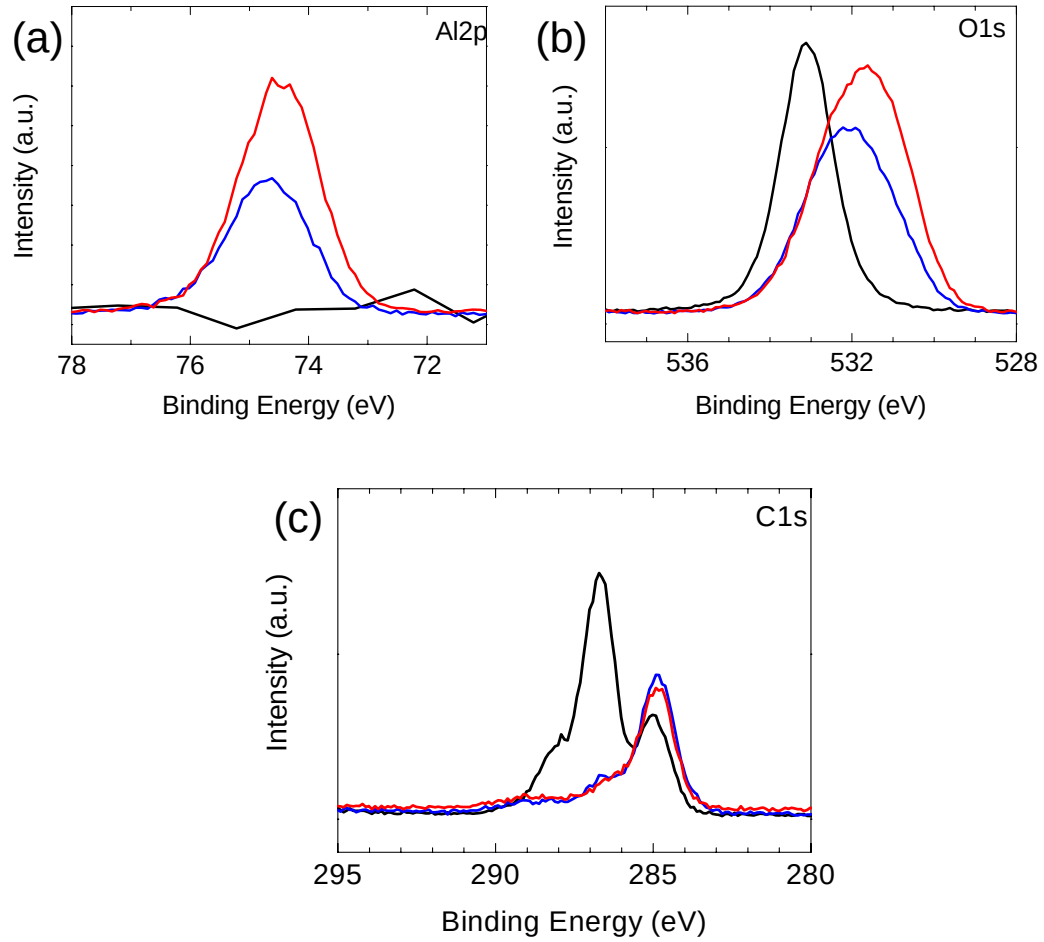

Figure 6.6. XPS spectra of Al_2O_3 on cotton substrates. (a) XPS detail spectra of Al2p (0 cycles: black line; 50 ALD cycles: blue line; 300 ALD cycles: red line). The Al2p signal can be seen to increase as the number of ALD cycles increases. (b) XPS detail spectra of O1s (0 cycles: black line; 50 ALD cycles: blue line; 300 ALD cycles: red line). A shift in the O1s peak can be seen as the number of ALD cycles increases. (c) XPS detail spectra of C1s (0 cycles: black line; 50 ALD cycles: blue line; 300 ALD cycles: red line). It can be seen that the C-O and O-C-O peaks found in the untreated cotton decrease as the fibers are coated with Al_2O_3.

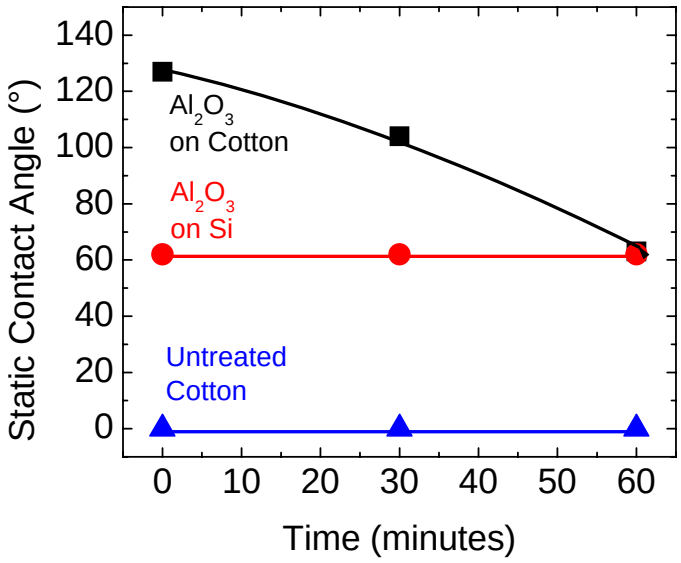

Figure 6.7. Static water contact angles on coated samples. The uncoated cotton fabric readily adsorbed water and had a contact angle of 0°. The Al_2O_3 coated silicon samples had a static water contact angle of 62°. Al_2O_3 coated cotton fabric had an initial static contact angle measurement of 127°. This contact angle can be seen to decrease with time under ambient air exposure.

Chapter 7 is a reprint of a paper that appeared on pages 719-722 of Nano Letters, Volume 7, Issue 3, in March 2007

Atomic Layer Deposition on Electrospun Polymer Fibers as a Direct Route to Al_2O_3 Microtubes with Precise Wall Thickness Control

Qing Peng,[1] Xiao-Yu Sun,[1] Joseph C. Spagnola,[2] G. Kevin Hyde,[3]
Richard J. Spontak[1] and Gregory N. Parsons[1*]

Departments of [1]Chemical and Biomolecular Engineering, [2]Materials Science & Engineering and [3]Textile Engineering, Chemistry and Science
North Carolina State University, Raleigh NC 27695

Abstract

Atomic layer deposition (ALD) of Al_2O_3 on electrospun poly(vinyl alcohol) microfiber templates is demonstrated as an effective and robust strategy by which to fabricate long and uniform metal-oxide microtubes. The wall thickness is shown to be precisely controlled within a molecular layer or so by adjusting the number of ALD cycles utilized. By judiciously selecting the electrospinning and ALD parameters, designer tubes of various sizes and inorganic materials can be synthesized.

Specific Contribution

For this article, I helped decide on appropriate conditions for the atomic layer deposition of the aluminum oxide onto the electrospun fibers. I then discussed with Qing Peng and Joe Spagnola the best ways to prepare the samples for TEM. After the samples were made, I was responsible for the TEM and EDS analysis of the samples. I helped with the revisions to the manuscript before it was submitted. After the manuscript was reviewed, I helped to answer questions from the reviewers and revise the final proofs of the paper.

Chapter 7: Atomic Layer Deposition on Electrospun Polymer Fibers as a Direct Route to Al_2O_3 Microtubes with Precise Wall Thickness Control

7.1 Introduction

Inorganic microtubes with precisely defined nano-scale walls have attracted considerable attention due to their potential application in technologies related, but not limited to, electronics, photonics, nanofluidics, medicine, sensing, catalysis, and controlled release.[1] A variety of different processes have been developed to fabricate such tubes from a variety of materials. Among those processes, the template-directed approach represents a straightforward and facile route to the fabrication of nano/micro-scale structures with hollow interiors. Nanorods,[2] carbon nanotubes[3,4] and porous media[5,6] have all been successfully used as templates in this vein. Such templates are, however, expensive and difficult to produce in large volume. Natural materials including cotton and paper[7,8] have also been used as templates, but the resultant nano/micro-scale structures are not easy controlled. In this work, we employ atomic layer deposition (ALD) on electrospun polymer fibers as a direct means by which to construct inorganic microtubes with well-defined nano-scale walls composed of Al_2O_3 after the templating polymer is removed. The results reported here indicate that this strategy provides an attractive, high-fidelity and low-cost route to inorganic microtubes, as well as nano-scale tubes and other complex shapes.

Electrospinning has become a valuable and versatile route by which to obtain exceptionally long polymer nano/micro-scale fibers possessing uniform diameter and good composition control.[9-14] Electrospun fibers are produced from polymer solutions as the

electric field between a spinneret and a target is increased until the electrostatic force at the tip of the spinneret exceeds the surface tension of the solution drop. The Taylor cone that forms is transformed into a continuous jet that forms solid fibers as the solvent evaporates. In combination with various surface modification tactics including physical vapor deposition (PVD),[15,16] chemical vapor deposition (CVD),[15] sol-gel processing,[7] and spin-on glass (SOG) incorporation,[16,17] electrospun templates have been used to fabricate metal,[15] metal oxide[7,16] and polymer[15,18] nanotubes. However each of these deposition methods is hindered by significant process limitations. For example, sol-gel chemistry has been successfully performed on electrospun fibers to generate TiO_2 nanotubes,[7] but uniform wetting of the huge surface area of the fiber matrix presents a significant and ongoing challenge for this method. In addition, PVD is a line-of-sight deposition technique that does not permit conformal deposition on fibers throughout the matrix. In CVD processes, depletion of precursor frequently limits uniform coating on large surface areas. Due to the limitations of these traditional deposition techniques, it is difficult to produce long nano/microtubes with smooth outer surfaces, uniform walls of controlled thicknesses at nanometer length scales.

7.2 Experimental

In this work, atomic layer deposition (ALD)[19-22] has been applied to matrices of electrospun polymer fibers to fabricate Al_2O_3 microtubes with smooth wall surfaces and precisely controlled wall thickness. This strategy exploits a sequential, self-limiting deposition process that operates on the principle of alternating saturating surface reactions. During ALD, a specimen is exposed to a precursor vapor that forms a (sub)monolayer of the

precursor on the substrate. After excess precursor is removed from the vapor phase by a purge gas (e.g., Ar), the reactant gas is subsequently pulsed onto the substrate, where it reacts with the adsorbed precursor layer to form a layer of the target film-forming material. Since no gas phase reaction occurs, the target film is grown layer-by-layer on the substrate, in which case the thickness of the deposited film can be accurately controlled by the number of cycles the process is repeated, as illustrated in Figure 7.1. Because of its unique process characteristics and controllability, ALD can be used to deposit conformal, uniformly thin films with precise thickness and composition control over large scales and onto substrates with complex topologies (including for example, fibers).[8,22,23] Moreover, ALD is chemically versatile and has been used to fabricate layers of metals,[24-26] metal oxides,[27] metal nitrides[22,24] and other materials. An additional benefit of ALD is that the deposition of Al_2O_3,[21,22] TiO_2[8] and TiN[24] can be conducted at relatively low temperatures (< 150˚C), thereby reducing, if not altogether eliminating, thermal damage to temperature-sensitive substrates such as organic media.

Poly(vinyl alcohol) (PVA) with a molecular weight of 127 kDa and a degree of hydrolysis of 88% was purchased from Aldrich and used without further purification. A 7 wt% PVA aqueous solution was prepared by dissolving PVA in deionized water (DI H_2O) at 60˚C and stirring gently for 2 h. Electrospinning was performed using the parallel-plate setup described elsewhere.[14] A stable jet was formed at a flow rate of 7 μl/min and an electric field of 1 kV/cm. Representative electrospun PVA fibers were sputter-coated with Au/Pd prior to field-emission scanning electron microscopy (FESEM) analysis performed on a JEOL 6400F microscope operated at 5 kV. Coated fiber composites were fabricated by

depositing thin Al_2O_3 films on the electrospun PVA fibers by ALD at 45˚C and a pressure of ~0.5 Torr. The aluminum precursor and oxygen reactant sources were $Al(CH_3)_3$ (TMA, 95%) and DI H_2O, respectively, and were delivered to the reactor as ambient-temperature vapors. During cycling, the TMA and DI H_2O were alternately introduced into the ALD chamber (base pressure ~10^{-6} Torr) in pulses of 5 and 0.5 s, respectively. Purge times were 20 s for TMA and 60 s for DI H_2O. In conjunction with each ALD on PVA fibers, a piece of native oxide Si wafer (measuring ~1 cm × 1.5 cm, treated by JTB® Baker Clean, rinsed in DI water and then N_2 blown-dry) was used as a reference substrate for growth rate measurements on a planar surface under identical deposition conditions. To remove the organic constituent after ALD, the Al_2O_3-coated PVA fibers were heated in air at 400˚C for 24 h. After removing the PVA by calcination, the resultant microtubes were likewise characterized by FESEM under the same conditions listed above. Transmission electron microscopy (TEM) was conducted by sonicating Al_2O_3 microtubes in ethanol for 1 min. Several drops of the suspension were pipetted onto TEM grids, which were allowed to dry at ambient temperature and then imaged with a Hitachi HF-2000 microscope operated at 200 kV. Complementary energy-dispersive x-ray spectroscopy (EDS) was performed with an Oxford Instruments Inca Energy 100 system to ascertain the chemical composition of the microtubes under different ALD conditions.

7.3 Results and Discussion

A representative FESEM image of individual as-electrospun PVA fibers is presented in Figure 7.2a. Depending on the duration of electrospinning, these fibers typically connect

to form a self-supporting web. The diameters of most of the PVA fibers used in this study range from 200 to 400 nm. To reflect this size scale, we hereafter refer to the fibers as *microfibers*. In comparison with poly(L-lactide) (PLA) electrospun fibers, which have been traditionally used as templates by which to generate tubes by PVD and CVD,[15,28] PVA with surface hydroxyl groups capable of reacting with deposited precursor species is much less expensive and likewise amenable to electrospinning from aqueous solution. These considerations are ultimately important in the mass production of high-quality templated microtubes. The resulting conformal deposition of Al_2O_3 on PVA fibers is shown in the FESEM images displayed in Figures 7.2b and 7.2c, as well as in the TEM image included in Figure 7.2d. Figure 7.2b indicates that the Al_2O_3 microtubes are connected together in a web, thereby preserving the original arrangement of the PVA electrospun fiber templates. This figure, which shows a large number of Al_2O_3 microtubes as only a very small part of the specimen investigated, also confirms that the ALD process yields uniform coverage over a relatively large area despite the apparent topological complexity. Most of the Al_2O_3 microtubes are observed to measure tens of micrometers in length, with many observed to extend into the millimeter range. The close-up FESEM image provided in Figure 7.2c reveals the structure of the hollow Al_2O_3 microtubes formed after removal of the PVA core. It is apparent from this and related images that the outer surface of the microtubes after 475 ALD cycles is relatively smooth. In this case, the wall thickness of these Al_2O_3 nanometer tubes is estimated to be about 38 nm on the basis of TEM images such as the one displayed in Figure 7.2d. As indicated by the arrow in this figure, the microtube replicates nano-scale features from the surface of the electrospun fiber. Attention is drawn here to a small neck in

the PVA fiber, along with some small surface blemishes and a peripheral circular feature. A similar circular feature is likewise evident on the interior of a microtube produced after 300 cycles of ALD (cf. Figure 7.3a).

Figure 7.3a is a TEM image of an Al_2O_3 replica of a PVA electrospun fiber template that was first exposed to Al_2O_3 ALD for 300 cycles prior to thermal treatment in air at 400˚C for 24 h. Despite their diameter (in excess of 200 nm), these microtubes appear electron transparent when observed by TEM. The high-magnification TEM image provided in Figure 7.3a demonstrates that the wall thickness of the microtubes is ~25 nm and is remarkably uniform along the length of a single tube. This observation extends to different tubes throughout the entire web. For comparison, Al_2O_3 microtubes formed after 150 ALD cycles are shown in the FESEM image in Figure 7.3c. In this case, the wall thickness is only ~14 nm, according to TEM (cf. Figure 7.3d). An EDS analysis performed on Al_2O_3 microtubes after 150, 300 and 475 ALD cycles and subsequent heating in air at 400°C for 24 h shows an Al:O ratio of 0.68:1 with 5% variation, thereby confirming that the elemental composition of the microtube walls is consistent with Al_2O_3. Corresponding analysis of the ALD wall thickness under these conditions is displayed in Figure 7.4. In this figure, the dependence of Al_2O_3 layer thickness on cycle number is discerned for (*i*) microtube walls on PVA fibers by TEM and (*ii*) planar films on Si wafers by ellipsometry. The average growth rate of Al_2O_3 on PVA fibers is ~0.08 nm/cycle, which is, within experimental uncertainty, virtually identical to the deposition rate (~0.07 nm/cycle) measured on the planar substrates under identical ALD conditions. A larger population of water molecules residing in the electrospun PVA fibers than on the Si substrate may explain the marginally higher growth rate on PVA.[21]

The results shown in Figure 7.4 indicate that the wall thickness of the Al_2O_3 microtubes generated here by ALD may be precisely (within a molecular layer or so) controlled by simply altering the number of deposition cycles. Carbonaceous residue has not been observed within the sensitivity of the EDS analysis (i.e., < 0.5%), as evidenced by the spectra provided in Figure 7.5.

For microfluidic applications, the porosity and permeability of fabricated microtubes constitute important design concerns. Previous reports[29,30] of Al_2O_3 ALD performed on planar polymer substrates indicate that films measuring tens of nanometers thick (similar to those fabricated here) perform as high-quality gas barriers. Although the TEM images in Figures 7.2 and 7.3 show evidence of breakage (presumably during calcination and/or sonication), the Al_2O_3 microtubes appear predominantly compact and smooth without discernible nanometer-size holes, suggesting that intact microtubes are most likely impermeable to liquids (e.g., water and organic solvents), while affording low permeability to gases. Even without process optimization, the results of this study unequivocally establish that ALD is an effective and robust strategy by which to fabricate long and uniform Al_2O_3 microtubes with precise control of wall thickness from electrospun PVA microfiber templates. By judiciously adjusting the electrospinning parameters, the diameter, alignment and structure of the templates can be further tuned as desired.[9-14] In similar fashion, the ALD process can be appropriately extended to synthesize designer microtubes of other inorganic materials such as TiO_2[8] and TiN.[24] Because ALD is a self-limiting vapor-phase process, it can be easily adapted to construct, via reactive layering, large numbers of tube structures

with nano-scale-precision dimensions and controlled composition, thereby providing an attractive complement to physical self-assembly.[31]

7.4 Acknowledgements

This work was supported by the STC Program of the National Science Foundation under Agreement No. CHE-9876674 (GNP) and the Department of Commerce through the National Textiles Center (RJS). GNP also acknowledges support from NSF under grant CTS-0626256.

7.5 References

1. Xia, Y.N. et al. One-dimensional nanostructures: Synthesis, characterization, and applications. *Advanced Materials* **15**, 353-389 (2003).

2. Lauhon, L.J., Gudiksen, M.S., Wang, C.L. & Lieber, C.M. Epitaxial core-shell and core-multishell nanowire heterostructures. *Nature* **420**, 57-61 (2002).

3. Lee, J.S. et al. Al2O3 nanotubes and nanorods fabricated by coating and filling of carbon nanotubes with atomic-layer deposition. *Journal of Crystal Growth* **254**, 443-448 (2003).

4. Min, Y.S. et al. Ruthenium oxide nanotube arrays fabricated by atomic layer deposition using a carbon nanotube template. *Advanced Materials* **15**, 1019-+ (2003).

5. Martin, C.R. Nanomaterials - a Membrane-Based Synthetic Approach. *Science* **266**, 1961-1966 (1994).

6. Steinhart, M. et al. Polymer nanotubes by wetting of ordered porous templates. *Science* **296**, 1997-1997 (2002).

7. Caruso, R.A., Schattka, J.H. & Greiner, A. Titanium dioxide tubes from sol-gel coating of electrospun polymer fibers. *Advanced Materials* **13**, 1577-+ (2001).

8. Kemell, M., Pore, V., Ritala, M., Leskela, M. & Linden, M. Atomic layer deposition in nanometer-level replication of cellulosic substances and preparation of photocatalytic TiO2/cellulose composites. *Journal of the American Chemical Society* **127**, 14178-14179 (2005).

9. Fridrikh, S.V., Yu, J.H., Brenner, M.P. & Rutledge, G.C. Controlling the fiber diameter during electrospinning. *Physical Review Letters* **90** (2003).

10. Li, D., Ouyang, G., McCann, J.T. & Xia, Y.N. Collecting electrospun nanofibers with patterned electrodes. *Nano Letters* **5**, 913-916 (2005).

11. Li, D. & Xia, Y.N. Electrospinning of nanofibers: Reinventing the wheel? *Advanced Materials* **16**, 1151-1170 (2004).

12. Li, D. & Xia, Y.N. Direct fabrication of composite and ceramic hollow nanofibers by electrospinning. *Nano Letters* **4**, 933-938 (2004).

13. Reneker, D.H. & Chun, I. Nanometre diameter fibres of polymer, produced by electrospinning. *Nanotechnology* **7**, 216-223 (1996).

14. Sun, X.Y., Shankar, R., Borner, H.G., Ghosh, T.K. & Spontak, R.J. Field-driven biofunctionalization of polymer fiber surfaces during electrospinning. *Advanced Materials* **19**, 87-+ (2007).

15. Bognitzki, M. et al. Polymer, metal, and hybrid nano- and mesotubes by coating degradable polymer template fibers (TUFT process). *Advanced Materials* **12**, 637-+ (2000).

16. Czaplewski, D.A., Kameoka, J., Mathers, R., Coates, G.W. & Craighead, H.G. Nanofluidic channels with elliptical cross sections formed using a nonlithographic process. *Applied Physics Letters* **83**, 4836-4838 (2003).

17. Kameoka, J., Verbridge, S.S., Liu, H.Q., Czaplewski, D.A. & Craighead, H.G. Fabrication of suspended silica glass nanofibers from polymeric materials using a scanned electrospinning source. *Nano Letters* **4**, 2105-2108 (2004).

18. Dong, H., Prasad, S., Nyame, V. & Jones, W.E. Sub-micrometer conducting polyaniline tubes prepared from polymer fiber templates. *Chemistry of Materials* **16**, 371-373 (2004).

19. Ferguson, J.D., Weimer, A.W. & George, S.M. Atomic layer deposition of Al2O3 films on polyethylene particles. *Chemistry of Materials* **16**, 5602-5609 (2004).

20. Gordon, R.G. Review of recent progress in atomic layer deposition (ALD) of materials for micro- and nano-electronics. *Abstracts of Papers of the American Chemical Society* **227**, U553-U554 (2004).

21. Groner, M.D., Fabreguette, F.H., Elam, J.W. & George, S.M. Low-temperature Al2O3 atomic layer deposition. *Chemistry of Materials* **16**, 639-645 (2004).

22. Ritala, M. et al. Perfectly conformal TiN and Al2O3 films deposited by atomic layer deposition. *Chemical Vapor Deposition* **5**, 7-9 (1999).

23. Knez, M. et al. Atomic layer deposition on biological macromolecules: Metal oxide coating of tobacco mosaic virus and ferritin. *Nano Letters* **6**, 1172-1177 (2006).

24. Kim, H. Atomic layer deposition of metal and nitride thin films: Current research efforts and applications for semiconductor device processing. *Journal of Vacuum Science & Technology B* **21**, 2231-2261 (2003).

25. Park, K.J., Doub, J.M., Gougousi, T. & Parsons, G.N. Microcontact patterning of ruthenium gate electrodes by selective area atomic layer deposition. *Applied Physics Letters* **86** (2005).

26. Park, K.J. & Parsons, G.N. Selective area atomic layer deposition of rhodium and effective work function characterization in capacitor structures. *Applied Physics Letters* **89** (2006).

27. Kim, H. & McIntyre, P.C. Atomic layer deposition of ultrathin metal-oxide films for nano-scale device applications. *Journal of the Korean Physical Society* **48**, 5-17 (2006).

28. Hou, H.Q. et al. Poly(p-xylylene) nanotubes by coating and removal of ultrathin polymer template fibers. *Macromolecules* **35**, 2429-2431 (2002).

29. Carcia, P.F., McLean, R.S., Reilly, M.H., Groner, M.D. & George, S.M. Ca test of Al2O3 gas diffusion barriers grown by atomic layer deposition on polymers. *Applied Physics Letters* **89** (2006).

30. Groner, M.D., George, S.M., McLean, R.S. & Carcia, P.F. Gas diffusion barriers on polymers using Al2O3 atomic layer deposition. *Applied Physics Letters* **88** (2006).

31. Zou, J., Ji, B.H., Feng, X.Q. & Gao, H.J. Self-assembly of single-walled carbon nanotubes into multiwalled carbon nanotubes in water: Molecular dynamics simulations. *Nano Letters* **6**, 430-434 (2006).

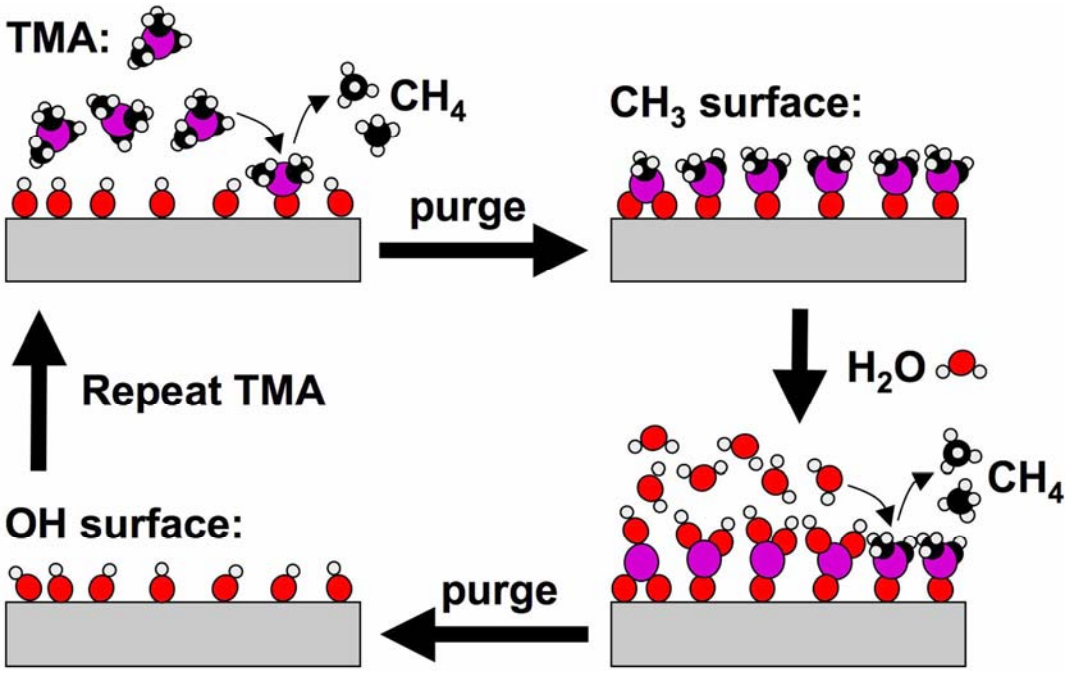

Figure 7.1. Schematic diagram of vapor-phase, self-limiting atomic layer deposition (ALD) illustrating the cyclic process by which an Al_2O_3 surface coating is controllably constructed layer-by-layer from TMA and H_2O precursors.

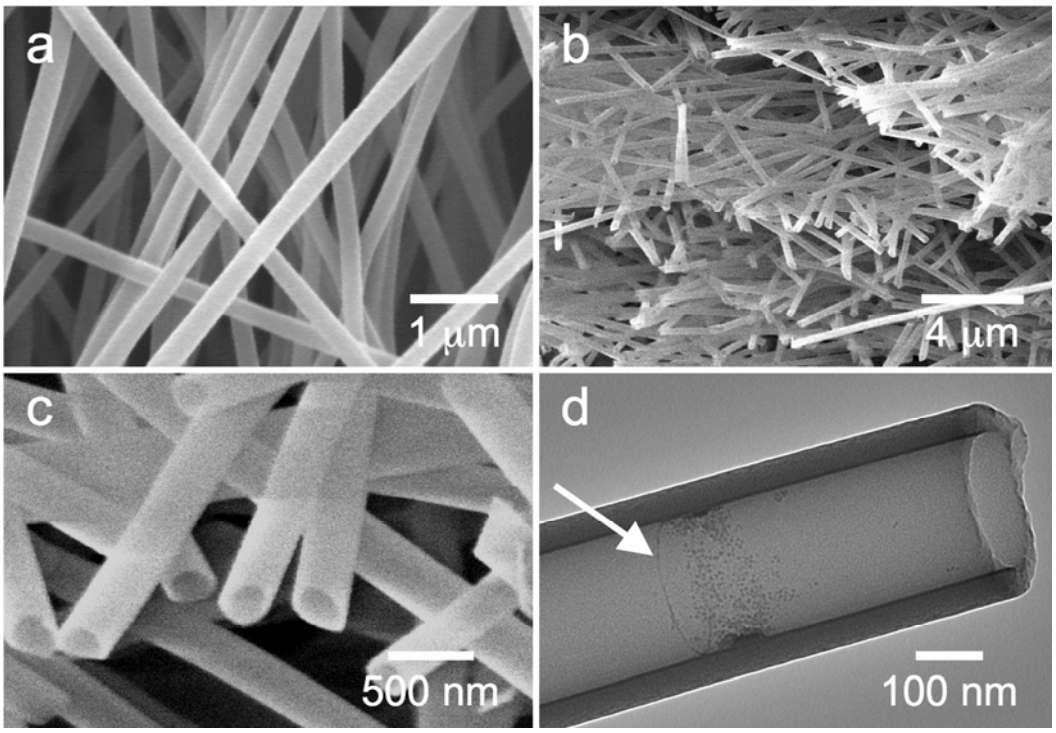

Figure 7.2. (a) FESEM image of electrospun PVA fibers. (b, c) FESEM images of Al_2O_3 microtube replicas prepared by ALD wherein the Al_2O_3 coating was deposited for 475 cycles at 45˚C. (d) TEM image of a corresponding Al_2O_3 microtube. The arrow in (d) identifies a peripheral circle formed inside the microtube near an apparent neck in the fiber template.

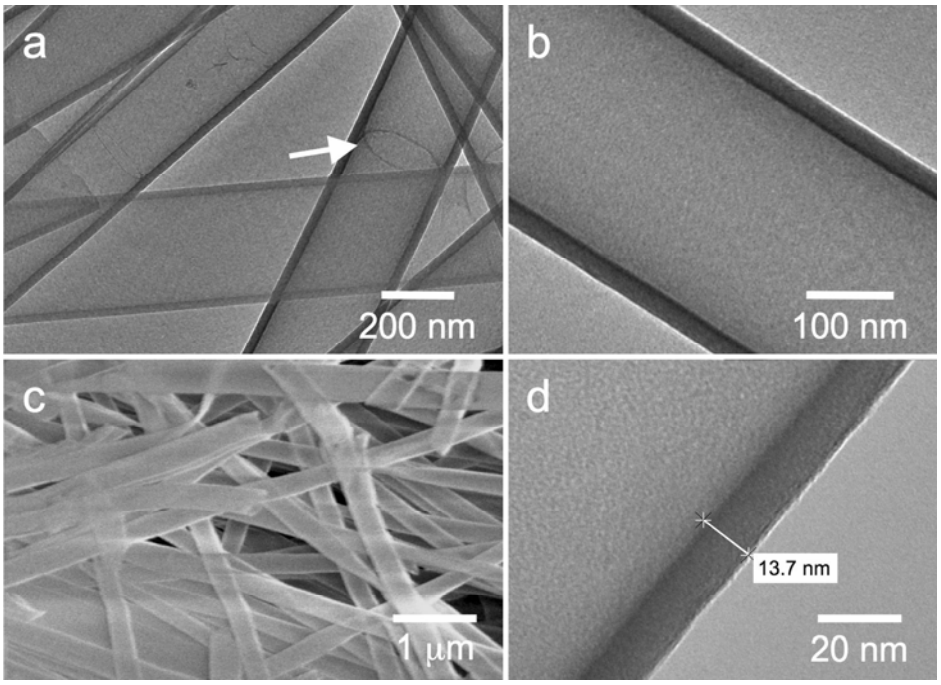

Figure 7.3. (a) FESEM image of an Al_2O_3 microtube in which ALD was performed on electrospun PVA fibers for 300 cycles at 45˚C. The arrow indicates a circle on the inside wall of the resultant microtube. (b) TEM image of the corresponding Al_2O_3 microtube illustrating the wall thickness. (c) FESEM and (d) TEM images of Al_2O_3 microtubes fabricated by ALD for 150 cycles at 45˚C. A wall thickness measurement is included in (d). In all cases, the electrospun PVA fiber templates were removed by heating in air at 400°C for 24 h.

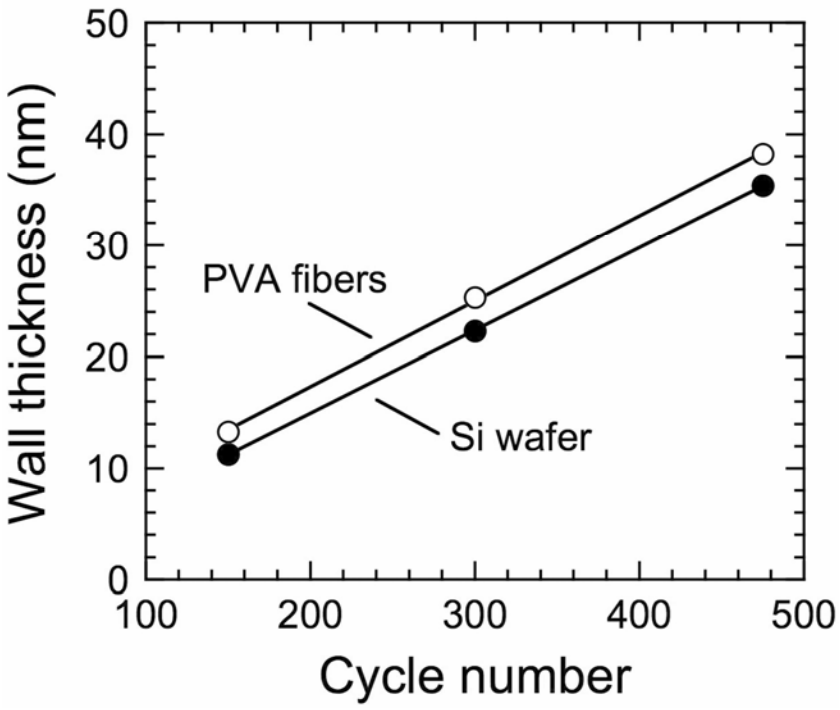

Figure 7.4. Wall thickness of Al_2O_3 microtubes prepared on electrospun PVA fibers (○) and measured by TEM as a function of ALD cycle number. Included for comparison is the Al_2O_3 film thickness on a planar Si substrate (●) measured by ellipsometry. The solid lines denote linear regressions of the data points. The corresponding average growth rates of Al_2O_3 are about 0.08 nm/cycle on the electrospun fibers and 0.07 nm/cycle on the Si substrate. Error bars (±1 standard deviation) deduced from analysis of 25 thickness measurements from each specimen are smaller than the symbols shown.

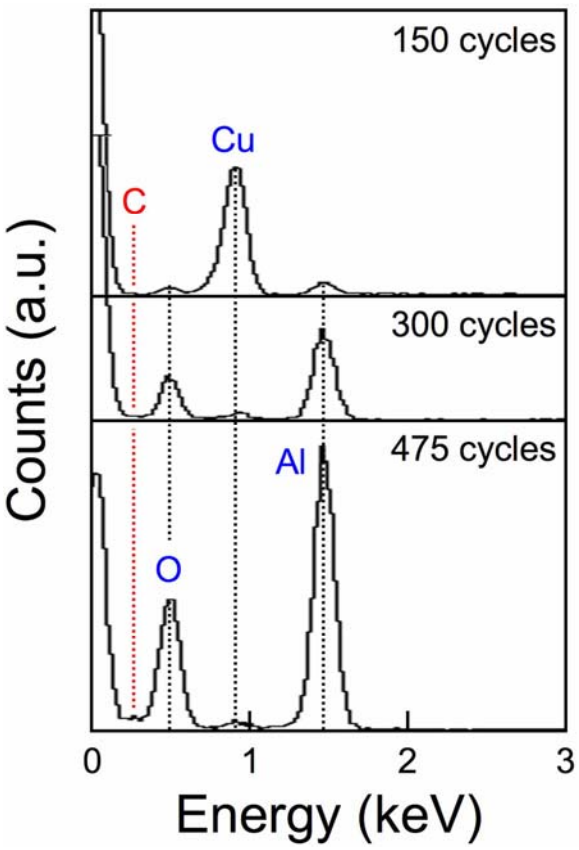

Figure 7.5. Representative EDS spectra acquired from the Al_2O_3 microtubes generated by ALD on electrospun polymer fibers after different cycle numbers (labeled). Note the presence of Al and O signals from Al_2O_3, as well as the absence of a discernible C peak from the polymer precursor (the instrument employed is capable of detecting C), after thermal treatment in air at 400°C for 24 h. The Cu signal is a consequence of the TEM grid and can be disregarded. The expected position for a signal due to C is also identified.

Chapter 8 is a reprint of a paper that will be submitted to the Journal of Applied Polymer Science

Uniform Coatings of Titanium Nitride onto High Surface Area Textile Materials using Atomic Layer Deposition

G. Kevin Hyde[1], S. Michael Stewart[2], Sunyeol Jeon[3]
and Gregory N. Parsons[2*]

[1]*Department of Textile Engineering, Chemistry, and Science*
[2]*Department of Chemical and Biomolecular Engineering*
North Carolina State University, Raleigh, NC 27695

[3]*Department of Chemical Engineering*
Hanyang University, Seoul, Korea

Abstract

Atomic layer deposition (ALD) is widely used in the semiconductor industry to produce inorganic insulating and metallic coatings on planar and irregular patterned surfaces. Recently, ALD applications have expanded into other areas, including nano-scale templating, optical coatings, thermal and chemical barrier layers, and for coatings on fibers where three dimensional conformation and structure are of particular interest. In this work, we show that vapor-phase ALD can be directly used to modify the chemical and structural properties of natural cotton textile fibers by depositing conformal nano-scale coatings of titanium nitride onto highly textured cotton surfaces. These results demonstrate the use of ALD on high surface area, highly complex cellulose-based natural fibers.

Specific Contribution

For this article, I worked with Michael Stewart to modify an existing ALD reactor for the low temperature deposition of titanium nitride. I worked with Michael to research possible precursors and reactants for the low temperature deposition of TiN. Once a suitable reaction scheme was decided on, we then built a new precursor cell to fit an existing ALD reactor. Michael and I also installed a new ammonia line in our group lab and attached it to the ALD reactor to use as the reactant. Once the reactor modifications were completed, I worked with Michael to test the TiN process on silicon samples and optimize the reaction conditions. I then planned a series of experiments for the deposition of TiN onto cotton samples. I helped train Sunyeol Jeon in the operation of the reactor. We then produced the samples of TiN modified cotton. A series of experiments were performed where dose times, cycles, and sample arrangement were varied. I was responsible for the XPS analysis of the samples and interpreting the results. Michael and I then conducted the contact angle analysis. I was responsible for interpreting the results. I also worked with Sunyeol to prepare samples for TEM. I wrote and revised the manuscript as well.

Chapter 8: Uniform Coatings of Titanium Nitride onto High Surface Area Textile Materials using Atomic Layer Deposition

8.1 Introduction

New molecular-scale process technologies that can controllably and uniformly modify complex textile structures such as fiber mats and bundles, woven fabrics, and engineered polymer structures, will enable and facilitate new emerging industrial products. Manufacturing techniques are of interest that can modify fiber surface functionality, as well as the bulk properties within a material such as a woven fabric to protect against mechanical, chemical, biological and thermal exposure, and effectively repel undesirable foreign substances, while maintaining the desired aesthetic and comfort characteristics.[1-6] Extending reactive systems and components to fabric platforms to produce catalytic mantles is another area of interest.[7] Inorganic insulator and metallic coatings are possible thin film materials that could achieve these desired properties.[1] Current methods for the coating of metallic compounds onto textile surfaces often result in non-uniform deposition, use large amounts of energy and raw materials, and create excess waste.[1,2,8] The development of new technologies for textile finishing could provide numerous opportunities for improved processes and new products.

The technique of atomic layer deposition (ALD) exploits a set of sequential, self-limiting deposition processes that operate on the principle of alternating saturating surface reactions. During ALD, a substrate is exposed to a precursor vapor that forms a (sub)monolayer of the precursor on the surface of the substrate. After excess precursor is

removed from the vapor phase by a purge gas (e.g., Ar), the reactant gas is subsequently pulsed onto the substrate, where it reacts with the adsorbed precursor layer to form a layer of the target film-forming material. Since no gas phase reaction occurs, the target film is grown layer-by-layer on the substrate, so that the thickness of the deposited film can be accurately controlled by the number of cycles the process is repeated.[9-12] Because of its unique process characteristics and controllability, ALD can be used to deposit conformal, uniformly thin films with precise thickness and composition control over large scales. Moreover, ALD is chemically versatile and has been used to fabricate layers of metals,[13-15] metal oxides,[16] metal nitrides[12,13] and other materials. An additional benefit of ALD is that the deposition of Al_2O_3,[11,12] TiO_2[17] and TiN[13] can be conducted at relatively low temperatures (< 150˚C), thereby reducing, if not altogether eliminating, thermal damage to temperature-sensitive substrates such as polymers. Also, selective deposition can be controlled by modifying the surface energy of the deposition substrate.[15] ALD, based on the fact that it is a vapor phase technology, can fully diffuse into porous textile structures, providing conformal and uniform coatings.

Titanium nitride (TiN) is a material of interest in a variety of applications. For example, TiN is one of the most used diffusion barrier films in semiconductor devices.[18] Titanium nitride films have low resistivity, high melting points, and good thermal and chemical stability.[19,20] In addition, TiN is a very strong material and is often used as a hard, wear-resistant coating.[21] Titanium nitride is also used in bioimplants and has been studied recently as an antibacterial coating.[22] Atomic layer deposition of TiN is often performed using titanium chloride and ammonia as precursor and reactant, respectively.[23,24] However,

chloride based precursors are not favorable for ALD due to the corrosive nature of the reaction products and the high temperatures needed to complete the reaction. More recent experiments have focused on the use of metal organic precursors for the deposition of TiN by ALD and in particular the use of tetrakis(dimethylamido)titanium (TDMAT) as a precursor.[25,26] The use of TDMAT as a precursor offers the ability to create uniform, conformal films of TiN at low temperatures (<150°C).

In this study, we investigate the low temperature ALD of TiN onto cotton fibers and fabrics using TDMAT as the metal organic precursor source and NH_3 as the reactant gas. Surface profilometry was used to measure the thickness of the TiN thin films on silicon substrates. The coated cotton fabrics were examined by X-ray photoelectron spectroscopy (XPS) and static contact angle measurements in order to understand the effect of film thickness on the surface energy and chemical composition of the fabric. These studies demonstrate that ALD of TiN is a feasible method for the uniform, conformal coating of textile materials useful in a variety of new applications.

8.2 Experimental

8.2.1 Sample Preparation

Tetrakis(dimethylamido)titanium (TDMAT, Strem Chemicals) was used as received from the supplier, and was maintained at 27ºC while being introduced into the reactor using argon as a carrier gas. Argon (National Welders) for both purging and precursor dosing was maintained at 100 sccm and was dried through a Drierite® gas drier. Ammonia (National Welders) was introduced as received into the reactor at the same flow rate as the argon.

Pressure was maintained at two Torr during processing and cycles consisted of a five second argon purge, five second TDMAT dose, five second argon purge, and finally a five second ammonia dose. During the deposition process, the substrates were introduced into the reactor and heated in vacuum ($5x10^{-6}$ Torr) to 100°C. TiN film growth advances by two self-limiting surface reactions that, when done in an alternating sequence, create a TiN film with controllable growth rate.

Silicon wafers were prepared from 0.0250-0.0250 resistivity, heavily boron-doped p-type silicon supplied by MEMC Electronic Materials, Inc. The silicon was initially cleaned using BakerClean™ (JT Baker) followed by submersion in 10% HF solution (BOE, JT Baker) until hydrophobicity was observed, then an additional twenty-five seconds of HF washing in the same solution. This treatment was followed by ten minutes of treatment in a 100mL DI water bath with 0.5mL of ammonium hydroxide solution (Fisher) and 2mL of 30% hydrogen peroxide solution (Fisher) at 45ºC to create a uniformly hydrogen terminated chemical oxide. Finally, the wafers were blown dry using nitrogen.

Bleached and mercerized woven cotton fabric (Textile Innovators) was used as received. Fiber fabric samples were cut into approximately 2 cm x 2 cm pieces before being used. The fabric samples were ~1 mm thick.

There were five one and a half inch spots available for samples on the quartz boat, whose positions were numbered one, pointing at the flow, to five, pointing towards the pump, so that position one was the first to receive doses from the source lines. To minimize variations, two distinct arrangements of the samples were used; one arrangement for growth rate studies and the second arrangement for surface characterization studies. To determine

the growth rate of the TiN step-height, samples were placed in the fourth position and glass slides were clipped to the samples to create a measurable step. For surface characterization samples, cotton samples for contact angle measurements were placed in the second position, cotton samples for XPS were placed in the third position, fabric samples for TEM measurements were placed in the fourth position, and silicon for profilometry measurements were placed in the fifth boat. All cotton samples were taped to the boat using two pieces of high temperature polyamide tape attached to the sides of the boat.

8.2.2 Sample Characterization

Step height measurements were taken by attaching a glass slide onto the silicon wafer using a clip. Measurements were taken using a Tencor Instruments Alpha-Step® 500 Surface Profiler with a scan distance of two-thousand micrometers, a scan speed of two-hundred micrometers per second, and a probe force of 31.4 milligrams.

X-ray photoelectron spectroscopy (XPS) was used to determine the film thickness and composition on the cotton fabric substrates. 5 mm x 5 mm samples of the cotton fabric were cut and attached to the XPS sample holder using double sided copper tape. XPS measurements were done using a Kratos AXIS Ultra spectrometer with an Al source and a spherical mirror analyzer working in spectrum mode. The total pressure in the main vacuum chamber during analysis was $\sim 4\times10^{-7}$ Torr. Spectra were collected with the stage containing the samples at 0°. The take-off angle of the electrons was 90° and the angle of the incident X-ray beam hitting the sample was 30°. The chemical elements present on the samples were identified from survey spectra. The survey scans started at 1200 eV and ended at −5 eV

taking 1 eV steps with a dwell time of 200 ms. High resolution detail scans were performed around peaks of interest. Charge effect was corrected using C1s at 285.0 eV as a reference position. Data processing was performed using CasaXPS software (London, UK).

Transmission electron microscopy (TEM) was used for characterizing film conformality and uniformity. TEM also allowed the thickness of the layers on the coated fibers to be determined. TEM images were obtained using a Hitachi HF-2000 system using a cold field emission electron source with an accelerating voltage of 200 kV. The TEM system was equipped with an Advanced Microscopy Techniques XR-60B camera system for digital imaging. Planar samples were prepared by randomly pulling individual fibers from the cotton fabrics using tweezers. The fibers were mounted to 200 mesh Cu grids using double sided tape. A second grid was then placed on top to hold the fibers between the grids. Cross-sectional samples were made by embedding the fabrics in an epoxy resin and then cutting the samples with an ultra-microtome into thin sections. The samples were then placed on Cu grids.

8.3 Results and Discussion

Titanium nitride was deposited on woven fabrics of cotton fibers using ALD. For this research, ALD of TiN was performed in a hot-wall, viscous-flow tube reactor that is described in detail elsewhere. One cycle of the process consisted of introduction of TDMAT, NH_3, and argon purge gases. Each gas was pulsed into the reactor for 5 second pulses in the order Ar/TDMAT/Ar/NH_3. Cotton is made up of the polymer cellulose $(C_6H_{10}O_5)_n$, which

presents –OH groups on the surface which are capable of reacting with the initial dose of TDMAT.

Growth rate studies on silicon were conducted to better understand TiN growth at low temperatures. As reported by other groups, growth of titanium nitride is non-ideal due to diffusion of precursor and reagent into the porous film during deposition.[25] Due to the surface area as well as the tortuousness of the path the TDMAT and ammonia have to take to move within the cotton, the amount of time required for the precursor and reagent to diffuse into the cotton should be much greater than that seen for silicon. As such, it is reasonable to assume that growth on the cotton is much different than for silicon as diffusion limitations do not give either reactant enough time to substantially diffuse into the film.

Growth rate studies were done by first varying the ammonia dose from two, three, five, and seven seconds with five seconds of TDMAT dosing, and then repeating the same dosing times for TDMAT at the optimized ammonia dose. For all samples used in growth rate studies, two hundred cycles were used. Film thicknesses were measured using surface profilometry.

Growth was seen to plateau after three seconds, indicating saturation. With increased dose times there is more likelihood that the reagents will diffuse into the films, thus there was a steady upward climb in the data as dose time was increased. A similar saturation curve was seen when varying TDMAT dose times, where a constant five second dose of ammonia was used. A plateau was again seen after three seconds. Based on the data from the saturation curves, a recipe of 5 second pulses in the order Ar/TDMAT/Ar/NH_3 and an operating

pressure of 2 Torr was used to deposit TiN on the cotton substrates. This ALD recipe is comparable to setups used by other research groups.[26]

Atomic layer deposition was performed on cotton fabric samples for a range of cycles at a temperature of 100°C. A change was observed in the color of the cotton samples during TiN ALD. There is very little color change from the untreated sample to the samples that underwent one cycle and five cycles of ALD. Starting with 10 cycles, a brownish-gold color begins to appear on the fabric samples. The TiN is very uniformly deposited on the surface of the cotton samples. It could also be seen that deposition also occurs on the bottom of the samples. Fabric samples up to 20 cycles appear to be uniformly coated by TiN. For 50 cycles and greater, the deposition is less uniform. The uniformity of the TiN film on the bottom of the samples could be improved by changing dosing times and the operating pressure.

The chemical composition of the TiN films deposited on the cotton substrates were analyzed using XPS. XPS analysis was performed on the top side of the cotton samples. It should also be noted that XPS analysis was performed two weeks after the initial samples were created. Samples were then stored in ambient conditions until they were analyzed. Figure 8.1 shows a comparison of the survey spectra for unmodified cotton and cotton coated with 100 cycles of TiN by ALD. Dominant signals for C and O are seen for the untreated cotton fabric. Signals of C, O, N, and Ti are detected for the TiN coated fabrics. Both the C and O peaks decrease in intensity as the fibers are coated with TiN.

High-resolution detail scans were performed around peaks of interest: Ti 2p, O 1s, C 1s, and N 1s. Changes in the chemical composition of the surface of the cotton substrates

were analyzed as a function of the number of ALD cycles. Figure 8.2(a) shows a high-resolution spectra of the Ti 2p signal. As expected, the Ti peak increases as the number of ALD cycles increase. As the TiN film becomes sufficiently thick at around 20 cycles, the Ti 2p signals become much more distinct. Two clear peaks can be seen for the TiN films, Ti $2p_{3/2}$ at 458.5 eV and Ti $2p_{1/2}$ at 464.0 eV. The structure of the signal is a result of different phases within the TiN film, in particular nitride, oxide, and oxynitride.[21,27] The peak at 458.5 eV corresponds to the existence of compounds such as TiN_xO_y and/or TiN_xO_{1-x} oxy-nitrides or reduced oxide states such as Ti_2O_3.[28] The Ti $2p_{1/2}$ peak at 464.0 eV can be ascribed to Ti-N bonds within the film.[29]

The O 1s spectrum is shown in Figure 8.2(b). The O 1s signal at 533.0 eV for untreated cotton is consistent with the expected peak position for C-O bonds.[30,31] As the thickness of the TiN film increases, the peak at 533.0 eV decreases while at the same time a signal becomes visible at 530.2 eV corresponding to O 1s from the surface layer of TiO_2.[32,33] A second component also becomes apparent at 532.0 eV. This second peak is likely associated with adsorbed water and oxygen or with N-O bonding and oxynitrides.[33,34]

The XPS spectrum of the C 1s peak is shown in Figure 8.2(c). It can be seen that the C 1s spectra can be divided into three components. The most intense signal for the untreated cotton fibers occurs at 286.7 eV, associated with the C-O bonds that make up the cellulose structure.[30] Less intense peaks are seen at 285.0 and 288.0 eV, corresponding to C-C and O-C-O bonds respectively. Again, a decrease in the intensity of the signals from the cellulose substrate can be observed as the fibers are coated with TiN. The sample treated with 100

cycles of TiN ALD shows the same three components at lower intensities. The carbon peaks for the thicker TiN films likely result from atmospheric contamination.[33]

Figure 8.2(d) shows the XPS spectra for N 1s. The dominant N 1s signal is located at a binding energy of 396.5 eV. It is generally accepted that this peak is characteristic of TiN.[32,33] The broad shoulder between 399.0 eV and 402.0 eV. The peak at 399.0 eV is normally attributed to the presence of N-O.[32,34] However, there is some disagreement in the literature in regards to the N 1s peak assignments, as the smaller signal could also be attributed to N-C bond formation.[33]

Based on the XPS data, it appears that oxygen bonds form on the surface of the samples due to air oxidation. Oxygen signals appear in the XPS spectra as a result of adsorbed molecules and the formation of oxides such as TiO_2. It has been shown that TiN is oxidized when exposed to air at room temperature. This forms a surface oxide layer of TiO_2 ($TiN + O_2 \rightarrow TiO_2 + (1/2)N_2$).[35] Beneath the oxidized surface layer, the coating exhibits more properties of a TiN film, as demonstrated by the characteristic gold color of the films and the presence of a clear Ti-N peak in the N 1s spectra.

The effect of the TiN coatings on the surface energy of the cotton fibers was examined using sessile drop experiments. Static water contact angle measurements show that fabric samples treated with a low number of ALD cycles exhibit very large contact angles when compared to untreated cotton and TiN coatings on silicon. It is well known that bleached and mercerized cotton fibers are exceedingly hydrophilic and easily absorb water, giving the uncoated fabrics a static water contact angle of 0°. SiO_2 treated with 5 cycles of TiN exhibited a static water contact angle of 55°. This is in contrast to a static water contact

angle of 122° for cotton fabric treated with 5 cycles of TiN. Cotton fabric treated with 1 cycle of TiN demonstrated an even greater static water contact angle of 133°. Figure 8.3 shows the static water contact angle on TiN treated cotton fabrics as a function of the number of ALD cycles. It can be seen that a critical point is reached between 10 and 20 cycles. After 20 cycles of TiN ALD, the cotton fabrics revert to a hydrophilic state.

Research has shown that the wettability of a surface is not only a function of the chemistry of the surface but also the topography and roughness of a sample material.[36-39] The large contact angle is ascribed to an increase in the rigidity of surface fibers by the more incompliant inorganic coating, effectively reducing the total contact area between the fiber and the water droplet and enhancing the hydrophobicity of the fabric surface. For fabrics treated with a low number of TiN ALD cycles (< 20 cycles), the TiN coating is very thin and increases the rigidity of the cotton fibers.

Static contact angle experiments were also used to demonstrate the ability of the ALD process to penetrate through the complex, three dimensional cotton fabrics. A fabric sample was folded during ALD, with the left-half of the sample folded under the right-half of the sample. The right side showed a darker, brownish gold color, except where thermal tape partially covered the surface to hold the sample in place. We noted that both sides of the sample clearly demonstrated hydrophobic behavior, which we ascribed to TiN deposition throughout the sample volume. The XPS presented confirms the presence of Ti within the coating. A similar control fabric sample that followed the same process method without the precursor exposures was completely hydrophilic. The darker top surface indicated non-uniformity of the coating thickness, which could be improved by more full understanding of

the process conditions. This ability to conformally modify woven textile materials with near monolayer precision may help enable new multifunctional textiles with properties and performance that deviate radically from current structured fabrics.

Figure 8.4 shows transmission electron microscopy of cotton samples coated with 200 cycles of TiN ALD at an operating pressure of 2 Torr and a temperature of 100°C. It should be noted that noted that the images in Figure 8.4 were obtained from individual fibers that were randomly extracted from the woven fabric samples. Figure 8.4(a) demonstrates the ability of ALD to conformally coat the complex surface of the cotton fiber. The TiN coating is also very uniform along the fiber surface. The white areas in Figure 8.4(a) are a result of separation of the fiber from the binding resin used for sample preparation. Defects and breaks in the TiN result from fracture during cross-sectioning of the samples.

The thickness of the TiN films is approximately 600 Å. Other random samples were imaged using the same ALD procedure and demonstrated similar thicknesses and uniformity. With a thickness of 600 Å, the growth rate of the TiN on the cotton fibers is approximately 2 Å per cycle. This growth rate is smaller than the 4 Å per cycle seen for the TiN films grown on silicon. The change in growth rate could be attributed to the fact that the reactants require longer to diffuse throughout the cotton samples. Also, the initial reactants may adsorb into the outer surface of the cotton fibers, requiring more time before a uniform film is created. Knudsen diffusion is the probable method of precursor diffusion through the bulk of the cotton fabric.

A more detailed electron microscopy with higher magnification is presented in Figure 8.4(b). The interface between the cotton fiber and the TiN coating can be clearly seen, with

the cotton fiber in the bottom left corner of the image and the TiN film being represented by the dark film. This film is sufficiently thick to change the color of the cotton fibers. The thickness of the coating is very uniform along the surface of the fiber. A gradient in the shade of the TiN film can be seen at the interface of the cotton fiber and the interface between the TiN coating and the embedding resin. This difference could be attributed to the formation of TiO_2 at the interfaces. An initial layer of TiO_2 could be formed during the first ALD cycle as the TDMAT precursor reacts with –OH groups on the surface of the cotton fibers. TiN ALD growth then occurs. When the samples are removed from the reactor and exposed to air, a portion of the TiN film oxidizes, forming a surface layer of TiO_2, which correlates to the XPS data. Microscopy images provide direct evidence of the conformal and uniform deposition of TiN onto the cotton fibers.

This work has characterized TiN films deposited onto cellulose fibers with ALD. In addition, TiN ALD was done at low temperatures, thereby reducing, if not altogether eliminating, thermal damage to the temperature-sensitive substrates. Contact angle analysis revealed the ability of TiN ALD to drastically change the surface characteristics of cellulose after a very small number of cycles. Further physical testing may suggest additional useful and unique applications for the ALD process.

8.4 Acknowledgements

The authors acknowledge support from the National Science Foundation under grant CTS-0626256.

8.5 References

1. Bajaj, P. Finishing of Textile Materials. *Journal Of Applied Polymer Science* **83**, 631-659 (2002).

2. Black, S., Kapsali, V., Bougourd, J. & Geesin, F. in Textiles for protection. (ed. R.A. Scott) 60-89 (Woodhead Publishing Limited, Cambridge; 2005).

3. Mahltig, B. & Bottcher, H. Modified silica sol coatings for water-repellent textiles. *J. Sol-Gel Sci. Technol.* **27**, 43-52 (2003).

4. Mahltig, B., Fiedler, D. & Bottcher, H. Antimicrobial sol-gel coatings. *J. Sol-Gel Sci. Technol.* **32**, 219-222 (2004).

5. Mahltig, B., Haufe, H. & Bottcher, H. Functionalisation of textiles by inorganic sol-gel coatings. *J. Mater. Chem.* **15**, 4385-4398 (2005).

6. Stull, J.O. in Textiles for protection. (ed. R.A. Scott) 295-354 (Woodhead Publishing Limited, Cambridge; 2005).

7. Besson, M., Gallezot, P., Perrard, A. & Pinel, C. Active carbons as catalysts for liquid phase reactions. *Catal Today* **102**, 160-165 (2005).

8. Leonas, K.K. in Textiles for Protection. (ed. R.A. Scott) 441-464 (Woodhead Publishing Limited, Cambridge; 2005).

9. Ferguson, J.D., Weimer, A.W. & George, S.M. Atomic layer deposition of Al2O3 films on polyethylene particles. *Chem Mater* **16**, 5602-5609 (2004).

10. Gordon, R.G. Review of recent progress in atomic layer deposition (ALD) of materials for micro- and nano-electronics. *Abstracts Of Papers Of The American Chemical Society* **227**, U553-U554 (2004).

11. Groner, M.D., Fabreguette, F.H., Elam, J.W. & George, S.M. Low-temperature Al_2O_3 atomic layer deposition. *Chem Mater* **16**, 639-645 (2004).

12. Ritala, M. et al. Perfectly conformal TiN and Al_2O_3 films deposited by atomic layer deposition. *Chem Vapor Depos* **5**, 7-9 (1999).

13. Kim, H. Atomic layer deposition of metal and nitride thin films: Current research efforts and applications for semiconductor device processing. *J Vac Sci Technol B* **21**, 2231-2261 (2003).

14. Park, K.J., Doub, J.M., Gougousi, T. & Parsons, G.N. Microcontact patterning of ruthenium gate electrodes by selective area atomic layer deposition. *Appl Phys Lett* **86** (2005).

15. Park, K.J. & Parsons, G.N. Selective area atomic layer deposition of rhodium and effective work function characterization in capacitor structures. *Appl Phys Lett* **89** (2006).

16. Kim, H. & McIntyre, P.C. Atomic layer deposition of ultrathin metal-oxide films for nano-scale device applications. *Journal Of The Korean Physical Society* **48**, 5-17 (2006).

17. Kemell, M., Pore, V., Ritala, M., Leskela, M. & Linden, M. Atomic layer deposition in nanometer-level replication of cellulosic substances and preparation of photocatalytic TiO2/cellulose composites. *Journal of the American Chemical Society* **127**, 14178-14179 (2005).

18. Kaloyeros, A.E. & Eisenbraun, E. Ultrathin diffusion barriers/liners for gigascale copper metallization. *Annu Rev Mater Sci* **30**, 363-385 (2000).

19. Ritala, M., Leskela, M., Rauhala, E. & Jokinen, J. Atomic layer epitaxy growth of TiN thin films from TiI4 and NH3. *J Electrochem Soc* **145**, 2914-2920 (1998).

20. Schulberg, M.T., Allendorf, M.D. & Outka, D.A. Aspects of nitrogen surface chemistry relevant to TIN chemical vapor deposition. *J Vac Sci Technol A* **14**, 3228-3235 (1996).

21. Kim, J., Hong, H., Ghosh, S., Oh, K.Y. & Lee, C. Physical properties of highly Conformal TiN thin films grown by atomic layer deposition. *Jpn J Appl Phys 1* **42**, 1375-1379 (2003).

22. Jeyachandran, Y.L. et al. Bacterial adhesion studies on titanium, titanium nitride and modified hydroxyapatite thin films. *Mat Sci Eng C-Bio S* **27**, 35-41 (2007).

23. Ritala, M., Leskela, M., Rauhala, E. & Haussalo, P. Atomic Layer Epitaxy Growth of Tin Thin-Films. *J Electrochem Soc* **142**, 2731-2737 (1995).

24. Uhm, J. & Jeon, H. TiN diffusion barrier grown by atomic layer deposition method for Cu metallization. *Jpn J Appl Phys 1* **40**, 4657-4660 (2001).

25. Elam, J.W., Schuisky, M., Ferguson, J.D. & George, S.M. Surface chemistry and film growth during TiN atomic layer deposition using TDMAT and NH3. *Thin Solid Films* **436**, 145-156 (2003).

26. Kim, J.Y., Choi, G.H., Kim, Y.D., Kim, Y. & Jeon, H. Comparison of TiN films deposited using tetrakisdimethylaminotitanium and tetrakisdiethylaminotitanium by the atomic layer deposition method. *Jpn J Appl Phys 1* **42**, 4245-4248 (2003).

27. Kim, J., Hong, H., Oh, K. & Lee, C. Properties including step coverage of TiN thin films prepared by atomic layer deposition. *Appl Surf Sci* **210**, 231-239 (2003).

28. Bertoti, I., Mohai, M., Sullivan, J.L. & Saied, S.O. Surface Characterization of Plasma-Nitrided Titanium - an Xps Study. *Appl Surf Sci* **84**, 357-371 (1995).

29. Devia, A., Benavides, V., Restrepo, E., Arias, D.F. & Ospina, R. Influence substrate temperature on structural properties of TiN/TiC bilayers produced by pulsed arc techniques. *Vacuum* **81**, 378-384 (2006).

30. Beamson, G. & Briggs, D. High Resolution XPS of Organic Polymers. (Wiley, Chichester, England; 1992).

31. Yeqiu, L., Jinlian, H., Yong, Z. & Zhuohong, Y. Surface modification of cotton fabric by grafting polyurethane. *Carbohydrate Polymers*, 276-280 (2005).

32. Ni, C.Y. et al. Effect of film thickness and the presence of surface fluorine on the structure of a thin barrier film deposited from tetrakis-(dimethylamino)-titanium onto a Si(100)-2 x 1 substrate. *Thin Solid Films* **515**, 3030-3039 (2007).

33. Vesel, A., Mozetic, M., Kovac, J. & Zalar, A. XPS study of the deposited Ti layer in a magnetron-type sputter ion pump. *Appl Surf Sci* **253**, 2941-2946 (2006).

34. Arias, D.F., Arango, Y.C. & Devia, A. Study of TiN and ZrN thin films grown by cathodic arc technique. *Appl Surf Sci* **253**, 1683-1690 (2006).

35. Saha, N.C. & Tompkins, H.G. Titanium Nitride Oxidation Chemistry - an X-Ray Photoelectron-Spectroscopy Study. *J Appl Phys* **72**, 3072-3079 (1992).

36. Daoud, W.A., Xin, J.H. & Tao, X.M. Superhydrophobic silica nanocomposite coating by a low-temperature process. *J Am Ceram Soc* **87**, 1782-1784 (2004).

37. Daoud, W.A., Xin, J.H. & Tao, X.M. Synthesis and characterization of hydrophobic silica nanocomposites. *Appl Surf Sci* **252**, 5368-5371 (2006).

38. Gao, L.C. & McCarthy, T.J. "Artificial lotus leaf" prepared using a 1945 patent and a commercial textile. *Langmuir* **22**, 5969-5973 (2006).

39. Gao, L.C. & McCarthy, T.J. A perfectly hydrophobic surface (theta(A)/theta(R)=180 degrees/180 degrees). *Journal of the American Chemical Society* **128**, 9052-9053 (2006).

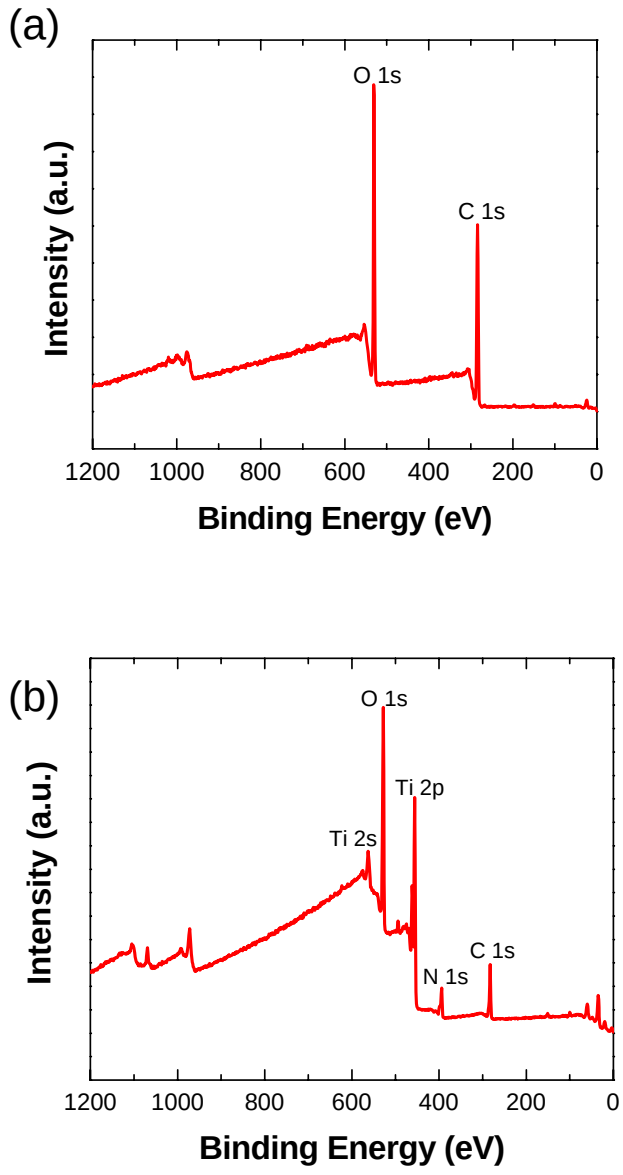

Figure 8.1. Comparison of XPS survey spectra of untreated cotton and cotton treated with 100 cycles of TiN ALD. (a) XPS survey spectra of untreated cotton. Dominant peaks of C and O can be seen. (b) XPS survey spectra of cotton treated with 100 cycles of TiN ALD. In addition to C and O peaks, peaks can now be seen for Ti and N, verifying the presence of a TiN coating.

Figure 8.2. XPS detail spectra of TiN on cotton substrates. For each of the graphs 0 cycles = black, 1 cycle = red, 5 cycles = green, 10 cycles = dark blue, 20 cycles = light blue, 50 cycles = magenta, 100 cycles = yellow (a) XPS detail spectra of Ti2p. The Ti2p signal, which consists of two distinct peaks, can be seen to increase as the number of ALD cycles increases. (b) XPS detail spectra of O1s. The peak can be seen to decrease and shift to lower binding energy as TiN is deposited. (c) XPS detail spectra of C1s. It can be seen that the C-O and O-C-O peaks found in the untreated cotton decrease as the fibers are coated with TiN while the C-C peak increases. (d) XPS detail spectra of N1s. As expected, there is no N peak for untreated cotton fibers. An increase in the N1s peak can be seen as the number of ALD cycles increases.

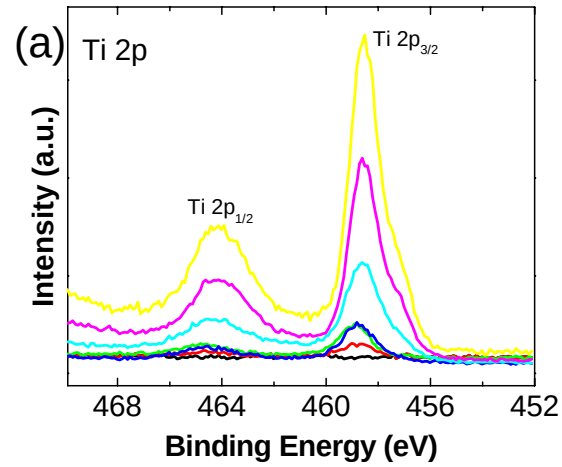
(a)
Ti 2p
Ti 2p3/2
Ti 2p1/2
Intensity (a.u.)
468
464
460
456
452
Binding Energy (eV)

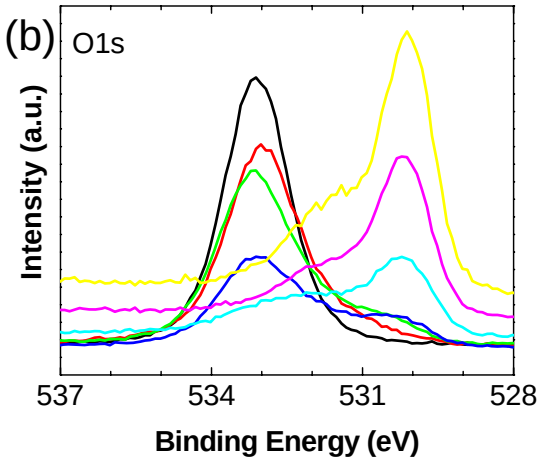
(b)
O1s
Intensity (a.u.)
537
534
531
528
Binding Energy (eV)

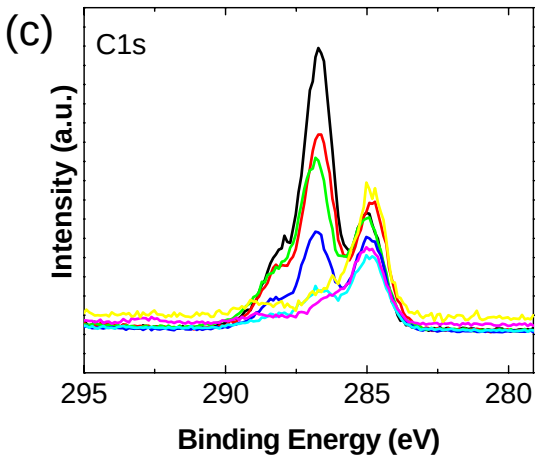
(c)
C1s
Intensity (a.u.)
295
290
285
280
Binding Energy (eV)

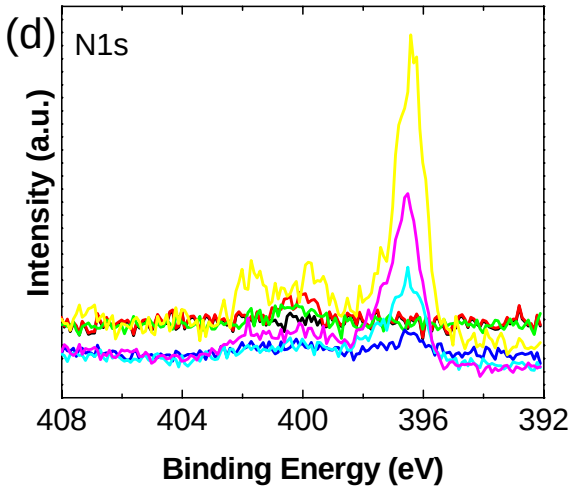
(d)
N1s
Intensity (a.u.)
408
404
400
396
392
Binding Energy (eV)

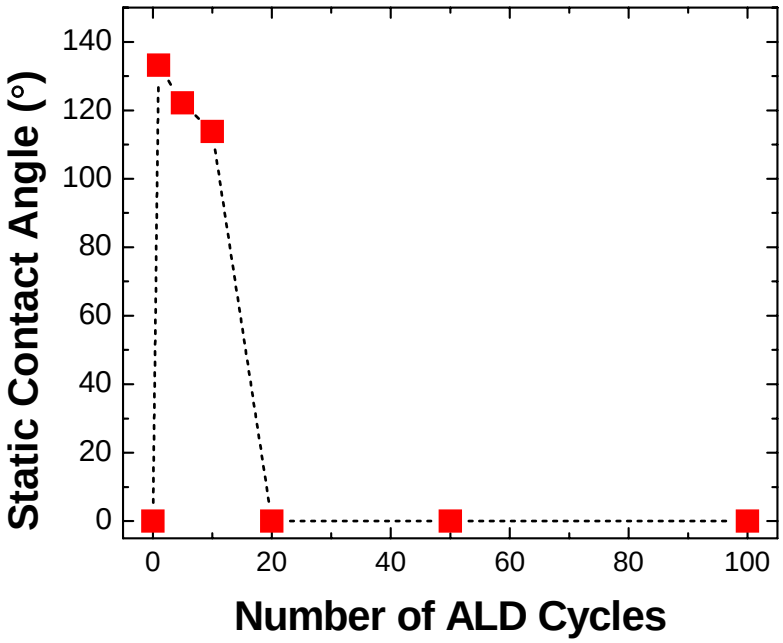

Figure 8.3. Static water contact angle on TiN coated fabric. ALD cycle number versus static water contact angle for TiN ALD coated fabric samples. The change in contact angle between 10 and 20 cycles can be clearly seen. The large contact angle is ascribed to an increase in the rigidity of surface fibers by the more incompliant inorganic coating.

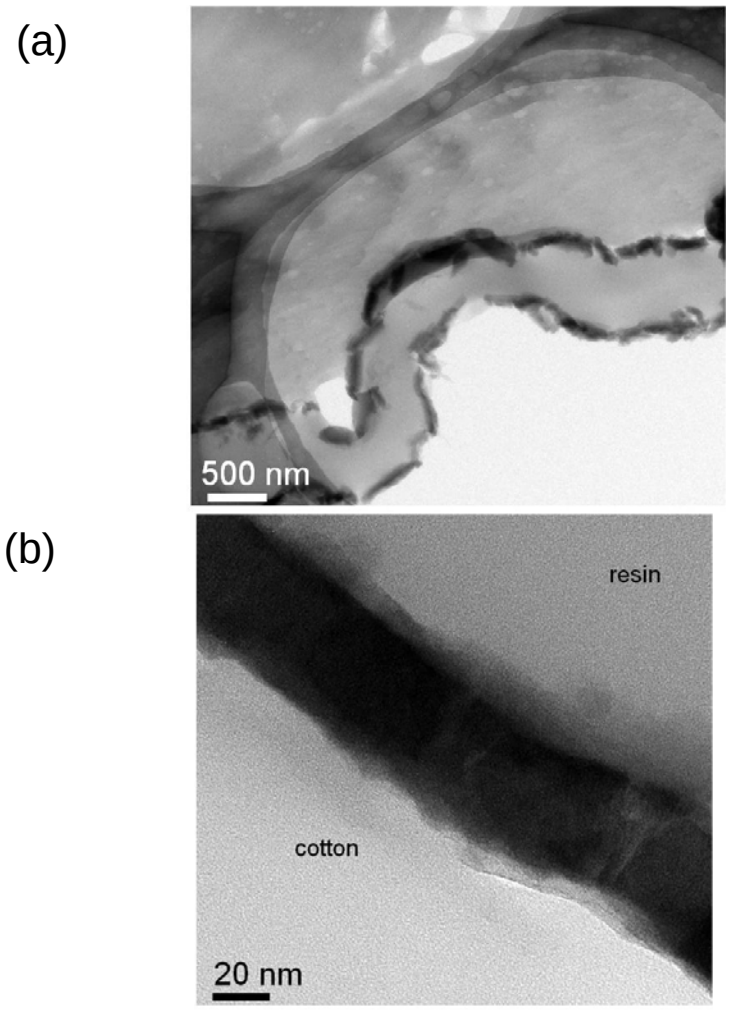

Figure 8.4. Transmission electron microscopy (TEM) of a TiN coated cotton textile fiber treated with 200 cycles of TiN ALD. (a) Cross-sectional image of cotton fiber showing conformal coating of TiN. Defects seen in the coating can be attributed to the sample preparation process. (b) High resolution cross-sectional image of cotton fiber detailing nature of TiN coating. A very thick layer of TiN can be seen on the surface of the cotton fiber. The change in gradient at the interface of the TiN film and the resin could be a result of the presence of a small layer of TiO_2 on the surface of the TiN coating.

Chapter 9 is a reprint of a paper that will be submitted to Chemical Vapor Deposition

Characteristics of TiO_2 Films Deposited on Cellulose Fibers by Atomic Layer Deposition

G. Kevin Hyde[1], S. Michael Stewart[2],
and Gregory N. Parsons[2*]

[1]*Department of Textile Engineering, Chemistry, and Science*
[2]*Department of Chemical and Biomolecular Engineering*
North Carolina State University, Raleigh, NC 27695

Abstract

Titanium dioxide thin films were grown by atomic layer deposition (ALD) on temperature sensitive substrates of cellulose based fabrics. ALD was conducted using tetrakis(dimethylamido)titanium (TDMAT) as the precursor and water as the reactant. Films were deposited at a deposition temperature of 100°C using purified argon as a carrier and purge gas. Growth rate as a function of cycles is shown to be linear. The films deposited are amorphous and highly pure. The characteristics of the films were studied by XPS, TEM, and static contact angle measurements. Contact angle measurements show a change in the surface energy of the cellulose fibers as they are coated. The results indicate that ALD of TiO_2 is a promising method for the modification of fibrous surfaces and the production of fiber based catalytic devices.

Specific Contribution

For this paper, I worked with Michael Stewart to prepare the reactor for deposition of the titanium dioxide films. We worked together to install a QMS systems for analysis of the reaction procedure. Initial experiments were done on silicon so that the film thickness could be easily determined. I determined a series of experiments for the deposition of TiO_2 onto cotton fabrics. I worked with Michael to prepare all of the samples. After sample preparation, I performed the XPS analysis and interpreted the results. Michael gathered the contact angle data and I did the analysis of the contact angle measurements. I prepared the manuscript that is presented in this dissertation. This paper requires some type of microscopy work before it is ready for publication.

Chapter 9: Characteristics of TiO_2 Films Deposited on Cellulose Fibers by Atomic Layer Deposition

9.1 Introduction

Titanium dioxide (TiO_2) is a material of interest for a variety of applications due to its beneficial properties. Applications of the material include coatings for solar cells[1,2], coatings for biomaterials[3,4], anti-reflective coatings[5], and photosensitive layers for photocatalysts.[6-9] Recently, TiO_2 has been studied as a photoactive coating for fibrous textile substrates.[4,10-12] Specific applications for TiO_2 modified textile materials include self-cleaning materials[10,11], materials with improved biocompatability[4,12] and high surface area substrates for coatings capable of photocatalytic oxidation.[13] Fibrous structures are of particular interest for TiO_2 based photocatalyis due to their large surface and illuminated areas when compared to traditional deposition platforms.[14,15]

Many different techniques have been used for the deposition of TiO_2 coatings and films. Coatings of particulate TiO_2 can be achieved using wet deposition techniques such as sol-gel deposition[10,11] and dip coating.[13] Thin films of TiO_2 have been created by numerous well known physical and chemical thin film deposition methods from liquid and gas phases.[8] Of the deposition methods available, atomic layer deposition (ALD) is becoming an increasingly popular method.[16] Atomic layer deposition is a modified form of chemical vapor deposition (CVD). Where CVD uses simultaneous dosing of reactants and relies on both gas and surface reactions, ALD uses alternating exposures of reactants to the substrate surface, resulting in self-limiting surface reactions. This alternating sequence ensures that surface reactions occur only with reactive sites created by the previous cycle. The self-

limiting nature of ALD allows atomic level thickness control and provides high quality, conformal films.[9,17,18] Recent studies have demonstrated the use of ALD at low temperatures (<100°C).[19,20] The ability to conduct ALD at lower temperatures has allowed the process to be applied to temperature sensitive materials such as natural fibers and polymers.[16]

Deposition of TiO_2 by ALD can be done with a variety of metal precursors and reactants. One of the most common systems makes use of titanium-tetrachloride ($TiCl_4$) as the metal precursor and water as the reactant.[9,21-23] Titanium-tetrachloride has the advantage of being a liquid at room temperature with a moderate vapor pressure. However, $TiCl_4$ is corrosive and forms HCl as a by-product. This has led to a search for other suitable precursors. Titanium alkoxides, in particular titanium- isopropoxide[16,24], titanium-ethoxide[6], and titanium-methoxides[8], have been used successfully for TiO_2 ALD. It is necessary for ALD precursors to have a high-reactivity with counter reactants formed during the ALD process, thereby reducing the processing times and producing films with higher purity. Metal amide compounds are of interest for ALD reactions due to their high reactivity with hydroxylated surfaces. Recent studies have demonstrated the use of tetrakis(dimethylamido)titanium (TDMAT) as a metal precursor and water[25,26] or hydrogen peroxide as the reactants.[17] One advantage of this reaction system is the fact that films can be grown at low temperatures (<150°C). These studies have shown that TiO_2 films created using TDMAT are uniform and also exhibit photocatalytic activity.

One of the most researched applications of TiO_2 is as a photocatalyst. Titanium dioxide can act as a photocatalyst under ultraviolet light, which limits efficiency. New research has shown that TiO_2 combined with non-metallic elements such as nitrogen[27] and

fluorine[28] improve photocatalytic activity of the TiO_2 in the visible region. Nitrogen in particular has been shown to have a great effect on the photocatalytic activity of TiO_2.[29] The use of a nitrogen containing precursor, such as TDMAT, may impact the photocatalytic efficiency of TiO_2 films deposited by ALD.

We have investigated the characteristics of TiO_2 films deposited on cellulose fibers by low temperature thermal atomic layer deposition. The use of TDMAT as a metal precursor allows for low temperature deposition of thin films, limiting or eliminating damage to the sensitive substrate materials. Fibrous structures modified by TiO_2 could enable numerous new applications such as materials with self-cleaning abilities, catalytic mantles, and biocompatible structures.

9.2 Experimental

9.2.1 Sample Preparation

Tetrakis(dimethylamido)titanium (TDMAT) was purchased from Strem Chemicals and used as received. The precursor cell was maintained at 27°C and the precursor was dosed into the reactor using an argon carrier gas. Argon was received from National Welders and was passed through a Drierite® Air Purifier to remove water. Deionized water was used as the reactant. DI water was obtained from a Millipore DI water system and was kept at 27°C during the runs in a stainless steel bubbler; water was introduced into the reactor without an argon carrier gas.

Silicon wafers were prepared from 0.0250-0.0250 resistivity, heavily boron-doped p-type silicon supplied by MEMC Electronic Materials, Inc. The silicon was initially cleaned

using BakerClean™ (JT Baker) followed by submersion in 10% HF solution (BOE, JT Baker) until hydrophobicity was observed, then underwent an additional twenty-five seconds of HF washing in the same solution. This treatment was followed by ten minutes of treatment in a 100mL DI water bath with 0.5mL of ammonium hydroxide solution (Fisher) and 2mL of 30% hydrogen peroxide solution (Fisher) at 45ºC to create a uniformly hydrogen terminated chemical oxide. Finally, the wafers were blown dry using nitrogen. Bleached and mercerized woven cotton fabric (Textile Innovators) was used as received. Cotton fabric samples were cut into approximately 2 cm x 2 cm pieces before being used. The fabric samples were ~1 mm thick.

Five one and a half inch spots were available for samples on the quartz boat, whose positions were numbered one, pointing at the flow, to five, pointing towards the pump, so that position one was the first to receive doses from the source lines. To minimize variations, cotton samples were placed in the second and third position and attached using a high-temperature polyamide tape, while a silicon wafer was placed in the fourth position and held in place using a metal clip.

For deposition, pressure was maintained at two Torr during processing and cycles consisted of a ten second argon purge, five second TDMAT dose, another ten second argon purge, and finally a five second ammonia dose. Prior to the deposition process, the substrates were introduced into the reactor, heated in vacuum ($5x10^{-6}$ Torr) to 100°C, and dried for thirty minutes. Optimal processing times for purging and dosing were determined using quadripole mass spectrometry (QMS) using a Leybold-Inficon TC100 quadripole mass spectrometer. Scans were conducted on a range of fifty Daltons with two points taken for

every point with a dwell of sixteen milliseconds. Because of the range and capability of the QMS, data points could only be taken every two seconds.

9.2.2 Sample Characterization

Growth rate measurements of the TiO_2 films on silicon substrates were measured by ellipsometry. A Rudolph Technologies Inc., Auto EL ellipsometer was used to conduct the measurements with an incidence angle of 75°. Three measurements were made at random spots on each sample in order to analyze the uniformity of the TiO_2 films.

X-ray photoelectron spectroscopy (XPS) was used to determine the film thickness and composition on the cotton fabric substrates. Samples of the cotton fabric were cut into 5 mm x 5 mm pieces and attached to the XPS sample holder using double sided copper tape. XPS measurements were done using a Kratos AXIS Ultra spectrometer with an Al source and a spherical mirror analyzer working in spectrum mode. The total pressure in the main vacuum chamber during analysis was $\sim 4\times10^{-7}$ Torr. Spectra were collected with the stage containing the samples at 0°. The take-off angle of the electrons was 90° and the angle of the incident X-ray beam hitting the sample was 30°. The chemical elements present on the samples were identified from survey spectra. The survey scans started at 1200 eV and ended at −5 eV taking 1 eV steps with a dwell time of 200 ms. High resolution detail scans were performed around peaks of interest. Charge effect was corrected using C1s at 285.0 eV as a reference position. Data processing was performed using CasaXPS software (London, UK).

The hydrophilicity of the TiO_2 films was evaluated by static water contact angle measurements. These measurements were performed at ambient conditions (relative

humidity of 60% and temperature of 25°C) by measuring the angle of a 1 μL droplet of water dropped onto the surface of the silicon or fabric from a 2 mm height. Angles were measured using ImageJ software.

9.3 Results and Discussion

Titanium dioxide was deposited onto silicon and cellulose fibers by atomic layer deposition. Deposition was carried out in a custom built, hot-wall viscous flow tube reactor that is described in detail elsewhere. Tetrakis(dimethylamido)titanium and water were used as precursor and reactant, respectively. A complete ALD cycle consists of a ten second argon purge, five seconds TDMAT dose, ten seconds argon purge, and five seconds water dose. Cellulose $(C_6H_{10}O_5)_n$, provides numerous –OH groups on the surface of the fibers. This chemical structure provides the TDMAT precursor with ample reaction groups for the initial ALD cycle. A proposed reaction scheme for TiO_2 ALD on cellulose fibers can be seen in Figure 9.1.

Optimal processing times for purging and dosing were determined using quadripole mass spectrometry (QMS). Signals were monitored for the TDMAT ligand, water, and argon. Each signal was normalized and placed side-by-side for comparison in Figure 9.2. As seen in the figure, the precursor's ligand signal increased during dosing of TDMAT, indicating a sharp increase in ligand concentration and thus attachment of the TDMAT to the surface. The ligand signal drops at the end of the TDMAT dose and is followed by a lower intensity signal indicative of a signal from the TDMAT and not a signal of the free ligand. This TDMAT signal ends before the end of the purge time indicating complete removal of

the unattached TDMAT. A similar trend is seen with the water; the water signal increases during dosing and falls off to beneath the detection limit of the QMS before purge time finishes. Also, it can be seen that during the water dose time, the ligand signal increases and drops before the end of the water signal, indicating complete removal of the ligand from the surface. Based on the results of the QMS analysis, an ALD recipe of ten seconds argon purge, five seconds TDMAT dose, ten seconds argon purge, and five seconds water dose was used to achieve ALD growth behavior.

A characteristic of ALD behavior is that deposited film thickness is linearly proportional to the number of ALD cycles. Figure 9.3 shows the increase in TiO_2 film thickness as a function of the number of cycles for deposition on silicon at 100°C with an operating pressure of 2 Torr. TiO_2 film thickness was measured by ellipsometry. Six measurements were taken at random spots on the sample in order to verify the uniformity and conformality of the film. Unlike characteristic ALD processes, the growth of TiO_2 using TDMAT and water at low temperatures does not demonstrate linear growth for the initial cycles. The growth rate for the first ten cycles shows some non-linearity. This behavior could be explained by incomplete saturation of the TDMAT on the silicon for the beginning ALD cycles. After ten cycles, the growth becomes much more linear. This behavior has been seen in other studies using TDMAT as a titanium precursor.[26] From the data presented in Figure 9.3, it was determined that the growth per cycle of titanium dioxide was 2.18±0.11 angstroms per cycle. This growth rate is comparable to reported growth rates using the same precursor and reactant.[25,26]

Using the same ALD procedure as the silicon, TiO_2 was deposited on cellulose fibers woven together into a fabric form. X-ray photoelectron spectroscopy was used to analyze the chemical composition of the films deposited on the fibers. It should be noted that XPS scans were done on fabric samples, allowing a multitude of individual fibers to be measured concurrently. The samples were stored in ambient conditions until analysis. The chemical composition of the films was measured in relation to the number of ALD cycles. A reference signal of 285.0 eV for C 1s was used to account for surface charging effects during XPS.

A detail scan of the Ti 2p signal is presented in Figure 9.4. The intensity of the Ti peak can be seen to increase with the number of ALD cycles. Distinct peaks can be seen at 458.8 eV and 464.7 eV representing Ti $2p_{3/2}$ and Ti $2p_{1/2}$, respectively. An accepted value for the Ti $2p_{3/2}$ signal in TiO_2 is 458.8 eV.[30] After one ALD cycle, a small peak for Ti $2p_{3/2}$ starts to become visible. This peak becomes much more pronounced between 10 and 20 ALD cycles. At this point, the TiO_2 film is sufficiently thick so that the XPS beam no longer interacts with the cellulose fiber substrate. The resulting XPS readings come solely from the TiO_2 film.

Figure 9.5 presents a detail scan of the O 1s spectrum. A peak can be seen at 533.0 eV for untreated cotton. This peak is representative of C-O bonds found in the structure of cellulose. The C-O peak decreases as the number of ALD cycles increases. A peak becomes visible at 530.3 eV as a result of Ti-O bonds found in TiO_2.[31,32]

The XPS detail scan of C 1s in presented in Figure 9.6. The C 1s spectra is separated into three different signals for the cellulose fibers. A peak can be seen at 286.6 eV, a signal of the C-O bonds found in the structure of cellulose. Shoulder peaks are also seen at 285.0

eV for C-C bonding and 288.0 eV for O-C-O bonding.[33] The peak signals representative of cellulose become less prominent as the number of ALD cycles increase and are eventually replaced by the signals from the TiO_2 film. The presence of C-C bonds near the surface of the films is most likely a result of atmospheric contamination. A more accurate understanding of the purity of the films could be obtained by limiting exposure to atmosphere before analysis.

Detail scans were also performed around the N 1s peak in order to determine the N contributed by the TDMAT precursor. As mentioned previously, nitrogen doped TiO_2 has been reported to be a more efficient photocatalyst. Figure 9.7 shows the detail spectra for N 1s. No clear nitrogen peaks can be seen in the data. Based on the XPS data, it can be seen that the TiO_2 films deposited by ALD are mainly TiO_2, without trace amounts of titanium nitrides or oxynitrides.

One important use of TiO_2 is to create photo-induced hydrophilic surfaces.[27,34,35] The hydrophilicity of titanium dioxide coatings can be increased by light irradiation in the long wave UV region (320-400 nm), this reaction mechanism has been described in detail elsewhere.[36,37] Static water contact angle measurements were conducted to examine the hydrophilic properties of the TiO_2 on the silicon and fiber substrates.

A comparison of the contact angles of the TiO_2 films on the two substrates can be seen in Figure 9.8. Examining the cellulose samples, it can be seen that the untreated fabric has a contact angle of 0°. After only one ALD cycle, the fabric substrates exhibit a contact angle of approximately 113°. This contact angle does not change until more than 25 cycles of TiO_2 ALD have occurred. Two possible explanations for this increased hydrophobicity

are the presence of un-reacted methyl groups on the surface of the cellulose fibers or that the TiO_2 film makes the nano-scale fibers more rigid, thus decreasing the contact between the water droplet and the fibers. For samples treated with more than 20 cycles of TiO_2, the cellulose fibers become very hydrophilic with contact angles of 0°. The contact angle measurements on the silicon samples are much different than the measurements on the cellulose based fabrics. After the initial ALD cycles, the TiO_2 films on silicon have a contact angle of approximately 80°. This contact angle decreases to 70° after 10 cycles and does not change greatly for up to 100 cycles.

9.4 Acknowledgements

The authors acknowledge support from the National Science Foundation under grant CTS-0626256.

9.5 References

1. Inoue, T., Fujishima, A., Konishi, S. & Honda, K. Photoelectrocatalytic Reduction of Carbon-Dioxide in Aqueous Suspensions of Semiconductor Powders. *Nature* **277**, 637-638 (1979).

2. Lancelle-Beltran, E. et al. Nanostructured hybrid solar cells based on self-assembled mesoporous titania thin films. *Chem Mater* **18**, 6152-6156 (2006).

3. Kommireddy, D.S., Sriram, S.M., Lvov, Y.M. & Mills, D.K. Stem cell attachment to layer-by-layer assembled TiO2 nanoparticle thin films. *Biomaterials* **27**, 4296-4303 (2006).

4. Huang, J.G., Ichinose, I. & Kunitake, T. Biomolecular modification of hierarchical cellulose fibers through titania nanocoating. *Angew Chem Int Edit* **45**, 2883-2886 (2006).

5. Durand, H.A. et al. Excimer-Laser Sputtering Deposition of Tio2 Optical Coating for Solar-Cells. *Appl Surf Sci* **86**, 122-127 (1995).

6. Aarik, J., Karlis, J., Mandar, H., Uustare, T. & Sammelselg, V. Influence of structure development on atomic layer deposition of TiO2 thin films. *Appl Surf Sci* **181**, 339-348 (2001).

7. Liu, Y.J., Wang, A.B. & Claus, R. Molecular self-assembly of TiO2/polymer nanocomposite films. *J Phys Chem B* **101**, 1385-1388 (1997).

8. Pore, V. et al. Atomic layer deposition of photocatalytic TiO2 thin films from titanium tetramethoxide and water. *Chem Vapor Depos* **10**, 143-148 (2004).

9. Sinha, A., Hess, D.W. & Henderson, C.L. Area selective atomic layer, deposition of titanium dioxide: Effect of precursor chemistry. *J Vac Sci Technol B* **24**, 2523-2532 (2006).

10. Bozzi, A., Yuranova, T., Guasaquillo, I., Laub, D. & Kiwi, J. Self-cleaning of modified cotton textiles by TiO2 at low temperatures under daylight irradiation. *J Photoch Photobio A* **174**, 156-164 (2005).

11. Yuranova, T., Mosteo, R., Bandara, J., Laub, D. & Kiwi, J. Self-cleaning cotton textiles surfaces modified by photoactive SiO2/TiO2 coating. *J Mol Catal a-Chem* **244**, 160-167 (2006).

12. Yuranova, T. et al. Performance and characterization of Ag-cotton and Ag/TiO2 loaded textiles during the abatement of E-coli. *J Photoch Photobio A* **181**, 363-369 (2006).

13. Wang, H.Q., Wu, Z.B., Zhao, W.R. & Guan, B.H. Photocatalytic oxidation of nitrogen oxides using TiO2 loading on woven glass fabric. *Chemosphere* **66**, 185-190 (2007).

14. Chen, S.F., Zhao, M.Y. & Tao, Y.W. Photocatalytic degradation of organophosphoros pesticides using TiO2 supported on fiberglass. *Microchem J* **54**, 54-58 (1996).

15. Mozia, S., Tomaszewska, M. & Morawski, A.W. Decomposition of nonionic surfactant in a labyrinth flow photoreactor with immobilized TiO2 bed. *Appl Catal B-Environ* **59**, 155-160 (2005).

16. Niskanen, A., Arstila, K., Leskela, M. & Ritala, M. Radical enhanced atomic layer deposition of titanium dioxide. *Chem Vapor Depos* **13**, 152-157 (2007).

17. Pheamhom, R., Sunwoo, C. & Kim, D.H. Characteristics of atomic layer deposited TiO2 films and their photocatalytic activity. *J Vac Sci Technol A* **24**, 1535-1539 (2006).

18. Kim, H. Atomic layer deposition of metal and nitride thin films: Current research efforts and applications for semiconductor device processing. *J Vac Sci Technol B* **21**, 2231-2261 (2003).

19. Groner, M.D., Fabreguette, F.H., Elam, J.W. & George, S.M. Low-temperature Al2O3 atomic layer deposition. *Chem Mater* **16**, 639-645 (2004).

20. Kim, H. & McIntyre, P.C. Atomic layer deposition of ultrathin metal-oxide films for nano-scale device applications. *Journal Of The Korean Physical Society* **48**, 5-17 (2006).

21. Finnie, K.S. et al. Influence of Si(100) surface pretreatment on the morphology of TiO2 films grown by atomic layer deposition. *Thin Solid Films* **440**, 109-116 (2003).

22. Jogi, I., Kukli, K., Aarik, J., Aidla, A. & Lu, J. Precursor-dependent structural and electrical characteristics of atomic layer deposited films: Case study on titanium oxide. *Mat Sci Semicon Proc* **9**, 1084-1089 (2006).

23. Mitchell, D.R.G. et al. Atomic layer deposition of TiO2 and Al2O3 thin films and nanolaminates. *Smart Mater Struct* **15**, S57-S64 (2006).

24. Park, M.H., Jang, Y.J., Sung-Suh, H.M. & Sung, M.M. Selective atomic layer deposition of titanium oxide on patterned self-assembled monolayers formed by microcontact printing. *Langmuir* **20**, 2257-2260 (2004).

25. Lim, G.T. & Kim, D.H. Characteristics of TiOx films prepared by chemical vapor deposition using tetrakis-dimethyl-amido-titanium and water. *Thin Solid Films* **498**, 254-258 (2006).

26. Maeng, W.J. & Kim, H. Thermal and plasma-enhanced ALD of Ta and Ti oxide thin films from alkylamide precursors. *Electrochem Solid St* **9**, G191-G194 (2006).

27. Asahi, R., Morikawa, T., Ohwaki, T., Aoki, K. & Taga, Y. Visible-light photocatalysis in nitrogen-doped titanium oxides. *Science* **293**, 269-271 (2001).

28. Li, D., Haneda, H., Labhsetwar, N.K., Hishita, S. & Ohashi, N. Visible-light-driven photocatalysis on fluorine-doped TIO2 powders by the creation of surface oxygen vacancies. *Chem Phys Lett* **401**, 579-584 (2005).

29. Shifu, C., Xuqiang, L., Yunzhang, L. & Gengyu, C. The preparation of nitrogen-doped $TiO_{2-x}N_x$ photocatalyst coated on hollow glass microbeads. *Appl Surf Sci* **253**, 3077-3082 (2007).

30. Moulder, J.F., Stickle, W.E., Sobol, P.E. & Bomben, K.D. Handbook of X-ray Photoelectron Spectroscopy. (Physical Electronics, Inc., Eden Prairie, Minnesota; 1995).

31. Ni, C.Y. et al. Effect of film thickness and the presence of surface fluorine on the structure of a thin barrier film deposited from tetrakis-(dimethylamino)-titanium onto a Si(100)-2 x 1 substrate. *Thin Solid Films* **515**, 3030-3039 (2007).

32. Vesel, A., Mozetic, M., Kovac, J. & Zalar, A. XPS study of the deposited Ti layer in a magnetron-type sputter ion pump. *Appl Surf Sci* **253**, 2941-2946 (2006).

33. Beamson, G. & Briggs, D. High Resolution XPS of Organic Polymers. (Wiley, Chichester, England; 1992).

34. Machida, M., Norimoto, K., Watanabe, T., Hashimoto, K. & Fujishima, A. The effect of SiO2 addition in super-hydrophilic property of TiO2 photocatalyst. *J Mater Sci* **34**, 2569-2574 (1999).

35. Wang, R. et al. Light-induced amphiphilic surfaces. *Nature* **388**, 431-432 (1997).

36. Sakai, N., Wang, R., Fujishima, A., Watanabe, T. & Hashimoto, K. Effect of ultrasonic treatment on highly hydrophilic TiO2 surfaces. *Langmuir* **14**, 5918-5920 (1998).

37. Ye, Q., Liu, P.Y., Tang, Z.F. & Zhai, L. Hydrophilic properties of nano-TiO2 thin films deposited by RF magnetron sputtering. *Vacuum* **81**, 627-631 (2007).

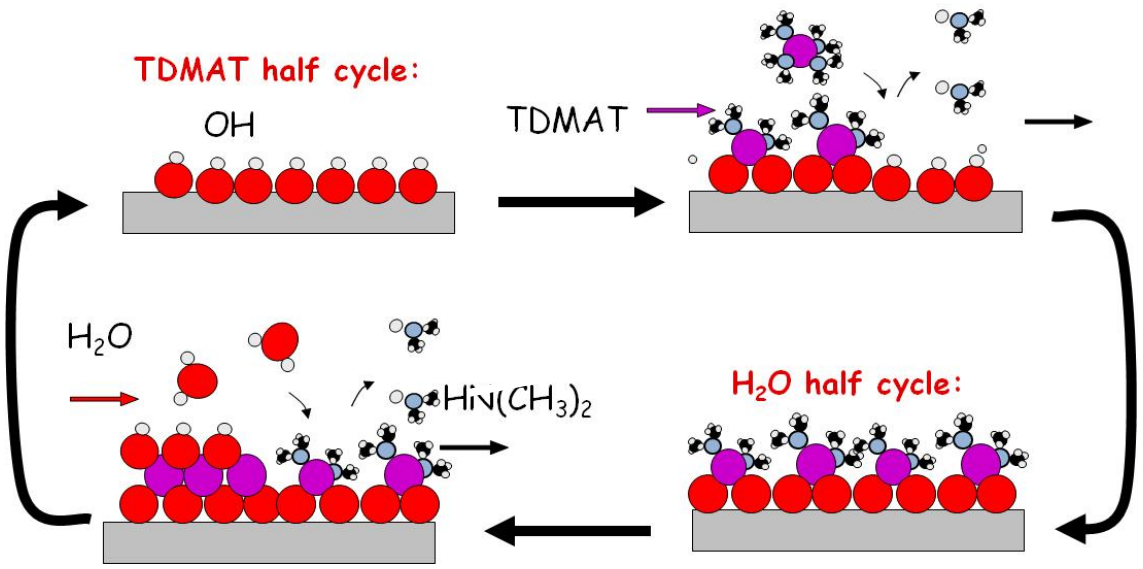

Figure 9.1. Schematic of TiO_2 ALD on cellulose fibers. The TDMAT reacts with the –OH terminated surface of the cellulose fibers, leaving a methyl terminated surface. The water then reacts with the methyl groups, creating a surface with –OH groups. This process is then repeated for the desired number of cycles.

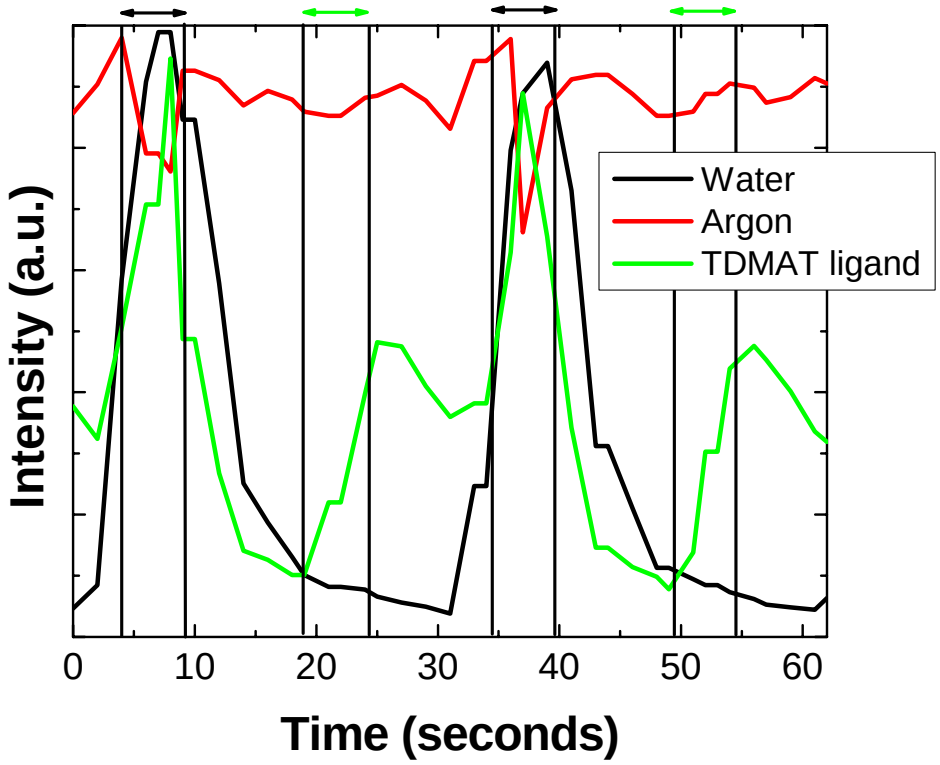

Figure 9.2. Quadripole mass spectrometry of TiO_2 ALD. Intensities of the TDMAT ligand, argon, and water are presented as functions of processing time. Green arrows indicate TDMAT dosing and black arrows indicate water dosing. Times between arrows represent argon purges.

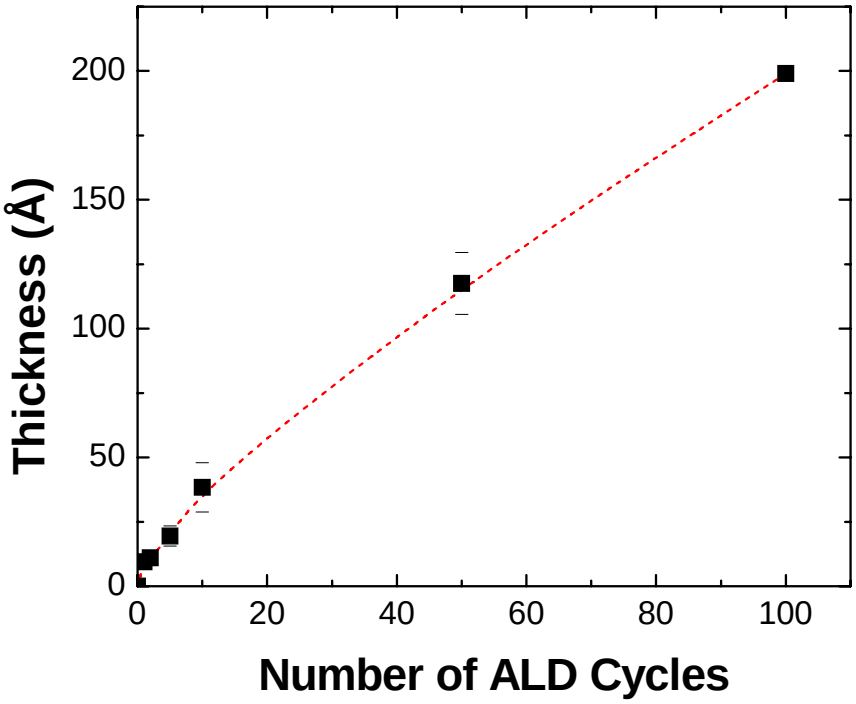

Figure 9.3. Growth rate of TiO_2 on silicon. Thickness of the TiO_2 film as a function of the number of ALD cycles as measured by ellipsometry. Titanium dioxide was deposited at 100°C and a process pressure of 2 Torr. The linear growth as a function of ALD cycles is indicative of an ALD process.

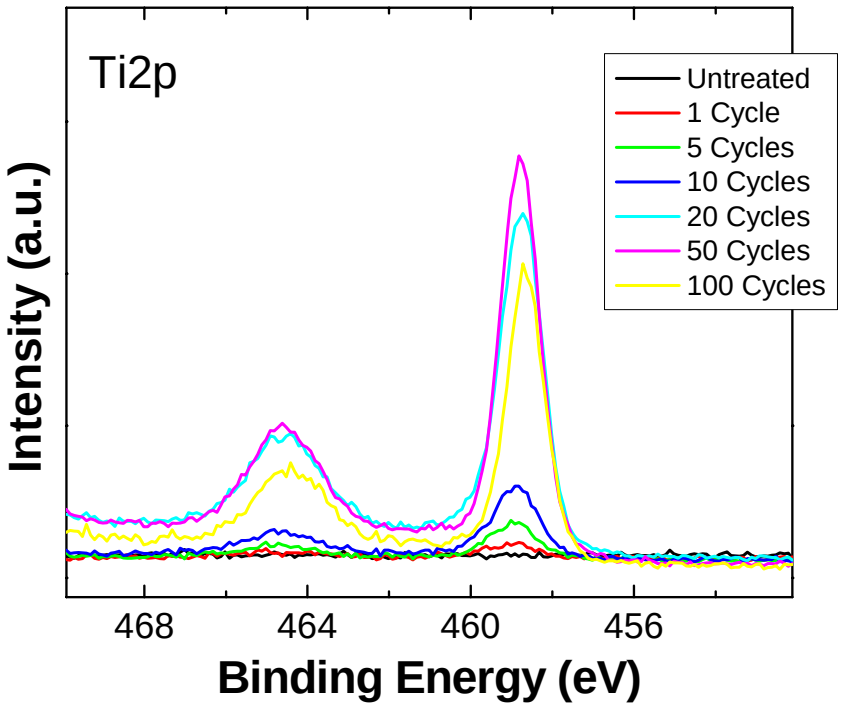

Figure 9.4. XPS detail spectra of Ti 2p for TiO_2 films deposited on cellulose fibers. The Ti2p signal, which consists of two distinct peaks, can be seen to increase as the number of ALD cycles increases.

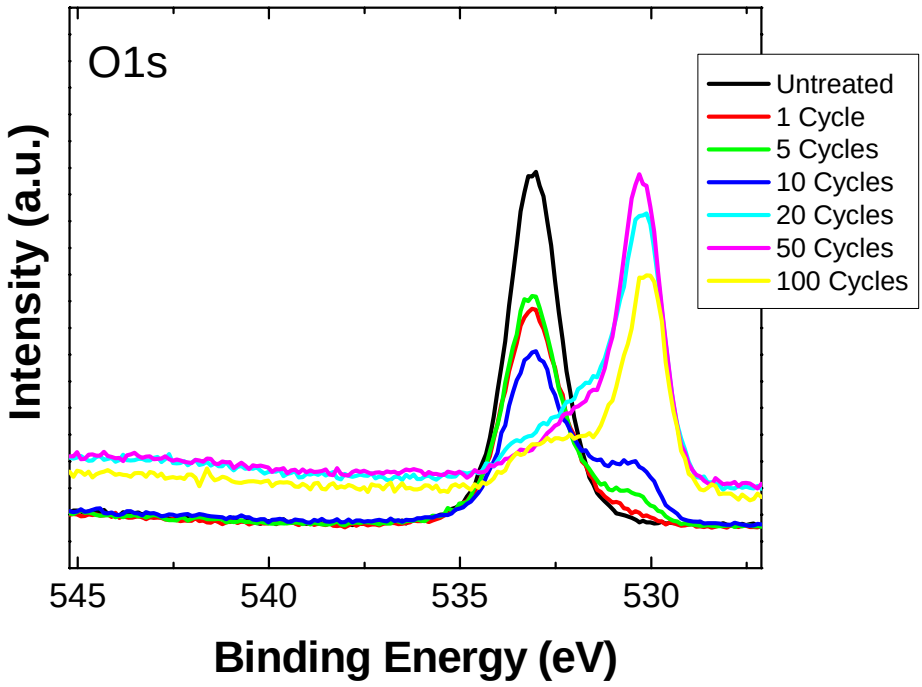

Figure 9.5. XPS detail spectra of O 1s for TiO_2 films deposited on cellulose fibers. The peak can be seen to shift to lower binding energy as TiO_2 is deposited, representing Ti-O bonding.

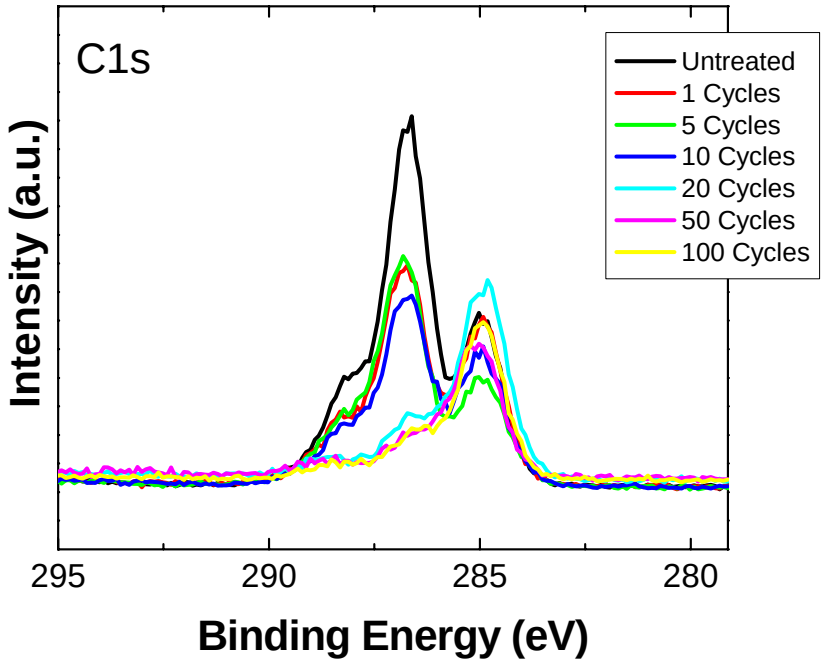

Figure 9.6. XPS detail spectra of C 1s for TiO_2 films deposited on cellulose fibers. The C-O and O-C-O peaks found in the untreated cotton decrease as the fibers are coated with TiO_2. The C-C peak increases as a result of contamination of the films.

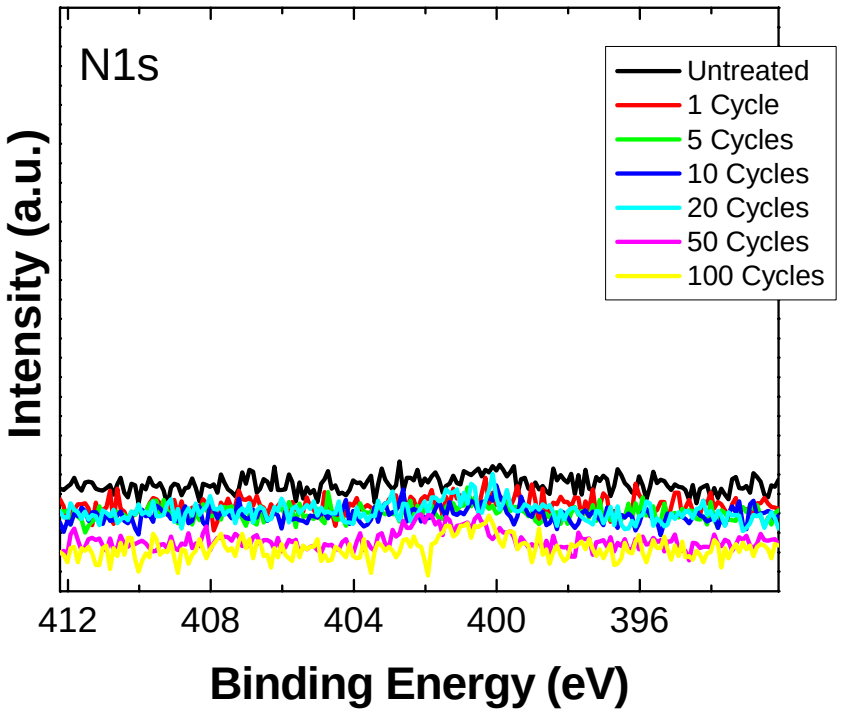

Figure 9.7. XPS detail spectra of N 1s for TiO_2 films deposited on cellulose fibers. No distinct peak can be seen for N 1s, demonstrating the purity of the TiO_2 films deposited.

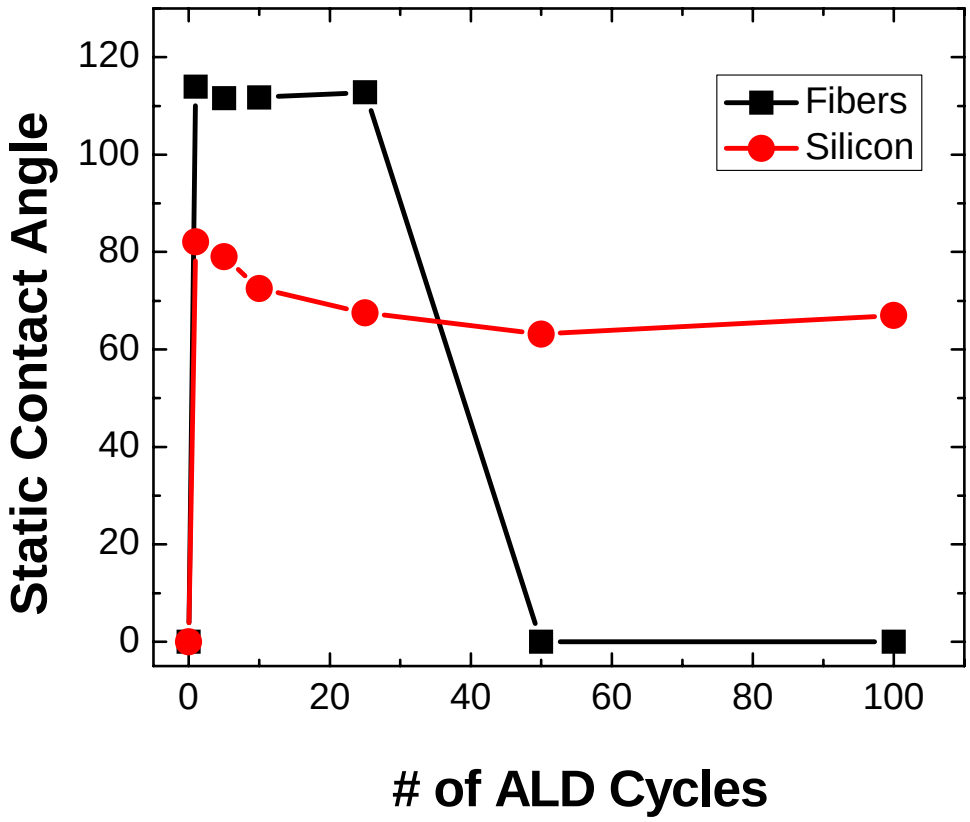

Figure 9.8. Static water contact angle on TiO_2 coated fabrics and silicon. ALD cycle number versus static water contact angle for TiO_2 ALD coated samples. This graph shows that very thin layers of TiO_2 (<50 Å) produce a hydrophobic effect on the normally hydrophilic cellulose fibers. The fabric samples are significantly more hydrophobic than the corresponding silicon samples. The metal oxides may act to reinforce nano-scale fibrils and thus increase the hydrophobicity.

CHAPTER 10: Conclusions and Future Work

This work has further established the use of LbL deposition as a surface modification technique for textile materials. Atomic layer deposition has also been shown to be a feasible method for nano-scale coatings of textile substrates. The deposited thin films are capable of changing macroscale properties of the substrates. The use of nano-scale deposition techniques such as LbL deposition and ALD provide a new range of materials to be used in textile applications. A few possible applications for conformal nano-scale coatings on textile substrates include new platforms for photovoltaic and fuel cell devices, scaffolds for tissue engineering, nano-magnetic structures, drug delivery systems, and high performance nano and biomolecule filtration and separation structures. The fundamental knowledge generated by this project has helped improve the understanding of surface functionalization and modification processes on textile substrates. The work presented should also help to expand the field of application of fiber-based systems.

The current results have demonstrated the unique potentials of LbL assembly and ALD to be transformative technologies leading to new research and product fields. At the same time, the results also point to some of the challenges that must be overcome in order to develop these techniques into functional nano-scale manufacturing procedures. Future work can be divided into several different objectives: 1) define the chemical reaction system requirements needed to create and promote new ALD and LbL deposition methods to coat and modify fiber-based surfaces; 2) develop a better understanding of reaction kinetics and effects of surface properties on coating and nucleation phenomena in complex fiber systems; and 3) understand how the surface modification process influences the function and

performance of modified fiber-based materials. In order to develop ALD and LbL technologies into textile manufacturing, it is important that the influence of characteristics of fibers such as porosity, tortuosity, and surface area on the deposition techniques be better understood.

Many new substrates could be investigated in future research. Synthetic materials such as polypropylene and nylon and natural materials such as silk and linen fibers are just a few of the possible substrate choices. In future studies, it would be useful to begin with planar substrates of similar composition to the fibers that will be investigated. This will allow better process optimization.

A variety of coatings could also be experimented with in future studies. Atomic layer deposition of metals such as silver, copper, nickel, ruthenium, and palladium would be of great interest. Many different materials can also be deposited using LbL deposition. It will be necessary to employ a variety of analysis techniques to determine the effect of the coatings on the structural, physical, and chemical properties of the modified materials.

CHAPTER 11: Appendix 1 – Combination of Layer-by-Layer and Atomic Layer Deposition Techniques

11.1 Introduction

This section describes experiments that have been done involving the combination of the LbL and ALD techniques. The purpose of this research is to better understand the creation of hybrid organic/inorganic structures at the nano-scale and the characteristics of the new composites. Combining LbL assembly and ALD could allow the creation of novel materials with increased functionality. This research will help to increase existing knowledge regarding inorganic and organic interfaces.

11.2 Experimental

11.2.1 Sample Preparation

Silicon wafers were prepared from 0.0250-0.0250 resistivity, heavily boron-doped p-type silicon supplied by MEMC Electronic Materials, Inc. The silicon was initially cleaned using BakerClean™ (JT Baker) followed by submersion in 10% HF solution (BOE, JT Baker) until hydrophobicity was observed, then underwent an additional twenty-five seconds of HF washing in the same solution. This treatment was followed by ten minutes of treatment in a 100mL DI water bath with 0.5mL of ammonium hydroxide solution (Fisher) and 2mL of 30% hydrogen peroxide solution (Fisher) at 45ºC to create a uniformly hydrogen terminated chemical oxide. Finally, the wafers were blown dry using nitrogen.

Poly (sodium 4-styrene sulfonate) (PSS), Mw 70000, and poly (allylamine hydrochloride) (PAH), Mw 70000, were purchased from Aldrich (St. Louis, MO) and used as

received. Aqueous solutions of the polyelectrolytes were made using deionized water at concentrations of 5 mM. A series of Petri dishes were used for the deposition process. The first row of dishes contained the cationic PAH solution, followed by a row of DI rinse water dishes. The third row contained the anionic PSS solution, followed by a fourth row of dishes containing the final DI rinse.

The deposition process began by placing the silicon substrate in the first PAH dish for five minutes. Tweezers were used to move the sample to the next dish containing deionized water. The rinse time was five minutes. The sample was then placed in the dish containing PSS. After five minutes, the sample was moved to the next dish containing deionized water to be rinsed for five minutes again. This process was repeated until a total of five bilayers of PAH/PSS were created. Once the polyelectrolyte deposition was completed, one sample was kept for analysis and the remaining samples were used as substrates for ALD.

For these studies, ALD of aluminum oxide was performed in a hot-wall viscous-flow tube reactor described elsewhere. Trimethylaluminum (TMA) (98%, Strem Chemical, Inc.) and deionized water were used as reactants for the deposition of Al_2O_3. The reactant lines were heated to 60°C in order to prevent condensation of water. Directly before deposition process, the substrates were placed in the reactor and heated in vacuum ($5x10^{-7}$ Torr) to ~100°C and allowed to equilibrate for 60 minutes. To begin deposition, the reactor was flushed with argon, and ambient temperature vapors of TMA and water were separately introduced into the reactor in pulses of 1 and 2 seconds respectively, with a 20 second Ar purge between each reactant exposure step. The TMA and water were carried into the reactor using Ar flow, and the Ar flow rate was constant at 100 standard cubic centimeters

per minute (sccm). The pressure was fixed at 1 Torr using a variable orifice valve downstream from the reactor. One hundred cycles of ALD were performed on top of the polyelectrolyte modified samples. After deposition, one sample was kept for analysis and the remaining samples were again used as substrates for LbL assembly. A total of five samples were created, each being topped by either a polyelectrolyte layer or an Al_2O_3 layer.

11.2.2 Sample Characterization

AFM measurements were taken using a Digital Instruments Atomic Force Microscope controlled using a Digital Instruments Nanoscope IIIa Scanning Probe Microscope Controller. A silicon nitride tip purchased from Veeco Nanoprobe Tips™. Specifically, measurements were taken in a tapping mode for a one micrometer square at 512 lines per square and 512 measurements per line, at a rate of 0.5003Hz. Data analysis and imaging was done using Nanotec© WSxM software.

X-ray photoelectron spectroscopy (XPS) was used to determine the composition on the cotton fabric substrates. Samples were attached to the XPS sample holder using double sided copper tape. XPS measurements were done using a Kratos AXIS Ultra spectrometer with an Al source and a spherical mirror analyzer working in spectrum mode. The total pressure in the main vacuum chamber during analysis was $\sim 4\times10^{-7}$ Torr. Spectra were collected with the stage containing the samples at 0°. The take-off angle of the electrons was 90° and the angle of the incident X-ray beam hitting the sample was 30°. The chemical elements present on the samples were identified from survey spectra. The survey scans started at 1200 eV and ended at −5 eV taking 1 eV steps with a dwell time of 200 ms. High

resolution detail scans were performed around peaks of interest. Charge effect was corrected using C1s at 285.0 eV as a reference position. Data processing was performed using CasaXPS software (London, UK).

11.3 Results and Discussion

From AFM measurements it was shown that the roughness of the initial polyelectrolyte layers on silicon was 0.220 nm. In Figure 11.1 it can be seen that the AFM tip actually dug into the film and created noticeable trenches along its path. However, on the first coating of aluminum oxide, the surface roughness decreased to 0.169 nm and the trenching of the AFM tip ceased as seen in Figure 11.2. The elimination of trenching on the surface is attributed to hardening of the surface due to the aluminum oxide. After, the second coating of polyelectrolytes, the surface roughness can be seen to increase to 2.665 nm as seen in Figure 11.3; at such small resolution, trenching of the polyelectrolytes due to the AFM tip could not be ascertained. On subsequent coating of aluminum oxide, the surface roughness was once again reduced to 0.546 nm as seen in Figure 11.4. Again, due to the small resolution, trenching due to the AFM tip could not be ascertained, but it can be clearly seen that aluminum oxide is successful in reducing the roughness of the surface. For the final electrolyte coating the surface roughness was 0.554 nm as seen in Figure 11.5.

The chemical composition of the hybrid structures were analyzed using XPS. It should be noted that XPS analysis was performed one week after the initial samples were created. Samples were then stored in ambient conditions until they were analyzed. Figure 11.6 provides a high resolution detail scan around the Al 2p peak. As expected no peak is

seen for sample A, which only has polyelectrolytes on the surface. After, Al_2O_3 deposition, a significant signal can be seen for samples B and D. The Al 2p peak decreases in intensity for samples with polyelectrolytes as the upper most layer. However, the presence of the Al 2p peak suggests that some interpenetration exists between the organic and inorganic layers.

Figure 11.7 shows high-resolution spectrum of the N 1s signal. The intensity of the N peak, which is attributed to the polyelectrolyte PAH, can be seen to increase in intensity for samples A, C, and E, which end with polyelectrolyte deposition. Samples B and D, which are topped with Al_2O_3, do not exhibit a peak at N 1s, demonstrating the ability of the ALD process to completely cover the polyelectrolyte layers. High-resolution spectra of S 2p can be seen in Figure 11.8. The S signal, which comes from the PSS, can be seen to increase for samples A, C, and E. Again, for the samples ending with ALD, no S signal can be seen.

The O 1s spectrum is shown in Figure 11.9. The O 1s signal at 534.0 eV is likely due to bonding from the O groups on the surface of the silicon and O groups present in the polyelectrolytes. After the initial Al_2O_3 deposition, the O 1s signal shifts to 532.0 eV, typical of Al-O bonding in Al_2O_3. The intensity of the peak is the greatest for samples B and D, which have Al_2O_3 as the top coating.

The XPS spectrum of the C 1s peak is shown in Figure 11.10. The initial signal can be seen to shift to approximately 285.0 eV. The peak for sample A is a result of C bonding between the polyelectrolytes and the silicon substrate. After ALD, the C signal is attributed to adventitious carbon.

The current results demonstrate that the combination of LbL assembly and ALD is a feasible technique for the creation of hybrid organic-inorganic nano-scale coatings.

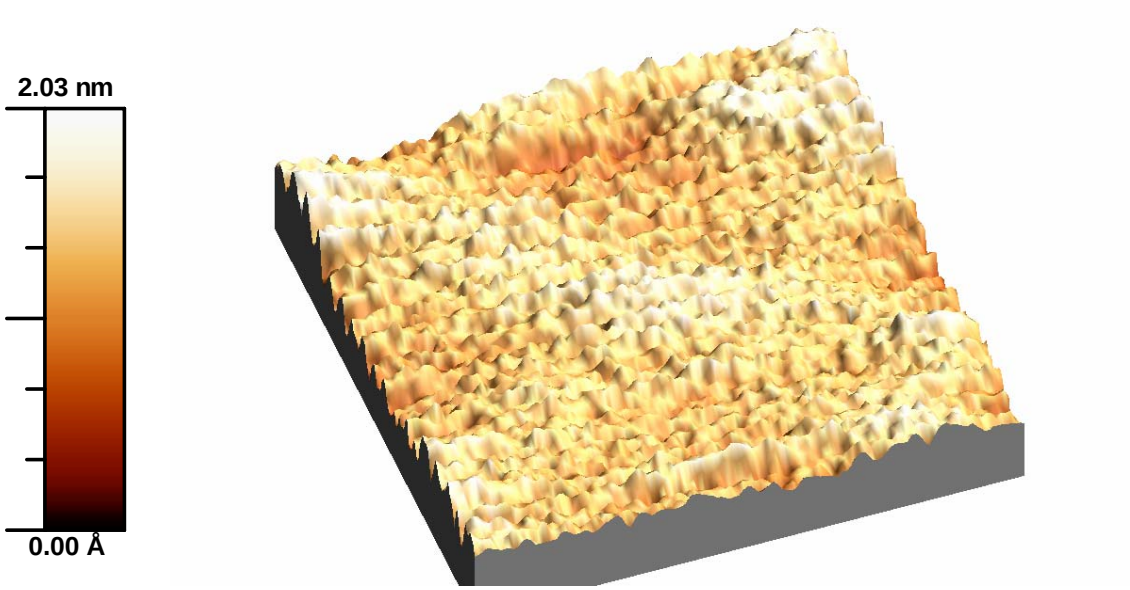

Figure 11.1. AFM image of 5 PAH/PSS bilayers on a silicon surface.

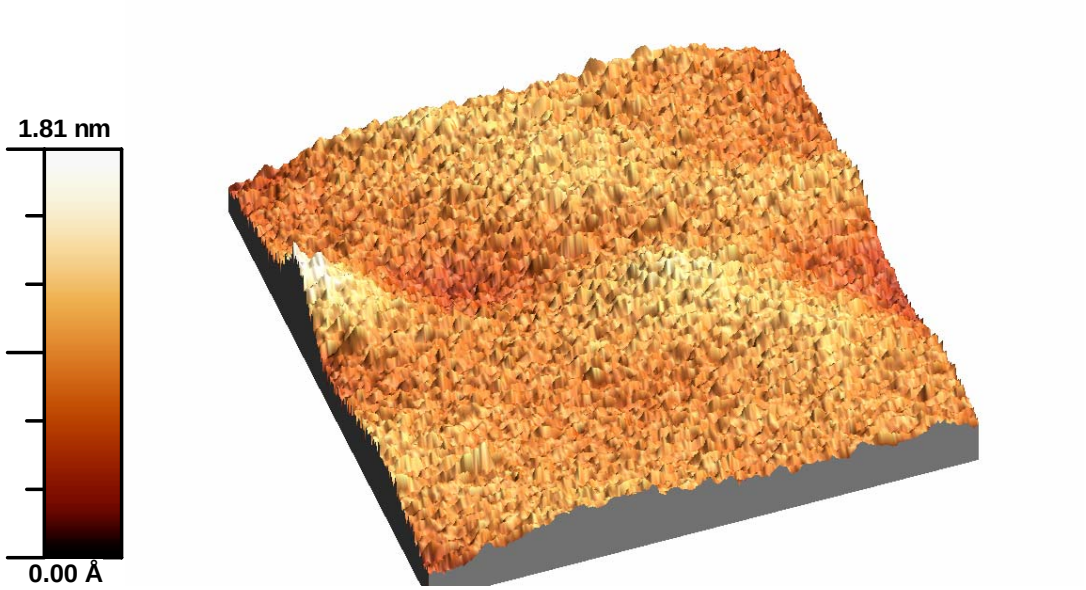

Figure 11.2. AFM image of 5 PAH/PSS bilayers on a silicon surface coated by 100 cycles of Al_2O_3 ALD.

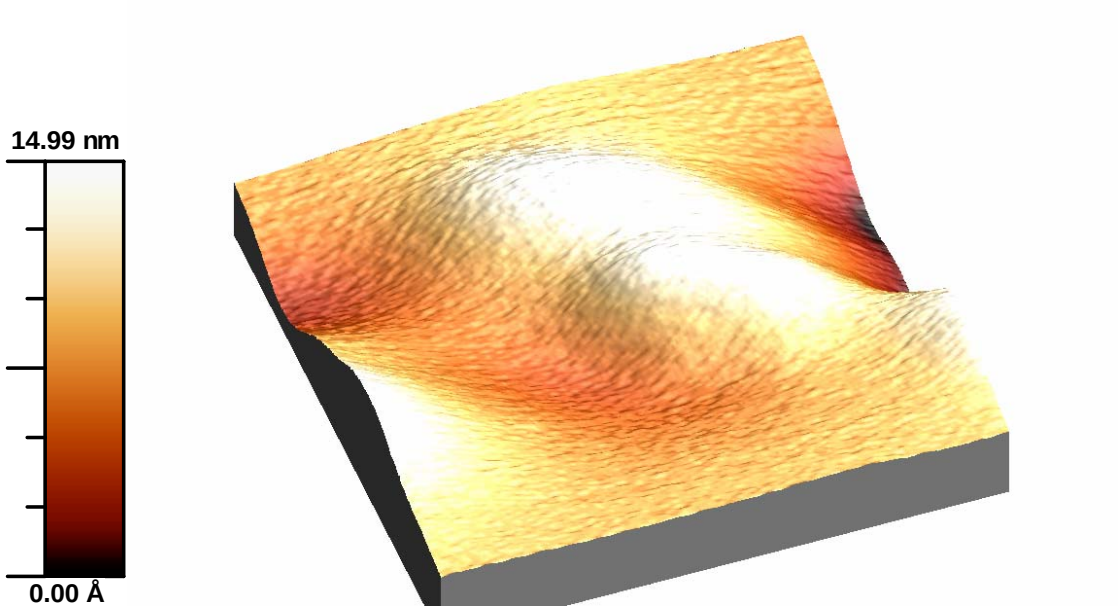

Figure 11.3. AFM image of a silicon sample with 5 PAH/PSS bilayers, 100 cycles of Al_2O_3 ALD, and 5 bilayers of PAH/PSS.

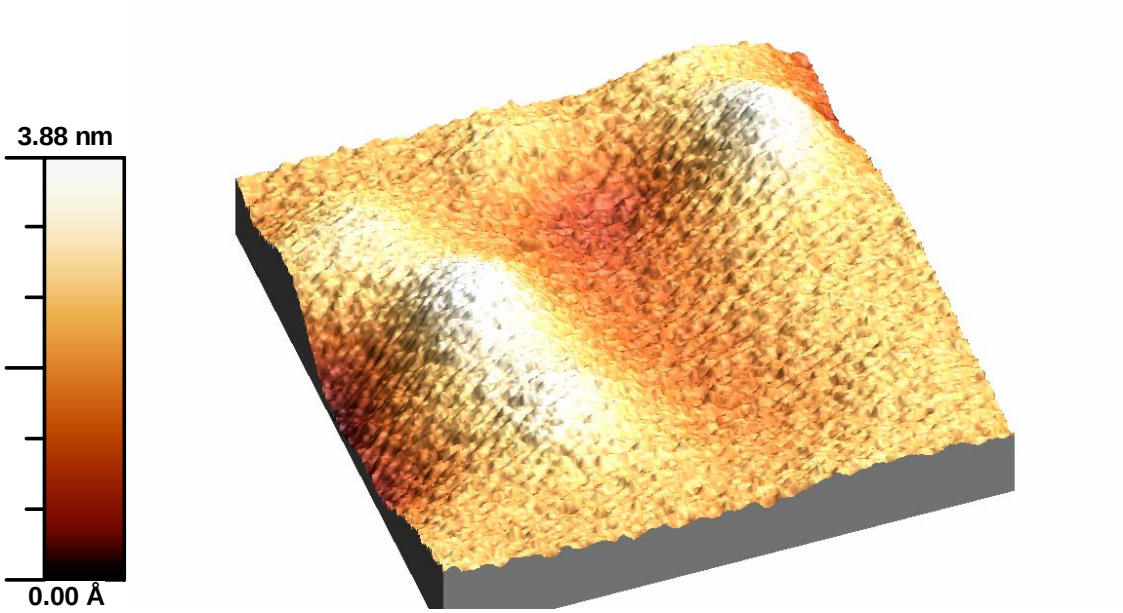

Figure 11.4. AFM image of a silicon sample with 5 PAH/PSS bilayers, 100 cycles of Al_2O_3 ALD, 5 bilayers of PAH/PSS, and 100 cycles of Al_2O_3 ALD.

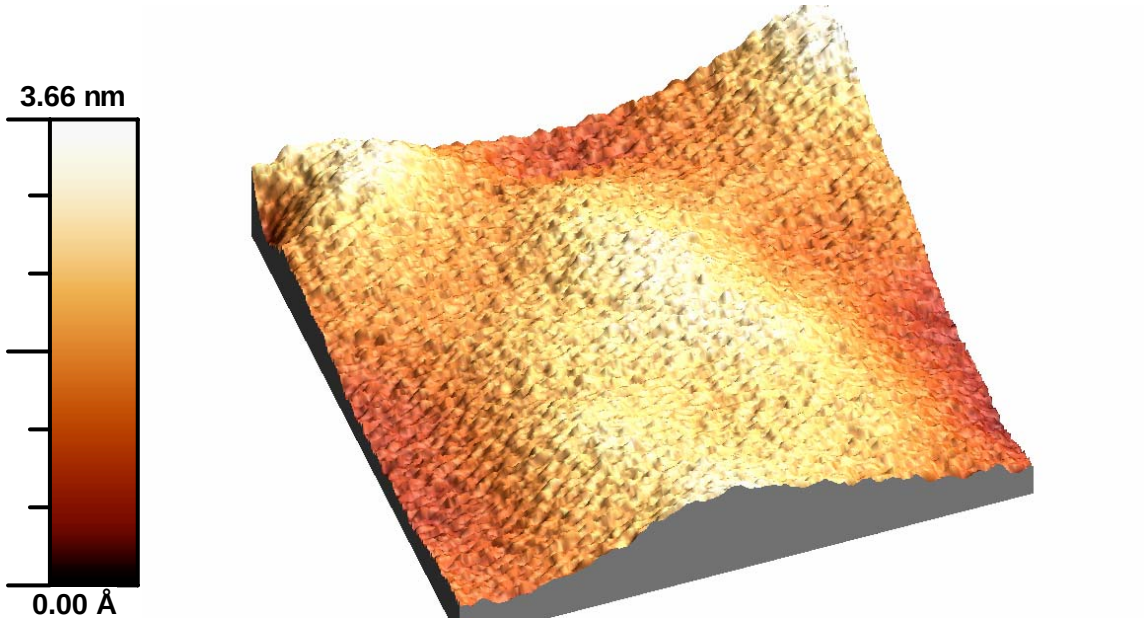

Figure 11.5. AFM image of a silicon sample with 5 PAH/PSS bilayers, 100 cycles of Al_2O_3 ALD, 5 bilayers of PAH/PSS, 100 cycles of Al_2O_3 ALD, and 5 bilayers of PAH/PSS.

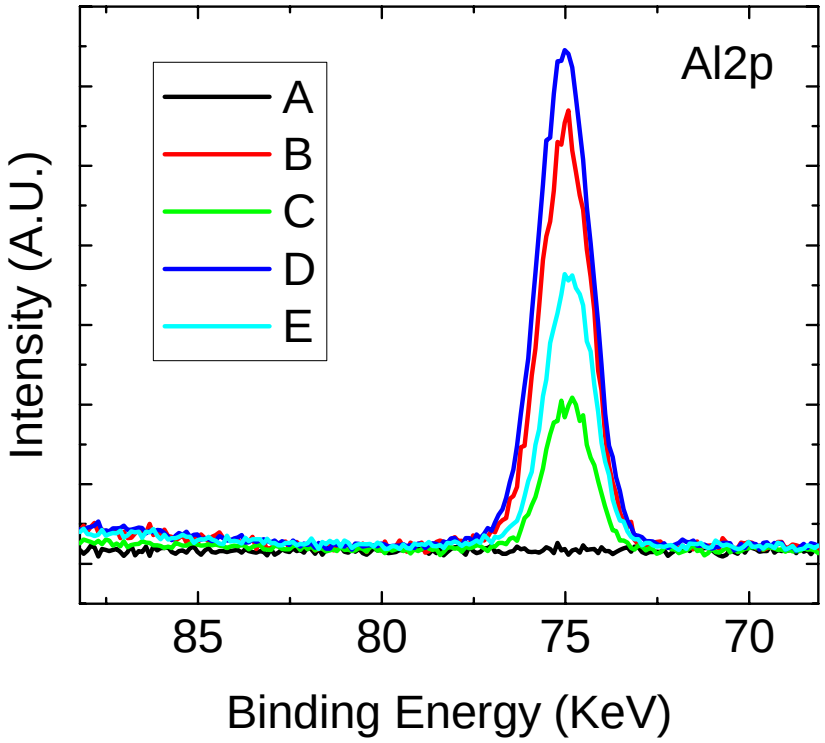

Figure 11.6. XPS detail spectra of Al 2p for silicon samples supporting alternating layers of polyelectrolytes and Al_2O_3. Samples A, C, and E have a PAH/PSS bilayer as the uppermost coating. Samples B and D have an Al_2O_3 layer as the uppermost coating. The intensity of the Al 2p peak can be seen to increase for samples B and D.

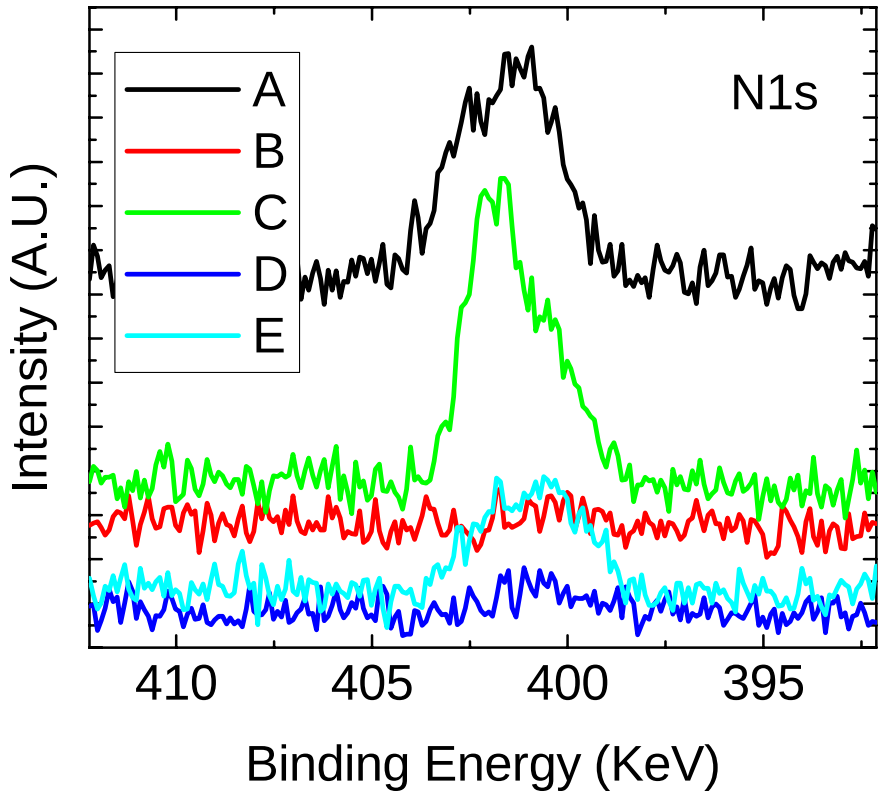

Figure 11.7. XPS detail spectra of N 1s for silicon samples supporting alternating layers of polyelectrolytes and Al_2O_3. Samples A, C, and E have a PAH/PSS bilayer as the uppermost coating. Samples B and D have an Al_2O_3 layer as the uppermost coating. The intensity of the N 1s peak can be seen to increase for samples A, C, and E.

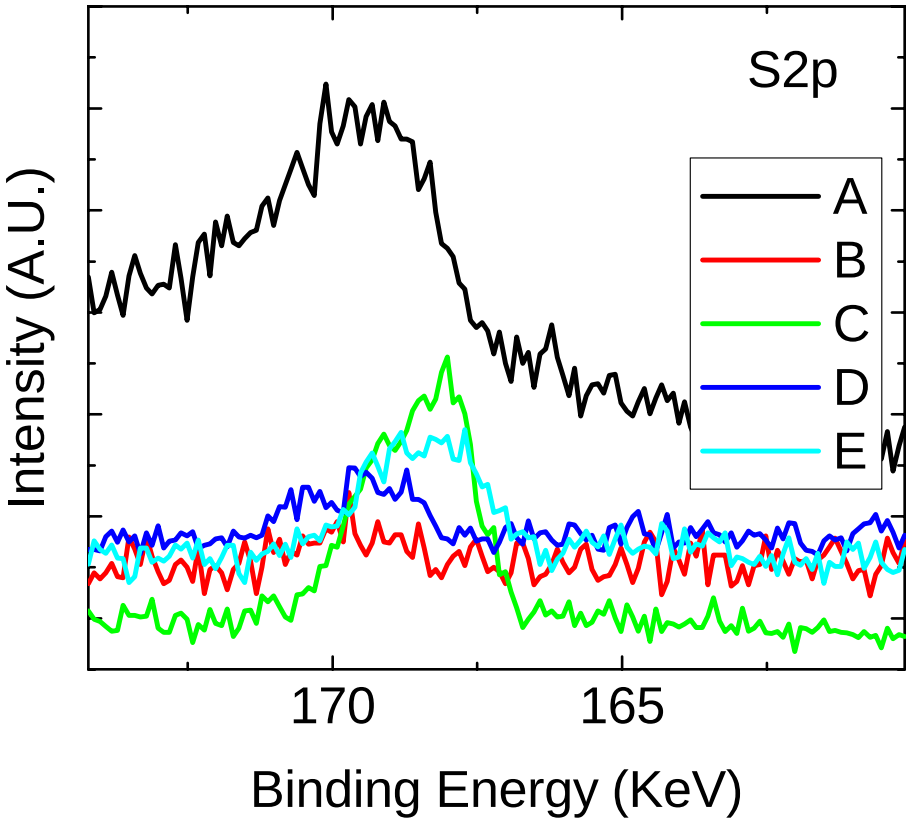

Figure 11.8. XPS detail spectra of S 2p for silicon samples supporting alternating layers of polyelectrolytes and Al_2O_3. Samples A, C, and E have a PAH/PSS bilayer as the uppermost coating. Samples B and D have an Al_2O_3 layer as the uppermost coating. The intensity of the S 2p peak can be seen to increase for samples A, C, and E.

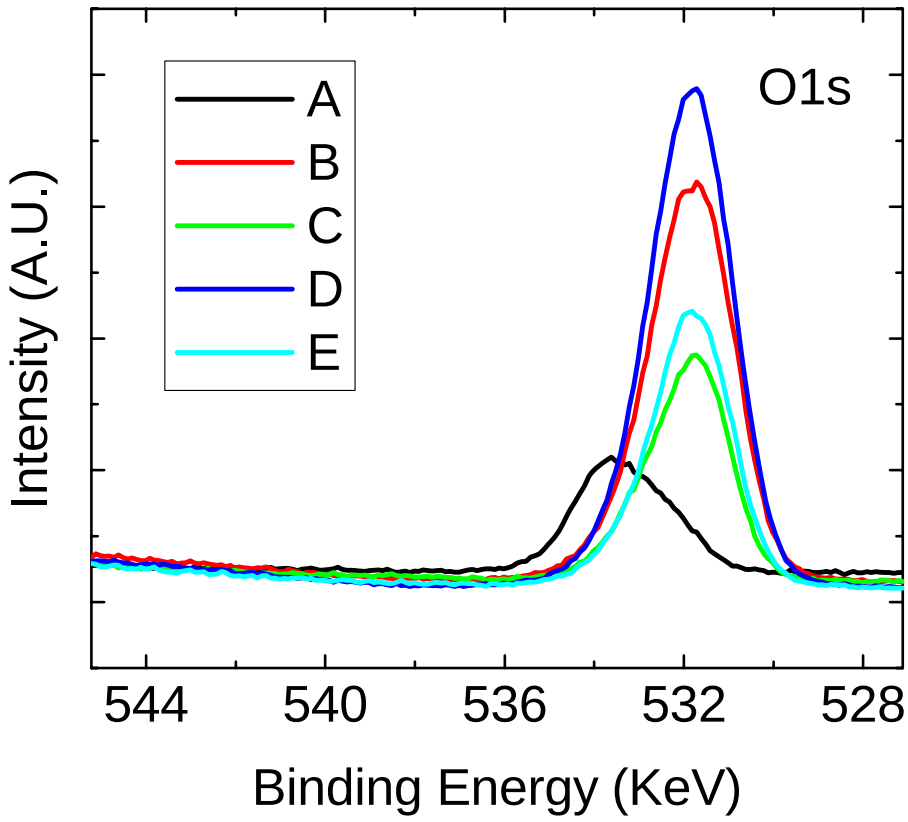

Figure 11.9. XPS detail spectra of O 1s for silicon samples supporting alternating layers of polyelectrolytes and Al_2O_3. Samples A, C, and E have a PAH/PSS bilayer as the uppermost coating. Samples B and D have an Al_2O_3 layer as the uppermost coating.

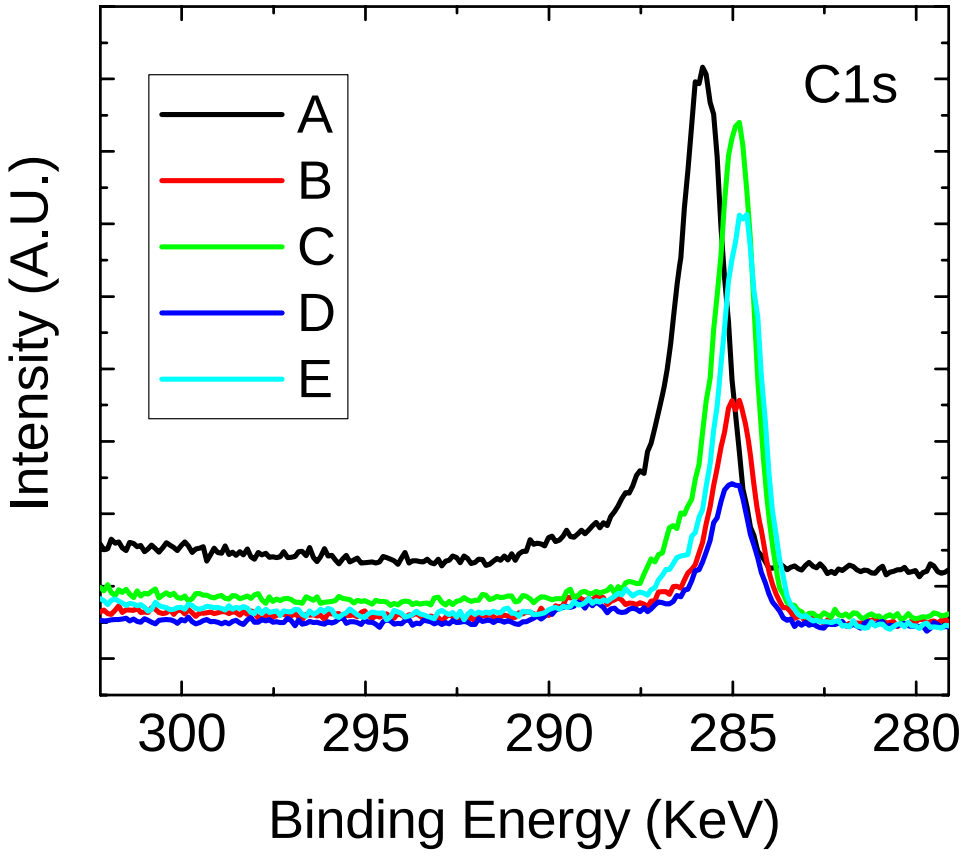

Figure 11.10. XPS detail spectra of C 1s for silicon samples supporting alternating layers of polyelectrolytes and Al_2O_3. Samples A, C, and E have a PAH/PSS bilayer as the uppermost coating. Samples B and D have an Al_2O_3 layer as the uppermost coating.